Design of a Weather Balloon Alternative

Final Report – Design Synthesis Exercise

Group 1

TU Delft

This page is intentionally left blank.

Design of a Weather Balloon Alternative

Final Report – Design Synthesis Exercise

by

Group 1

Florian Voetter	5326168
Giel Otte	5314372
Han Van Lierde	5222575
Marten Schutte	5337828
Menno Wijkhuizen	5284732
Rafael Milla-Koch	5222826
Roan van der Voort	4646452
Tobias Laier	4549228
Varun Gottumukkala	5263883
Wouter Cijsouw	5207584

Tuesday 27th June, 2023

Tutor:	Paul Roling
Coaches:	Stein Stroobants & Rens van der Zwaard
Experts:	Paul de Jong & Tiemo Mathijssen
Faculty:	Aerospace Engineering, TU Delft

TU Delft

Executive Summary

Weather balloons have been used for decades as a means of measuring atmospheric properties. Balloons are launched twice a day from almost 900 locations worldwide, carrying measurement instruments called radiosondes. Along with data from ground-based sensors, aircraft, and remote-sensing satellites, the collected meteorological data is fed into numerical weather forecasts and climate models. The weather balloons typically burst at altitudes of around 33 km, after which the radiosonde falls back with a parachute but without any control. This leads to large amounts of waste scattered over land and sea. While the balloon material itself is fully biodegradable, the loss of radiosondes and their associated electronics can be an environmental threat. Furthermore, the loss of the filling gases such as helium and hydrogen also poses a threat to the environment – helium is a non-renewable resource and hydrogen indirectly causes warming effects when released in the upper atmosphere. These factors present the need to develop sustainable and reusable alternatives to current weather balloons.

In response to this pressing need, the BRAVO family of gliders has been developed, which is short for “Balloon-Released Aerial Vehicle for weather Observation”. This report provides a comprehensive overview of the design process of creating these gliders. It introduces the detailed final design and outlines the logistical and operational procedures associated with their usage. Furthermore, the report encompasses meticulous analyses of cost and market factors, technical risks, and sustainability considerations. To ensure reliability, the gliders undergo thorough verification and validation processes. Finally, the report concludes with gained insights, recommendations, and directions for future work.

System Layout

After trade-offs in previous reports yielded a balloon lifted glider as the best option, a number of design choices for the system layout remained.

Fuselage and wing configuration: The configuration options considered were the conventional design, blended wing with tail, blended flying wing, and canard. After evaluating the criteria, it was concluded that the conventional design and blended wing with tail were the most suitable options. The conventional design offers simplicity, cost-effectiveness, and ease of manufacturing, while the blended wing with tail provides better insulation, innovative design, and structural efficiency. Therefore, the final configuration combines the two, featuring a conventional layout with a lift-generating fuselage for improved insulation.

Empennage configuration: Several empennage options, including conventional tail, T-tail, cruciform tail, H-tail, V-tail, and twin vertical tail, were analysed based on criteria such as vertical stabilizer size, weight, structural efficiency, aerodynamic efficiency, required fuselage size, stability, controllability, and redundancy. Ultimately, the H-tail was chosen, as its design offers advantages such as increased aerodynamic efficiency due to end-plate effects, improved lateral control with a shorter vertical tail span, and better resilience to turbulence for enhanced stability. Additionally, the possibility of installing the tail on one or more booms allows for a smaller fuselage size.

Number of gliders: Due to the large range of different payload weights, it was considered to use multiple gliders with different sizes. The trade-off analysis considered four options: one glider accommodating all payloads, two gliders optimized for different payloads, three gliders dedicated to specific payloads, and a modular glider with interchangeable sections. Based on the desire to optimize operational cost while maintaining performance, the analysis determined that a two-glider system is the most suitable choice. This system includes one glider for radiosonde-only launches and another glider capable of carrying both radiosonde and ozonesonde, as well as custom payloads. This configuration offers flexibility, cost-effectiveness, and manageable operational complexity. Both options were dubbed BRAVO Mini and BRAVO Max respectively.

Methods

The design of any aerospace vehicle is a complex undertaking, as there are a lot of subsystems that interact with, and depend on, one another. To get an initial design as a starting point for the design iterations, an algorithm was written to provide basic fundamental properties such as wing surface area, maximum lift coefficient, and fuselage volume. From this preliminary design, a number of methods were employed to iterate until a final design was reached.

Performance Analysis

A flight performance tool was developed to determine the gliders' performance given certain conditions. It includes an optimisation algorithm focusing on maximizing the ratio of ground speed over descent rate to maximize their geographic range. The analysis reveals that the system's performance is influenced by two primary factors: wind speed and wing loading (W/S). Higher wind speeds and higher wing loading contribute to improved performance, resulting in higher true airspeed and ground speed. On the other hand, average wind conditions and lower payload mass can lead to decreased range for the BRAVO Max glider.

To assess the system's performance in diverse locations worldwide, a selection of locations representing different weather patterns was analysed. Past ozonesonde data from these locations was utilized to calculate the system's performance for each data point. The drift from launch to burst was determined based on GPS locations, and a wind profile was generated from the available wind data. The flight performance tool was then used to calculate the range, considering the drift. The excess range, which represents the difference between the calculated range and the drift, was used as a metric to evaluate the system's performance.

The analysis shows that, in most cases, the BRAVO gliders can return to the launch site in at least 90% of days, and in half of the locations even 99% of the days. However, the performance may be affected by factors such as launch time flexibility, adverse weather conditions, and the altitude reached by the balloons.

Aerodynamic Design

For the aerodynamic design, the openVSP software was utilised for things like estimating C_{D_0}. It utilises the vortex lattice method to determine the aerodynamic properties of the wing and horizontal and vertical stabilizers, however, it can not be employed for the fuselage, which imposed limitations on drag calculations. Furthermore, steady stability analyses were conducted with it.

Icing emerged as a significant challenge, coming from various sources, and depending highly on prevailing conditions. The small scale of the glider relative to the size of ice crystals worsened this issue. Extensive investigation into mitigating measures was undertaken, encompassing both passive and active solutions for de-icing and anti-icing.

The final choice was decided to be a combination of different options, such as the installation of an icing protection system, as well as improved flight path planning to avoid certain climatic conditions. Furthermore, the selection of the airfoil was made with icing in mind.

Airfoil selection was particularly difficult, as it was affected by the very low Reynolds numbers ranging from 20000 to 175000 and a wide range of Mach numbers, ranging from 0.1 to 0.47. In the end, the Dillner 20-32c airfoil, with its thin profile and high camber, was chosen for the wing. In contrast, to keep the tail design simple, the NACA 0010 airfoil was used.

The aerodynamic design went through multiple iterations, with a single design at first before being split up into BRAVO Mini and BRAVO Max.

Stability Analysis

In order to ensure that the aircraft will be stable in flight, a stability analysis was performed. For this, multiple steps were taken, ranging from sizing based on historical data to simulation based on aerodynamic analysis.

Firstly, the horizontal and vertical tail surfaces were sized based on a number of H-tail aircraft and gliders, which provided aspect ratios and geometrical relations. From this initial sizing, a first design

was made, which was used to generate basic aerodynamic control and stability coefficients.

These coefficients were used as an input for a scissor plot, which resulted in a more accurate estimate for the tail size and the required position of the centre of gravity. Once these changes were implemented, another aerodynamic analysis was performed, although more expansive this time around.

From this, the static- and dynamic stability was analysed. Although the spiral mode was initially unstable, this was alleviated by adding dihedral to the design. Furthermore, the control surface requirements were generated by optimizing the state-space coefficients such that the required manoeuvres were met

Structural Analysis

To perform structural analysis on the BRAVO Mini and BRAVO Max wings, a small Python toolkit was developed. This toolkit was used to analyse the stress and deflection of the wings and determine the appropriate sizing of the wing structure.

The stress analysis focused on two criteria: breaking strength and rigidity. The maximum stress, which determines the breaking strength, was analysed at the wing root as it typically experiences the highest stress. The analysis considered three stresses: normal stress from bending moments, shear stress from torsional moments, and shear stress from shear forces. However, the shear stresses were neglected due to their lower magnitude compared to bending normal stresses. To account for simplifications and assumptions, a safety factor of 1.2 was applied.

The bending stresses were determined using standard beam bending equations, considering the sectional properties of the wing. The foam core's contribution was neglected due to its negligible stiffness compared to the skin. The sectional properties were calculated by treating the wing skin as a series of thin angled plates and summing up their properties.

Material selection: One of the simplest construction methods involves cutting or moulding a wing out of polymer foam, such as expanded polystyrene (EPS) or expanded polypropylene (EPP). However, this method is suitable only for lightweight aircraft, as they tend to deform when subjected to excessive weight. To overcome this limitation, a stiff load-carrying skin, typically a strong woven fibre mat, is added to cover the foam core. This composite skin, attached to the foam core with a resin, provides strength and stiffness to the wing structure while preventing buckling and collapse. For added stiffness, composite spars can be embedded in the foam core, but this increases the weight of the wing. The structural analysis, however, concluded, that this was not necessary.

The material selection process involves choosing the type of polymer foam, skin fibre reinforcement, and matrix for the composite skin. EPP was chosen as the foam core material due to its flexibility, resilience, and superior energy absorption properties compared to expanded EPS. EPP is also easier to recycle, making it the more sustainable option.

For the skin reinforcement, various materials were considered, including carbon, aramid (e.g., Kevlar), E-Glass, and Diolen fibres. A trade-off analysis was conducted, considering criteria such as failure stress, impact resistance, stiffness, cost, and sustainability. Aramid fibres scored the highest due to their high impact resistance, making them the chosen option.

Epoxy was selected as the matrix material for the composite skin due to its balanced strength, workability, and compatibility with EPP and aramid fibres. Epoxy can also be obtained in partially plant-based form, adding to its sustainability. However, epoxy is susceptible to ultraviolet (UV) radiation, requiring a protective coating or covering to shield it from UV exposure.

BRAVO family

The BRAVO family of gliders uses the same systems and infrastructure wherever possible. The first example of this are the ground systems, which play a crucial role in the overall operation of the system, including launch, recovery, and communication with the vehicle. The launch system offers two options: manual procedures as they are now launched or a semi-automatic launcher. While the manual procedures are familiar and simple, they require staff to be present during late-night launches, leading to significant costs. The semi-automatic launcher streamlines the process, reducing manual effort and enabling automated nighttime launches. It incorporates components like an automatic hydrogen gen-

erator, automated clamping mechanisms, and a scheduled release system for optimal performance. Even though it was determined to be out of scope for this report, this launcher has the potential to greatly reduce launch cost, or even be sold separately as it can launch balloons with any payload.

For the landing system, a trade-off was performed to determine the most suitable design solution. Several design options were evaluated based on criteria such as cost, space requirements, added mass to the aircraft, complexity, weather handling, ease of retrieval, and the effect of failure. The horizontal net design option emerged as the most favourable choice, excelling in multiple criteria. It addresses the limited ground space available, adds no additional mass to the aircraft, and exhibits superior performance in handling strong winds. While it requires additional effort for retrieval and involves higher costs, its overall effectiveness and efficiency outweigh these drawbacks. It was found that two 16 by 16 metre nets for the two different gliders were required. The polypropylene nets are mounted 5 metres above the ground.

Both gliders are launched using balloons. The choice of hydrogen as the lifting gas is justified based on its better lifting performance compared to helium and its cost-effectiveness and sustainability. The handling of hydrogen by the personnel is evaluated separately. The sizing of the balloon is crucial to maintain economic feasibility. The approach used involves calculating the burst altitude for different commercially available balloon sizes and payload weights. The calculations consider the buoyancy force, drag coefficient, ascent velocity, and other factors. The results indicate the burst altitudes for each combination of balloon size and payload weight, determining their feasibility for reaching the required altitude of 33 km. Based on the results, for the small glider, a 1000g balloon is suitable for most days, while a 1200g balloon is required in windy conditions. Launching the big glider with an ozonesonde payload can be done with a 2000g balloon on most days, but a 3000g balloon is necessary in windy conditions. For the big glider with a full 2 kg payload, a 3000g balloon is always sufficient. The attachment of the balloon to the glider requires a strong and biodegradable line. The line length of 33 to 40 metres was determined based on historical data and scaled linearly with the balloon radius. Cotton material was chosen for best fulfilling the necessary requirements. For the separation mechanism, methods analysed include balloon bursting, hot-wire cutting, pyrotechnics, 3 ring detachment, and quick-release snap shackle. The hot-wire system was ultimately chosen based on a trade-off evaluation. Additionally, a passive system is proposed as a backup, utilizing a pressure differential to cut off the balloon line at the predetermined altitude.

Furthermore, the navigation and guidance logic is common to both glider variants. The requirements for the flight navigation and control sub-system include communication with the ADS-B transponder, adaptive flight path capability, avoidance of restricted airspace, a user-friendly interface, and the ability to determine and land at designated sites. Air traffic management considerations show that controlled airspace is not a significant issue for the glider's trajectory. However, precautions are taken to avoid specific parachute jumping exercise zones and a no-fly zone around Hilversum airport. The GNC system autonomously steers the glider back to the launch site, using navigation system data for position, attitude, and speed. An autopilot system controls the glider based on trajectory optimization methods. The return trajectory logic involves generating cones for each landing site based on pre-flight parameters and wind data. The 'Martini Method' determines cone boundaries, centred around each landing site, based on optimal trajectories for maximum range. Wind data is obtained, and the glider's range is calculated to ensure return to the main launch site in over 95% of wind conditions, with possible diversion if needed.

The Performance of the BRAVO system was also evaluated in various conditions and locations. The system's range was assessed based on wind speeds and wing loading. Higher wind speeds benefited from higher wing loading, while lower payload mass affected BRAVO Max's range in average wind conditions.

Performance from selected locations was evaluated using past ozonesonde data. The percentage of returns to the launch site was considered a key metric. Results showed that the BRAVO system achieved return rates above 90% for all locations except Macquarie Island. Table 1 provides the return percentages for BRAVO Mini and BRAVO Max in different configurations across the selected locations.

Table 1: The probability of returning to the launch site for BRAVO Mini and BRAVO Max

	BRAVO Mini	BRAVO Max + ozonesonde	BRAVO Max + 2 kg payload
Broadmeadows, AU	96.5%	96.5%	98.2%
Boulder, US	99.0%	99.0%	99.2%
De Bilt, NL	90.9%	90.6%	92.5%
Macquarie, AU	63.9%	63.4%	67.4%
Paramaribo, SR	100.0%	100.0%	100.0%
South Pole, AQ	99.0%	99.0%	99.4%

BRAVO Mini

BRAVO Mini is the smaller brother in the BRAVO family, designed to replace standard radiosondes. This chapter will give an overview of all relevant design characteristics. A render is provided in Figure 1, and main aerodynamic characteristics are given in Table 2.

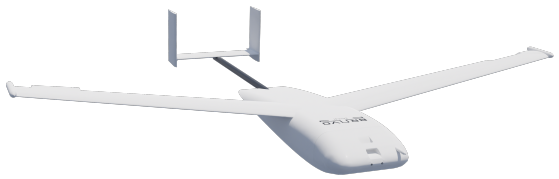

Figure 1: Final design of BRAVO

Table 2: Final aerodynamic design parameters for BRAVO mini

Parameter	**Value**	**Unit**
Wingspan	0.775	m
Surface area	0.05	m^2
Aspect ratio	12	-
Dihedral	8.00	degrees
Fuselage chord	0.367	m
Fuselage surface area	0.0275	m^2
Fuselage t/c	0.15	-
Taper ratio	0.600	-
LE sweep	4.76	degrees
Total mass	0.753	kg
Stall speed	13.2	m/s

During the design iterations, a number of challenges were encountered and changes made. The blending of the wing and body was abandoned, as for the small payload the added volume was not necessary any more. At the same time, it introduced challenges by making estimations more difficult, having a destabilizing effect from having lift generated in front of the wing, as well as the uncertainty of interference between the two. It was discovered that a higher wing loading gives better range due to higher speeds. But since weight can't be increased due to the launch system, the area was decreased. Care was taken to ensure neither $C_{L_{max}}$ was reached, nor too high Mach numbers. Since the effect of increasing the aspect ratio was small, it was chosen with durability in mind. Finally, since the lift of the fuselage was determined to be negligible, the corners were rounded to reduce vortices and drag. Another important influence in the aerodynamic design was the stability and controllability of the aircraft. Using the previously described method of initial sizing, followed by scissor plot analysis and analysis of the stability derivatives, a stable design was iterated for. For the finalized design, the static stability derivatives C_{m_α}, C_{l_β} and C_{n_β} had a value of -0.736, -0.0912 and 0.108, respectively. Observing the signs of these derivatives shows that the aircraft is statically stable. For the dynamic stability, the eigenvalues of the eigenmotions are shown in the table below.

Eigenmotion	**Eigenvalue**	**Damp. Ratio**	**Eigenmotion**	**Eigenvalue**	**Damp. Ratio**
Short Period	-3924	1	Aperiodic Roll	-25.4	1
	-13.6	1	Dutch Roll	-2.81+20.4j	0.1367
Phugoid	-0.0157+0.313j	0.05018		-2.81-20.4j	0.1367
	-0.0157-0.313j	0.05018	Spiral	-0.0127	1

As all real parts of the eigenmotions are negative, the aircraft is considered stable in all eigenmotions,

thus demonstrating total dynamic stability. Lastly, the control surfaces were sized using the previously mentioned method of simulating for the required manoeuvres. This resulted in a $C_{Z_{\delta e}}$, $C_{m_{\delta e}}$ and $C_{l_{\delta a}}$ of -0.384, -1.54 and -0.0570, respectively.

Payload and electronics:

For the mission measurements, the electronics need to perform various functions, including determining air temperature, relative humidity, pressure, and wind speed and direction. The temperature sensing device selected is a platinum RTD due to its linearity, resolution, and accuracy. It will be placed outside the craft to prevent interference from the heat generated by the electronics. Relative humidity will be measured using off-the-shelf sensors commonly used in radiosondes, with additional protection and easy replacement being considerations. To measure pressure, a combination of GNSS altitude, temperature, and sea level pressure will be used to infer the pressure at a given altitude. Additionally, an off-the-shelf pressure sensor with a range of 1100 hPa to 260 hPa and high accuracy will be incorporated for increased accuracy at low altitudes. Wind direction and magnitude will be determined by analysing the drift of the balloon using GNSS position data.

The electronics system requires on-board energy storage in the form of a battery to function continuously for a long period of time, even in no-light conditions. After considering different battery chemistries and trade-offs, lithium-ion batteries are selected due to their specific density, temperature range, and safety. Insulation and a small heating element will be added to meet the temperature range requirement without significantly impacting the overall mass/specific energy of the battery. The battery decided upon is made of four cells with a combined capacity of 50.4 Wh and a weight of 197 grams, capable of providing the peak power of 33.1 Watts.

The flight control system relies on electronics with a sufficiently powerful processor and additional sensors to enable effective operations. Interfaces are necessary for interaction with humans and other systems. The required interfaces include a charging interface for the battery pack, a data interface (USB) for compatibility and ease of use, a payload interface for power and data exchange, a system interface for control lines and antenna signals, and a human interface for power control and operator interaction.

Regarding communications, an active continual downlink is essential for timely data collection, as weather models depend on it. The use of the radio spectrum from 400.15 to 406 MHz is regulated for meteorological aid devices, with a maximum transmission power of 200mW. To ensure effective long-range communication, careful design choices were made. Two main considerations were the antenna's ability to handle the required data rate and provide a sufficient link budget for reliable transmission. A quarter-wave monopole antenna and a half-wave dipole antenna were evaluated. While the quarter-wave antenna was smaller and lighter, its limited radiation pattern made it less suitable for a craft with changing orientation. The dipole antenna, with slightly increased gain, solved this issue and was integrated into the wing to maintain optimal orientation. The preferred antenna orientation was determined through coverage analysis, favouring ascent coverage to minimize data loss. Additional factors such as free-space path loss, receiver sensitivity, and maximum communication range were considered, leading to the selection of specific parameters for successful long-range communication. The maximum communication range was determined by analysing a receiver's sensitivity for various bit rates. Then, using the antenna gain, transmitted power and free space loss, the attainable range at a certain bitrate for commonly available transceivers in the market were obtained. To attain the required maximum range, a bitrate of 9600kbps using GFSK modulation is achievable, which doubles the bandwidth of current systems. For shorter ranges, a higher bitrate is achievable, going up to 200kbps within 100km. Making a variable bitrate system a solution to increase the data gathered.

BRAVO Max

BRAVO Max is the bigger glider in the BRAVO family, designed to replace ozonesondes, as well as enabling custom payloads of up to two kilograms. This chapter will give an overview of all relevant design characteristics. A render is provided in Figure 2, and main aerodynamic characteristics are given in Table 3.

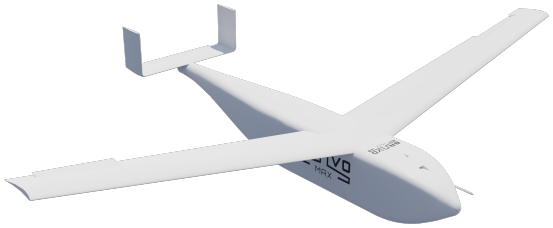

Figure 2: Final design of BRAVO Max

Table 3: Final aerodynamic design parameters for BRAVO max

Parameter	Value	Unit
Wingspan	1.61	m
Surface area	0.215	m^2
Aspect ratio	12	-
Dihedral	10	degrees
Taper ratio	0.600	-
LE sweep	4.76	degrees
Total mass	4.02	kg
Stall speed	14.7	m/s

One of the major challenges for BRAVO Max was the large size of the payload. This combined with the need for 2 cm of insulation lead to a large size of the fuselage and therefore a lot of drag. Similar to BRAVO Mini, increasing the aspect ratio was not providing enough benefit to counter the reduced durability and was therefore kept at 12. As with BRAVO Mini, an important influence in the aerodynamic design was the stability and controllability of the aircraft. Using the same method of initial sizing, followed by scissor plot analysis and analysis of the stability derivatives, a stable design was iterated for. For the finalized design, the static stability derivatives C_{m_α}, C_{l_β} and C_{n_β} had a value of -0.848, -0.259 and 0.0985, respectively. Observing the signs of these derivatives shows that the aircraft is statically stable. For the dynamic stability, the eigenvalues of the eigenmotions are shown in the table below.

Eigenmotion	Eigenvalue	Damp. Ratio	Eigenmotion	Eigenvalue	Damp. Ratio
Short Period	-1348	1	Aperiodic Roll	-13.1	1
	-8.27	1	Dutch Roll	-0.101+6.76j	0.0149
Phugoid	-0.00956+0.197j	0.04854		-0.101-6.76j	0.0149
	-0.00956-0.197j	0.04854	Spiral	-0.0404	1

As all real parts of the eigenmotions are less than 0, the aircraft is considered stable in all eigenmotions, thus demonstrating total dynamic stability. Lastly, the control surfaces were sized using the previously mentioned method of simulating for the required manoeuvres. This resulted in a $C_{Z_{\delta e}}$, $C_{m_{\delta e}}$ and $C_{l_{\delta a}}$ of -0.271, -1.355 and -0.121, respectively.

Payload and electronics: For BRAVO max, the sensors for the flight control are the same as for BRAVO mini, however in addition to the sounding sensors a custom payload of up to two kilos can be loaded, for which a 12V power rail at 2W is provided. The installed 8-cell battery has a capacity of 100.8 Wh and weights 394 grams is able to accommodate the peak power of 44.1 W. The communication system is identical to BRAVO Mini again and described in the respective section.

Operations & logistics

Among the challenges for logistics and operations is the landing site selection and return protocols for safe and reliable vehicle returns. Compliance with UAV regulations is another critical consideration. As the drone system has the capability to actively control itself, it must adhere to the relevant regulations for unmanned aerial vehicles (UAVs) to ensure safe and legal operations. Furthermore, given the significant changes introduced by the drone system, adjustments to launch preparation procedures have to be made, including the calibration of instruments. Maintenance is another important aspect of the operations. Some key areas were identified to inspect, such as deformations, control surfaces, and lighting functionality. Having proactive maintenance procedures in place is key for ensuring a high availability of the system. Besides that, procedures for tasks such as light and wing replacements were developed to ensure that repairs can be undertaken quickly, and the glider returned to service.

Sustainability

Sustainability was a driving factor at every step of the design process and the entire life-cycle of the gliders, from manufacturing to operational use and end-of-life considerations. This is because it was the explicit mission of BRAVO to reduce the emissions of conducting high altitude measurements.

Operational emissions of the BRAVO system primarily involve the release of hydrogen, which contributes to global warming indirectly. The size of the balloon and the corresponding amount of hydrogen released upon bursting can be controlled to limit operating emissions. The use of hydrogen as a filling gas offers advantages over helium in terms of renewability and minimal impact on warming due to its ability to escape Earth's atmosphere. Additionally, manufacturing emissions contribute significantly to the gliders' life-cycle emissions. The materials used, such as EPP foam and aramid fibres, have recycling capabilities, however, the energy-intensive manufacturing processes and the use of sulphuric acid during production raise sustainability concerns. Similar issues arise with the production of electronics and batteries.

The mission's impact on overall sustainability is significant, as frequent and accurate meteorological and climate data collection improves weather forecasts, climate models, and disaster response planning. The BRAVO gliders' ability to provide more frequent soundings at low costs contributes to economic and societal benefits, particularly in addressing the climate crisis and achieving the United Nations' Sustainable Development Goals.

Risk

During the design process, various technical risks were identified for the system. The biggest risks which were categorized as catastrophic or critical include the balloon catching fire during launch, the system colliding with other air traffic, glider missing the landing net, flight control system failure, control surfaces icing up, and scientific sensors getting blocked by icing. To mitigate these risks, several measures were implemented. For instance, a spark-free environment was ensured during launch to reduce the risk of fire. Transponders were included to detect and avoid other air traffic. Grass was allowed to grow high around the landing net to reduce the severity of a landing there. Control surfaces were regularly moved to maximum positions to prevent ice build-up. Additional flight plans and landing zones were prepared in case of premature balloon burst. Heating elements were added to the scientific sensors to prevent icing. Passive automatic release mechanisms and secondary landing sites were incorporated to address the risk of disconnection from the balloon. These mitigation measures, along with routine inspections and component replacements, helped reduce the severity of the identified risks. An updated risk map showed that most risks were now in the yellow and orange zones, indicating that no highly probable risks with critical or catastrophic effects remain.

Cost and Market analysis

The cost estimation for the BRAVO system involves breaking down the composition into known or estimated cost components. This breakdown is applicable to both BRAVO Mini and BRAVO Max, with separate quantitative breakdowns provided for each. The primary cost driver for both gliders is operational expenses, particularly the cost of balloons. Excluding the balloon, the launch cost is only around €10 for Mini and €18 for Max, highlighting the potential for reusable and retrievable balloons to significantly reduce expenses. However, developing such balloons falls outside the scope of this project and requires advancements in materials science. While the gliders can greatly reduce the cost of radiosonde launches, they are only part of the overall solution. Operational costs, excluding the balloon, account for approximately 30% of the remaining costs. It should be noted that many operations will be carried out by employees of KNMI or other institutes as an additional responsibility, making the extra labour cost estimation conservative. A summary table of key costs can be found in Table 4.

Table 4: Cost overview

	BRAVO Mini	BRAVO Max
Total investment cost	€58,400	€58,400
Vehicle Cost	€642	€1040
Lifetime Cost per vehicle	€24,100	€87,100
Cost per launch	€121	€436

While re-evaluating market segments, the market for high-altitude balloons (HAB) remains relevant, as it aligns with the main aim of the project and the unique selling points (USPs) of the BRAVO concept. However, the market for high-altitude pseudo satellites (HAPS) is no longer attractive due to the low endurance of the BRAVO concept. The market for satellite testing, particularly for nano-satellites, still provides potential opportunities for BRAVO, especially with its return-to-base capability. Additionally, new market opportunities include scientific missions in fields like earth observation and atmospheric science, military applications such as reconnaissance missions, and monitoring and surveillance applications like forest fire monitoring. Each of these segments has its specific requirements and advantages, but BRAVO's low cost makes it an attractive option in these markets. A number of competitors were identified and competitiveness against BRAVO analysed.

The market size and share section focuses on the earth observation market and the high-altitude balloons market for meteorological institutes. The earth observation market is projected to increase in size, with the largest market segment being military and intelligence. The target for BRAVO is to achieve a 5% market share in the aerial vehicles segment of the earth observation market within two years of operation. For meteorological institutes, the target is to achieve a 15% market share after two years.

The target cost and return on investment analysis estimate the target cost per launch of the BRAVO system based on the cost of conventional systems. The target cost is set 20% lower than the current cost to undercut competitors. The return on investment is calculated based on the target cost, income generated, and initial investment. The estimated return on investment for BRAVO Mini is 147%, while for BRAVO Max, it is 52%.

RAMS

The RAMS (Reliability, Availability, Maintainability, and Safety) method is utilized to assess the performance of the system. In terms of reliability, the system experiences three types of failure: teething failure, random failure, and age-related failure. The teething failure period is addressed during the integration test phase, while efforts are made to prevent age-related failure through early retirement of parts. The reliability of individual components needs to be quantified.

Availability is categorized into planned and unplanned causes. Planned unavailability includes maintenance and system tests, which are limited but can be scheduled without major impact on operations. Unplanned unavailability accounts for unexpected system failures, such as electrical component failures or structural damage. To ensure availability, multiple drones of each size are utilized interchangeably. External boundary conditions, particularly wind conditions and the formation of ice, influence availability. Launch availability is high, with over 99% availability as long as a person can physically step outside. Landing availability considers early bursts, and the chance of a glider not being able to return to any base is estimated to be very low. Wind conditions are the main factor affecting availability.

Maintenance planning aims to avoid scheduling maintenance during periods with unpredictable weather, to make sure the system is available to take measurements during these most important times. The regular maintenance work packages should be completed within eight hours, and calibration and impact damage inspections are performed before and after each launch.

Safety is analysed from both internal and external perspectives. Internal safety addresses concerns related to balloon filling, construction, landing, and calibration/charging processes. The KNMI has experience in safely handling hydrogen and can adapt procedures accordingly. External safety considers uncontrolled and controlled but unplanned landings. Fatality rates must be below a certain threshold, and precautions are taken to minimize the risk of impact during landing

V&V

It is important to verify and validate tools used in the development process to ensure that they accurately reflect reality and produce accurate results. The V-model is used to break down the system into subsystems and tasks for unit testing. Mathematical and computational tools are verified first. After unit tests, parent subsystem and complete system tests are conducted. Since the design is not yet completed and the verification and validation process therefore ongoing, a plan of future efforts was devised.

Conclusion and Recommendations

This report aimed to design a sustainable alternative to single-use weather balloons by developing a detailed design of a balloon-lifted glider capable of autonomous return to the launch site. The design process involved the development of various subsystems, including Aerodynamics, Stability and Control, and Structures. Additionally, logistics, manufacturing, sustainability, risk analysis, and market analysis were performed to provide a comprehensive understanding of the system. The design phase encompassed the selection of configuration, determination of glider count, and iterative development of subsystems. The challenge of achieving the required range for reliable return proved crucial, with high winds posing the greatest limitation. To address this, a smaller design with higher wing loading was adopted to increase speed and overcome wind resistance. A landing system was also designed, featuring a net for safe and reliable landings in all weather conditions. BRAVO Mini has a range of 463 km in zero wind conditions and 143 km in 2 SSD wind conditions, based on historical weather data. Analysis of balloon burst locations and wind data indicated that BRAVO Mini could successfully return home in 90.9% of cases. While two final designs have been achieved, further detailed development is required before prototyping and testing can commence. Recommendations for further development include simulated icing and research on the Reynolds number effect. Furthermore, the development of a semi-automatic launcher has the potential to significantly lower the launch cost.

Nomenclature

Acronyms

A/C	Aircraft
ADS-B	Automatic Dependent Surveillance-Broadcast
AFRP	Aramid Fibre Reinforced Polymer
BLE	Bluetooth Low Energy
BOM	Bill Of Materials
CFRP	Carbon Fibre Reinforced Polymer
CNC	Computer Numerical Control
DOT	Design Option Tree
GNSS	Global Navigation Satellite System
HAB	High Altitude Balloon
HALE	High Altitude Long Endurance
IMU	Inetertial Measurement Unit
IPS	Icing Protection System
ISA	International Standard Atmosphere
KNMI	Koninklijk Nederlands Meteorologisch Instituut *Royal Dutch Meteorological Institute*
LTI	Linear Time Invariant
LVNL	Luchtverkeersleiding Nederland *Air Traffic Control the Netherlands*
MAC	Mean aerodynamic chord
OpenVSP	Open Vehicle Sketch Pad
RAMS	Reliability, Availability, Maintainability, and Safety
ROC	Rate of Climb
SAF	Sustainable Aviation Fuel
TRL	Technological Readiness Level
VLM	Vortex Lattice Method
WBS	Work Breakdown Structure
WFD	Work Flow Diagram

Greek Symbols

α	Angle of attack	rad
β	Sideslip angle	rad
δ	Vertical deflection	m
ϵ	Downwash angle	rad
η	Efficiency	-
γ	Flight path angle	rad
λ	Eigenvalue	-
μ	Relative density	-
ρ	Density	$kg \cdot m^{-3}$
σ	Stress	$N \cdot m^{-2}$
θ	Twist angle	radians

Latin Symbols

$\bar{c}$	Mean aerodynamic chord	m
$\bar{x_{ac}}$	Location of the aerodynamic centre on the MAC as a fraction of the MAC	-
$\bar{x_{cg}}$	Location of the centre of gravity on the MAC as a fraction of the MAC	-
$\ldots_h$	(subscript) Of the horizontal tail	-
$\ldots_v$	(subscript) Of the vertical tail	-
$\mathcal{M}$	Molar mass	$g \cdot \text{mol}^{-1}$
A	Area	m^2

a	Speed of sound	$m \cdot s^{-1}$
AR	Aspect ratio	-
b	Span	m
c	Speed of light	m
C_D	Drag coefficient	-
C_L	Lift coefficient	-
C_P	Propeller force coefficient	-
C_{D_0}	Zero-lift Drag coefficient	-
D	Drag force	N
d	Diameter	m
d	Distance	m
e	Oswald efficiency	-
f	Frequency	Hz
f_s	Safety factor	-
F_T	Thrust force	N
$FSPL$	Free Space Loss	dB
g	Gravitational acceleration at sea-level	9.81 $m \cdot s^{-2}$
h	Height	m
I_{SP}	Specific impulse	s
I_{xx}	Mass moment of inertia	m^4
J	Polar moment of inertia	m^4
K	Radius of gyration	m
L	Lift force	N
l_h	Tail length	N
M	Mach number	-
m	Mass	kg
N	Number of moles	mol
n	Rotational speed	Hz
n_{max}	Maximum load factor	-
p	Pressure	$N \cdot m^{-2}$
p	Roll rate	$rad \cdot s^{-1}$
q	Pitch rate	$rad \cdot s^{-1}$
R	Gas constant	8.314 $J \cdot mol^{-1}K^{-1}$
r	Radius	m
r	Yaw rate	$rad \cdot s^{-1}$
Re	Reynolds number	-
S	Surface area	m^2
T	Temperature	K
t	Thickness	m
V	Volume	m^3
v	Velocity	$m \cdot s^{-1}$
$V_{descent}$	Descent speed	$m \cdot s^{-1}$
V_{ground}	Ground speed	$m \cdot s^{-1}$
V_{TAS}	True airspeed	$m \cdot s^{-1}$
W	Weight	N

Contents

1 Introduction

In order to predict the weather and track climate change, scientists still rely on a century old technology: weather balloons. Though the sensors are much more advanced in modern times, the basic system is the same as in the early 1900s: A balloon that is filled with helium or hydrogen is attached to an electronic sensor package called a radiosonde, and released into the atmosphere. After reaching the desired altitude, the balloon bursts and the payload descends back to the surface in an uncontrolled manner, sometimes under a parachute. The payload is almost never reused, leading to a large amount of waste. Often the payload and balloon remnants are left in the environment, leading to pollution.

In addition, the gas used to fill the balloon, most commonly helium or hydrogen, is wasted when the balloon bursts. Helium in particular is a scarce resource which is primarily extracted from natural gas deposits, which are producing decreasing amounts of helium each year [1]. With almost 900 launch sites worldwide launching up to two balloons per day [2], and the growing concern for the Earth's climate, a need is presented for a more sustainable alternative that is reusable and less damaging to environment and climate. The Royal Dutch Meteorological Institute (KNMI), which operates one of these launch sites in De Bilt, has expressed a desire to switch to such an alternative, and has been the primary stakeholder in this project.

The aim of this report is to generate a detailed design of a sustainable alternative to the current system of single-use weather balloons. The solution was named BRAVO, which is short for Balloon Released Aerial Vehicle for weather Observations. This new system shall be able to reach the same maximum altitude of 33 km that the weather balloons currently deployed by KNMI can reach, perform the same measurements, while being more sustainable by returning the system to base and reusing components.

This report builds on previous work done in this design synthesis exercise, where the concept and requirements were already established. Specifically, the previous report led to the selection of the balloon-launched glider concept further developed in this report. This resulted from a trade-off performed against other concepts, including a powered aircraft, rocket aircraft, a steerable balloon and a parafoil. The powered and rocket aircraft were dropped due to their unpractical size and noise concerns. The steerable balloon would not be able to fight the winds encountered during operations. The balloon lifted glider and parafoil were the most practical concepts, but the glider won out in the end due to its better wind handling capacity and because there were less unknowns involved compared to the parafoil.

The report possesses the following structure. First, some ancillaries relating to the design processes are presented in chapter 2. Then the initial system layout is given in chapter 3, which is used as a starting point for the detailed subsystem design. chapter 4 shows the shared tools and methods used during the subsystem design, including first and second order sizing. In-depth designs per subsystem are presented in chapter 5 through chapter 12, which are then summarized in chapter 13. Additionally, Sustainability, Market, Risk and RAMS analyses are performed in chapter 16 through chapter 20. Finally, verification and validation on the final design is performed in chapter 21.

2
Design Logic

2.1. Project Objectives
Before progressing any further in the design for this project, it is essential to update/redefine the technical and organisational objectives previously defined in [3] for this ten-week period.

2.1.1. Technical Objectives
The main goal of this project is to design a reusable and sustainable alternative aerial vehicle to replace the current solution, which is a non-reusable weather and radiosonde/ozonesonde combination. Analysing prior attempts and literature on the scientific challenges involved, the technical aspect of this project will be a challenge. Compromises will likely need to be made in order to fulfil the mission need statement and deliver a feasible design for a product.

The mission need statement is as follows:
To design a sustainable and reusable system to replace the current high altitude meteorological measurement devices at a lower cost per launch.

From this statement, several critical requirements can be derived. First, the system must be more sustainable than the current meteorological balloons. Second, the system must have a lower cost per launch than the current solution. Third, the solution must be reusable, which stems from the first two points.

2.1.2. Organisational Objectives
Due to the scale of the Design Synthesis Exercise (DSE), proper organisation plays a vital role in the success of the project. As such, the project plan [3] provided a detailed overview of all tasks and their respective timelines required to develop the project. Overall, three aspects are identified to be of importance. In no particular order, these are manpower, scheduling and sustainability. Manpower takes into account crude developmental resources, such as the number of full-time equivalents available. Scheduling concerns the assignment of these resources, along with internal deadlines. Lastly, sustainability assures that the development of the project proceeds with low waste.

From this, the project objective statement is formulated:
Develop a sustainable and reusable alternative for the current weather balloon system with a team of 10 students in 10 weeks.

2.2. User Requirements
The primary user requirements are listed below. These are the top-level requirements that drove the design process and were derived from the main stakeholder, KNMI. For a complete list of the formulated requirements, the Baseline Report [4] can be referred to.

- WBA-STK-KNMI-001: The system shall accomplish at least the same measurements as done by conventional weather balloons
- WBA-STK-KNMI-002: The system shall be reusable
- WBA-STK-KNMI-003: The system shall take off in a distance of less than 200 [m]
- WBA-STK-KNMI-004: The system shall land in a distance of less than 200 [m]
- WBA-STK-KNMI-005: The system shall carry a maximum payload of at least 2 [kg]

- WBA-STK-KNMI-006: The system shall be transportable in a standard 20 [ft] container
- WBA-STK-KNMI-007: The system shall have a maximum unit production cost of 75000 [Euros]
- WBA-STK-KNMI-008: The system shall be able to fly autonomously
- WBA-STK-KNMI-009: The system shall be able to take measurements at a time resolution of at most 10 [s]
- WBA-STK-KNMI-010: The system shall be able to take measurements at a distance resolution of at most 50 [m]

2.3. Project Design & Development Logic

A project design and development logic diagram is provided in Figure 2.1, which outlines the logical order of activities expected following the design activities discussed in this report.

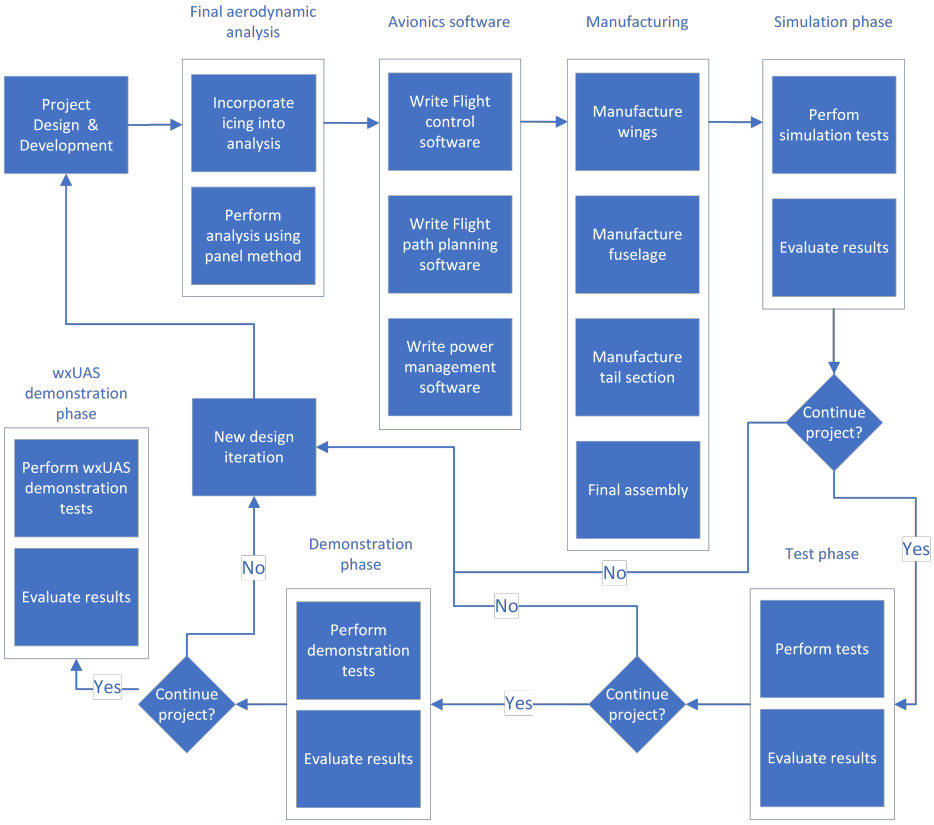

Figure 2.1: Project design and development logic diagram

2.4. FFD and FBS

The functional flow diagram (FFD) and functional breakdown structure (FBS) are provided on the next two pages. The functional flow diagram is used to visualise the relationship between different functions and how these are interconnected to achieve the goal. As it shows how the different functions, and systems performing them, interact it is possible to see possible problems and optimise the design for maximum performance, and make sure the design meets all the customer's requirements. The functional breakdown structure is similar to the functional flow diagram and is created from it, however, instead of showing the interconnection and flow between functions, it is shaped as a tree, and provides a higher level of detail. The entire project is first broken down into the main functions the product needs to achieve. The breaking down is repeated until the required level of detail was achieved. This way, a systematic overview is created, allowing to organise and prioritise all functions.

Functional Flow Diagram

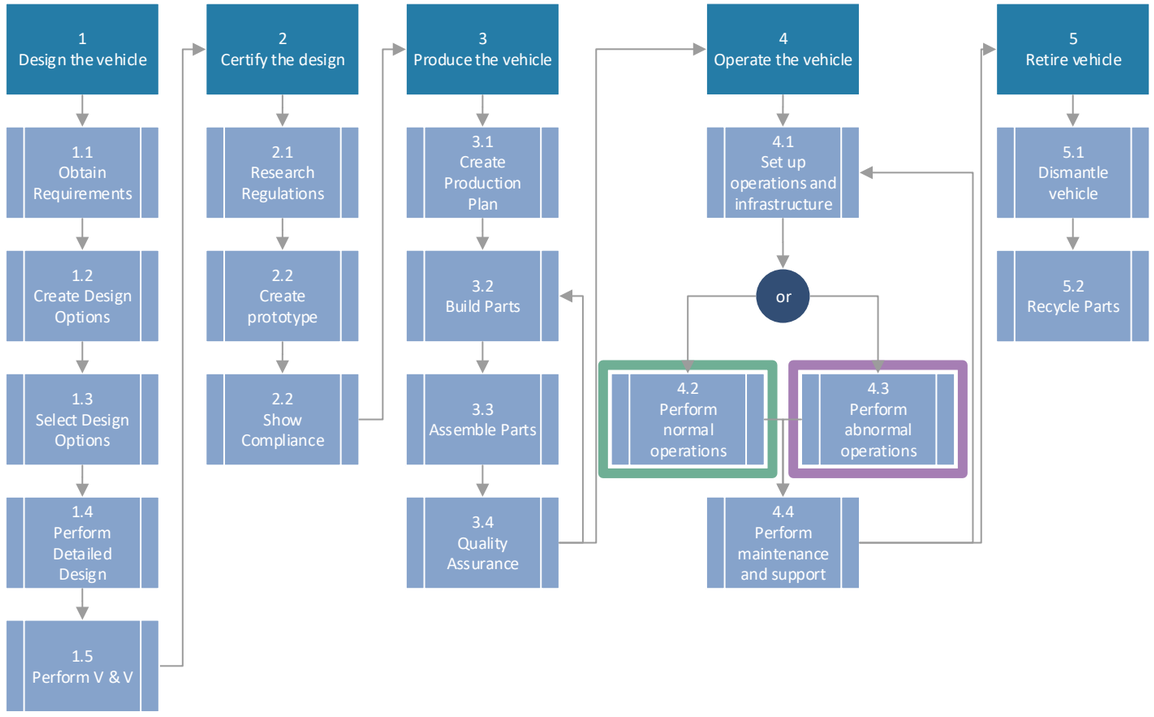

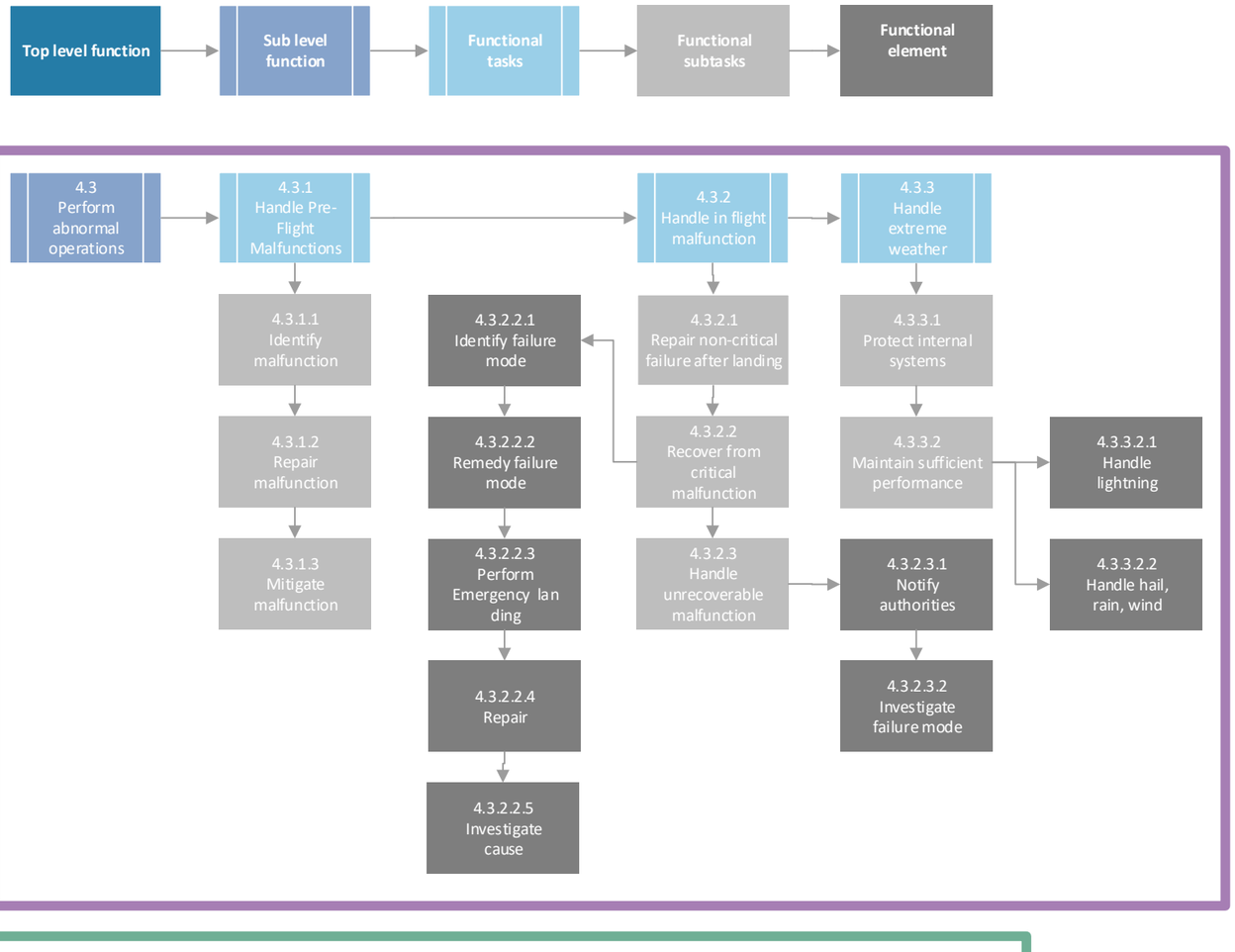

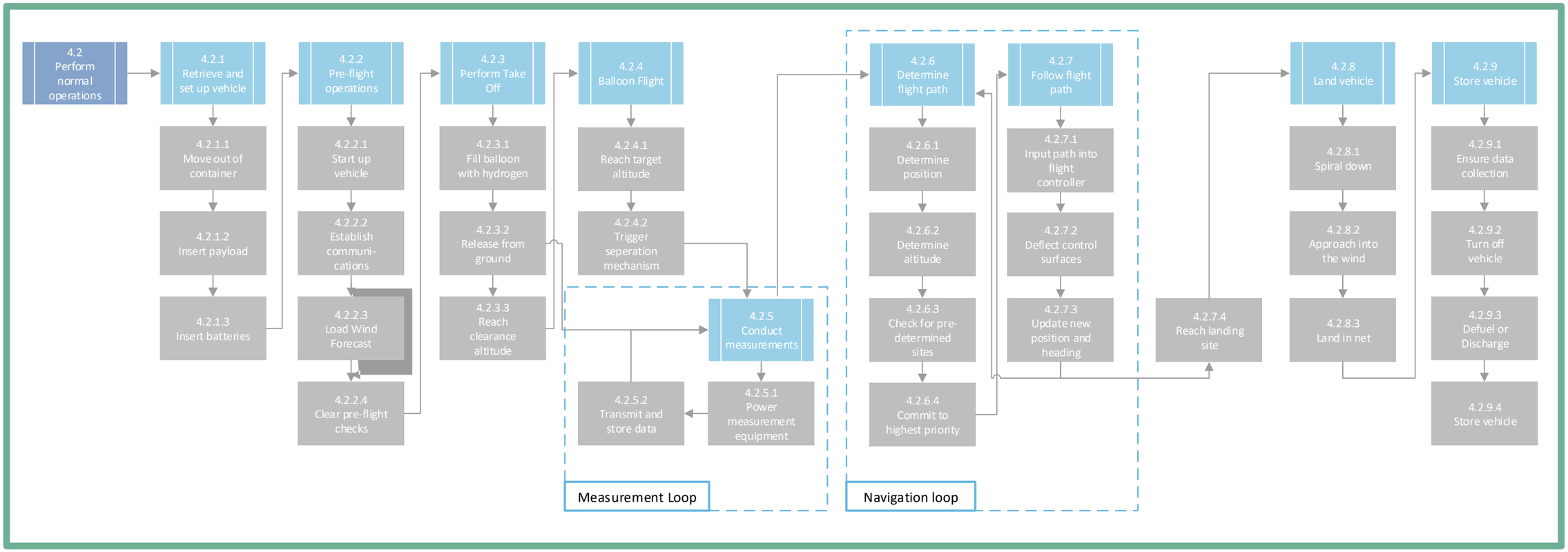

Functional Breakdown Structure

- Product cycle
  - 1 Design the vehicle
    - 1.1 Obtain Requirements
      - 1.1.1 Obtain mission requirements
      - 1.1.2 Obtain stakeholder requirements
      - 1.1.3 Setup system requirements
    - 1.2 Create Design Options
      - 1.2.1 Create design option tree
    - 1.3 Select Design Options
      - 1.3.1 Discard unfeasible options
      - 1.3.2 Perform preliminary trade off
      - 1.3.3 Analyse remaining designs
      - 1.3.4 Perform trade off
    - 1.4 Detail Design
      - 1.4.1 Detailed subsystem design
      - 1.4.2 Ensure final design meets requirements
      - 1.4.3 Iterate design for requirements and performance
    - 1.5 Perform V & V
  - 2 Certify the design
    - 2.1 Research Regulations
    - 2.2 Create prototype
    - 2.3 Show Compliance
  - 3 Produce the vehicle
    - 3.1 Create Production Plan
      - 3.1.1 Create Technical Drawings
    - 3.2 Build Parts
      - 3.3.1 Assemble sub assemblies
    - 3.3 Assemble Parts
      - 3.3.2 Assemble parts
    - 3.4 Quality Assurance
      - 3.3.3 Assemble vehicle
  - 4 Operate the vehicle
    - 4.1 Set up operations
      - 4.2.1 Retrieve and set up vehicle
        - 4.2.1.1 Chose glider size
        - 4.2.1.2 Move out of storage
        - 4.2.1.3 Attach electronics slide into the glider
      - 4.2.2 Pre-flight operations
        - 4.2.2.1 Obtain green light from visual inspection
        - 4.2.2.2 Start up vehicle
        - 4.2.2.3 Establish communi-cations
        - 4.2.2.4 Check battery levels
        - 4.2.2.5 Check control surface actuations
        - 4.2.2.6 Load wind forecast data
      - 4.2.3 Perform Launch
        - 4.2.3.1 Fill balloon with hydrogen
        - 4.2.3.2 Attach balloon to the glider
        - 4.2.3.3 Release from launch site
      - 4.2.4 Balloon Flight
        - 4.2.4.1 Reach target altitude
        - 4.2.4.2 Trigger seperation mechanism
      - 4.2.5 Determine Flight Path
        - 4.2.5.1 Determine position
        - 4.2.5.2 Determine altitude
        - 4.2.5.3 Cbeck for pre-determined sites
        - 4.2.5.4 Commit to highest priority
      - 4.2.6 Conduct measurements
        - 4.2.6.1 Carry measurement equipment
        - 4.2.6.2 Power measurement equipment
        - 4.2.6.3 Transit and store data
      - 4.2.7 Follow flight path
        - 4.2.7.1 Input path into flight controller
        - 4.2.7.2 Deflect control surfaces
        - 4.2.7.3 Update new position and heading
        - 4.2.7.4 Reach landing site
      - 4.2.8 Land vehicle
        - 4.2.8.1 Spiral down
        - 4.2.8.2 Approach into the wind
        - 4.2.8.3 Land in net
      - 4.2.9 Store vehicle
        - 4.2.9.1 Ensure data collection
        - 4.2.9.2 Turn off vehicle
        - 4.2.9.3 Discharge
        - 4.2.9.4 Store vehicle
    - 4.3 Perform abnormal operations
      - 4.3.1 Handle Pre-Flight Malfunction
        - 4.3.1.1 Identify malfunction
        - 4.3.1.2 Repair malfunction
        - 4.3.1.3 Mitigate malfunction
      - 4.3.2 Handle in flight malfunction
        - 4.3.2.1 Repair non-critical failure after landing
        - 4.3.2.2 Recover from critical malfunction
          - 4.3.2.2.1 Identify failure mode
          - 4.3.2.2.2 Remedy failure mode
          - 4.3.2.2.3 Perform Emergency landing
          - 4.3.2.2.4 Repair
          - 4.3.2.2.5 Investigate cause
        - 4.3.2.3 Handle unrecoverable malfunction
          - 4.3.2.3.1 Notify authorities
          - 4.3.2.3.2 Investigate failure mode
      - 4.3.3 Handle extreme weather
        - 4.3.3.1 Protect internal systems
        - 4.3.3.2 Maintain sufficient performance
        - 4.3.3.2.1 Handle lightning
        - 4.3.3.2.2 Handle hail, rain, wind
    - 4.4 Perform maintenance and support
  - 5 Retire vehicle
    - 5.1 Dismantle vehicle
      - 5.2.1 Seperate recyclable components
    - 5.2 Recycle Parts
      - 5.2.2 Recycle recyclable parts
    - 5.3 Reuse Parts
      - 5.2.3 Dispose uncrecyclable parts
      - 5.3.1 Build new vehicles
      - 5.3.2 Repurpose into other systems

Project Objective → System → Task → Subtask → Fuction → Elementary function

3
System Configurations

3.1. Initial Concept Trade-off Summary
Following the exclusion of several concepts based on feasibility and technology-readiness, a trade-off was conducted on the remaining concepts. These concepts were evaluated on their performance, operations, sustainability, cost, and risk. However, the trade-off was not very conclusive, so a second trade-off was conducted on four updated concepts: a rocket-powered aircraft, a propeller-powered aircraft, a glider with a disposable balloon, and a parafoil with a disposable balloon. The winning concept of the second trade-off was the glider with a disposable balloon. This concept also came out on top of the first trade-off, but the result of the second trade-off was much more conclusive.

3.2. Configuration
One of the first steps in the design process is to decide on a configuration of the glider. This design choice effects multiple subsystems, like: Aerodynamics, stability & control, and structures. To ensure the final design is in compliance with the requirements, selecting the configuration with minimum compromises is crucial. It is important to do this while taking into account the mission profile of the glider system. This will be done with a trade-off.

Figure 3.1: Different Design Configurations

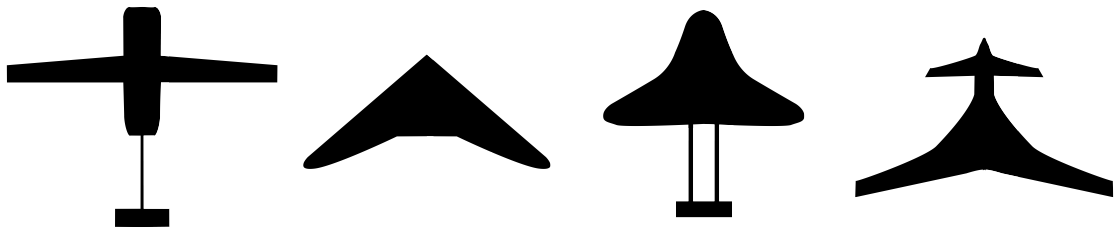

(a) Conventional **(b)** Blended Flying Wing **(c)** Blended Wing Body With Tail **(d)** Canard

Conventional
A conventional configuration consists of a non-blended wing, fuselage, and a tail. The main advantages with this design would be the simplicity and the vast historical data. In addition, manufacturing conventional aircraft would be much easier compared to the blended options as all the components can be separately manufactured/tested and then attached to the fuselage. This however creates the problem of having an external payload bay, since the fuselage is not large enough to house the components. With this in mind, the landing durability is also compromised, as there are many protruding parts such as the wings and the stabilizers. This is shown in Figure 3.1a.

Flying Wing
The flying wing configuration is a tailless, blended wing design, shown in Figure 3.1b. This setup is known for its low wetted area and therefore low parasitic drag. In addition, the large wing blended fuselage section enables for a large and sleek payload bay, located inside the structure. This however makes production of such a configuration more difficult. Another notable disadvantage of the flying wing is the low stability at low speeds and Reynolds number, which can negatively impact the system

at landing conditions and stall conditions at altitude. Despite being used commonly for powered drones at similar sizes, for gliders blended wings are not used due to less efficient airfoils being necessary. This makes the initial sizing of the system difficult, as data on historical aircraft is low.

Blended Wing Body with Boom Tail

The blended wing body with boom tail configuration combines the conventional design with the flying wing. In this configuration, the lower parasitic drag is sacrificed to increase stability and controlability, but the lift over drag is still 20% better than a conventional design (L/D = 20). Having a horizontal stabilizer increases the stability of the glider especially at lower speeds and the large amount of space inside the structure allows for payload storage and insulation while not adding significant drag, however, the disadvantages of the blended wing when it comes to manufacturing are still evident. In addition, the durability of the system is compromised as more fragile components such as the boom and stabilizer are included, which especially in landing could increase repair costs. A representation of this configuration is shown in Figure 3.1c.

Canard

The main advantages of the canard configuration come from the upstream placement of the control surfaces. This means additional pitch control and delay in loss of control at stall. However, the main disadvantage of the canard configuration would be the landing durability with a long nose sticking out in front of the main wing. Furthermore, the aerodynamic interference of the canard with the main wing would be difficult to quantify. Finaly the added complexity to the controls system and the restricted payload space in the fuselage are limitations of the canard configuration, which can be seen in Figure 3.1d.

Table 3.1: Trade-off: Glider configuration

Criteria	**Weight**	Conventional	Blended	BWB with tail	Canard
Stability and control	5	5	2	5	3
Durability	4	2	4	3	1
S/W	1	3	5	4	3
Wetted area	2	3	4	3	3
Technological readiness	3	5	2	2	4
Manufacturability	1	4	3	3	4
Total		61	48	56	44

In Table 3.1, the design configurations are traded off with criteria; stability and control, durability, S/W, Wetted area, technological readiness and manufacturability. These criteria have been selected to find the optimal performing glider configuration by looking at possible challenges in the design process. The weights and scores are ranging 1-5 and the highest total scoring configuration is selected as the winner after a sanity check.

As a result of the trade-off, the conventional configuration has the highest score and is the most logical choice for this glider concept. However, to improve on its weaker areas such as wetted area with respect to surface area, the fuselage and therefore the payload bay will be designed as lifting bodies. This will pull the bad scoring areas of the design more towards the blended wing body with tail option, while also keeping the manufacturability and stability as high as possible.

3.3. Number of Gliders

The glider must have the capability of carrying a radiosonde and ozonesonde, but ozonesondes are only launched once a day. Therefore, designing a glider to accommodate both a radiosonde and ozonesonde would lead to an over-designed glider during radiosonde-only launches. Therefore, to ensure that each launch is optimised for performance, the possibilities of having multiple gliders or introducing modularity were considered. To facilitate the selection of the number of gliders or modularity, a trade-off was performed for the following options:

- **One Glider**: A single glider that can accommodate at least a radiosonde and ozonesonde.
- **Two Gliders**: One glider optimised for carrying only a radiosonde, and another one for carrying a radiosonde, ozonesonde and custom payloads.
- **Three Gliders**: One glider optimised for carrying only a radiosonde, another one for carrying only a radiosonde and ozonesonde, and a third glider for custom payloads.
- **Modular Glider**: A single glider with interchangeable sections for different payloads.

The following criteria and weights (given in parentheses, on a scale of 1 to 5) were deemed relevant for the trade-off:

- **Unit Cost (2)**: The unit cost criteria includes the cost of purchasing the glider/s. While important, the operational cost significantly outweighs it.
- **Operational Cost (5)**: The operational cost is the most important criteria, as reducing it is one of KNMI's main desires. The operational cost includes the cost of having smaller/larger balloons for different gliders.
- **Infrastructure Cost (3)**: The infrastructure cost criterion includes the additional infrastructure needed in order to store and operate the glider/s. It is an important consideration, considering the existing infrastructure for weather balloon launches is limited, but it is still not as important as the operational cost.
- **Payload Flexibility (2)**: The payload flexibility criterion indicates the possibility and ease of using different payloads. It is not a very important criteria, though, because the ability to use custom payloads is not a requirement, but a desire.
- **Performance (4)**: The performance of the glider/s is very important, and determines the overall capability of the glider to return to the launch site. It is not as important as the operational cost, though, as that is still the driving desire.
- **Operational Complexity (3)**: The operational complexity relates to the time, number of personnel, and training required to prepare, launch, recover and stow the glider/s.

The trade-off and results are shown in Table 3.2.

Table 3.2: Trade-off: Glider number and modularity

Criteria	**Weight**	One Glider	Two Gliders	Three Gliders	Modular Glider
Unit cost	2	5	3	1	3
Operational cost	5	2	3	4	3
Infrastructure cost	3	4	3	2	2
Payload flexibility	2	2	4	5	4
Performance	4	2	4	5	4
Operational complexity	3	5	4	3	2
Total		59	66	63	61

The results of the trade-off indicate that using two gliders would be the best option, even though the difference in scores is not that convincing. The two glider system provides an optimised option for radiosonde-only launches, while also providing an additional option for ozonesondes and larger, custom payloads. The two glider system provides sufficient payload flexibility while ensuring the best performance for the radiosonde-only launches, which constitute the majority of launches. In addition, the operational complexity and infrastructure costs are relatively low.

4 Methods

In this chapter, the overall method of the design process is laid out. The method was developed in more detail at the same the design work was taking place, therefore multiple methods for sizing will be explained in this chapter. The methods here are still top level and above the different subsystems. In this project however, most of the design decisions been taken up by the Aerodynamics department, so most of the documentation of iterations will be covered there.

4.1. Subsystem interfacing

All subsystems in the design process are dependent on each other in a complex may. Because of that, an N2 chart, created previously[5], was created to visualize all connections between these systems. This N2 chart is hard to read through and hard to draw conclusions from, therefore the most important connections are listed below that drove the design process.

1. **Aerodynamics:** The aerodynamics subsystem mainly needs the internal component sizes and weight to be able to size the shape of the glider. Also, FC & navigation will require a certain maximum C_{D_0} and wing loading in order to fly through the wind and have a high range. Lastly, the landing system requires a certain landing speed, which has to be designed for.
2. **Stability & Control:** The S&C subsystem needs the distribution of masses in the aircraft together all Aerodynamic coefficients from Aerodynamics.
3. **Power & electronics:** needs the power required for all internal components, their sizes and their operating temperature.
4. **FC & Navigation:** FC & Navigation needs to know the aerodynamic parameters and mass of the glider in order to plan an appropriate flight path.
5. **Payload & data handling:** P& DHis mainly giving out requirements to other subsystems, but it does need to know if sensors can be placed in the right places from Aerodynamics.
6. **Communications:** Communications needs to know what telemetry data needs to be sent to ground.
7. **Structures:** Structures needs all possible loading conditions during flight and landing together with the sizing of the glider to perform the structural calculations.
8. **Ground systems:** Ground systems needs the mass and stall speed of the glider to size the landing system.
9. **Balloon system:** The balloon system has the glider mass as an input to size the balloon.

4.2. Initial method

Initially, the design was a blank sheet and some sort of first general iteration had to be done. For this, some limiting input values had to be thought of in order to constrain the design to the extent that a result can be generated. This is covered in the first order sizing, section 4.3, which can also be seen as the second box in Figure 4.1. Here, the logic behind the first few iterations is laid out in a flow chart. The outputs of the first order sizing are inputted into the Aerodynamic analysis. This method is described in section 5.1 in the Aerodynamics chapter. Finally, inputs of both the first order sizing and the Aerodynamic analysis are inputted into the flight profile analysis, which is described in section 4.4.

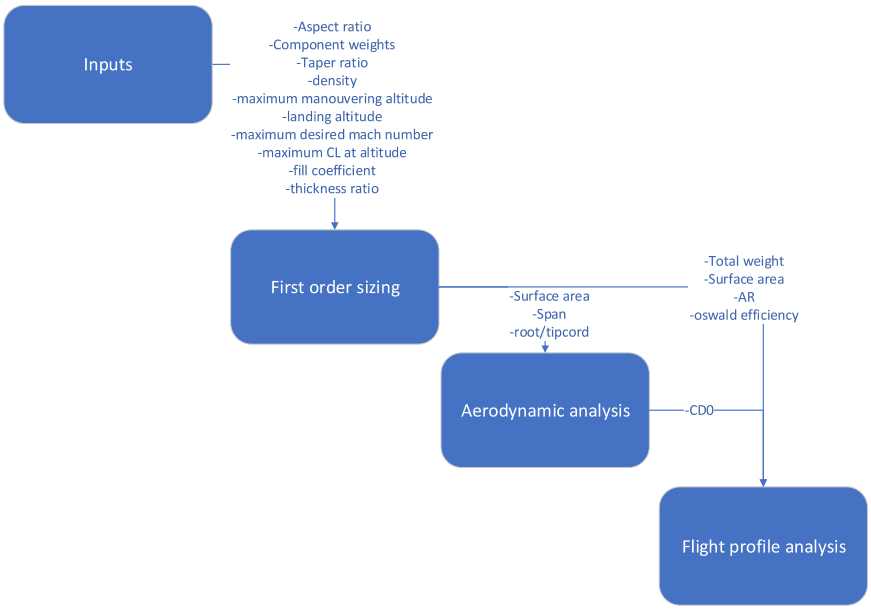

Figure 4.1: Initial design approach visualized

4.3. First Order Sizing

In the first order sizing, the main aim is to find the surface area and weight of the aircraft. for this, an iterative algorithm is written. First, the inputs are defined. These include the weights of the components that are presumed to be fixed for the preliminary phase and will change later on:

- fuselage volume
- density of the wing
- mass of the electronics
- mass of the payload
- spar weight per meter
- maximum C_L
- maximum operating height
- landing height
- aspect ratio
- taper ratio
- fill coefficient
- tail mass

as a first step in this process, the speed at landing conditions is calculated by assuming equal dynamic pressure at the maximum altitude stall speed and the landing height stall speed. This comes down to:

$$V_{ground} = V_{alt} \cdot \sqrt{\frac{\rho_{alt}}{\rho_{ground}}} \tag{4.1}$$

These dynamic pressure conditions will be used throughout the calculations.

After this, an iterative loop is started where, first, the surface area that is required based on the weight and the dynamic pressure conditions. Based on this surface area and other wing parameters, the weight of the wing is calculated. After this, the weight is updated to the new weight, after which a new surface area is calculated. This method stops once the weight is within a pre-specified limit. This method converges fairly quickly and gives a result as shown below:

```
######################REPORT#####################
number of iterations required for convergence: <NUMBER>
total weight: <NUMBER> [N]
wing weight: <NUMBER> [N]
```

```
spar weight: <NUMBER> [N]
payload weight:  <NUMBER> [N]
fuselage weight: <NUMBER> [N]
tail weight: <NUMBER> [N]
electronics weight: <NUMBER> [N]
surface area:  <NUMBER> [m^2]
mean aerodynamic cord <NUMBER> [m]
root cord <NUMBER> [m]
span <NUMBER> [m]
landing speed: <NUMBER> [m/s]
####################END REPORT###################
```

From this report, the inputs for the Aerodynamic analysis can be deduced and used for the initial sizing of the aircraft.

4.4. Flight Profile Analysis

In order to determine the ideal optimization algorithm, a closer look had to be taken at what was necessary from these gliding aircraft. The goal of these vehicles is to return to their launch site in the majority of cases. From the user requirements, found in chapter 2 a range of 150 km in severe wind conditions was decided upon as the target for this design.

To be able to do meaningful calculations with this, the wind needs to be accurately estimated. After analysing publicly available ozonesonde data [6], an atmospheric wind profile was attained by averaging the winds across the dataset for each altitude. After this, anywhere from zero to two standard deviations of extra wind speed could be added to the average wind profile. For all configurations that are run in this program, three wind conditions are tested:

1. **No wind** gives a baseline insight
2. **Average wind** gives insight into the average day performance
3. **2 SSD wind** gives the range for a 97.5 percent confidence interval

For this, it will be assumed that the wind will always be blowing in exactly the opposite direction to the flight path that needs to be followed. In the case of this design, severe wind conditions were defined to be 2 SSD.

Now that a target has been defined, the focus can be put on the simplified model, Figure 4.2a shows the relation between the various contributors to the airspeed. For traditional gliders, the descent speed, $V_{descent}$, is minimized in order to maximize the endurance of the aircraft, however, depending on the wind speed their geographic range varies greatly. High winds can even result in negative ground speed, V_{ground}, which is very undesirable for this use case. Therefore, it was determined that in order to maximize the geographic range of these gliders, it would be necessary to maximize the ratio of ground speed over descent rate, $\frac{V_{ground}}{V_{descent}}$.

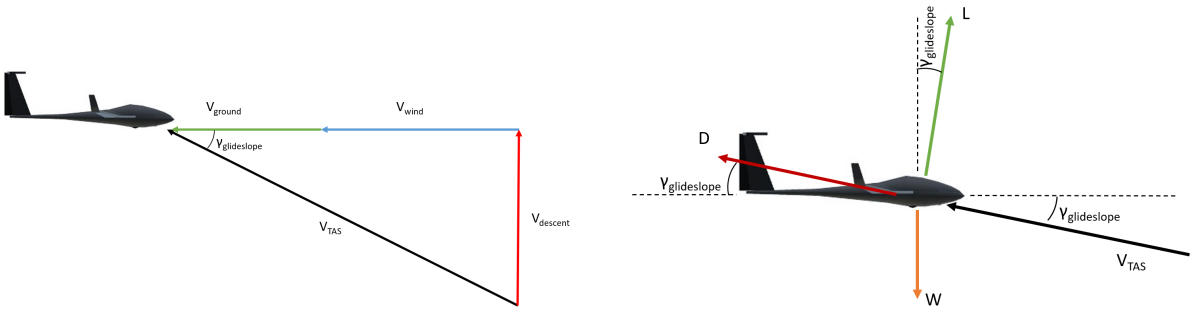

(a) Velocity diagram for a typical gliding aircraft

(b) Free body diagram for a Glider

Figure 4.2: Velocity and free body diagram for a simple glider

In order to determine the relationship between the ground speed, descent rate, weight, lift and drag a free-body diagram was generated which can be seen in Figure 4.2b.

From this point, the method could be simplified even further, assuming small angle approximation,

which is likely to be a valid assumption for a high-performance glider. With this assumption, Lift is assumed to be equal to drag, and furthermore, V_{TAS} is assumed equal to $V_{ground} + V_{descent}$.

From these relations, Equation 4.2 was generated, where V_{TAS} is defined as in Equation 4.3 and C_D as in Equation 4.4.

$$\frac{V_{ground}}{V_{descent}} = \frac{V_{TAS} - V_{wind}}{V_{TAS} \cdot \frac{C_D}{C_L}} \tag{4.2}$$

with:

$$V_TAS = \sqrt{\frac{W}{S}\frac{2}{\rho}\frac{1}{C_L}} \tag{4.3}$$

$$C_D = C_{D_0} + \frac{C_L^2}{\pi \cdot AR \cdot e} \tag{4.4}$$

In this equation it is important to realise that one is optimizing for the ground speed, the airspeed is irrelevant for the sake of this calculation. Also, readers might have noticed that when the wind speed is positive in sign, this is perceived as a headwind. From this formula and the known wind and atmospheric parameters, a numerically optimized C_L and L/D ratio can be determined for maximum range. Alongside the range, flight time, true airspeed, Reynolds number and a number of other parameters are calculated. The inputs to this method are listed bellow, and they can be changed at any point along the design process.

```
{"AR": 12, "e": 0.9, "m": 0.75, "S": 0.05, "CD_0": None, "CD_0_base": 0.02771,
"CD_0_h": 5.714285714285715e-07, "CL_max": 0.666 * 1.55, "CL_alpha": 0.10796535}
```

Some things to note are: all units are SI aside from C_{L_α} which is in the units of 1/°. Additionally, the C_{D_0} constant can be swapped out for a variable C_{D_0} which changes with altitude by using the $C_{D_{0,base}}$ and $C_{D_{0,h}}$ parameters.

The exact method used can be found on the team's GitHub [1] in the FlightPerformance Python Class.

4.5. Updated method

When initial sizing methods were applied and an initial design was generated, a need for a new method of sizing was deemed necessary to optimise the design for the to be performed mission, illustrated in Figure 4.3. The flight profile analysis was made the first step for the iteration process. It would analyse which surface area, weight combination gives the best range and pass that onto the sizing. In the sizing, all necessary changes to the design are made, and subsequently the Aerodynamic analysis is performed again to get better range estimates in the flight profile analysis. This method optimized the important goal of getting back to base in almost all weather conditions. It should be noted though that there were still constraints though that needed to be adhered to from all subsystems, but those are not included in the figure for clarity. They are mostly part of the second order sizing, which became more sophisticated while subsystems became more sophisticated. It should be noted that the iterations shown in the figure were not distinct iterations, but instead a more constant update of design parameters which became more certain over time.

[1] Github repo: https://github.com/Weather-Balloon-Alternative/bravo-aero-structures/tree/first_order_sizing

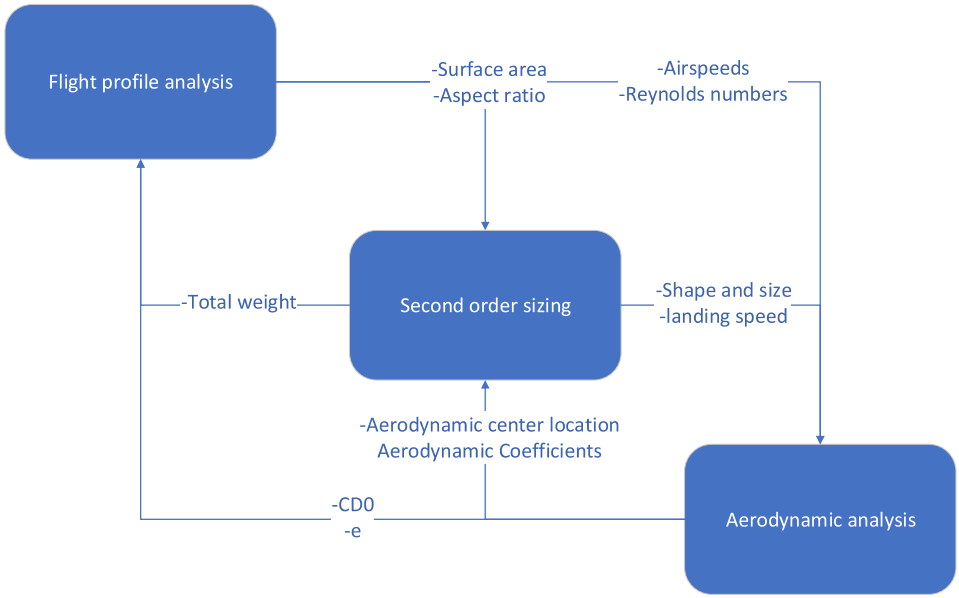

Figure 4.3: Initial design approach visualized

4.6. Second order sizing

As said in section 4.3 and section 4.5, the task of the second order sizing is to go from a few limiting parameters like wing size and aerodynamic properties to a full sizing of the aircraft. There are many subsystems which perform their task in this part of the design process, but they are described in their own subsystem. This section will just cover the overarching design steps which do not fit in a certain subsystem. The second order sizing in this section was performed in Excel, with a different sheet for each iteration. This made sharing data of the current iteration simple, but the cost was a manual connection with the Python code and OpenVSP. It was realised halfway though the design process that a fully integrated code would have been better but at this point, changing it would have costed too much time.

4.6.1. Mass estimation

Besides the simple mass estimation done in section 4.3, a more accurate mass estimation was also done in the Excel sheet. There is more detail in the mass of the individual components together with their x location, measured from the nose of the aircraft, which will be used for the centre of gravity estimation. The mass of the electronics was given by the Payload and Electronics subsystems, together with the insulation thickness required to be able to adequately heat the internals. The following assumptions were made in this simplified mass estimation.

- All components are filled with foam of $60g/m^3$
- Each component has a uniform covering thickness distribution, determined by structures
- Fill factor, $FF = \frac{S_{airfoil}}{c \cdot t}$, is measured to be 0.7
- A factor of 1.3 is used in the covered area of the wing to account for the roundness of the airfoil shape.

The structural mass of the fuselage was either the shape of the centre airfoil, in case of the small glider, or a combination of cubes and square cones for the big glider. These cones approximate the smooth, flowing shape of the nose and tail. The shapes used to approximate the fuselage shape are shown in Figure 4.4. Surface area approximations were also made to calculate the covering mass. The structures subsystem is given the current iteration and then gives back the required amount of covering

layers per component given by structures. The structures subsystem also gives the required tail boom diameter and mass per length.

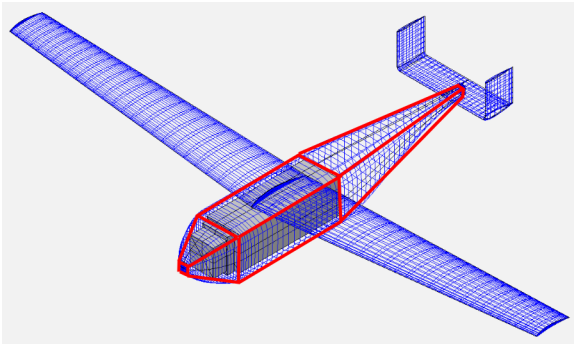

Figure 4.4: Shapes used to approximate the fuselage mass of the big glider

In the end, a final mass estimation is obtained, which of course still has uncertainties and discrepancies. These are included in a contingency factor, which is normally added on top of the mass, since that normally decreases range. Also, a higher mass results in a more expensive balloon. However, with the optimal flight path described in chapter 10, a higher mass results in a better range. Therefore, a contingency factor is used to both subtract and add mass, to account for the discrepancies.

4.6.2. Layout and Center of Gravity

The aerodynamic design is not just automatic calculations, it is also about fitting all internal components in the right position to make the plane balance in the right position. The tail length and size are dictated by stability, but the wing position and nose length need to be decided based on the mass distribution. The centre of gravity location is a weighted sum of all components, and the equation for this is given in Equation 4.5. The assumptions and simplifications made for the CG position are listed below.

- CG of a thin airfoil is at half of the chord
- CG of a foam cone is 0.3 from the base and for covering it is 0.4
- CG of electrical components is in the centre of the part

The stability analysis has not been done when the layout is decided, so a preliminary CG location has to be decided. This CG position is chosen to be the same location as the aerodynamic centre. For most wings it is located at 25% of the MAC but if there is a lifting body fuselage, such as for the small glider as will be seen later, the fuselage will also have a contribution to it. This contribution is hard to estimate, so a test is set up using OpenVSP to derive the position of the AC. Equation 4.6 uses moment and lift coefficient at two angles of attack to give the location of the AC. With the CG and AC locations known, they can be placed at the right location with respect to each other. The layout and component placement are then moved around until the CG is in the right spot. Often this necessitates a longer nose or a wing position shift, so this is an essential part of the design process.

$$x_{cg} = \frac{\sum x_i \cdot m_i}{\sum m_i} \tag{4.5}$$

$$x_{ac} = c_{ref} \cdot \frac{C_{m_2} - C_{m_1}}{C_{L_1} - C_{L_2}} \tag{4.6}$$

5 Aerodynamics

The aerodynamic design of a glider is a complicated process which requires extensive communication with other subsystems to iterate to a final design which will meet the requirements set. The most important requirements of these are the ones related to range, the capacity to fly in strong winds and the payload size of BRAVO max. No additional requirements were set, but instead constraints were enforced by other subsystems. This chapter will cover the main iterations done to the glider designs throughout the process, since aerodynamic design comes from the mass estimation and internal layout of the components. Due to the design process being a mix of three programs which had to communicate with each other for iterations, an automated way of iterating the design to a perfect design was not an option. Also, because manual changes to the design had to be done in OpenVSP and design decisions had to be made by human engineering insight. This chapter will follow the design choices made which resulted in the final designs. First an OpenVSP introduction, the issue of icing and the airfoil choice will be covered before moving on to the main design iterations.

5.1. OpenVSP

The aerodynamic analysis program that was chosen is OpenVSP, which stands for open vehicle sketch pad. It is an aircraft preliminary design software developed by NASA in the early 1990s and has been made open source in 2014. It has a graphical user interface which allows the user to make 3d models of aircraft using wing shapes and fuselage shapes. The program has built in engineering and aerodynamic functionalities, including a vortex lattice method, which is the main method used in the aerodynamic design of the glider.

Interface The main advantage of OpenVSP over other available programs is the user-friendly 3d modelling tool, where a plane can be made out of wing and fuselage parts. All parameters of these wing sections can be changed and the model updates parametrically, allowing quick iterations in the design. The 3d model was besides the analysis functions also used for volume estimation and placing the electronic packages. Figure 5.1 shows the model for the final BRAVO Mini in the user interface of OpenVSP. The internal components are visualised with the grey boxes, and from that their location and insulation thickness around them can be verified. Also, the mesh can be seen which was used during analysis, which was adjusted to the accuracy needed for different analyses.

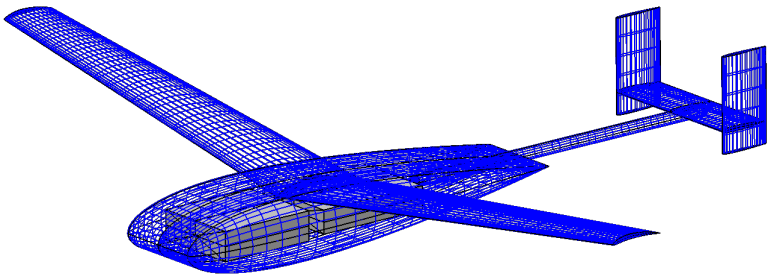

Figure 5.1: OpenVSP model of the final BRAVO Mini internal components visible

Parasitic drag OpenVSP has a built-in parasitic drag calculator where a C_{D_0} value is calculated per component and a total C_{D_0} given as an output. The estimator used is the Schlichting compressible method, which was deemed appropriate due to part of the flight being in the compressible region of Mach numbers. It was found during testing that C_{D_0} changed over altitude and velocity due to changes in Reynolds number. This change in C_{D_0} is plotted in Figure 5.2, with the influence of altitude on the left and the influence of velocity on the right. A simple linear relation was set up from OpenVSP data using a linear approximation which would change a base C_{D_0}, at v=30m/s and h=0, to a C_{D_0} estimate at a specific flight condition. The relation obtained for this can be seen in Equation 5.1, with altitude in m and velocity in m/s as inputs. It was realised that this cannot be approximated to be linear, but Reynolds number influence is complicated and hard to approximate accurately. There is more influence of Reynolds number not covered in OpenVSP like flow separation at altitudes like 30 kilometres. This has to be researched more in future design work, but the effect will be a slightly different C_{D_0}, changing the range, but will not be critical to the overall mission.

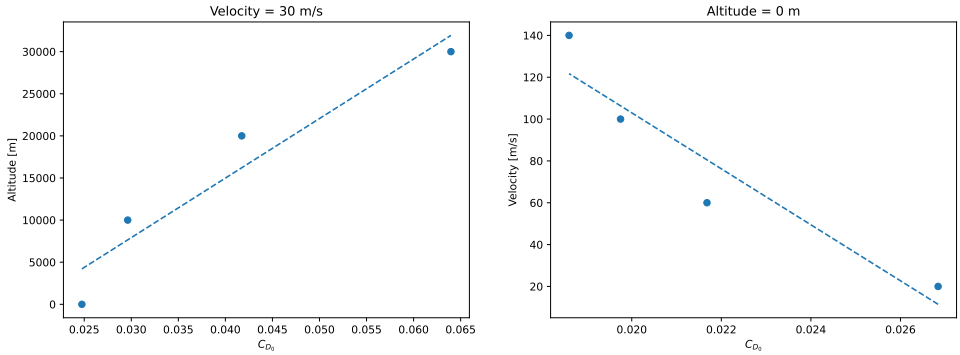

Figure 5.2: The influence of altitude and velocity on C_{D_0}

$$C_{D_0}(h, V) = 0.0257 + 1.415 \cdot 10^{-6} \cdot h - 7.473 \cdot 10^{-5} \cdot V \tag{5.1}$$

Vortex Lattice Method The main tool used in openVSP is the VSPaero solver in vortex lattice mode. This method is great for calculating Aerodynamic properties of the wing and stabilizers, but it can not analyse a fuselage shape, which limits it in the drag calculation department. It can however calculate induced drag, moments and lift accurately. OpenVSP also has a 3d viewer to visualize the analysis that has been done. Here the pressure difference distribution on the wing can be seen for different angles of attack and wakes visualize the vortices generated. Such a viewer can be used for checking if the analysis did not have any errors in the pressure distribution. The VLM, Vortex Lattice Method, is also used for doing steady stability analyses for the control department, providing all necessary coefficients for analysing stability and control and sizing the control surfaces. These surfaces are modelled as sub-surfaces and can be moved to a specific angle, and the output from the VLM solver will give the moments created by these surfaces. Finally, through testing, it was found that the Oswald Efficiency factor estimation by OpenVSP is not trustworthy. It often gave values above one, like 1.1. Therefore, an Oswald efficiency factor for a wing that has a taper ratio of 0.6 was assumed to be 0.9. This would give more realistic results from the drag calculations.

5.2. Icing

Icing is a phenomenon which occurs when super cooled liquid water collides with the aircraft. the droplets freeze when they contact the aircraft. [7] This liquid can be present in the air as is or in the form of clouds. Water vapour clouds can significantly increase the accretion rate. However, clouds made up of snow or ice crystals do so to a much smaller extent. Besides icing from water vapour in air and clouds, super cooled rain can be a source of ice growth. Because the droplets are much larger, this can have a larger effect on the icing. But this conditions occurs less often.

For icing, there are several conditions in which the ice can form and which influence the eventual impact

it will have on the aircraft. these are:

- RIME: droplets are significantly below freezing and super cooled. This causes them to freeze immediately on impact with the surface. It builds in more streamlined geometries, which lowers the potential to disrupt the airfoil significantly[8].
- GLAZE: forms when the droplet temperature is close to the freezing point. Either the droplet itself is only slightly below freezing, or the aircraft surface is below freezing. In this regime, the droplets instantly freeze upon impact, but remain liquid. This can then run back over the airfoil. The ice resulting from this is clear and smooth. It can grow irregular ice geometries such as horns and can therefore have a significant effect on the airfoil performance. [9][8].
- mixed: a mixture of both conditions above. Which can also significantly effect airfoil performance.

These conditions can form ice in various different areas and structures. While four main geometry types can be identified, the build up will usually be a combination of various types.[8] types of icing geometries:

- Roughness: small ice build up which increases the roughness of the airfoil.
- Horn ice: horn like protrusions which can grow from the leading edge, significantly changing the geometry of the airfoil.
- stream-wise ice: builds up in streamlined shapes. Influences aerodynamics the least.
- span-wise ice: forms ridges in the spanwise direction.

5.2.1. Effects of icing

Icing on small scale UAVs can be a major problem. A millimetre of Ice build up on a 737 wing might not be much but add that same millimetre to a small UAV wing, and it can pose a significant flow disruption. This flow disruption effects the lift generated by the airfoils, increases the drag on the aircraft and because of increased non uniformity's decreases the stability of the aircraft. Risk of icing greatest when in cloud layers, especially in vapour clouds as opposed to ice clouds.

The severity of icing on a UAV varies a lot with conditions, but can have a very significant effect on the performance. Figure 5.3 shows how this various icing conditions affect the performance of a UAV system. This was done for a UAV craft with similar enough characteristics[10] that lessons from this can be applied to the current design. The consequence of icing will however be limited to performance and the aircraft will still be able to glide down, but just with a lower lift over drag, as long as the control surfaces are moved regularly.

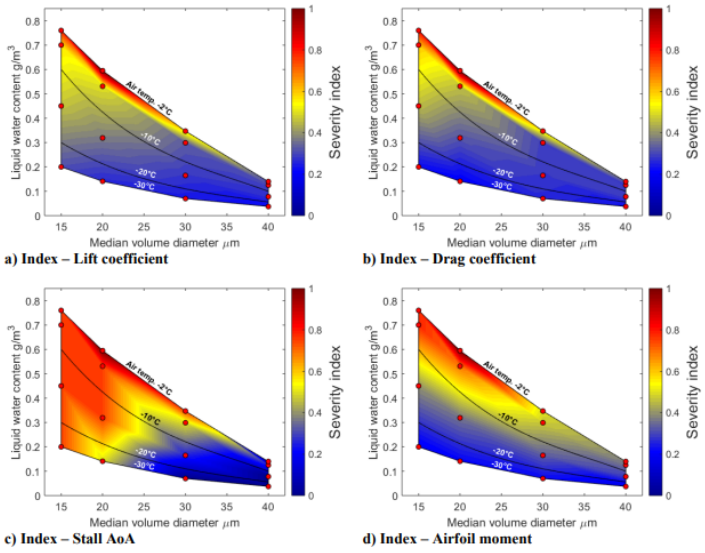

Figure 5.3: severity index of icing for various parameters for various temperature regimes [10]. 0 is no influence, 1 is severe influence

Considering the temperatures the aircraft will be exposed to and the severity index from Figure 5.3 the main problems with icing will only some into play below about 10km. This is also corroborated with the cloud altitudes[7].

5.2.2. Mitigations

In order to handle icing within the design, there are a series of options to mitigate the problem. First of, for the design of the wings and airfoil, a thin airfoil with increased camber seem to have a reducing effect on icing[11]. The effect of a thin airfoil is logical, as this would decrease the surface area available for accretion. In addition, consideration apply to the performance envelope[12]. Designing the airfoil right on the edge of allowable performance will make it less tolerant to disturbances of the flow due to icing. If possible, the design should be chosen such that even with degraded performance, the mission can still be completed. Second, part of it can be mitigated in mission planning. Selecting the conditions in which the vehicles can be used such that the icing risk it will have is allowable. This can already mitigate a lot of the risk. Further, the flight path planning can be adjusted such that major manoeuvres are performed above or around zones with increased icing risk. Such that the performance penalty is no longer of issue. Finally, an Icing Protection System (IPS) can be implemented. These come in various types and sizes. Anti-icing systems completely prevent the build-up of ice on the wing surface. De-icing systems allow some build-up, but will periodically clear the wing of ice. This could be done by for example embedding heating elements in the skin of the wing to melt the ice.

5.2.3. Final choices

Taking in to consideration the effects of icing, the following mitigation strategies have been taken. First in aerodynamic design the effect of icing will be considered for the foil selection. Second, an Icing Protection System will be integrated in to the vehicle. This will be elaborated upon in more detail in subsection 9.2.8. Finally, in flight path routing, most routing will be attempted before performance degradation due to icing becomes too severe. This all combined should lead to a robust system which can perform in normal icing conditions.

5.3. Airfoil selection

Selecting the correct airfoil is a critical part of designing an aircraft, or in this case, a glider. From the mission profile, the flight regime helps to determine the range of Reynolds number that the aircraft will encounter, however, the Reynolds number depends not only on atmospheric conditions but also on chord length and airspeed. The Reynolds number that the aircraft is flying at will determine the performance of the wing with respect to the lift, drag, and moment generated. In addition, from a structural aspect, a wing must have a sufficient thickness in order to incorporate systems such as flaps, fuel tanks, ailerons, and landing gear. And of course, the wing must sustain the forces it generates during the whole mission profile.

Starting with the systems that are traditionally located in the wing, Both BRAVO and BRAVO XL will have an external landing system and therefore, will not require landing gear nor a place to store it. Furthermore, both systems will be battery-powered, with the battery located in the fuselage. Finally, the system will not make use of any flaps, just ailerons, which will be controlled with servo motors, which can be located within the fuselage. The conclusion from this is that structural strength is the only consideration aside from flight performance, which will be touched on next.

One of the drivers when selecting an airfoil is flight performance. As the BRAVO family will reach altitudes of up to 33 km, and will remain below a Mach one, the first design challenge will be to fly at extremely low Reynolds numbers, from as low as 20,000 and up to 175,000. The typical regime for hobby aircraft is between 10^5 and 10^6, however, these vehicles never fly at such significant altitudes. Additionally, A high maximum lift coefficient is required during landings in order to have as low of a stall speed as possible.

From this short analysis, it is visible that the ideal choice of airfoil is something which is able to perform well in a broad range of Reynolds numbers, and can still produce sufficient lift at extremely low Reynolds numbers. From [13], one can see that the performance of an airfoil at low Reynolds number is highly dependent on how the airfoil controls flow separation. Furthermore, a curved plate outperforms conventional airfoils at Reynolds numbers as low as 40,000 as it is thin leading edge disturbs the flow

very little and is able to avoid laminar flow separation.

Comparing a number of airfoils, specifically, low thickness, high camber airfoils such as the Dillner 20-32-C [14] and cr001sm [15] airfoils along with the Drela Apex 16 [16] and NACA2412 [17] airfoils a consensus can be made. After performing a preliminary flight profile analysis using the first order sizing tool generated in section 4.4 a maximum required lift coefficient at altitude was determined to be no higher than 0.8 as can be seen in Figure 5.4. Also, here a C_L of zero can be seen for the initial phase where the glider is free falling. Besides the low lift coefficients, a high lift coefficient is still required at higher Reynolds numbers to ensure reasonable landing speeds.

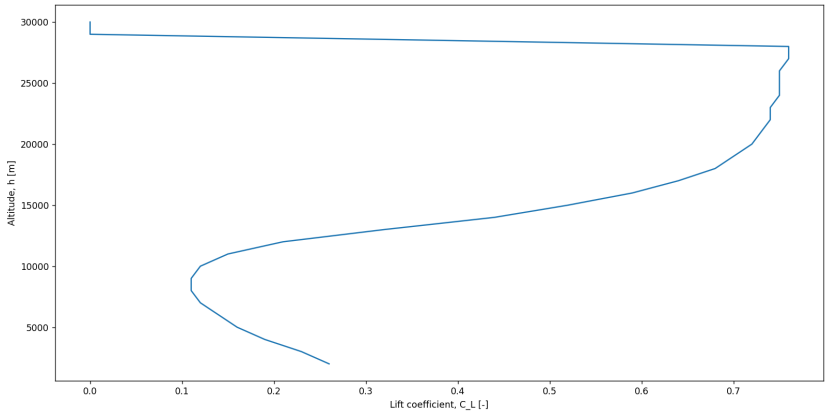

Figure 5.4: Altitude vs lift coefficient for the parameters: C_{D0} = 0.0336, AR = 12, e = 0.9 mass = .840 kg, S = 0.05 m^2 and a headwind of two standard deviations above average headwinds.

Looking at the Airfoil Tools data for all airfoils at a Reynolds number of 50,000 (the lowest that Airfoil Tools supports) the maximum 2d lift coefficient is approximately 1.2 for all the aforementioned airfoils. However, at lower Reynolds numbers it is likely that the thinner, higher-cambered airfoils will significantly outperform an airfoil such as the NACA2412. In addition, the Drela Apex 16 is designed for the transonic regime (Mach 0.8 to 1.2), and is not likely to perform optimally for these subsonic speeds.

Now looking at the polars for the selected airfoils at a Reynolds number of 100,000, the 20-32C airfoil and the cr001sm both have the highest lift coefficient at sim1.55 and sim1.4 respectively. This makes the 2032C airfoil, a thin highly cambered airfoil, the best choice for both low and high Reynolds numbers.

The horizontal and vertical tail also need an airfoil. For this, the choice was made to keep it simple and stick to a 0010 airfoil. This airfoil is commonly used on tail surfaces because of its symmetry. A cambered airfoil is not an option for the tail because it needs to work in both down force and lift equally

Now, for some final notes and remarks for this section. First, the effects of flying over a large range of Mach numbers from 0.1 to 0.47, where speeds of Mach 0.47 are achieved at minimum Reynolds numbers, these conditions will likely cause early flow separation and therefore a lower $C_{L_{max}}$. Exact numbers on this influence is however left as future work. The consequence of the lower Reynolds numbers are not expected to be too severe since the glider's C_L are not near the $C_{L_{max}}$ and a flight at lower lift coefficient is possible, however some range will be lost.

The Dillner 20-32C is not available in openVSP. It was therefore replicated with a four digit airfoil. The thickness to chord ratio, camber location and camber height. Figure 5.5 shows the 2 airfoils above each other.

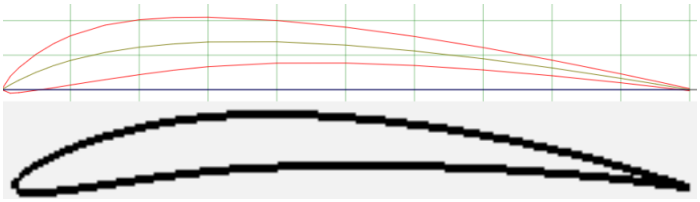

Figure 5.5: Comparison of Dillner 20-32C (on top) and the replica of it using a 4 digit airfoil (below).

5.4. General sizing

At the time at which the first iteration was performed, it was still uncertain whether multiple designs were necessary. The glider was therefore designed with a payload mass of 2kg in mind and expected to fulfil all missions that need to be carried out. It was therefore meant to get a better idea of the size and the challenges that lay ahead. The configuration was however chosen already at the time of starting the general sizing.

5.4.1. Preliminary sizing

To start the design process, the first-order weight and size estimation method was run to find the initial estimations of the glider. The report generated by the first-order sizing method is shown below. This estimation is done based on the inputs described in Table 5.1

```
#####################REPORT#####################
number of itterations required
for convergene: 5
total weight: 44.579 [N]
wing weight: 4.318 [N]
spar weight: 5.681 [N]
payload weight:  19.62 [N]
fuselage weight: 4.169 [N]
tail weight: 1.962 [N]
electronics weight: 8.83 [N]
surface area:  0.21 [m^2]
mean aerodynamic cord 0.145 [m]
root cord 0.181 [m]
span 1.448 [m]
landing speed: 20.433 [m/s]
####################END REPORT###################
```

Table 5.1: input data for the first order estimation

variable	input	unit
payload weight	2	kg
electronics weight	0.9	kg
density of foam	25	kgm^{-3}
taper ratio	0.6	-
maximum lift coefficient	1.1	-
maximum Mach number	0.6	-
Aspect Ratio	10	-
airfoil thickness	0.12	
fuselage volume	0.017	m^3

These sizes were then roughly modelled in OpenVSP and a new mass estimation of the fuselage was made in Excel. A new C_{D_0} value was found from the parasitic drag functionality in OpenVSP, run using landing conditions, which was then filled back into the initial sizing. This iteration was repeated a few times until an initial sizing was found. The 4 different iterations made in this initial sizing are shown in Figure 5.6 where the top-left model shows the first iteration and the bottom-left one shows the fourth iteration. As can be seen, the fuselage size pretty much stays constant, since that was limited by the payload size. The wing size did increase over the iterations though partly due to the higher total mass, but mostly due to the relative size of the fuselage compared to the wing getting smaller, thus decreasing C_{D_0}. The fourth version was done, right around the time the decision was made to split the design up in two versions, thus this concept was not developed further at this point. The final outputs from these iterations are used in the next section to obtain the parameters required for a range calculation.

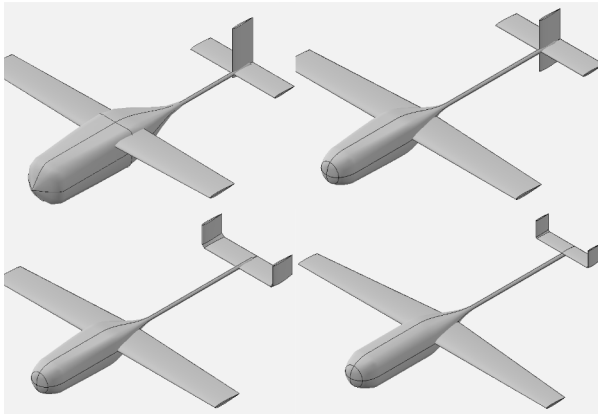

Figure 5.6: 3d models of the first four iterations, going from top-left to bottom-right.

5.4.2. Flight profile

Using the average wind speed data in the atmosphere, the optimized flight path through the atmosphere was modelled in Figure 5.7 for the fourth design using the method described in section 4.4. Furthermore, the range and the approximate descent time, given that the assumption that the vehicle is in full control at 27 kilometres altitude, resulted in the table presented in Table 5.2.

Table 5.2: first iteration results from range and descent calculations

condition	range [km]	descent time [hr]
No wind	408.0	2.2
0 SSD (average)	266.5	1.5
2 SSD (97.5%)	158.0	0.8
3 SSD (99.8%)	123.5	0.6

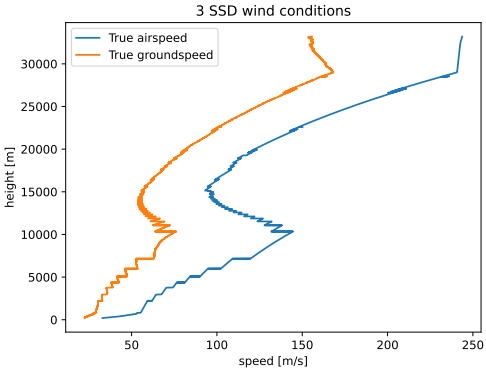

Figure 5.7: Height and speed plotted for the fourth iteration in 3 SSD wind conditions

5.4.3. Conclusion

From the first few iterations, it became clear that 2 gliders will be necessary to fulfil the mission for the lowest cost, as described in chapter 3. The reasons coming from this aerodynamic analysis are as follows. Firstly, having a single glider like this will result in a heavier glider than necessary, even for flights which only need a radiosonde. Secondly, decreasing the wing size while keeping the payload bay size will result in a high C_{D_0} and therefore decrease range too much. So for the next iterations, the two designs will be treated separately.

5.5. BRAVO Mini

With the first round of sizing done, it was realized that two different gliders will be necessary to achieve the full mission spectrum the system has to perform. The iteration this section will focus on is the one for a glider which is as light as possible while still being able to perform the same measurements as a radiosonde.

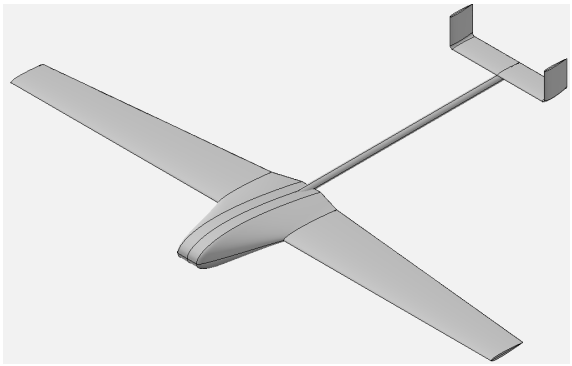

(a) Initial blended wing and fuselage design of BRAVO Mini

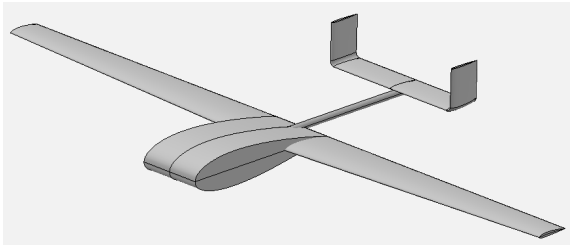

(b) BRAVO Mini iteration with separate lifting fuselage

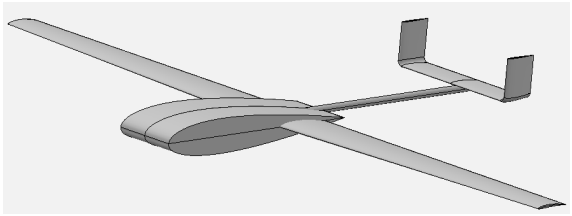

(c) BRAVO Mini iteration with longer fuselage

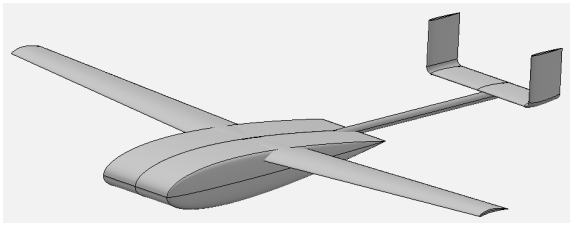

(d) BRAVO Mini iteration with smaller surface area

Figure 5.8: Versions 5 (top left), 8 (top right), 9 (bottom left) and 10 (bottom right) of the BRAVO Mini glider

5.5.1. Preliminary sizing

The initial weight estimation has to be done for the small glider as well, just like in section 5.4. Electronic masses were obtained from the payload and electronics subsystems together with their respective sizes, which were in turn used to size a rough foam box around them.

```
######################REPORT#####################
number of itterations required for convergene: 9
total weight: 18.671 [N]
wing weight: 4.34 [N]
spar weight: 0.748 [N]
payload weight:  1.961 [N]
fuselage weight: 1.4 [N]
tail weight: 1.01 [N]
electronics weight: 4.9 [N]
surface area:  0.0878 [m^2]
mean aerodynamic cord 0.077 [m]
root cord 0.096 [m]
span 1.148 [m]
landing speed: 20.433 [m/s]
####################END REPORT###################
```

5.5.2. Design process

The data from the preliminary sizing was used to start designing the initial iterations of BRAVO Mini. The choice was made to design a glider with a fuselage that would also be lifting. This fuselage would then also be blended with the wing at the wing roots to end up with a semi blended body configuration. The choice was made because compared to the large size of the first iteration, this plane will have a flexible, small payload size which would easily fit inside the lifting fuselage. The first iteration that resulted from this is shown in Figure 5.8a. The fuselage is sized to tightly fit the electronic modules designed by the electronics and power subsystem.

There are several problems with this configuration that would have to be investigated for further design work. The first one is the destabilizing effect of the fuselage creating lift in front of the main wing, therefore moving the aerodynamic centre and centre of pressure forward, necessitating more weight in the nose to balance the aircraft. The second one are the vortices coming from the fuselage wing blended section, interfering with the tail. The severity of this interference is hard to estimate, but it is something to keep in mind. Also, the blended nature of the wing and fuselage made estimations hard to do. It was unclear whether wing surface area was just the slender wings or also the fuselage contribution.

Additionally, if the fuselage section is included in the surface area, what is then its contribution to the total aspect ratio of the glider. Despite these uncertainties, the glider was iterated a couple of times, resulting in a lower surface area and therefore a bigger contribution of the fuselage blended section. The decision was made at this point to continue with a separate fuselage and wing, but still keep the fuselage in an airfoil shape to investigate the possible advantages further, see Figure 5.8b.

The surface area at this point still has not been changed from the initial sizing, so it was still sized for the stall Mach number requirement at altitude, S = 0.878. At this point in the design process, the ground system did not have a landing speed requirement yet and the net was thought to be able to handle high speeds, so this surface area was kept, durability of the airframe was a high priority though according to structures. Also, no specific airfoil was chosen yet at this point, but it became clear a decision had to be made soon.

With a clear separation between the fuselage and the wing, it was easier to weigh the contributions of the two lifting surfaces against each other. Using a lift analysis in OpenVSP, the fuselage was found to have a C_L of 0.3 when the wing had a C_L of 0.8. This correction factor was used to do estimate the aerodynamic centre location with a weighted average between the wing and fuselage. A location which is the datum point for the tail length, received from the Stability and Control subsystem.

After a more accurate internal layout planning, the fuselage was found to be too small to fit all components comfortably. Therefore, the decision was made to decrease the fuselage thickness to chord ratio from 0.2 to 0.15. The result of this design change and some other small changes can be seen in Figure 5.8c.

Looking at these past two iterations, the observation was made that the glider mass was significantly lower than anticipated. Preliminary sizing estimated 1.9 kg, but the new accurate mass estimation came to 0.879 kg. A new sizing had to be done to come to better surface area, for this the updated design method described in section 4.5 was implemented. The mass and surface area were now iteratively chosen to come to the best range. With this new approach, the realisation was made that a higher wing loading resulted in a higher range in high wind conditions, due to it then flying faster and being more able to penetrate the wind. The mass could not be increased because this would give the landing system and balloon system problems. Instead, the surface area was significantly reduced to 0.05 m^2.

Careful attention was given to the C_L values over the entire flight path to make sure the $C_{L,max}$ is never reached. The chosen airfoil, Dillner 20-32-C, has a $C_{l,max}$ of 1.55, which is adjusted to a 3d: $C_{L,max} = 1.55 \cdot 0.9 = 1.395$. The design never came close to this lift coefficient, so that was deemed not to be a problem. To avoid issues with speed of sound, a maximum Mach number was also set.

Finally, the aspect ratio of the wing was varied to determine its impact on range. However, it was found that changing the surface area had a considerably greater effect than varying the aspect ratio. Therefore, a high aspect ratio was not chosen to make the design more durable and lighter due to less covering material being needed for structures. Added to this is the change of Reynolds number with aspect ratio. A higher aspect ratio results in a smaller chord, further decreasing the Reynolds number, making the low Reynolds numbers more of a problem. For the same reason, the aspect ratio of the horizontal tail was lowered to AR=3. The resulting glider design of this iteration is shown below in Figure 5.8d.

Even though the design at this point had the right overall sizing, there were still adjustments to made to optimise it further. Firstly, an aerodynamic analysis showed that the lift contribution of the fuselage is pretty much negligible, as explained in the next section. Therefore, the sides of the fuselage were rounded, so reduce weight and reduce the severity of vortices around the sides of the fuselage. Also, it was investigated whether shortening the fuselage and increasing thickness to decrease wetted area was effective. A parasitic drag analysis showed the fuselage drag go from $C_{D_0} = 0.0113$ to $C_{D_0} = 0.01254$. Additionally, the internal components had less space to move around, which would cause problems later on with component integration. As a result, the thickness to chord ratio was kept at 0.2. The fuselage was however moved back to decrease the destabilizing effect of it, and balance calculations showed that having the battery in the nose will still allow the aircraft to balance on the AC.

The main improvement in this final iteration was the detailed stability analysis. OpenVSP was run in steady stability mode at zero angle of attack, and all stability coefficients are put out in a CSV file by

OpenVSP. Stability and Control then uses these value to check the scissor plots and all eigenmotions to check if the glider is stable and balancing in the right spot. Multiple changes to the wing position, tail length, and component location were made until the plane balanced at the right location and had a sufficient tail volume. In the first stability iteration, the glider had unstable spiral and the Dutch roll did not dampen out fast enough. The latter problem was solved by increasing the vertical stabilizer. The spiral instability was solved by increasing the dihedral to an angle of 8 degrees. The final aerodynamic design of BRAVO Mini is shown below in Figure 5.9 and the corresponding values of the main aerodynamic parameters in Table 5.3.

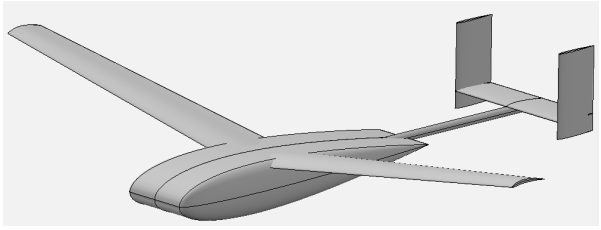

Figure 5.9: Final design of BRAVO Mini with stability design done

Table 5.3: Final aerodynamic design parameters for BRAVO Mini

Parameter	Value	Unit
Wingspan	0.7746	m
Surface area	0.05	m^2
Aspect ratio	12	-
Dihedral	8.0000	degrees
Fuselage chord	0.3667	m
Fuselage surface area	0.0275	m^2
Fuselage t/c	0.15	-
Taper ratio	0.6000	-
LE sweep	4.7636	degrees
Total mass	0.7527	kg
Stall speed	13.15	m/s

5.5.3. Control surface sizing

Besides the overall planform of the glider, the control surfaces also have to be designed to obtain enough control. The Stability and Control subsystem, described in chapter 6, needs a certain roll moment and pitch moment from the aerodynamics subsystem. In the interface of OpenVSP, the fraction of the chord and the position along the wing can be adjusted. The VLM analysis is then run with 15 degrees of deflection and the moments are read off from the interface. Iterating the sizes is a manual process, since OpenVSP does not have a function for giving the effect of a control surface for different sizes. The results of the sizing are given in Table 5.4, showing that the requirements from S&C are indeed met.

Table 5.4: Required control derivatives and control derivatives delivered from Aerodynamic design for BRAVO Mini.

Surface	Required [1/deg]	Max deflection 15 deg	Result [1/deg]
Elevator	$C_{z_{de}} = -0.0067$	$C_z = -0.1026$	$C_{z_{de}} = -0.00684$
Aileron	$C_{l_{da}} = -0.000995$	$C_{mx} = 0.01741$	$C_{l_{da}} = -0.00116$

Table 5.5: Control surface sizes for BRAVO Mini

Parameter	Value	Unit
start aileron from root	0.3099	m
end aileron from root	0.3680	m
aileron/local chord	0.25	-
end elevator from centre	0.0716	m
elevator/local chord	0.4	-

5.5.4. Final design analysis

During the design process, a C_{D_0} was obtained repeatedly to estimate the obtainable range. Table 5.6 lists the final influence of different components and the total C_{D0} in landing conditions. The landing condition C_{D0} is then extrapolated to a new C_{D_0} at a different altitude and velocity, as described in section 5.1 for the range calculation.

Table 5.6: Parasitic drag analysis for final BRAVO Mini (v=30, h=0)

Component Name	C_{D_0}	% Total
Tail tube	0.000612	2.147704
Main Wing	0.014059	49.35903
Horizontal	0.002779	9.758263
Fuselage	0.011033	38.735
total	0.028483	100

When estimating the Oswald efficiency with OpenVSP, an inaccurate result of e = 1.1 was returned. Since it is above 1, which is impossible, it is not usable for the range estimations. Therefore, a Oswald efficiency factor of 0.9 was kept for the final range calculation. The final range calculation can be found in the design summary chapter in section 13.1.

One other aspect to analyse of BRAVO Mini is the effectiveness of the lifting body. It was hoped that it would add some extra lift with a low penalty on extra drag, but the graphs in Figure 5.10 show this is not the case. The lift coefficient in yellow and induced drag coefficient in red are plotted both against angle of attack. The graph on the left shows the regular behaviour of the glider without the fuselage, with logical lift coefficient values. On the contrary, the fuselage on the right has lift coefficients of 0.02 at 6 degrees, which is negligible compared to the C_L of the rest of the aircraft of 1.25. From this, it can be concluded that the lifting fuselage does not add significantly to overall lift of the aircraft. It is not a big problem though, since the induced drag from the fuselage is also still low compared to the overall glider. Having a fuselage in the shape of a wing was advantageous for the VLM analysis, as it could be included in the stability analysis, as can be seen in Figure 5.11. Here, pressure distributions and wake lines are shown to check the analysis method. The fuselage wing shape is mostly purple in these images, meaning that the pressure difference produced is low compared to the main wing. Also, the right figure shows some vortices coming from the fuselage, indicating that the analysis indeed takes this into account.

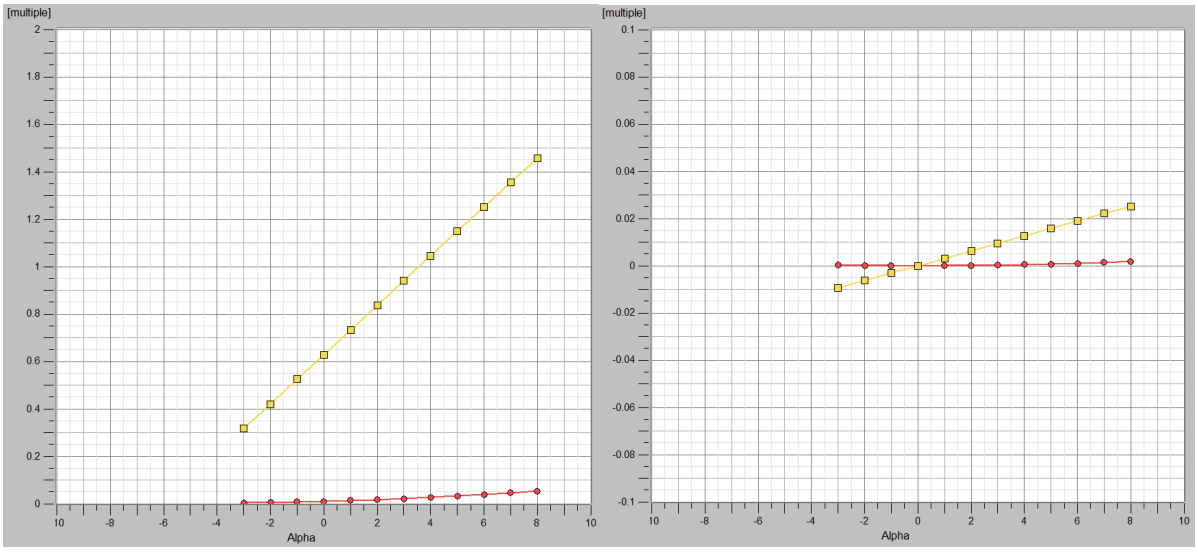

Figure 5.10: C_L and C_{Di} over alpha for BRAVO Mini without fuselage on the left and just the fuselage on the right.

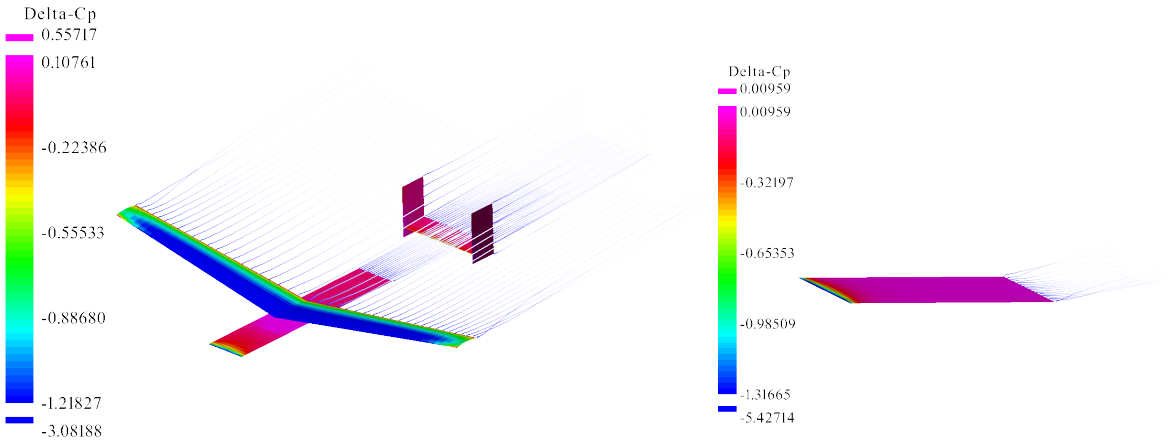

(a) VLM viewer for BRAVO Mini at an AOA of 4 degrees

(b) VLM viewer of the lifting fuselage at an AOA of 10 degrees

Figure 5.11: VLM viewer for BRAVO mini

5.6. BRAVO Max

BRAVO Max was designed after the Mini was designed, therefore most methods could be reused to make going thought the iteration process faster. There were still some differences though in the design philosophy which made this one different. Most importantly, the wing sizing did not use the preliminary sizing code, but instead jumped to the second order sizing method and used the range estimation code iteratively to obtain the optimal range. Therefore, this chapter will start off with describing the design process.

5.6.1. Design process

The design process started with setting up a mass estimation and balance method to get a mass estimate from a surface area. There was already a preliminary mass and surface area from the general sizing in section 5.4 which gave a starting point. By iterating the mass and surface area with the range estimation code, a surface area of 0.215 m^2 was found relatively quickly compared to BRAVO mini. One reason for this is the fact that most masses in BRAVO Max do not change with wing size, like the 2kg payload and electronics. The same aspect ratio was chosen as with Mini and kept at 12. Tests were again performed to see if an increase in aspect ratio would help with range, but the advantages were not enough to continue beyond 12.

The mayor challenge with BRAVO Max was the payload bay needing to be placed right below the centre of gravity to facilitate swapping of payloads without throwing the glider off balance. Initially, the CG could be assumed to be located below the aerodynamic centre for an initial wing position and tail length. The electronics were placed in front of the payload and an initial tail size was estimated by Stability & Control. Figure 5.12 shows the OpenVSP model of this iteration. The fuselage design is based around the payload size with 2cm of insulation around it, and aerodynamic shapes for the nose and tail cones.

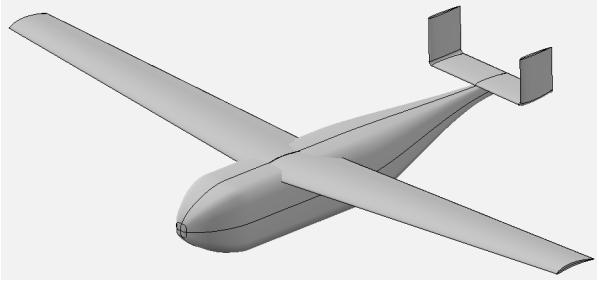

Figure 5.12: First iteration of BRAVO Max

The stability analysis was run using this model to see what needs to be changed to make it stable. From the stability analysis it was learned that the CG needs to be a certain distance behind the aerodynamic centre and the tail length had to be increased. This also caused the nose length to increase, since the weight of the tail had to be balanced out with the electronics in the nose. With these changes, multiple stability iterations were performed until a stable design was reached. This process was completely manual, so it took some time. The final design of BRAVO Max is shown in Figure 5.13 with the corresponding parameters in Table 5.7.

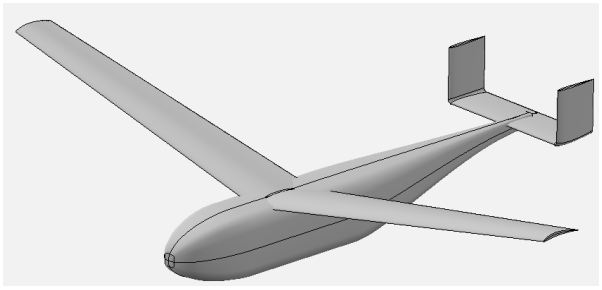

Figure 5.13: Final design of BRAVO Max with stability design done

Table 5.7: Final aerodynamic design parameters for BRAVO max

Parameter	Value	Unit
Wingspan	1.6062	m
Surface area	0.215	m^2
Aspect ratio	12	-
Dihedral	10	degrees
Taper ratio	0.6000	-
LE sweep	4.7636	degrees
Total mass	4.0212	kg
Stall speed	14.65	m/s

5.6.2. Control surface sizing

Just like with BRAVO Mini, BRAVO Max also has control surfaces to be sized. This was done in the exact same way. Table 5.8 shows that the control surface sizing requirements from stability and control are met, and the sizes are listed in Table 5.9.

Table 5.8: Required control derivatives and control derivatives delivered from Aerodynamic design for BRAVO Max.

Surface	Required [1/deg]	Max deflection 20 deg	Result [1/deg]
Elevator	$C_{z_{de}} = -0.00473$	$C_z = -0.1013$	$C_{z_{de}} = -0.00507$
Aileron	$C_{l_{da}} = -0.00211$	$C_{mx} = 0.04455$	$C_{l_{da}} = -0,00223$

Table 5.9: Control surface sizes for BRAVO Max

Parameter	Value	Unit
start aileron from root	0.5944	m
end aileron from root	0.7630	m
aileron/local chord	0.25	-
end elevator from centre	0.1244	m
elevator/local chord	0.4	-

5.6.3. Final design analysis

Just like with BRAVO Mini, BRAVO Max was also analysed with the parasitic drag calculation. The final results from this are listed in Table 5.10. It is notable that the C_{D_0} of BRAVO Max is lower compared to BRAVO Mini with 0.02562 compared to 0.02848. This can be explained by the fact the relative size of the fuselage compared to the wings is lower for BRAVO Max. Since C_{D_0} is relative to the surface area of the wings, it is smaller.

Table 5.10: Parasitic drag analysis for final BRAVO Max (v=30, h=0)

Component Name	C_{D_0}	% Total
Fuselage	0.007549	29.46384
Wing	0.013618	53.15395
Stabilizer	0.004453	17.3822
Total	0.02562	100

6
Stability & Control

The verification that an aircraft is both stable and controllable is not only vital for achieving mission completion, but also for safety of personnel and bystanders. During active control, the aircraft also needs to be able to perform all required manoeuvres for completing the mission while drawing minimal power to limit the required battery size. To accomplish these goals, the following steps are devised.

Firstly, an empennage layout is selected based on requirements and qualitative grounds in section 6.1. After this, historical data is gathered to give an initial estimate of the empennage dimensions in section 6.2. This is then given to the Aerodynamics department in order to obtain initial estimates for aerodynamic coefficients, which are then used as an input for a scissor plot shown in section 6.3. This results in more accurate sizing for the tail length and the tail area.

With these results, the Aerodynamics department performs a detailed analysis, obtaining the required coefficients for stability analysis. Here, stability in the required eigenmodes is tested in subsection 6.4.2 and section 6.5. Finally, once stability is demonstrated in section 6.6, the control surfaces are sized by observing which respective coefficients are required to attain the required manoeuvring rates. Finally, limitations of this method are discussed in section 6.7.

6.1. Empennage Selection

For the selection of an empennage, the options will be explored first. Hence, a diverging phase is started in subsection 6.1.1. Then, the options that are selected are put into a trade-off converging back to a final selection in subsection 6.1.2

6.1.1. Empennage options

Firstly, an empennage is selected. To make a selection, a list of possible layouts was compiled along with criteria, from which a ranking was made amongst the options. These options are listed below, along with their inherent properties[18] and with the decision to keep them for the ranking or not. Visualizations of the options are shown in Figure 6.1.

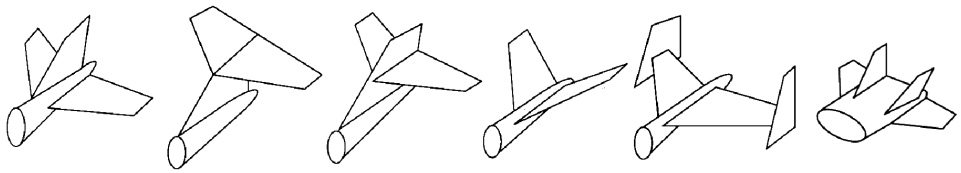

Figure 6.1: Options for the empennage[18]. From left to right: Conventional tail, T-tail, Cruciform tai, V-tail, H-tail. Twin vertical tail.

- Conventional tail: This configuration, together with the T-tail, is the most convenient layout for performing the functions of the empennage. All control surfaces are kept relatively close to the fuselage, which can help with maintaining low mass moments of inertia and keeping the required structural support in check. However, due to the positioning of the horizontal tail wake effects do occur, decreasing efficiency.
  Decision: Keep option for the ranking.
- T-tail: As mentioned in the conventional tail, this configuration has a straightforward performance

of all the functions of the tail. Furthermore, due to the fact that the horizontal tailplane is moved out of the main wing wake, efficiency of the horizontal tail is increased, resulting in a smaller tail planform. However, due to the horizontal tail position, the structure is heavier when compared to the conventional tail. Furthermore, the location of the horizontal tail opens up the possibility of a deep stall, which can be unrecoverable. As such, this configuration does not meet the requirement of being able to recover from any stall angle.
Decision: Do not keep option for the ranking.

- Cruciform tail: The cruciform tail attempts to alleviate the issues of the conventional and T-tail by moving the horizontal tail to the middle of the vertical tail. This relieves the structural load while keeping the vertical tail largely out of the wake of the main wing. However, this configuration does not fully alleviate the risk of deep stall, and as such does not meet the requirement of being able to recover from any stall angle.
  Decision: Do not keep option for the ranking.
- H-tail: The H-tail is a different approach to tail design where instead of the vertical tail being situated between the horizontal tail, it is split apart and moved to the tips of the horizontal tail. This makes it so that the vertical tail surfaces act as end-plates for the horizontal tail, which increases efficiency. A more mission-specific benefit is that the vertical tail span can be decreased, which is desired for the landing. The lateral control is also increased due to the shorter vertical tail span. However, the structural design is more complicated and the required support of the vertical tail increases the mass.
  Decision: Keep option for the ranking.
- V-tail: Although complicated to control due to the merging of the vertical and horizontal tail, the V-tail offers a reduction in drag. This is due to the reduction in total tail area. However, this does come at a cost of adverse roll/yaw coupling.
  Decision: Keep option for the ranking.
- Twin vertical tail: Similarly to the H-tail, this configuration splits up the vertical tail into two surfaces, which lowers the vertical tail span. However, due to the fact that the end of the empennage is slim, the vertical tails would have to be placed so close together that they would heavily interfere, and as such is not kept for the ranking.
  Decision: Do not keep option for the ranking.

6.1.2. Empennage ranking

The empennage configurations that were kept are then put into a ranking, where their qualitative performance is compared. For this comparison, the conventional tail is used as a baseline. The ranking is done based on a number of factors deemed important for either the mission or the ease of design. These factors are listed below.

- Vertical stabilizer size: When landing in a net, it is key to keep the aerodynamic surfaces as small as possible to minimize the risk of breakage. However, this factor also eases design struggles somewhat due to the lower mass moment of inertia it provides.
- Weight: As with any aircraft, minimization of mass is one of the most important design goals. Less weight means less required lift, which means a reduction in wing size and therefore less weight. Another aspect which increases the importance of this factor is that a lower mass might allow for a smaller lifting balloon, which reduces system cost.
- Structural efficiency: A better structural efficiency means that less structural support is required for the design. While related to weight, this factor was included separately due to the fact that the required structural supports are expected to be some of the most expensive parts of the tail.
- Aerodynamic efficiency: A greater aerodynamic efficiency is especially desired for this design as it implies a larger L/D ratio, which means a greater glide slope.
- Required fuselage size: A smaller required fuselage size has a number of advantages. Other than offering improvements in structural efficiency, weight and wetted area, it is also beneficial for ground operations due to less required effort for transporting, along with a reduction in cost and production difficulty.
- Stability (More is better): A more stable design is desired due to the fact that it automatically resists changes in attitude, which means it inherently resists destabilizing forces and moments, allowing for a less complex flight computer.

- Controllability: Controllability is an important aspect of the tail due to the fact that the aircraft needs to be able to quickly compensate for disturbances in flight, along with being able to perform all required manoeuvres for performing the mission.
- Redundancy: With the aircraft experiencing such a large range of temperatures, inherent redundancy of the design is desired. After all, being able to repair is preferred over having to replace.

The resultant ranking can be seen in Table 6.1.

Table 6.1: Empennage Ranking

	Conv.	**V-tail**	**H-tail**
Vertical stabilizer size	+/-	+/- Although the total surface area of the tail is reduced, the size of the vertical stabilizer tends to be the same due to also having to function as the horizontal stabilizer.	+ Due to the vertical stabilizer being split into two, the H-tail has a significantly smaller vertical stabilizer.
Weight	+/-	+ Since the V-tail requires a similar amount of reinforcement, there is a pure saving.	- The horizontal tail must support both vertical tails, which increases weight.
Structural efficiency	+/-	+/- V-tails tend to have comparable structural efficiencies to conventional tails.	- The horizontal tail must support both vertical tails, which decreases structural efficiency.
Aerodynamic efficiency	+/-	+ V-tails have an inherently lower drag due to the reduced wetted area.	+ H-tails benefit from end-plate effects, which increases aerodynamic efficiency.
Req. fuselage size	+/-	+/- V-tails require a similar fuselage size compared to conventional tails.	+ Due to the possibility of installing the tail on one or more booms, the fuselage can be made smaller.
Stability	+/-	- V-tails tend to have issues with maintaining longitudinal and directional stability.	+ H-tails tend to have a better resilience to turbulence, which is beneficial for stability.
Controllability	+/-	- V-tails tend to be more difficult to control due to the ruddervators.	+/- H-tails tend to have similar controllability to conventional tails.
Redundancy	+/-	- Due to the merged functionality, failure of a control surface means loss of multiple degrees of control.	+ Due to having multiple vertical stabilizer surfaces, failure of a rudder does not mean an automatic loss of control in yaw.
Result	**2nd**	**3rd**	**1st**

As is visible, the H-tail comes out as the best option. Therefore, from here on out the aircraft will be designed with an H-tail. This configuration will also serve as a basis for the initial sizing of the empennage.

6.2. Initial Empennage Sizing

As the concept of the aircraft is quite unique in the sense that it is balloon-launched to an extremely high altitude, after which it lands in a net, finding missions which are similar is difficult. Because of this, it is chosen to base the sizing of the empennage off of two different sources. Firstly, glider aircraft are used as a basis for the initial estimates of the $\frac{l_h}{c}$ ratio and the $\frac{S_h}{S}$ ratio, while H-tail aircraft are used for the initial sizing of AR_h and AR_v. For ease of calculation, all values obtained from statistical relations will be rounded to 1 significant figure. Furthermore, sweep of both the horizontal and vertical tail will not be considered. $\bar{c_v}$ will be set equal to $\bar{c_h}$.

Table 6.2: Historical glider data for the tail length-to-chord ratio and the horizontal tail area-to-main wing area ratio.[19]

Aircraft	l_h/c	S_h/S
Phoebus B1	4.87	0.12
LS 1c	3.53	0.15
ASW 15B	4.73	0.10
T49 Capstan	2.96	0.17
Mosquito	4.62	0.05
Average:	**4.14**	**0.12**

Table 6.3: Historical H-tail aircraft data for the aspect ratios of the horizontal and vertical tailplane.[20]

Aircraft	AR_h	AR_v
A-10 Thunderbolt II	2.70	1.05
Britten Sheriff	5.50	1.43
Shorts Skyvan Series 3M	3.70	2.16
Short 330	4.01	2.41
Bell XV-15	3.34	2.17
Average	**3.85**	**1.84**

From these datasets, an initial sizing was decided, which can be seen in Table 6.4.

Table 6.4: Initial parameters for the empennage sizing.

Parameter	l_h/c	S_h/S	AR_h	AR_v
Value	4	0.1	4	2
Allowed excursion	1	0.05	1	1

6.3. Scissor Plot

With the initial wing sizing performed, a more in-depth analysis was desired before moving on to stability analysis. For this, it was decided to generate a scissor plot in order to get a more accurate value for the tail length and the horizontal tail surface area. The scissor plot is generated in subsection 6.3.1 and the results are discussed in subsection 6.3.2.

6.3.1. Scissor plot generation

In order to generate said scissor plots for the BRAVO aircraft, the equations for generating the stability and controllability lines were used from [21] and [22]. Things to note are: In order to maintain stability, the $\bar{x}_{cg}$ should remain to the left of the stability line. Furthermore, the $\bar{x}_{cg}$ should remain to the right of the controllability line. an example of this can be seen in Figure 6.2a, where the stability line (orange) and controllability line (blue) are clearly visible.

To start off, $\frac{V_h}{V}$ and $\frac{d\epsilon}{d\alpha}$ were set to be equal to 0.95 and 0.725, respectively[19]. These values were updated during the design iterations in order to come t a minimum required tail area.

6.3.2. Scissor plot results

With all parameters now available, the scissor plots were generated and iterated. After obtaining a satisfactory solution, new tail sizing and tail lengths were provided to the Aerodynamics department for new analysis. Starting off, the scissor plots for BRAVO Mini are shown in Figure 6.2a and Figure 6.2b.

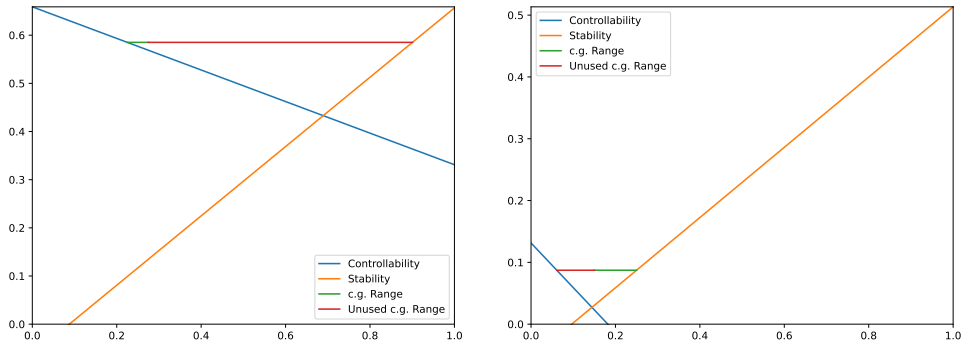

(a) Scissor plot of the initial design for BRAVO Mini

(b) Scissor plot of the final design for BRAVO Mini

Figure 6.2: Scissor plots of the first and final designs of BRAVO Mini

As is visible from the plot, there was an effective reduction in the minimum required relative tail size from 0.59 to 0.087. In the final iteration, AR_h was changed to 3 for structural reasons. It should be noted that a sizable improvement was still available, but it was chosen not to pursue this due to structural and aerodynamic reasons. The actual value of $\frac{S_h}{S}$ was set to 0.11, however. This was due to fears of the wake of the fuselage interfering with the vertical tail surfaces. $\frac{l_h}{c}$ was kept equal to 4. $\bar{x_{cg}}$ was moved to 0.200 while $\bar{x_{ac}}$ was positioned at 0.146.

After this, the scissor plots for BRAVO Max were generated. The scissor plots of the first and final iterations are visible in Figure 6.3a and Figure 6.3b, respectively.

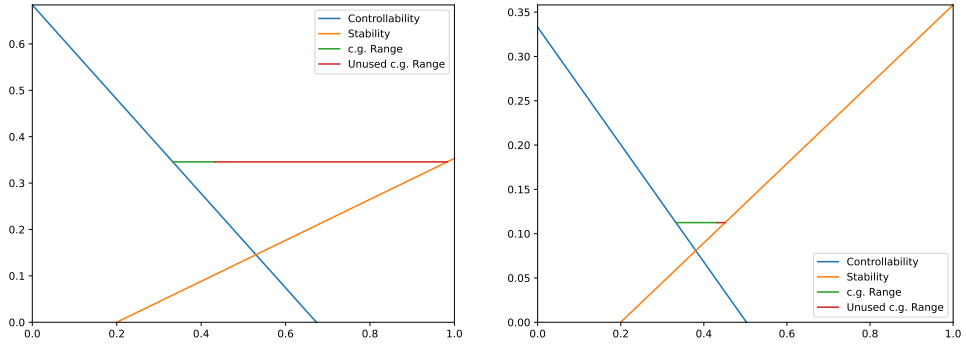

(a) Scissor plot of the initial design for BRAVO Max

(b) Scissor plot of the final design for BRAVO Max

Figure 6.3: Scissor plots of the first and final designs of BRAVO Max

For BRAVO Max, a sizable reduction in the minimum required relative tail size was achieved, namely from 0.34 to 0.11. Again, the aspect ratio of the horizontal tail was changed to 3 for structural reasons. The actual size of the horizontal tail was set to 0.15 for balance reasons. $\frac{l_h}{c}$ was set to 5. $\bar{x_{cg}}$ was moved to 0.383 while $\bar{x_{ac}}$ was positioned at 0.250.

6.4. Longitudinal Stability

To achieve a longitudinally stable aircraft, both static and dynamic longitudinal stability is required. While a dynamically stable aircraft is automatically statically stable, demonstrating this is more difficult and has a higher chance of containing errors, be it because of calculations or through uncertainty in simulation outputs. As such, both will be demonstrated independently, starting with static stability in subsection 6.4.1 and dynamic stability in subsection 6.4.2.

6.4.1. Static Stability

For achieving static stability, one of the most important design goals is to have an aircraft that resists a change in angle of attack. To achieve this, the aircraft must have a C_{m_α} which is less than zero. As

this can be obtained with relative ease from aerodynamic analysis, no heavy calculation is required.

6.4.2. Dynamic Stability

In order to demonstrate longitudinal dynamical stability, it must be shown that all longitudinal eigenmotions are stable. To ensure that all eigenmotions are stable, the real part of the eigenvalues must be less than 0. All of the necessary equations of motions including linearization and relevant assumptions, all of which are relevant for the flight profile of these gliders, can be found in [23].

$$\dot{\mathbf{x}} = \mathbf{A}\mathbf{x} + \mathbf{B}\mathbf{u} \tag{6.1}$$

It is important to note that in order to run numerical simulations using the provided equations, they must be transformed into state-space matrices in the form of Equation 6.1. This can be done by following the steps outlined in [23]. Using these relations, it is possible to simulate the short period and phugoid (long period) oscillations.

6.5. Lateral Stability

Similarly to longitudinal stability, it is required to have both dynamic and static lateral stability. Again, the demonstration of this will be done separately due to the increased chance of errors with dynamic stability, even though dynamic stability automatically implies static stability. In subsection 6.5.1, the lateral static stability will be discussed. In subsection 6.5.2, the dynamic stability will be discussed.

6.5.1. Static stability

In order to achieve static lateral stability, two design goals must be achieved. Firstly, it is desired that the aircraft will automatically want to cause a rolling moment that returns the aircraft to an even keel in the case of the appearance of sideslip. Furthermore, the aircraft must also want to reduce the sideslip angle down to 0. there C_{l_β} must be less than 0 and C_{n_β} must be more than 0[18]. These parameters are also obtained directly from aerodynamic analysis, no further attention is paid to obtaining them.

6.5.2. Dynamic stability

As was the case for longitudinal stability, dynamical stability is demonstrated through the observation of the eigenvalues, albeit of the linearized asymmetrical equations of motions in this case. These equations of motion can again be found in [23] and can be converted for numerical analysis in a similar fashion as subsection 6.4.2, using [23] as a guide.

Unlike longitudinal stability, three eigenmotions can be seen when analysing the lateral dynamic stability of an aircraft. These are namely, the aperiodic roll, Dutch roll, and aperiodic spiral.

6.6. Final Control and Stability Sizing

With all criteria established, the final sizing was performed. This was done by firstly implementing the more accurate tail size estimates as described in section 6.3, and then observing whether the eigenmotions are stable as described in section 6.4 and section 6.5. This was done for both BRAVO Mini in subsection 6.6.1 and BRAVO Max in subsection 6.6.2. After this, the control surfaces were sized by looking at what pitch or roll moment was required for the elevator and ailerons respectively in subsection 6.6.4. After review of the mission plan, it was determined that no manoeuvres or conditions required the use of rudders, and as such were not included in the design to reduce both the weight and the number of possible failure points.

6.6.1. BRAVO Mini stability sizing

For the sizing of BRAVO Mini, the initial concept was analyzed for static stability first. As discussed in subsection 6.4.1 and subsection 6.5.1, C_{m_α} and C_{l_β} must be less than 0, while C_{n_β} must be more than 0. As can be observed in Table 6.5, these requirements are met in the initial design. As such, there were no changes needed for the static stability.

Table 6.5: Static stability coefficients of the initial BRAVO Mini concept

Coefficient	C_{m_α}	C_{l_β}	C_{n_β}
Value	-0.736	-0.0912	0.108

With the static stability requirements met, the longitudinal dynamic stability was analysed. The resultant eigenvalues, as obtained via the procedure described in subsection 6.4.2 and subsection 6.5.2 are summarized in Table 6.6 along with their associated damping ratios.

Table 6.6: Eigenvalues and damping coefficients of the longitudinal and lateral eigenmotions of the initial BRAVO Mini concept.

Eigenmotion	**Eigenvalue**	**Damp. Ratio**	**Eigenmotion**	**Eigenvalue**	**Damp. Ratio**
Short Period	-3064	1	Aperiodic Roll	-24.6	1
	-12.4	1	Dutch Roll	-1.371+14.4j	0.0951
Phugoid	-0.0144+0.283j	0.05067		-1.371-14.4j	0.0951
	-0.0144-0.283j	0.05067	Spiral	0.0985	1

As is visible from the eigenvalues, both longitudinal eigenmotions are stable. An unexpected result here is that the short period oscillation has no imaginary component, and thus actually doesn't oscillate. As will be seen during later designs, this is a common issue and will be further discussed in section 6.7.

For the lateral eigenmotions, it is observed that this design has the issue of a divergent spiral eigenmotion. To counter this, a iteration process was started in which the minimal integer value of dihedral was found where this issue was countered. However, this had the negative effect of degrading the performance of the Dutch roll to such an extent that it became unstable itself. The vertical tail was therefore resized to bring this coupling back to acceptable levels.

The resultant design was double-checked for stability. Again, the static stability was verified first. The values of C_{m_α}, C_{l_β} and C_{n_β} are visible in Table 6.11.

As can be seen, all static stability coefficients still have the right sign assigned to them. There is no visible penalty observed, with all static stability coefficients experiencing an increase in magnitude, some even more than doubling. With static stability demonstrated, dynamic longitudinal and lateral stability was analysed. The resultant eigenvalues of the longitudinal and lateral eigenmotions are summarized in Table 6.7 along with their damping ratios.

Table 6.7: Eigenvalues and damping coefficients of the longitudinal and lateral eigenmotions of the finalized BRAVO Mini concept.

Eigenmotion	**Eigenvalue**	**Damp. Ratio**	**Eigenmotion**	**Eigenvalue**	**Damp. Ratio**
Short Period	-3924	1	Aperiodic Roll	-25.4	1
	-13.6	1	Dutch Roll	-2.81+20.4j	0.1367
Phugoid	-0.0157+0.313j	0.05018		-2.81-20.4j	0.1367
	-0.0157-0.313j	0.05018	Spiral	-0.0127	1

As visible, the stability of the longitudinal eigenmotions remain roughly similar to the original version. This corresponds to the low amount of impact that was expected due to the changes for the lateral stability. The short period oscillation became even more strongly negative, while the phugoid became more damped.

Comparing the finalized design to the initial one in terms of lateral stability, improvement are visible across the board. Most importantly, the spiral eigenmotion has been stabilized, while the Dutch roll obtained a higher damping ratio. The aperiodic roll became more stable as well.

6.6.2. BRAVO Max stability sizing

The sizing of BRAVO Max was done similarly to BRAVO Mini. Firstly, it was observed whether C_{m_α} and C_{l_β} were less than 0, and whether C_{n_β} was more than 0. As is visible in Table 6.8, these requirements are met in the initial design. As such, there were no changes needed for the static stability.

Table 6.8: Static stability coefficients of the initial BRAVO Max concept

Coefficient	C_{m_α}	C_{l_β}	C_{n_β}
Value	-1.32	-0.0498	0.0615

From the eigenvalues as displayed in Table 6.9, it is visible that the initial design of BRAVO Max has quite similar characteristics to the initial design of BRAVO Mini. Firstly and most critically, the spiral is unstable. The short period oscillation has the same characteristic of not oscillating, although it is fully stable. With the exception of the aperiodic spiral, all other eigenmotions are stable, although special attention should be paid during the iteration process to the phugoid as it appears to be edging on instability.

Table 6.9: Eigenvalues and damping coefficients of the longitudinal and lateral eigenmotions of the initial BRAVO Max concept.

Eigenmotion	**Eigenvalue**	**Damp. Ratio**	**Eigenmotion**	**Eigenvalue**	**Damp. Ratio**
Short Period	-623	1	Aperiodic Roll	-11.9	1
	-19.1	1	Dutch Roll	-0.313+4.86j	0.06439
Phugoid	-0.0138+0.102j	0.1333		-0.313-4.86j	0.06439
	-0.0138-0.102j	0.1333	Spiral	0.119	1

During the iteration process, the effect of dihedral on the Dutch roll appeared to be less severe than for BRAVO Mini, although it still degraded performance. As such, no resizing of the vertical tail was required. The resultant design was again checked first for static stability. The values of C_{m_α}, C_{l_β} and C_{n_β} are visible in Table 6.12. Again, all static stability coefficients still had the right sign assigned to them. Both C_{m_α} and C_{l_β} increased in magnitude and thus stability, while C_{n_β} slightly decreased.

After this, the dynamic stability was again analysed. Once again, the values of the eigenvalues and their damping ratios are shown in Table 6.10.

Table 6.10: Eigenvalues and damping coefficients of the longitudinal and lateral eigenmotions of the finalized BRAVO Max concept.

Eigenmotion	**Eigenvalue**	**Damp. Ratio**	**Eigenmotion**	**Eigenvalue**	**Damp. Ratio**
Short Period	-1348	1	Aperiodic Roll	-13.1	1
	-8.27	1	Dutch Roll	-0.101+6.76j	0.0149
Phugoid	-0.00956+0.197j	0.04854		-0.101-6.76j	0.0149
	-0.00956-0.197j	0.04854	Spiral	-0.0404	1

Comparing the dynamic stability of the finalized design to that of the initial one, a number of observations can be made. First and foremost, the spiral eigenmotion became stable, which was the primary purpose of the iteration process. However, this did come at the cost of the short period, phugoid and Dutch roll becoming less stable. However, due to the fact that this design does not need to keep comfort of flight in mind, this degradation of performance is accepted.

6.6.3. Final Aircraft Characteristics

After a number of iterations, the final values for the LTI system were calculated. In Table 6.11 and Table 6.12, the coefficients for the LTI system representations for both aircraft are summarized. These can be used for simulation, along with control surface sizing

Table 6.11: Stability and control parameters of the finalized BRAVO Mini concept.

V	=	30	$\frac{m}{s}$	m	=	0.75273	kg	b	=	0.7746
S	=	0.05	m^2	$\bar{c}$	=	0.06455	m	μ_c	=	190.387
$\bar{x_{cg}}$	=	0.19994		C_L	=	0.62602		μ_b	=	15.86558
K_X^2	=	0.01551		K_Y^2	=	0.0189		K_Z^2	=	0.02732
K_{XZ}	=	0		I_h	=	0.25820				
$C_{Z_{\dot{\alpha}}}$	=	-3.66174		C_{Z_u}	=	-0.0616		C_{m_q}	=	-46.3011
$C_{m_{\dot{\alpha}}}$	=	-15.4337		C_{Z_α}	=	-6.09275		$C_{X_{\delta e}}$	=	0
C_{X_u}	=	-0.00243		C_{X_0}	=	-0.04068		$C_{N_{\delta e}}$	=	0
C_{X_α}	=	0.49195		C_{Z_q}	=	-10.9852		$C_{Z_{\delta e}}$	=	-0.384
C_{X_q}	=	-0.23997		C_{m_u}	=	0.02024		$C_{m_{\delta e}}$	=	-1.536
C_{Z_0}	=	-0.62602		C_{m_α}	=	-1.09774				
$C_{Y_{\dot{\beta}}}$	=	0.61632		C_{l_p}	=	-0.61897		$C_{Y_{\delta r}}$	=	0
C_{Y_β}	=	-0.59881		C_{l_r}	=	0.20493		$C_{l_{\delta a}}$	=	-0.057
C_L	=	0.62602		C_{n_β}	=	0.22471		$C_{l_{\delta r}}$	=	0
C_{Y_p}	=	-0.26446		C_{n_p}	=	-0.04852		$C_{n_{\delta a}}$	=	0
C_{Y_r}	=	0.61632		C_{n_r}	=	-0.26435		$C_{n_{\delta r}}$	=	0
C_{l_β}	=	-0.18388		$C_{Y_{\delta a}}$	=	0				

Table 6.12: Stability and control parameters of the finalized BRAVO Max concept.

V	=	30	$\frac{m}{s}$	m	=	4.02119	kg	b	=	1.60624
S	=	0.215	m^2	$\bar{c}$	=	0.13385	m	μ_c	=	114.0646
$\bar{x_{cg}}$	=	0.38289		C_L	=	0.62016		μ_b	=	9.50539
K_X^2	=	0.02603		K_Y^2	=	0.03022		K_Z^2	=	0.0555
K_{XZ}	=	0		I_h	=	0.66927				
$C_{Z_{\dot{\alpha}}}$	=	-2.81191		C_{Z_u}	=	-0.06186		C_{m_q}	=	-31.5451
$C_{m_{\dot{\alpha}}}$	=	-10.515		C_{Z_α}	=	-5.29817		$C_{X_{\delta e}}$	=	0
C_{X_u}	=	-0.00231		C_{X_0}	=	-0.03141		$C_{N_{\delta e}}$	=	0
C_{X_α}	=	0.51316		C_{Z_q}	=	-8.43573		$C_{Z_{\delta e}}$	=	-0.271
C_{X_q}	=	-0.10352		C_{m_u}	=	0.00905		$C_{m_{\delta e}}$	=	-1.355
C_{Z_0}	=	-0.62016		C_{m_α}	=	-0.84841				
$C_{Y_{\dot{\beta}}}$	=	0.31196		C_{l_p}	=	-0.63809		$C_{Y_{\delta r}}$	=	0
C_{Y_β}	=	-0.42201		C_{l_r}	=	0.19495		$C_{l_{\delta a}}$	=	-0.121
C_L	=	0.62016		C_{n_β}	=	0.09847		$C_{l_{\delta r}}$	=	0
C_{Y_p}	=	-0.32337		C_{n_p}	=	-0.05404		$C_{n_{\delta a}}$	=	0
C_{Y_r}	=	0.31196		C_{n_r}	=	-0.09841		$C_{n_{\delta r}}$	=	0
C_{l_β}	=	-0.25878		$C_{Y_{\delta a}}$	=	0				

6.6.4. Control surface sizing

With static and dynamic stability demonstrated for both BRAVO Mini and BRAVO Max, the last remaining point is the sizing of the control surfaces. As previously mentioned, the decision was made to not include rudders into the design. As such, only the elevator and the ailerons required sizing.

The elevator will be placed on the horizontal tail surface to obtain the maximum moment arm, while the ailerons will be placed towards the trailing edge of the main wing tips in order to create the largest possible couple. This has the added benefit of being stall resistant, since it is strongly expected that the wing root will experience stall first and then travel out towards the tips[18]. This means that the ailerons will be last to experience stall, ensuring roll authority throughout the flight envelope.

The control surfaces were sized using two separate methods. The elevator was sized based on limit load conditions. Its coefficients were determined to meet the pitch rate needed to generate the highest load factor, multiplied by a safety factor, during all moments in the active control phase. The analysis showed that the highest pitch rate for required to attain this would occur just before landing, from which

an altitude of approximately 0 meters and a velocity of 30 meters per second was assumed. After this, the required pitch rate could be determined according to Equation 6.2. With both aircraft being designed with a maximum load factor of 2.5, a resultant q_{max} of $1.63\frac{rad}{s}$ is obtained when considering a safety factor of 2.

$$q_{max} = S.F.\frac{n_{max}g}{V} \tag{6.2}$$

For roll rate requirements it is more difficult to obtain requirements from the mission profile, as in the ideal mission no rolling takes place. As such, it was decided to make use of existing regulations for aircraft. As the most strict requirement obtainable for roll rate is a time-to-60-degree-bank of 1.3 seconds[18], this figure was used for the aileron sizing.

To gain insights into the requirements for the control surfaces, a state-space simulation was made for both aircraft in which the values $C_{Z_{\delta_e}}$ and $C_{l_{\delta_a}}$ were optimized to attain these requirements. $C_{m_{\delta_e}}$ was approximated by multiplying $C_{Z_{\delta_e}}$ by $\frac{l_h}{\bar{c}}$. The sizing results can be seen in Table 6.11 and Table 6.12. These coefficients were then sized for physically in subsection 5.5.3 and subsection 5.6.2. Furthermore, the overview of the stability and control derivatives of both aircraft can be seen in Table 6.11 and Table 6.12.

6.7. Limitations

This section addresses limitations in stability and control analyses, including assumptions and decisions made to address these issues. Firstly, mass moments of inertia were determined using a crude method, approximating all components as a cuboid for simplicity. However, the actual values will differ from these estimates, and the impact of this approximation is yet to be determined until a more accurate analysis is conducted.

Another issue with the analysis is the scale. Due to the low Reynold's number caused by the small chord, OpenVSP is operating in a region where it usually is not. Proper verification and validation of OpenVSP at low Reynold's numbers would need to occur to determine whether results are accurate.

Staying on the topic of OpenVSP, a major limitation is that VLM cannot analyze the fuselage effects on the stability and control derivatives. The $\dot{\alpha}$- and $\dot{\beta}$-derivatives were also unobtainable and had to be estimated using statistical relations with the pitch rate and yaw rate derivatives.

Last but not least, the lack of oscillations occurring during the short period eigenmotion for both aircraft. While the root of the issue cannot be attributed to a single coefficient, but instead by an interaction of multiple, it does suggest some inaccuracies in the analysis and would motivate the investment into more accurate simulations in the future.

7
Structures

Having an aircraft with perfect aerodynamics is useless if it breaks due to loads sustained during flight. It is therefore vital that the BRAVO Mini and Max gliders have a structure that is properly designed to withstand these loads. At the same time, the structure should also remain light in order to keep the total weight of the system low. A very challenging aspect of the structural design was the small scale; many traditional construction techniques used for full sized aircraft are hard or impossible to construct at the scale of millimetres and centimetres. This required the use of more unique structural designs for the components. This chapter is broken down into the four main parts, representing the main structural components of the gliders: The wings in section 7.1, then the empennage in section 7.2, the fuselage in section 7.3 and finally the tail boom in section 7.4. Per section, results for both BRAVO Mini and Max are separately presented.

7.1. Wing Design

Designing the wing structure of small wings brings a number of challenges and differences from wing structures on full sized aircraft. The complex structures used in full sized aircraft are difficult to scale down to wings with thicknesses measured in millimetres (the thickness at MAC for BRAVO Mini is $0.08 \cdot 64 = 5.12mm$). A more useful source of reference proved to be remote controlled hobby aircraft.

The simplest construction method used in these aircraft is to cut or mould a wing out of a polymer foam, like the example in Figure 7.1a. Various foams can be used, such as expanded polystyrene (EPS), or expanded polypropylene (EPP), which is stronger but more flexible than EPS. However, this construction style only works for very light aircraft, since they will deform a lot once the aircraft gets too heavy. This can be remedied by covering the foam with a stiff load carrying skin, like as shown in Figure 7.1b. This usually takes the form of strong woven fibre mat that is attached to the foam core with a resin, thus forming a composite skin. The foam core then does not contribute much to strength and stiffness, but it provides a mould to shape the skin, and prevents the skin from buckling and collapsing.

Composite spars can also be embedded in the foam to add additional stiffness if required, though this adds a lot of weight. When using spars, the foam core can also be entirely omitted. The composite skin is kept in shape by strategically placing the spars, see for instance Figure 7.1c. This construction method is the strongest, since it combines multiple spars with a strong composite skin, but is also the most complex and difficult to construct.

For both BRAVO Mini and BRAVO Max, the choice was made to use the foam core plus composite skin construction method. The primary reasons are that it is feasible to manufacture at the scales required and offers good strength and stiffness performance. For the BRAVO Max, a spar could be embedded if required, but the BRAVO Mini wing is too thin to do this. A schematic overview of the wing construction is given in Figure 7.7. The preliminary design of the wing will primarily entail selecting the materials for the core, skin and aileron, and then sizing the thickness of the composite skin.

7.1.1. Material selection

As explained in the previous subsection, the structure of the glider will consist of two main components: a low density (foam) core and a load-carrying composite skin. This leads to three material choices to be made: The type of polymer foam, the skin fibre reinforcement and the matrix.

The foam core primarily gives shape to the structural skin of the glider, but also acts as insulation for

(a) Example of foam wing construction. Source: circondo.com

(b) Example of foam core composite wing construction. Source: instructables.com

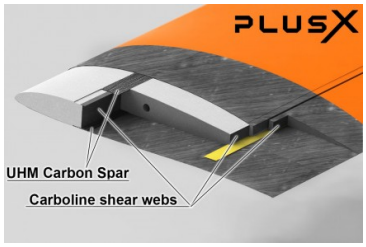

(c) Example of full composite wing construction. Src: Kennedy Composites

Figure 7.1: Various wing construction methods for small scale aircraft.

the payload within the fuselage. Two types were considered: expanded polystyrene (EPS), expanded polypropylene(EPP). EPS is a harder and more brittle type of foam, whereas EPP is more flexible and resilient. EPP foam was chosen because its properties make it less likely to break internally as the surrounding structure flexes. It also has great energy absorption, which is important during (crash) landings. In addition, it is much easier to recycle than EPS [24], which makes it a more sustainable option.

The properties of EPP can be adjusted by varying the density, which typically varies between 20 and 200 kg/m^3 [1]. Since the foam is less structural in nature, the main driving factors for selecting a specific density were insulation properties for the payload and workability during manufacturing. Based on these considerations, a density of 60 kg/m^3 was selected.

For the skin reinforcement, a number of materials were considered: Carbon, Aramid(e.g. Kevlar), E-Glass and Diolen fibre. Table 7.1 Shows a trade-off for these materials.

Table 7.1: Skin reinforcement material trade-off

Criteria	**Weight**	Carbon	Aramid	E-Glass	Diolen
Failure stress	3	5	3	4	1
Impact resistance	4	1	5	3	5
Stiffness	2	5	4	3	1
Cost	1	2	1	5	5
Sustainability	2	1	1	1	3
Total		33	40	37	36

Failure stress
The maximum failure stress is of high importance since a higher maximum stress allows for a thinner skin, reducing weight. Carbon fibres are the best in this regard, the pure fibres have a breaking strength up to 7 GPa [25], when embedded in a matrix this can yield strengths of a round 1 GPa (unidirectional) [26]. Glass fibres are not quite as strong, typically maxing out around 3GPa for the pure fibres. Aramid fibres have similar tensile strengths to glass fibres, but when embedded in a matrix, they tend to underperform in compressive strength [26]. Lastly, Diolen fibres perform much worse than the other fibre types in this regard.

Impact resistance
Impact resistance is a measure of how good a material can dissipate concentrated energetic impacts. This was given the highest weight of 4 since such impacts may occur frequently during landing. Aramid

[1] https://www.bpf.co.uk/plastipedia/polymers/Expanded_Polypropylene_EPP.aspx accessed on Tuesday 27th June, 2023

fibres are well known for their high impact resistance for their low weight; consider their frequent use in bullet-proof vests. For this reason, they score the highest. Diolen fibres are also excellent in this regard. fibreglass and especially carbon fibres are much more brittle, though, which is why they score lower[27].

Stiffness
Stiffness was considered to be less important than failure strength, since as will be seen later, the manner in which the wing is constructed makes it inherently quite stiff. This criterion was given a weight of 2. In general, stiffness scales close to proportionally with failure strength, so carbon fibre scores highest, whereas Diolen scores quite low [26].

Cost
Another factor to consider is the cost of the material. This was given a low weight since the size of the gliders is quite small, so in the end the material costs will be quite low in comparison to the labour costs as discussed in chapter 17. Carbon and aramid fibres are the most expensive types at around €20 per m^2 for both carbon [2] and aramid [3]. Glass fibres and Diolen are much less expensive, at around €5 per m^2 [4] [5].

Summing up the total scores shows that aramid fibres are the highest scoring option, though all options are quite close in score. The final choice was still to use the aramid fibres, primarily because of their high impact resistance, making the glider more resilient during landings and crashes.

Considering the small scale of the glider, a low mass per m^2 fabric is needed for the reinforcement. The lowest weight aramid fabric readily available is 60 g/m^2, such as [6]. This fabric has a dry thickness of about 0.1mm.

To complete the composite skin, a matrix is also required to provide support for the fibres. The matrix needs to be compatible with lamination construction. A number of different options were considered, such as polyester, vinyl ester and epoxy. Epoxy was chosen since it offers a good balance of strength and workability, bonds well to EPP and aramids, and can be obtained in partially plant-based form, making it a more sustainable option. One downside of epoxy is that it is susceptible to ultraviolet radiation, which the gliders will be exposed to quite heavily. For this reason, a coating, or covering is required to shield it, which can also be replaced over time to avoid degrading the epoxy resin. This covering also allows controlling the aerodynamic properties of the skin, regardless of the composite chosen. The wrap covering could be rougher or smoother, depending on what is more optimal for aerodynamics and icing.

7.1.2. Properties of selected materials

After having selected the exact materials to be used, detailed properties were collected on their engineering properties. For the foam, the main relevant property is the density, which was already selected at 60 kg/m^3 .

Reference data was used to estimate the material properties of the combined aramid/epoxy (AFRP) composite. Based on [28] and [26], properties were compiled in Table 7.2. When combining fibre directions, properties are averaged between directions, like shown in the bottom of Table 7.2. The ply thickness was determined using Equation 7.1. The area mass $\frac{m}{A}$ for aramid fibres is 60 g/m^2 as mentioned before, and using a matrix to fibre mass ratio of 55 to 45 gives an area mass of 71 g/m^2 for the epoxy. Together with their densities, this results in a ply thickness of 0.105 mm. These are very thin layers, since the fabric is so light.

$$t = \frac{m_{fib}}{A}\frac{1}{\rho_{fib}} + \frac{m_{epox}}{A}\frac{1}{\rho_{epox}} \tag{7.1}$$

[2] https://www.easycomposites.eu/200g-22-twill-3k-hexcel-primetex-carbon-fibre, accessed Tuesday 27th June, 2023
[3] https://www.easycomposites.eu/Kevlar-satin-175g-1m, accessed Tuesday 27th June, 2023
[4] https://www.easycomposites.eu/300g-plain-weave-diolen-cloth, accessed Tuesday 27th June, 2023
[5] https://www.easycomposites.eu/200g-22-twill-woven-glass-cloth, accessed Tuesday 27th June, 2023
[6] https://www.compositeshop.de/xoshop/lng/en/fibers/aramide-fiber/woven-aramide-fiber-fabric-61gm-plain.html accessed Tuesday 27th June, 2023

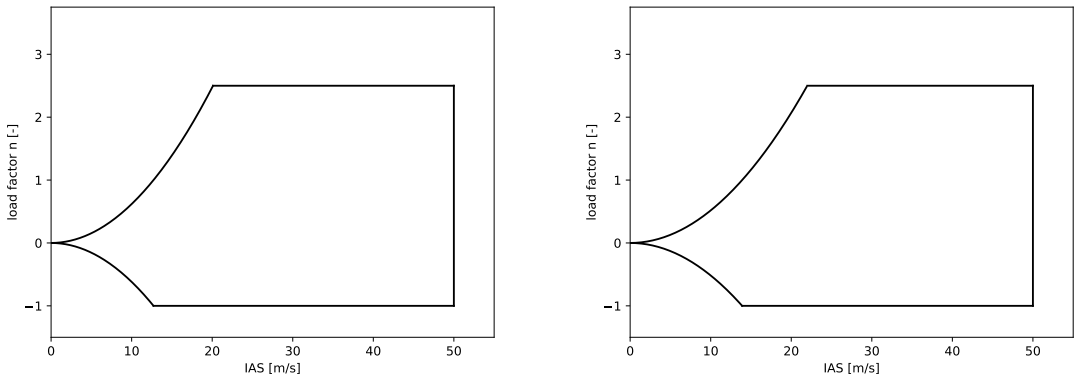

(a) Flight envelope for the BRAVO Mini glider

(b) Flight envelope for the BRAVO Max glider

Figure 7.2: Flight envelope for both BRAVO designs

7

Table 7.2: Material properties of the AFRP composite. Thickness and relative mass is given per layer.

Orientation	E[GPa]	G[GPa]	$\sigma_{ult,T}$[MPa]	$\sigma_{ult,C}$[MPa]	t[mm]	Rel. mass[kg/m^2]
0/90	30	5	480	190	0.105	0.129
$\pm$ 45	15	14	100	100	0.105	0.129
Comb. 0/90$\pm$45	22.5	9.5	290	145	0.52	0.258

For the covering above the structural skin, the weight was based off of 3M 1080 Cast vinyl wrap [8], which has a weight of 150g/m^2.

7.1.3. Load cases

For sizing the wing structure, two main load cases were identified. The first is flight under a load factor. The load factor is defined as the ratio of lift over weight, see Equation 7.2.

$$n = 1 + \frac{\Delta L}{W} = \frac{L}{W} \tag{7.2}$$

During steady level flight, lift, and weight are in equilibrium and thus the load factor is 1. However, when executing manoeuvres such as turning or levelling out of a high-speed dive, the lift can be higher or lower than the weight, thus resulting in a higher or lower load factor. For the design of both BRAVO Mini and BRAVO Max a maximum load factor of 2.5 was selected, which is common for transports under CS-23 [29]. This value was chosen since both designs are not expected to perform aerobatic manoeuvres, unlike for example competition gliders. The flight characteristics will be more similar to transport aircraft during flight. The flight envelope for both glider designs is shown in Figure 7.2.

The second load case considered is landing. As will be explained in section 12.2, the landing will make use of a net to catch the glider as it flies in near its stall speed, during which it will experience high G-forces as it decelerates. If the glider does not fly in perfectly straight, the wings may have to carry some deceleration loads. The exact dynamics of this are very hard to predict without complex simulations or real world experiments. Thus, for this initial analysis, a number of assumptions and simplifications have to be made in order to predict the forces experienced.

- The net is fine enough such that the nose of the glider cannot poke through. This ensures that the nose will always carry some forces. This puts a requirement on the sizing of the net.

[7] https://www.easycomposites.eu/LB2-epoxy-laminating-resinaccessed Tuesday 27th June, 2023

[8] https://multimedia.3m.com/mws/media/767410O/3m-scotchprint-car-wrap-film-series-1080.pdf accessed Tuesday 27th June, 2023

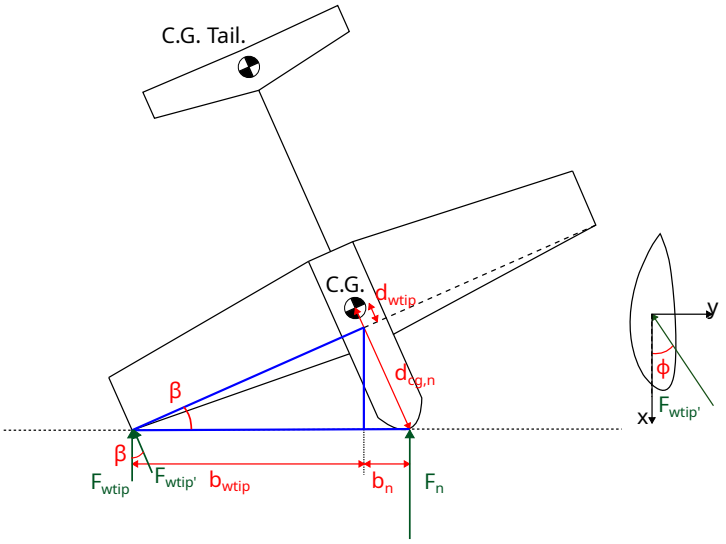

Figure 7.3: Schematic representation of forces on glider during landing

- The incidence angle ϕ is limited to $\pm 15°$. This limits the bending moment in the weak direction of the wing. The justification for this is that the guidance of the glider is expected to be accurate enough to ensure this angle.
- If the glider hits the net off-axis in the span-wise direction (angle β) and the wing tip strikes first, it will rotate until the nose also strikes the net, at which point it will start to decelerate. During the rotation, the forces are neglected.

The landing forces follow from deceleration experienced during landing in the net. This deceleration is about 9g, as determined in chapter 12. This then translates in to a force that depends on the gliders mass, as given by Equation 7.3. With some trigonometry, the force acting on the wing tip can be calculated, resulting in Equation 7.4. This force can then be broken down into forces in the coordinate frame of the wing section, F_x and F_y, as given by Equation 7.5 and Equation 7.6. Since F_y creates a moment in the weakest axis of the wing section, the limiting case is when the glider lands in the net at the maximum incidence angle.

$$F_{land} = ma_{land} \tag{7.3}$$

$$F_{wtip} = F_{land} \frac{b_n / b_{wtip}}{1 + b_n / b_{wtip}} \tag{7.4}$$

$$F_x = F_{wtip} \cos\beta \cos\phi \tag{7.5}$$

$$F_y = F_{wtip} \cos\beta \sin\phi \tag{7.6}$$

7.1.4. Methods

In order to perform structural analysis on the BRAVO Mini and Max wing, a small python toolkit was developed to perform stress and deflection analysis. This was then used to size the wing structure accordingly. The general analysis methods used in this toolkit are described below.

Stress analysis

There are two criteria used to size the wing structure: breaking strength and rigidity. The first to be investigated is breaking strength, which requires the determination of the maximum stress. This stress analysis is performed at the wing root, as this is where the highest stress typically occurs, which is also proven in Figure 7.6 and Figure 7.5.

The three stresses at the wing root are normal stress from bending moments, shear stress from torsional moments, and shear stress from shear forces. The shear stresses were ignored during this analysis, since initial calculations showed them to be much lower than the bending normal stresses (in the order of 5 MPa vs >100 MPa). To account for this simplification as well as others made during the analysis,

a safety factor of 1.2 was applied. The bending stresses can be determined using Equation 7.7, where M_x and M_y are the internal bending moments in the x and y direction respectively, x and y represent the location of the point to calculate the stress at, and I_{xx}, I_{yy} and I_{xy} are the sectional properties.

$$\sigma = \frac{M_x I_{yy} y}{I_{xx} I_{yy} - I_{xy}^2} + \frac{M_y I_{xx} x}{I_{yy} I_{xx} - I_{xy}^2} \tag{7.7}$$

The contribution of the foam core can be ignored, since its stiffness is negligible compared to that of the skin. Since the load carrying structure does not have a simple shape like a plate or a tube, determining the sectional properties requires some extra steps. The strategy chosen was to consider the wing skin as a discrete number of thin angled plates at an offset from the centroid of the shape. This situation is illustrated in Figure 7.4. The sectional properties of each individual plate can then be determined using Equation 7.8, Equation 7.9 for the area moments of inertia and Equation 7.10 for the product of inertia. The total properties of the section can then be simply found by summing up the properties of every i-th plate.

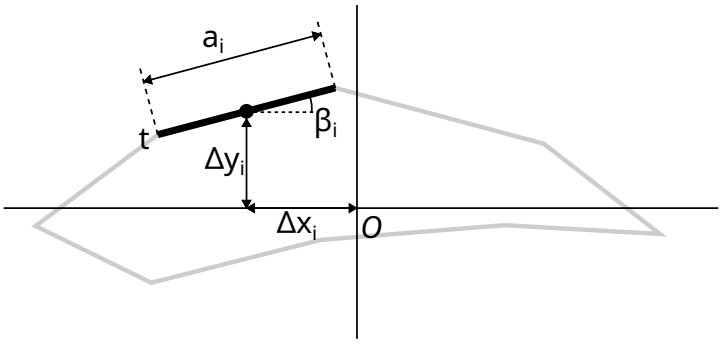

Figure 7.4: Calculating wing skin sectional properties

$$I_{xx} = \frac{a_i^3 t \sin^2 \beta_i}{12} + a_i t \Delta y_i^2 \tag{7.8}$$

$$I_{yy} = \frac{a_i^3 t \cos^2 \beta_i}{12} + a_i t \Delta x_i^2 \tag{7.9}$$

$$I_{xy} = \frac{a_i^3 t \sin 2\beta_i}{24} + a_i t \Delta x_i \Delta y_i \tag{7.10}$$

The perimeter points of the Dillner 20-32C wing profile were obtained from airfoiltools[9] and loaded into a python program which performed the area moment estimation method detailed above. After applying the moments, the point of maximum stress was found by simply calculating the stress for many points on the airfoil and selecting the (absolute) maximum value.

$$f_s \cdot \sigma_{max} < \sigma_y \tag{7.11}$$

Deformation

The total deformation of the wing must also be analysed, since even if nothing breaks, the structure could deform too much. Too much deformation can significantly reduce the aerodynamic efficiency of the wing, and can also lead to aeroelastic effects, where the interaction of the structural deformation and aerodynamic forces leads to strong oscillations that could destabilize the glider or cause a structural failure.

The two modes of deformation analysed are bending and twisting. For bending, the deformation is assumed to be primarily caused by the lift distribution over the wing, which acts in the most flexible axis of the wing section. The deformation of the wing in this direction was determined using the classic beam deformation formula, given by Equation 7.12. Here z denotes the length along the (half) wing, and the moment sectional properties must be determined as a function of z since the wing tapers. The resulting curvature $\frac{d^2v}{dz^2}$ can then be integrated twice to find the deflection v.

[9] http://airfoiltools.com/airfoil/details?airfoil=2032c-il, accessed on Tuesday 27th June, 2023

$$\frac{d^2v}{dz^2} = \frac{M_x(z)I_{yy}(z)}{E(I_{xx}(z)I_{yy}(z) - I_{xy}^2(z))} \tag{7.12}$$

To perform this integration, the geometry of the wing planform as well as the section geometry was loaded into a python program, where this section was scaled linearly with the taper of the wing while the skin thickness was kept constant. M_x was determined by doubly numerically integrating the elliptical lift distribution (at maximum load factor). The beam curvature was then also integrated twice to find the maximum deflection.

The wing twist was determined using Equation 7.13, which is valid for thin-walled closed sections, and a constant wall thickness t and shear modulus G along the section circumference s. For this equation the torque T needs to be found as a function of z as well. This was found by integrating the aerodynamic moment coefficient over the wing, and adding the hinge moment from the aileron. The twist rate $\frac{d\phi}{dz}$ can then be integrated to find the total twist. Just like for the deflection, this was done using a numerical integration in python.

$$\frac{d\phi}{dz} = \frac{T(z)s}{4A_{encl}^2(z)Gt} \tag{7.13}$$

7.1.5. Results

The analysis methods described above were combined into a python program that could determine skin thickness based on maximum allowable stresses induced by the loads encountered. In addition, maximum tip twist and deflection for the wings were also generated by the program. These results, along with other considerations, were then used to determine the thickness and lay-up of the skin material.

This was done for each iteration of the design, where wing shape and size were pre-determined by performance and aerodynamic analysis as described in chapter 5. The weight of the structure would then have an impact on the next iteration. The results of the wing structural analysis for both glider models, BRAVO Mini and Max, are presented below. The final geometries and weights, which were also used for the final iteration of the structural analysis, can be found in chapter 13

BRAVO Mini

Table 7.3 Summarizes the wing structural analysis results for BRAVO Mini, showing a limited set of inputs. The analysis also required the remaining geometry as input, which for the final iteration can be seen in chapter 13. The material properties (E, $\sigma_{ult,t}$ and $\sigma_{ult,c}$) come from the skin material and lay-up as described in subsection 7.1.1. Two safety factors were also applied. A safety factor of 1.5 was used to limit stresses away from the actual ultimate stress, which is common in the aerospace industry [30]. In addition, a safety factor of 1.2 was applied to account for the simplifications and assumptions made in the design tool, which was deemed appropriate.

Running these inputs through the design tool gave the results shown in the bottom half of Table 7.3. The minimum skin thickness required for the BRAVO Mini wing is 0.149 mm, where the limiting load case is flight under maximum load factor. Since the AFRP layers are 0.105 mm each, this requires an actual skin thickness of 0.21 mm. As described in subsection 7.1.1, For two layers the lay-up will be 1 layer of $90/0^\circ$ and 1 layer of $\pm 45^\circ$, where the second layer is less effective in tensile forces (which is already accounted for in the maximum compressive and tensile stresses) but is very effective in resisting torsion.

Figure 7.5 shows the wing deflection for the BRAVO Mini wing with the selected skin thickness, under maximum load factor. When taken over the entire wing half, the tip deflection is quite small, and most of the curvature is in the wing root. The tip, which is where the ailerons are located, remains quite flat. A stress heat map is plotted on the deflected beam, which shows that the maximum stress is at the root, as assumed.

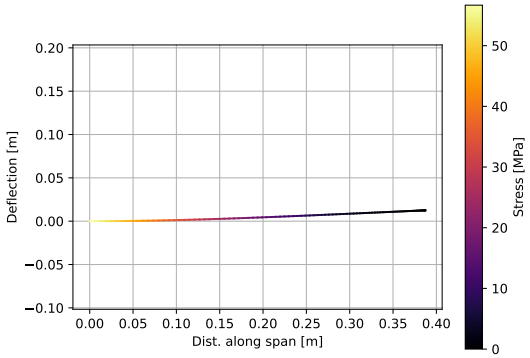

Figure 7.5: Bending diagram and stress heat map of BRAVO Mini wing.

Table 7.3: Structural analysis results for BRAVO Mini wing

Parameter	Value	Unit
n_{max}	2.5	-
a_{land}	9.2	g
f_s	$1.5 \cdot 1.2$	-
min. t_{skin}	0.149	mm
chosen t_{skin}	0.21	mm
σ_{max}	56.67	MPa
max tip deflection	12.53	mm
max tip twist	0.30	deg

BRAVO Max

Table 7.4 shows the analysis results for the larger BRAVO max. Since the flight profile is shared between the two models, many of the inputs remain the same, only the weight and geometry changes. The analysis showed that a skin thickness of 0.29 mm is required, where the limiting factor is also flight under maximum load factor. This leads to an actual skin thickness of 0.315 mm, with an AFRP lay-up of $90/0°$,$\pm 45°$, $90/0°$. Again, the 45 degree layer provides stiffness in the torsion direction, which the $90/0°$ does not have.

The wing deformation under maximum load factor is also plotted for the BRAVO Max wing in Figure 7.6. The tip deflection for the Max wing is also quite small when the proportions of the wing are taken into account.

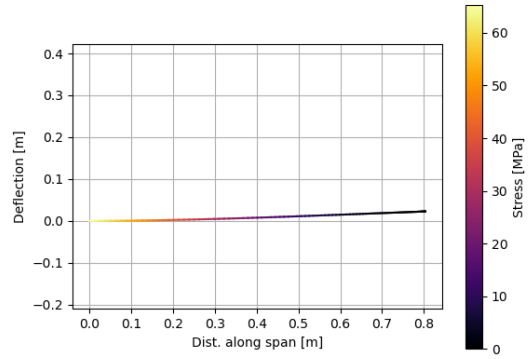

Figure 7.6: Bending diagram and stress heat map of BRAVO Max wing.

Table 7.4: Structural analysis results for BRAVO Max wing

Parameter	Value	Unit
n_{max}	2.5	-
a_{land}	9.2	g
f_s	$1.5 \cdot 1.2$	-
min. t_{skin}	0.29	mm
chosen t_{skin}	0.315	mm
σ_{max}	83	MPa
max tip deflection	38.1	mm
max tip twist	0.214	deg

To summarize the design of the wing, a schematic overview of the wing section is shown in Figure 7.7, along with some extra details. Note that this figure does not include any dimensions and applies for both BRAVO sizes. The wing is constructed out of a foam core with an aramid fibre composite laminated over it. This is then covered with a vinyl covering to protect the composite. Inside the wing are two channels: one to carry wires to power lights at the wing tip, and another to carry a push-pull rod to actuate the aileron. To prevent icing, the wing tip also incorporates a heater pad, which is placed under the composite layer. At the wing tips, the aileron is present. This is made out of a solid piece of composite, and attached with a separate flap of aramid fibre to act as the hinge. The ailerons are then actuated by the push-pull rod.

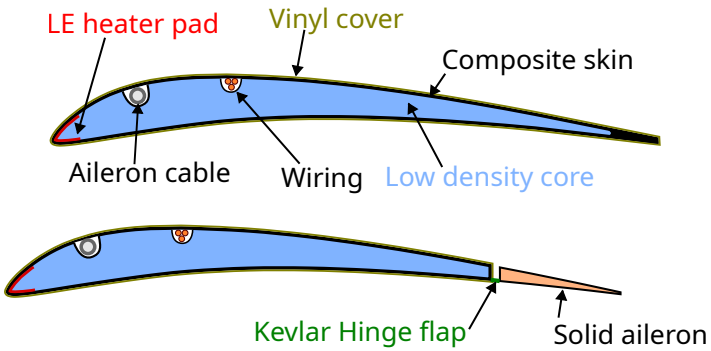

Figure 7.7: Structure of wing section

7.2. Empennage Design

In order to simplify the design, the construction method for the empennage was selected to be the same as for the wing. This thus entails a foam core covered by a hard skin, with the same materials as selected and described in subsection 7.1.1. To size the structure, the same method as used for the wing was modified to analyse the stresses and deformations in the tail.

7.2.1. Load cases

For the tail structure sizing, only the loads during maximum load factor flight were taken into account, since the tail cannot strike the net first during landing as the glider will dive in nose first.

To obtain the maximum lift for the tail surfaces, the total lift nW can be scaled by the respective surface area ratio, yielding Equation 7.14 and Equation 7.15 for the horizontal and vertical tail lift forces respectively.

$$L_h = nW\frac{S_h}{S} \tag{7.14}$$

$$L_v = nW\frac{S_v}{S} \tag{7.15}$$

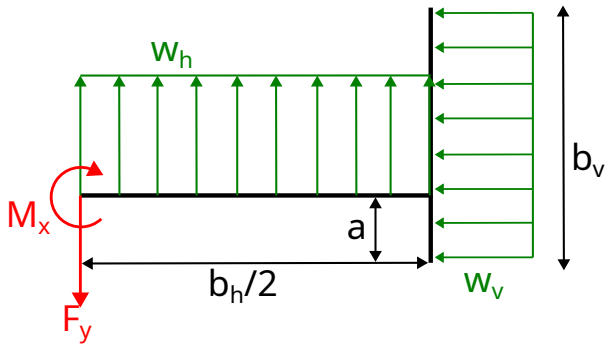

Figure 7.8: Free body diagram of forces acting on half tail structure

The distribution of forces over half of the tail is shown in Figure 7.8. During aerodynamic analysis, the lift forces over the tail surfaces turned out to be roughly uniform due to their low aspect ratio, so this distribution was used during further analysis. The critical point of analysis is once again at the root, where the moment M_x is not only the resultant of w_h but also the side force of the vertical tail, w_v which causes an extra moment depending on the offset of the tail a. In the worst case, these forces act in the direction as shown in the figure, in which case the largest moment is created at the root.

7.2.2. Results

BRAVO Mini The analysis results for the BRAVO Mini tail are presented in Table 7.5. Since the tail is much smaller in chord, the stresses are lower. Even though 1 layer of skin would be sufficient in theory, in practice this would require the fabric to be placed either in the 45 degree or 90 degree direction. This would lead to low stiffness in twisting or bending. Since the tail surface is so small compared to the rest of the glider, the weight penalty is comparatively small, and a stiffer tail reduces

the likelihood of aeroelastic effects occurring. Figure 7.9 shows that the tail is indeed very stiff with the current configuration.

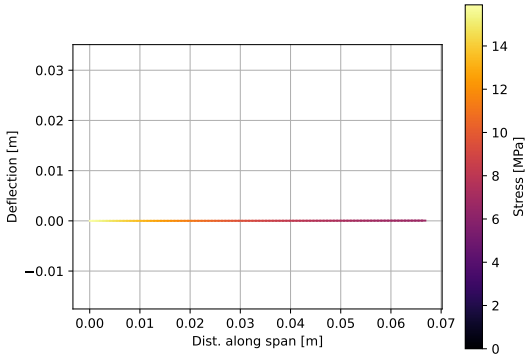

Figure 7.9: Bending diagram and stress heat map of BRAVO Mini horizontal tail.

Table 7.5: Structural analysis results for BRAVO Mini wing

Parameter	Value	Unit
n_{max}	2.5	-
a_{land}	9.2	g
Sh/S	0.112	-
f_s	$1.5 \cdot 1.2$	-
min. t_{skin}	0.05	mm
chosen t_{skin}	0.21	mm
σ_{max}	15.9	MPa
max tip deflection	0.05	mm

BRAVO Max

The results of the BRAVO Max tail analysis are shown in Table 7.6. Again the loads on the tail are much lower, but in this case two layers of AFRP are just barely required. giving a total of 0.21 mm. Though, for the same reasons as explained in the BRAVO Mini tail design, less than two layers would not have been ideal anyway. Figure Figure 7.10 also shows that the deflection for the horizontal tail of the BRAVO Max is quite small, which is good as the tail needs to be quite stiff to provide effective control authority.

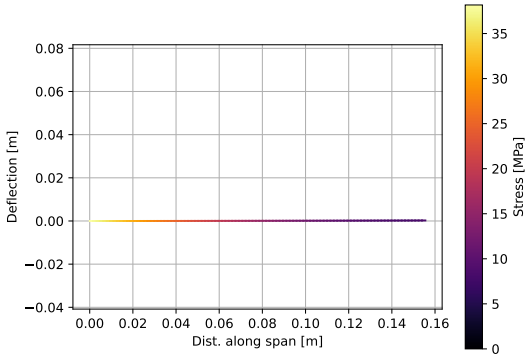

Figure 7.10: Bending diagram and stress heat map of BRAVO Max horizontal tail.

Table 7.6: Structural analysis results for BRAVO Max tail

Parameter	Value	Unit
n_{max}	2.5	-
a_{land}	9.2	g
Sh/S	0.15	-
f_s	$1.5 \cdot 1.2$	-
min. t_{skin}	0.11	mm
chosen t_{skin}	0.21	mm
σ_{max}	38.2	MPa
max tip deflection	0.24	mm

7.3. Fuselage Design

Now that a wing design has been chosen, the focus will shift to the fuselage design, for both the BRAVO Mini and the Max. To start, it was decided that the fuselage would be broken down into two pieces, one which houses the majority of the electronics, including the battery, flight computer, onboard sensors and configurable payload bay (in the case of BRAVO Max) and the other piece, which would serve as an attachment point for the wing and tail surfaces, as well as serving as an insulator for the electronics.

7.3.1. Electronics Slide

Due to the small dimension of the BRAVO Mini's and Max's fuselage design, access to the payload and electronics are at a premium. This means a clever design must be thought up in order to allow for sufficient access, whilst maintaining the structural and aerodynamic integrity of the aircraft. Furthermore, access in order to remove and calibrate the onboard sensors was essential as the crafts themselves are too large in order to fit in the required calibration chambers, more about this can be found in section 8.3. In conclusion, the decision was made to have the nose, of both the Max and Mini, removable. This would allow the delicate sensors to stay in place, protected in the nose duct. Furthermore, this makes payload modification easy, as the user will have access to all sides prior to sliding the nose and electronics back into place pre-flight. Another critical function of the electronics slide sub-structure is to support the vehicle during the ascent phase, as seen in Figure 7.11, for both the BRAVO Max and Mini, the release hook is attached directly to the sub-structure, therefore it must hold up the weight of the remaining aircraft. More about this release hook can be found in chapter 11.

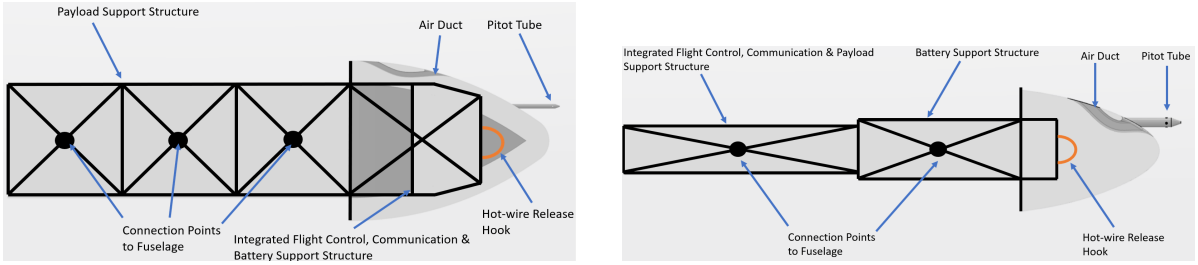

(a) Integrated structure for the payload and electronics slide BRAVO Max

(b) Integrated structure for the payload and electronics slide of BRAVO Mini

Figure 7.11: Integrated structure for the payload and electronics slide of the BRAVO family

Figure 7.11 shows the integrated truss structure which will support the payload, flight computer and battery, all while being fixed to the nose of the aircraft. This structure will then house connection points, which will have threaded holes for flat-head machine screws to pass through the body of the aircraft and screw into. This will securely hold the electronics slide to the remainder of the aircraft fuselage and will not disturb the surrounding airflow during flight. As the fuselage construction is made of foam with only a thin covering of AFRP. Plastic inserts will be glued into the foam of the fuselage where the screws pass through. Furthermore, nylon screws will be used in order to reduce the heat transfer between the outside and inside the fuselage. The structure itself can also be made of durable plastic, which will aid to keep the weight to a minimum.

The structure can be fixed to the nose of the aircraft via a number of different methods, glue being the simplest. However, damage to the nose would result in a write-off of the entire electronics slide. Furthermore, the replaceability of the temperature and humidity sensor along with the Pitot tube must be considered. For this, the top of the air duct, which can be seen in both Figure 7.11a and Figure 7.11b, shall be made of a durable, temperature-resistant plastic which can be fixed to the nose in a number of different ways.

A low-cost solution in order to solve the replaceability aspect of the nose design is to have the nose itself and the protective duct cover attached using hook and loop fastening. Solutions such as VELCRO® are suitable. This allows the user to easily remove and replace the sensors and/or the nose of the aircraft if either becomes damaged.

In order for these aforementioned components to be removable certain design decisions must be made, namely, the Pitot tube shall be attached directly to the electronics slide sub-structure, and the temperature and humidity sensors shall be fixed to the nose. Wire extensions will be added to the sensors to allow for them to be plugged into prior to sliding the nose over the Pitot tube and sub-structure, which will then be held in place with hook and loop to the vertical plate of the sub-structure. The top of the air duct can then also be attached with hook and look, completing this part of the fuselage.

During pre-launch assembly, the nose section can be passed over the string before fixing it to the release hook, then the nose can be slid into place and the assembly attached to the main fuselage.

7.3.2. Main Fuselage

Now that a design has been settled on for the electronics slide. The remainder of the fuselage can be designed, incorporating all the crucial components such as the wing, tail, and electronics into one aircraft. Furthermore, the Fuselage will house the servos which will be used to move the control surfaces during flight. Therefore, this part of the design was done in tandem with stability and control (chapter 6) as well as Electronics (chapter 9) in order to determine the required servo strength and by extension the size. Working with these other subsystems ensured that there was enough space inside the fuselage to house these components.

Starting with the overall fuselage design, similar construction to the wing was decided on as this would allow (in the case of BRAVO Mini) a homogeneous aircraft, with fewer interconnections and lower weight. As for BRAVO Max, a similar construction method was chosen. However, in its case the wings shall remain removable for transport, this is required as the wingspan is $\sim$ 1.6 m and the fuselage $\sim$1 m. Due to the relatively low weight of the solution, the loads acting through the fuselage will be quite minimal. The main wing will consist of a single piece, meaning all bending loads will be resolved within the wing section and the fuselage is simply required to support the mass of itself and its payload. Additionally, it must sustain the loads generated by the vertical and horizontal stabilizers, which are significantly less than that of the main wing. The largest load case will be during landing, at which point it must be sufficiently strong in order not crumple once it hits the net. Unfortunately, the exact force that it will need to sustain during this manoeuvre is difficult to know, as this depends on the mass distribution of the glider along with g-loading. The g-loading during landing was estimated in chapter 12. The team felt it was acceptable to move this analysis into future work and for the moment assume that a similar construction to the wing would suffice as a placeholder until a more in-depth analysis could begin.

As mentioned previously in section 7.1, the choice of low-density internal core will be EPP foam, which will provide insulation for the electronics, battery, and payload as well as provide some resilient structure for landing. This will be covered with a single layer of AFRP which will carry the majority of the loads, all while providing the impact resistance required for a highly reusable glider. Again, epoxy resin will serve as the matrix for this composite. The thickness of the foam was determined in collaboration with the electronics team as well as the aerodynamics team, as this would directly affect both the battery size and the drag. Therefore, a balance was struck at 15 mm.

Now that a general design has been made for the fuselage construction, it is time to move on to servo placement. Due to the low thickness of the wing cross-section, there is no possibility to mount the servo motors within the wing itself. An alternative would be to mount fairings in order to cover the servos in a more aerodynamic shape however this is not optimal, furthermore, it increases the mass moment of inertia, which in turn requires larger control surfaces and larger servos, turning the process into a runaway snowball. Several other options were considered, the first being wing pods mounted at the wing tips, but this presents the same problem as the fairing-covered servos. Both of these options would also result in a lower lift-to-drag ratio. Having the control surfaces extend all the way to where the wing meets the fuselage would allow the servos to be placed within the fuselage, exposing only their control horns to the airflow. Unfortunately, this poses several control issues, the first of which relating to control during stall. More detail about why the control surfaces cannot be placed near the wing root can be found in chapter 6.

This left one option. to locate the servos remotely in the fuselage and have some sort of linkage system to transfer the forces from the servos to the control surfaces. This in general is not such a difficult task, as there is usually sufficient space within the wing to mount such linkages. However, for both BRAVO Max and Mini, space is at a premium. Because of this, it was determined that a push/pull rod would ultimately be the best solution, embedding the servos on either side of the fuselage. The large advantage of push/pull rods is that they are low profile, low maintenance and bendable. All things that will be absolutely necessary for the BRAVO aircraft. They will have to make a 90-degree turn in order to attach to a control horn located in the middle of the ailerons, close to the point of rotation. The biggest disadvantage that comes with this system is the added friction, and by extension, a lower efficiency. This can be minimized by using low-friction materials for the housing of the rod, such as PTFE tubing. Figure 7.12 and Figure 7.14 shows how this configuration might look in the aircraft. Note that the main servo body (in black) is to scale with the aircraft, however, the linkage, consisting of the control horns (in white), the housing (in light blue) and the rod (in dark blue) are not sized.

This system will have to be installed during assembly, prior to the wing skin being applied, furthermore, for BRAVO Max, as the wings must be removable, so too must the servos. Therefore, the servos shall be mounted to the bottom of the wing section (only for BRAVO Max) and

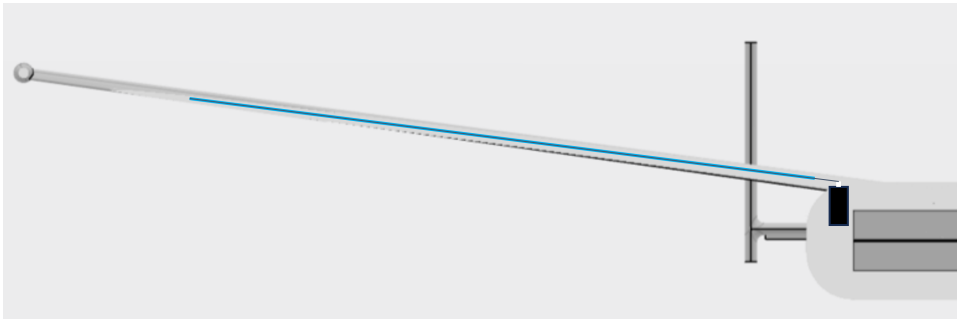

(a) Aileron control servo placement for BRAVO Mini

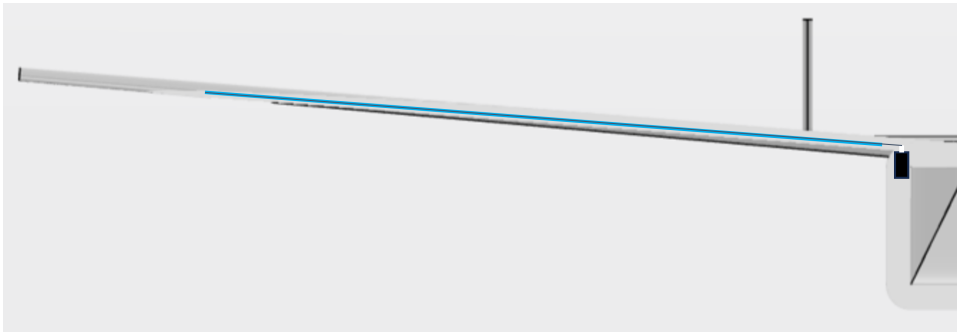

(b) Aileron control servo placement for BRAVO Max

Figure 7.12: Aileron control servo placement for the BRAVO family (servos, in black, are to scale, control arms, in white, and push/pull rod and sheath, in dark and light blue, are subject to change)

For the elevator, packaging was less of a challenge. Although for BRAVO Mini, the space was still limited, furthermore, the required control force for the elevator led to the need for a larger more powerful servo than what was necessary for the ailerons. As for the connection between control surface and servo, this will be handled by a stiff push/pull rod. The path from servo to control surface is almost a straight shot and allows for such a simple mechanism to be employed. For BRAVO Mini, the push/pull rod will pass through the tail boom, as seen in Figure 7.13a, again allowing the servo to be placed in the main fuselage body. The elevator servo placement for both gliders can be seen in Figure 7.13 and Figure 7.14.

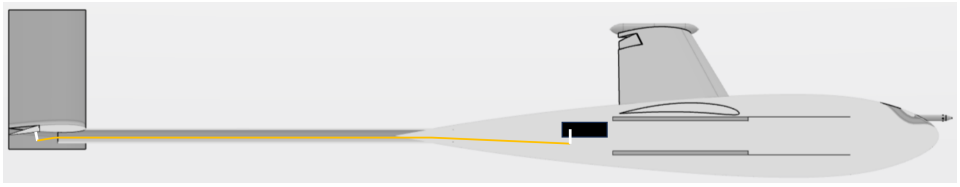

(a) Elevator control servo placement for BRAVO Mini

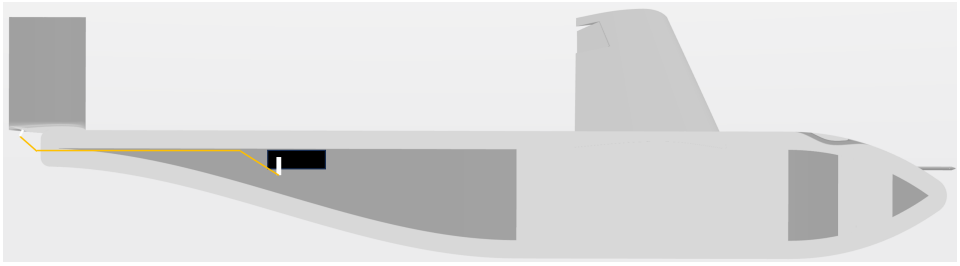

(b) Elevator control servo placement for BRAVO Max

Figure 7.13: Elevator control servo placement for the BRAVO family (servos, in black, are to scale, control arms, in white, and push/pull rods, in yellow, are subject to change)

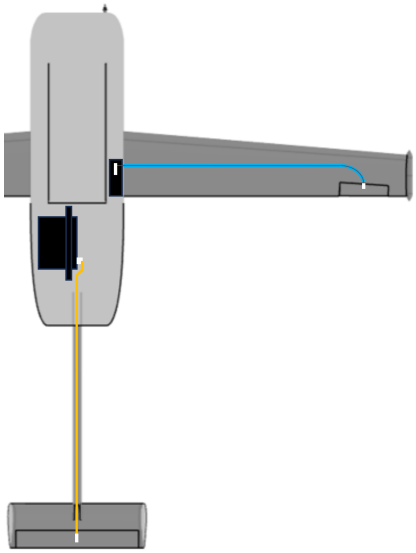

(a) Aileron and Elevator control servo placement for BRAVO Mini

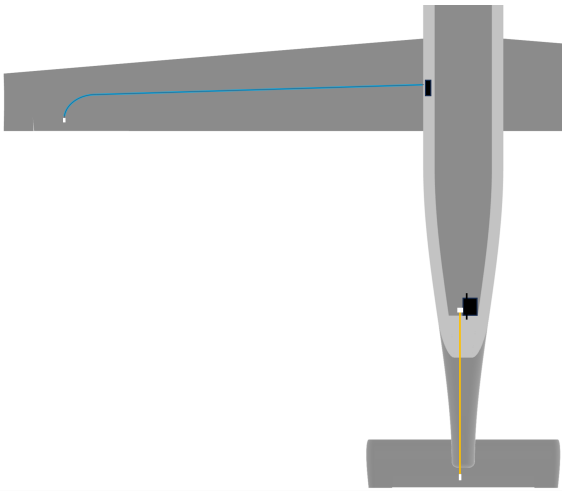

(b) Aileron and Elevator servo placement for BRAVO Max

Figure 7.14: Aileron and Elevator servo placement for the BRAVO family (servos, in black, are to scale, control arms, in white, push/pull rods, in yellow, and push/pull rod and sheath, in dark and light blue, are subject to change)

7.4. Tail boom design

In this section, the design of the boom connecting the empennage structure to the fuselage is explained for both BRAVO Mini and BRAVO Max. subsection 7.4.1 presents the trade-off which determines the choice of material for the boom. After this, subsection 7.4.2 discusses the method used to find the optimal cross-section of the boom.

7.4.1. Tail boom material trade-off

To choose the material for the tail boom, a trade-off is performed considering various materials used in gliders. The criteria are explained below in Table 7.7.

Table 7.7: Table showing the trade-off for the tail boom material

Criteria	**Weight**	CFRP	GFRP	AFRP	Aluminium	Balsa wood
Density	5	3	3	3	1	5
Mechanical properties	5	5	3	3	4	1
Cost	1	2	1	1	3	4
Sustainability	2	1	1	1	3	4
Total		44	33	33	34	42

Density

Density has the highest weight attainable. As with any aircraft design, weight minimization is high on the agenda. In this project especially, since the size of the balloon necessary to lift a certain glider to the required altitude, and thus the price, increases rapidly with the payload mass.

Balsa wood clearly scores the best in this category. It has a density of around 150 [kg/m^3][31]. This is a lot lower than the composites, which have densities in the range of 1400-1900 [kg/m^3][32]. Lastly, Aluminium has a density of about 2800 [kg/m^3] [33] and scores poorly.

Mechanical properties

Stiffness and strength is weighed just high as density. These parameters determine the required cross-section of the boom to withstand the loads. For this criterion, the E-modulus, G-modulus and yield or ultimate strength of the materials were taken into account.

In this criterion, CFRP outscores the other materials by far. It has an E-modulus of 175 [GPa] and a UTS of 1000 [MPa]. The other composites follow with similar strength, but lower E-modulus of 40 [GPa] for GFRP and 75 [GPa] for AFRP. One important note is that these are the unidirectional properties, so these properties are significantly lower in a non-unidirectional tube. Aluminium alloys have similar mechanical properties, but it is unidirectional and therefore scores slightly higher and balsa wood are a lot lower with 10.4 [GPa] and 3.71 [GPa] respectively.

Cost

The lowest weighed criterion is cost. The low weight is due to the small contribution this part has to the overall costs. The composites score low in this category since they require a lot of resources to manufacture. Meanwhile, Aluminium and especially balsa wood are readily available for lower prices.

Sustainability

The last criterion is sustainability. This takes into account the resources materials require and the end-of-life emissions of the materials. Again, the composites score poorly since they require a lot of resources and are arduous to recycle. Aluminium scores better because it is more commonly recycled, although the alloys used in aviation also put up challenges for that. Lastly, balsa wood is theoretically carbon-neutral, although the sustainability of the source of the wood is often a concern.

Looking at Table 7.7. The winner is CFRP. This is a logical result, since it is the most common material in this application. Balsa wood scores quite close to it. But it mainly excels in the lower weighted criteria. Therefore, CFRP is deemed the best option.

7.4.2. Tail boom sizing

The boom connecting the tail to the fuselage has to be sized for bending and torsion due to wing loading. The bending moment, shear force and torsion moment are calculated using Equation 7.16, Equation 7.17 and Equation 7.18.

$$M_x = nW\frac{S_h}{S} \cdot l_{tail} \quad (7.16) \qquad V_y = (n - 1 - n\frac{S_h}{S})W \quad (7.17)$$

$$T_z = nW(L_{centre} + L_{centre_{tail}}\frac{S_h}{S}) \quad (7.18)$$

All of these loads are the maximum internal load, which occurs at the root, the connection of the boom to the fuselage. The tail boom will be a hollow tube with radius r and thickness t. A range of radii of 0.001 [m] to 0.01 [m] and a range of thicknesses of 0.0005 [m] to 0.01 [m] is considered. For every resulting section, the moment of inertia, polar moment of inertia and cross-sectional area are computed using Equation 7.19, Equation 7.20 and Equation 7.21.

$$I_{xx} = \frac{\pi r^4}{4} - \frac{\pi(r-t)^4}{4} \quad (7.19) \qquad J = \frac{\pi r^4}{2} - \frac{\pi(r-t)^4}{2} \quad (7.20)$$

$$A = \pi(r^2 - (r-t)^2) \quad (7.21)$$

These are then used to obtain the maximum internal bending and shear stresses with Equation 7.22 and Equation 7.23.

$$\sigma_x = \frac{M_x r}{I_{xx}} \quad (7.22) \qquad \tau = \frac{T_z r}{J} - \frac{V_y}{I_{xx}} \cdot 2\pi r^3 sin(\frac{1}{4 * r}) \quad (7.23)$$

Additionally, the maximum twist angle and vertical deformation at the aft tip are computed using Equation 7.24 and Equation 7.25.

$$\theta = \frac{T_z}{GJ} \cdot l_{tail} \quad (7.24) \qquad \delta = \frac{M_x {l_{tail}}^2}{3EI_{xx}} \quad (7.25)$$

These values are then compared to the maximum allowable values to find the minimum viable cross-section. For the stresses, this is based on the ultimate tensile strength (UTS) and ultimate shear strength (USS) of the CFRP to be used. The deflections are compared to maximum allowable deflections. The maximum values can be found in Table 7.8.

Table 7.8: Table listing the maximum allowable values used for sizing the tail boom cross-section

Parameter	Value	Unit
CFRP UTS	110	MPa
CFRP USS	260	MPa
Max vertical deformation	1.0	cm
Max twist angle	2.0	radians

Through the above analysis, the resulting design options were found to have the parameters as specified in Table 7.9.

Table 7.9: Table listing the resulting design parameters of the tail boom for both BRAVO mini

Parameter	BRAVO mini	Unit
r	5	mm
t	1	mm
A	28.3	mm^2
m	20.9	gr

8 Payload

This chapter discusses the different payloads that will be onboard the BRAVO Mini and Max. The payload types are first explained and the way they will be packaged within the gliders will then be shown.

8.1. Functions

The functional requirements for the payload subsystem are mainly derived from KNMI's measurement requirements. The measurement requirements stem from requirement WBA-STK-KNMI-001, which necessitates BRAVO to collect meteorological data – temperature, pressure, humidity, wind speed and wind direction – as well as ozone data. In addition to the meteorological and ozone measurements, the glider allows for custom payloads, such as greenhouse gas measurement instruments.

The first step is measuring the atmospheric variables: for the radiosonde, it is temperature, pressure, and humidity, while for the ozonesonde it is ozone concentration. Wind speed and direction are not directly measured, but are calculated from the timestamps of the GPS coordinates. For conventional radiosonde/ozonesonde payloads, no correction is made for the drag experienced by the balloon and payload. However, for the BRAVO Mini and Max, the drag experienced by the glider will be significant enough such that the wind speed measured by the GPS coordinates of the balloon and glider system significantly deviates from the actual wind speed. Therefore, the calculation of the wind speed must include a correction factor for each glider. This correction factor can be determined by testing the BRAVO Mini and Max in a wind tunnel, and measuring the extent to which the glider is affected by wind speeds.

Figure 8.1 shows the interface of how the payload system will work. The meteorological and/or greenhouse gas data is measured by sensors, and the measurements are converted and manipulated into a digital format that can be transmitted. Using the battery as a power source, the radio transmitter transmits the sensor data along with the GPS coordinates to the ground station. The data is processed at the ground station and distributed to weather-prediction centres, scientists, and other relevant institutions.

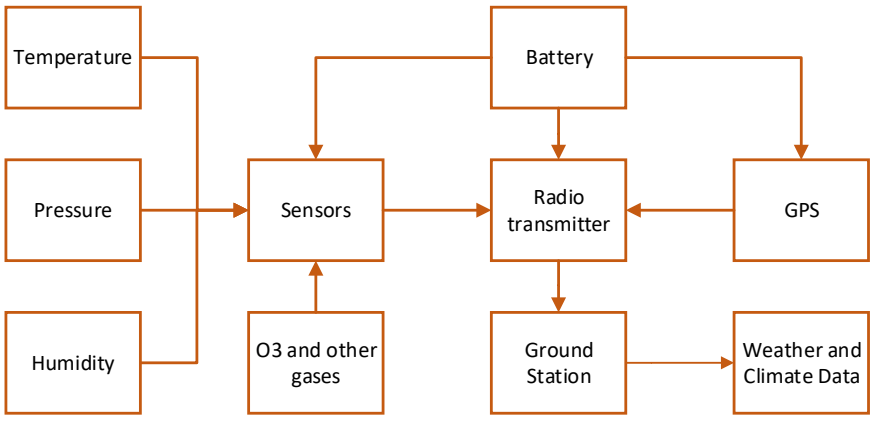

Figure 8.1: Top-level Payload Interface Diagram

8.2. Payload Types

To conduct the same measurements as current weather balloons, BRAVO must have the capability of being equipped with a radiosonde and ozonesonde. As discussed in chapter 3, it was decided that having two gliders would be the most optimal to fulfilling the requirements and maximising the performance.

The radiosonde is the payload most commonly launched for meteorological measurements. A global distributor of radiosondes is a company called Vaisala. KNMI uses their RS-41 radiosonde, which provides temperature, humidity, air pressure, and wind speed/direction data. The data is transmitted back to the ground station once every second. The radiosonde can be tied to the balloon winding and directly launched. However, the packaging of the radiosonde is not optimised for volume, since it is not designed to be carried by a vehicle. Further, the plastic casing is unnecessary if the sensors will be carried within the glider.

The ozonesonde contains the sensors, insulated by a bulky foam box. An interface is used to attach the radiosonde to the ozonesonde. The ozonesonde and the interface are also provided by Vaisala. The limiting factor when reducing the occupied volume of the radiosonde is the amount of insulation required to ensure that the sensors are within operating temperatures.

The custom payload is meant to provide the customer with freedom to add extra sensors up to the 2 kg payload limit. Our primary stakeholder, expressed desires to conduct additional measurements, apart from their standard radiosonde and ozonesonde measurements. In particular, sensors to measure greenhouse gases such as CO_2, CH_4, and N_2O. The extra space is also intended for testing new sensors and instruments. In addition to in-situ sensors, remote-sensing instruments can also be tested.

8.3. Packaging

Due to the different payloads and gliders, the way packaging methods for each payload will be different. This section briefly explains the methods in which the payloads in BRAVO Mini and BRAVO Max can be accessed.

8.3.1. Radiosonde

The radiosonde payload can be accessed by pulling out the nose section of the BRAVO Mini, as shown in Figure 8.2. The RS-41 radiosonde manufactured by Vaisala will not fit inside the payload bay of the BRAVO Mini. Due to Vaisala's patented technology, the exact sensors being used inside the radiosonde are not known. Therefore, sensors that provide sufficient accuracy, resolution, and range were used and packaged into the compact volume within the glider. The sensors used are further discussed in chapter 9. An air duct is included on the nose of the BRAVO Mini, as can be seen in Figure 8.2, to allow the temperature and humidity sensors to function correctly.

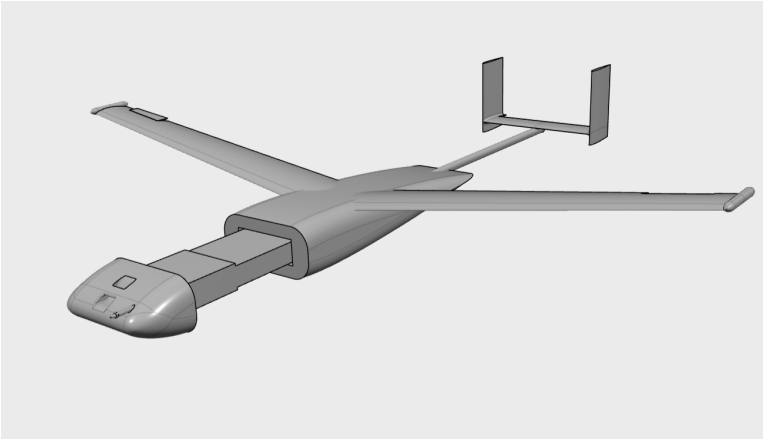

Figure 8.2: BRAVO Mini Radiosonde Payload Bay Removed

8.3.2. Ozonesonde

Measuring 191 × 191 × 254 mm, the Vaisala ozonesonde payload currently used by KNMI will not fit within the 100 × 100 mm cross-section of the BRAVO Max payload bay. The ozone sensor is a very precise instrument, and works by measuring the current, in nA, produced by a chemical reaction with ozone in the atmosphere. To work correctly, the sensor must operate within a temperature of 0 and 30 °C. The foam used for insulation around the sensor is very bulky, and it is responsible for most of the volume of the ozonesonde. The sensor itself measures only 100 × 70 mm, and can easily fit within the BRAVO Max payload bay [34]. Therefore, instead of completely redesigning the packaging of the ozonesonde, it was decided to only use the ozone sensor and not the foam insulation. Instead, to ensure that the sensor operates within its temperature limits, the same thickness of foam used for the insulation box was used in the core of the gliders.

8.3.3. Custom

Along with measuring meteorological and atmospheric variables, a new market was discovered: testing CubeSats. Weather balloons are the only vehicles apart from launchers that routinely reach altitudes above 30 km. While 30 km is much lower than typical CubeSat orbit altitudes of 200-1000 km, the environment at 30 km shows similar characteristics to the space environment [35]. Verifying the flight-readiness of the hardware and software of CubeSats is very expensive compared to the cost of the CubeSat itself. The near-space environment in the upper stratosphere can be used as a low-cost method to test the functioning of systems on CubeSats. at around 35 km, a CubeSat experiences almost identical environmental conditions that it would experience in low-Earth orbit. Thermal conditions can be recreated by allowing for more airflow cooling down the payload.

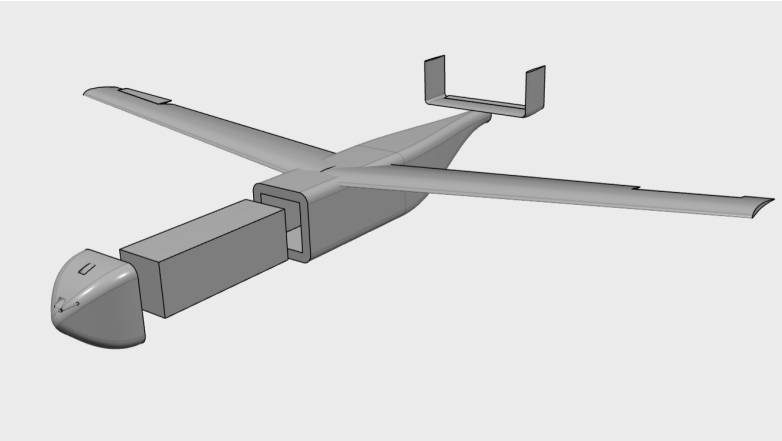

Figure 8.3: BRAVO Max CubeSat payload

The large interior volume of the BRAVO XL is meant to accommodate a 3U CubeSat, which measures 10 × 10 × 30 cm. One phenomenon that cannot be simulated on a balloon for CubeSats is the effect of space radiation. However, this is not a primary concern, since the orbits of 3U or smaller CubeSats will decay and burn up in the atmosphere before space radiation can have a significant cumulative effect [36]. When a CubeSat is not used as a payload, there is a large interior volume that can be utilised for custom payloads. The mass of the payload used affects the performance of the BRAVO Max, which is discussed in chapter 13. A duct is also included on the nose of the BRAVO Max, as shown in Figure 8.3, to aid with measurements requiring air flow.

9

Power & Electronics

In this section, the design of the electronics will be discussed. First, the functional description of this section will be broken down in section 9.1. This is then followed up by a section examining the various subsystems present to fulfil the functions, and what requirements those need to adhere to. In this section, trade-offs with respect to the technology used will also be made. With everything clearly laid out in section 9.2 the choices will be implemented to a prototype design level in section 9.3. One thing to note is the great similarity between the BRAVO Mini and Max. The electronics will be close to the same between them, except for the payload. For all other components, it can be assumed that the exact glider type is irrelevant from an electronics point of view.

9.1. Functional description of the electronics

The electrical system is what ties most components together. It needs to facilitate a large range of functions performed by the other subsystems. In order to examine what all these functions are, it was useful to make a functional flow diagram of the processes the electrical system need to perform in various stage of a mission. These various stages are shown in Figure 9.1. These main functionalities were then further split up into the smaller functions the electrical system needs to perform. Note that some function seem to be very large, such as “execute flight system”. This is due to that function being the domain of another subsystem.

Figure 9.1: Summary of the functional flow diagram for the electrical system

Before the vehicle can be launched, certain preparations need to be made. The steps performed in this stage are shown in Figure 9.2. Notable here are the calibration step of the various sensors required for the mission and uploading the flight profile data. For the flight profile a flight solution will be pre-calculated using prediction data and this will then be transferred to the vehicle. What this exactly entail will be discussed in subsection 9.2.3, but the electronics system needs to facilitate this data transfer efficiently. This is somewhat similar for calibration. The electronics system needs to be able to store the calibration coefficients such that it can correct its sensor measurements before transmission.

After preparation, the vehicle can be transported to the launch site, where it can be turned on. The moment it is turned on, the electrical system goes through some checks in order to make sure it is ready for a launch. These checks are depicted in Figure 9.3. After going through the checks, it will attempt to acquire a GNSS signal. Once that is acquired and the system performs as it expects, the lights on the craft will indicate it is ready. In addition to that, an initial message will be transmitted to check the communications system. After this is finished, the balloon can be launched. The electronics detect the balloon launch and switch the system from pre-launch mode to ascend mode, as depicted in Figure 9.4.

During ascent, the system continually performs measurements of the environment and transmits this to the base station. The functional flow during this phase is depicted in Figure 9.5. During this phase,

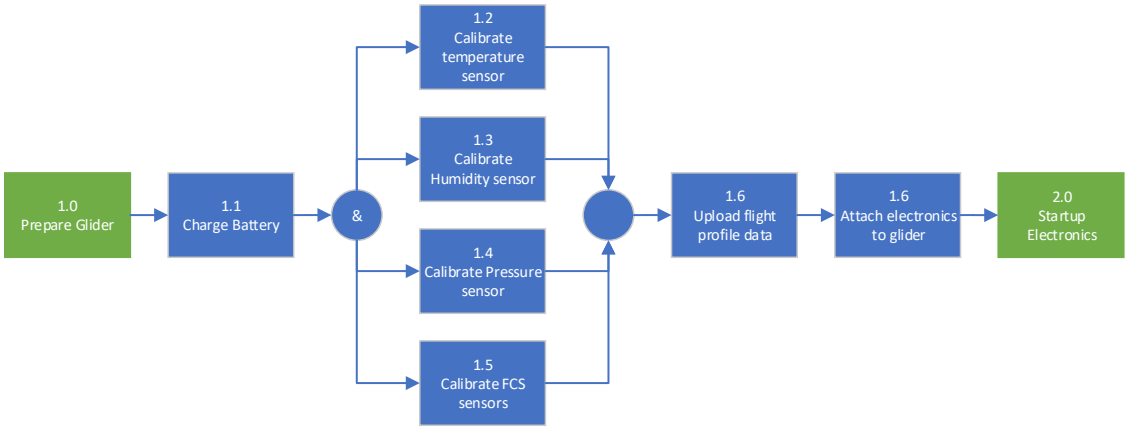

Figure 9.2: preparation of the electrical system

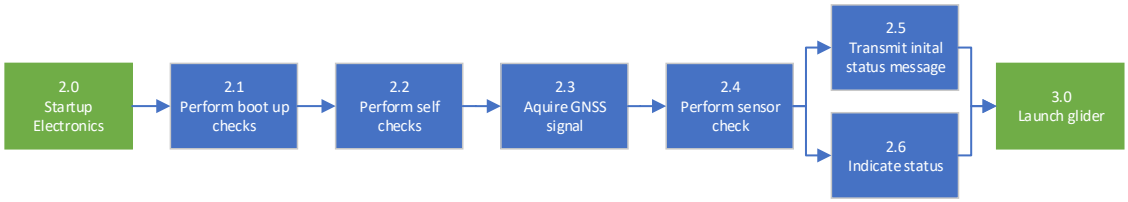

Figure 9.3: startup functional flow diagram for the electronics system.

the electronics system checks whether it has reached its desired altitude. Once it has done so, or the balloon has burst premature, the balloon is released, and the flight control system is switched in to flight mode. After this, it enters into the descend phase.

Shown in Figure 9.6 is the functional flow diagram during the descend phase. In this phase, the vehicle has the most functions to perform simultaneously. It still performs the mission measurements and in addition, the vehicle also runs the flight control loop and aims to follow the flight path selection.

Continuing, the moment the craft lands, it transmits a message indicating as such, and goes into a lower power mode. This is depicted in Figure 9.7.

Finally, when the craft is retrieved all the collected data will need to be downloaded from it as not all of it will be transmitted. The functional process for this is depicted in Figure 9.8. It will need to transfer the detailed flight measurements and the detailed telemetry data of the flight. Then some post flight checks will have to be performed by the system before it shuts down, ready to be prepared for the next mission.

9.2. Main Design Process

In this section, the main design of the electronics section is introduced. in subsection 9.2.1 a method for accurately obtaining the measurement data is introduced. Continuing, the battery selection, sizing and the usage of power is presented in subsection 9.2.2. In subsection 9.2.3 the sensor and the computer supporting flight control are introduced. In subsection 9.2.4 a brief touch will be done on the interface and the payload of the gliders. In subsection 9.2.5 an introduction to how the communications are going to work is presented. Since the system will do most of the flying at night, safety lights are needed and their exact functioning will be introduced in subsection 9.2.6. Being able to determine direction and flight path is rarely of any use if the system cannot act upon these inputs. Therefore, in subsection 9.2.7 the working of the actuators will be laid out. It has been identified that icing could form a major issue,

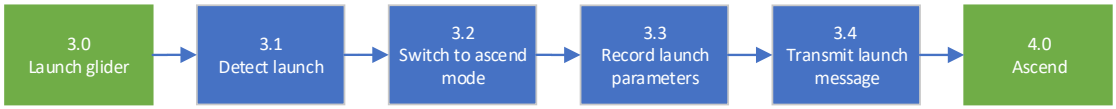

Figure 9.4: functions executed during launch

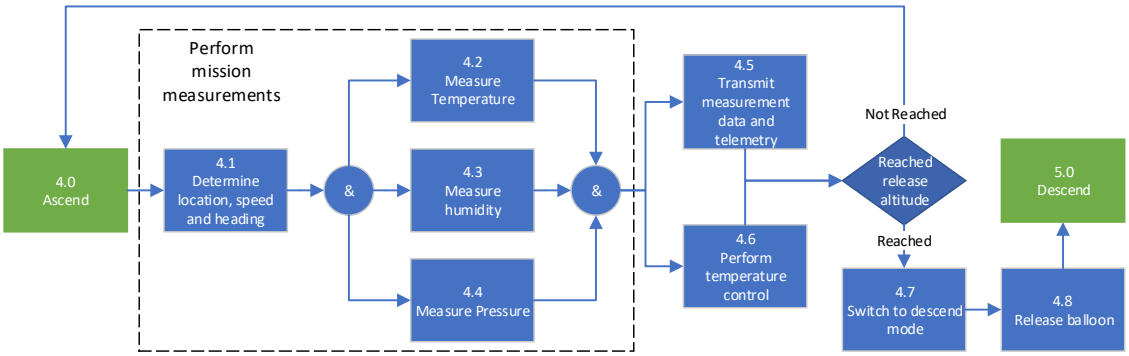

Figure 9.5: Functions executed during the ascent phase.

therefore an icing protection system is presented in subsection 9.2.8. Finally, the internal temperature control is mentioned in subsection 9.2.9.

9.2.1. mission measurements

For the mission measurements, the electronics need to perform the following functions:

- determine air temperature
- determine relative humidity
- determine pressure
- determine wind magnitude and direction

In addition to these base measurements that both the BRAVO mini and BRAVO max need to perform, the BRAVO max also needs to accommodate an additional scientific payload. For this, it will need to make a power and communications interface available. But the exact electronics of such payloads are out of scope for the integrated electrical system.

Determining the temperature

From the requirement, the temperature measurement range is from 180K up to 350K, and it should be able to determine temperature within this range with an accuracy of at least 0.01K.

For determining temperature, there are several well-established methods:

- Resistive temperature detectors
- Thermocouples
- Thermistors
- Silicon diodes
- Infrared sensors

Each of these methods have their own pro's and cons. To determine the sensor type, the measurement range, accuracy, and stability over time were compared against one another in a trade-off shown in Table 9.1. What becomes immediately clear is the performance of the RTD and thermocouple. All other methods compare relatively unfavourable. First thermistors, either the negative or positive temperature coefficient variety, are nonlinear, especially over broad ranges. This non-linearity unevenly distributes

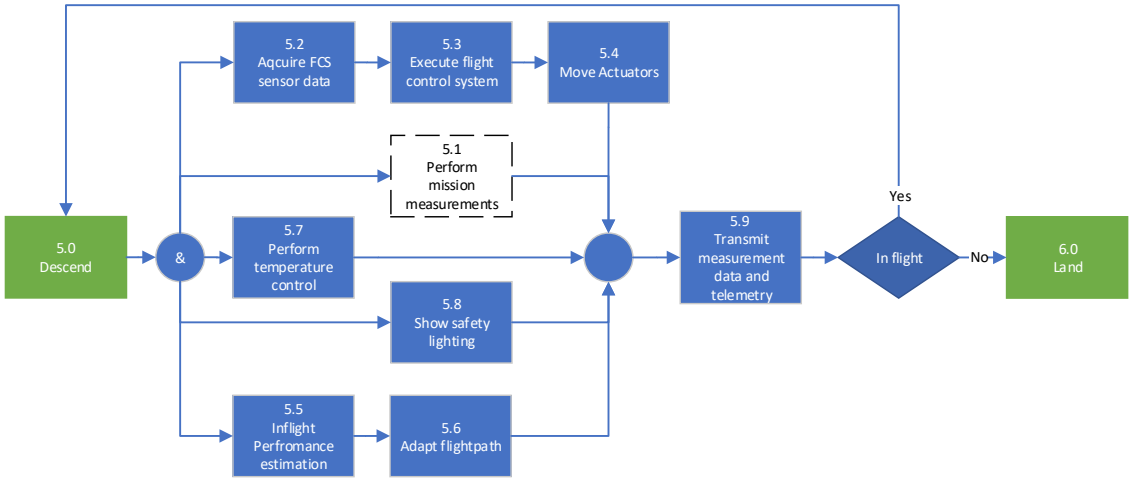

Figure 9.6

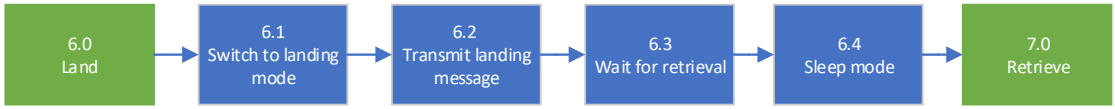

Figure 9.7

the resolution across the measurement range. This can be acceptable for a lot of applications, but is detrimental for scientific applications like these. Silicon diodes perform great for a cryogenic range of temperature, as their conductivity is linear in the regime. But become nonlinear in warmer temperature ranges, making them unsuitable for this application. Lastly, infrared sensors: With proper calibration these can be accurate enough, but due to the lower stability with time and temperature of this method it was chosen to pursue another direction.

Table 9.1: Trade-off on temperature sensing devices

Criteria	**Weight**	Resistive temperature detector	Thermocouple	Thermistor	Silicon diode	Infrared sensor
Measurement Range	3	3	4	3	2	3
Accuracy	4	5	5	2	3	2
Stability	3	5	3	3	3	1
Resolution	2	4	3	1	3	1
Total		75	64	38	48	28

To conclude, the method used for temperature sensing will be a platinum RTD. Because of its linearity, resolution, and accuracy. It will need to be placed on the outside of the craft to prevent interference from the heat generated by the electronics.

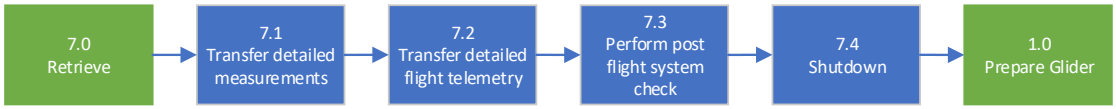

Figure 9.8

Relative humidity

For the measure of relative humidity, there are several off-the-shelf sensors available which are commonly used in radiosondes. Integration of one such sensor would meet the requirements of matching the measurement accuracy of the current radiosonde system. These sensors are very sensitive, however. if they are touched or make contact with anything, their function is degraded, and the measurements produced are no longer usable. Therefore, if we want to increase the reusability of the system, additional effort has to be expended on designing build in protection for this sensor. In addition, the placement should allow for easier replacement of this sensor in case of damage or contamination.

Determining pressure

The total range of measurement spans from 1100 hPa down to 1 hPa, aligning with the resolution and uncertainty of the radiosondes. This wide range is achieved by combining GPS altitude with temperature and sea level pressure to infer the pressure at a given altitude [37]. The uncertainties associated with different pressure regimes are as follows:

- Pressure > 100 hPa: 1 hPa
- Pressure 100 – 10 hPa: 0.3 hPa
- Pressure < 10 hPa: 0.04 hPa

To enhance the accuracy of these measurements, an additional pressure sensor can be incorporated. Common off-the-shelf pressure sensors utilized for this purpose typically have a range of 1100 hPa to 260 hPa, a resolution of 0.0065 hPa, an absolute accuracy of approximately 0.5 hPa, and a relative accuracy as low as 0.025 hPa. This inclusion has the potential to improve the measurement system's accuracy up to an altitude of 10 km and, with additional ground station information, possibly even further.

Moreover, a barometric pressure sensor can be employed to more accurately estimate altitude, surpassing the sole reliance on GNSS and proving useful for flight control. As a result, the additional barometric pressure sensor is integrated into the system. However, the method of calculating pressure based on geopotential altitude and temperature will be used when operating beyond the pressure sensor's range.

Determining wind direction and magnitude

Determining wind direction and magnitude involves analysing the drift of a balloon caused by wind. By observing the balloon's movement using GNSS position data, it becomes possible to calculate the wind direction and velocity. In the case of the descent phase, parameters such as True Airspeed (TAS) and heading are measured. These values are then combined with GNSS speed over ground and GNSS heading measurements to accurately determine the wind direction and velocity.

9.2.2. Battery and Power conversion

In order to function continuously for a long period of time and in no light conditions, on board energy storage is necessary. A battery serves this purpose. There are several battery types and chemistry's. Not all chemistries are suitable for every application. In this application, there are a few very important considerations. Firstly, the specific density: A lighter battery means a smaller and cheaper balloon. Second is the temperature range, especially below zero degrees Celsius is tricky for a lot of battery chemistry's, so special considerations need to go into this choice. Finally, safety of the battery system is a concern. Some types of chemistry and package type are more stable than others, and for a product this is important to consider. These considerations are represented in a trade-off in Table 9.3, with information gathered from [38][39][40] presented in Table 9.2.

Table 9.2: Battery chemistry specifications

Battery chemistry	Specific energy density [Wh/kg]	Thermal Range [ºC]
Lead-acid	30 - 50	-20 to 50
NiCd	45 - 80	-40 to 60
NiMh	60 - 120	-20 to 60
Lithium Ion	170 - 240	-20 to 60
Lithium Polymer	140 - 200	-20 to 60
Lithium Phosphate	90 - 160	-20 to 60

Table 9.3: Battery chemistry trade off table

Criteria	**Weight**	Lead-acid	NiCd	NiMh	Lithium Ion	Lithium Polymer	Lithium Phosphate
Specific energy density	5	1	1	2	3	3	2
Thermal stability	4	1	1	2	3	3	2
Thermal range	4	2	3	2	2	2	2
Safety	5	2	2	2	2	1	2
Total		27	31	36	45	40	36

After considering the trade-off analysis of different chemistries, it is evident that the most suitable solution is to opt for lithium-ion batteries.Although lithium-ion batteries alone do not meet the temperature range requirement, a proposed solution involves incorporating insulation and a small heating element.By implementing insulation and a heating element, it is possible to fulfil the temperature range requirement without significantly impacting the overall mass/specific energy of the battery.

Power conversion

Converting the energy stored in the battery into stable voltages is essential to make it usable for various systems, as the battery voltage varies significantly with its charge level. The sensors and processor in the system typically operate at common voltages of 5V and 3.3V. Additionally, a 12V rail has been incorporated to power the lights, offering a suitable voltage level for their operation, and to provide to possible payloads in the BRAVO Max. Depending on the specific requirements, the actuators will be powered by either the 5V or 12V rail.

9.2.3. flight control

The flight control system relies on electronics to enable its operation. Essential requirements for the electronics include a sufficiently powerful processor capable of executing the necessary algorithms. Additionally, depending on the specific functions of the flight control system, the presence of additional sensors may be necessary to support its operations effectively.

flight control sensors

For the flight control system, there are several parameters which need to be measured:

- Accelerations
- Angular accelerations
- Speed over ground
- Airspeed

- Location in 3D

This then translates to the following sensors being required:

- IMU (Inertial Measurement Unit)
- Gyroscope
- GNSS (Global Navigation Satellite System) Receiver
- Pitot tube

Flight computer

The systems need a processor capable enough to run various real time algorithms for stability and control, do flight path determination, internal telemetry upkeep, perform sensor measurements and handle the data and communication. While this may seem like a lot of things to do. The actual computational power required to perform all these task can fit into a surprisingly small and efficient package.

Finally, in addition to the sensors, some additional memory is required for storing flight path data and data of diversion stations. This can be added in the form of some additional non-volatile memory available to the flight computer.

9.2.4. Interfaces and payload

Any device will need interfaces in order to be interacted with by both humans and other systems. The BRAVO systems are no exception to this. The several interfaces which are required are: Charging interface, data interface, payload interface, system interface and finally a human interface.

- Charging interface: The battery pack needs to be charged, but also balanced such that the cell voltage of all cells is equal. This balancing and charging logic can be done by an external charging device, as this is only required once before each mission and would save some weight. This therefore requires a charging plug with positive negative lead as well as leads for in between the cells and for increased safety a lead for a temperature sensor(NTC or something similar)
- Data interface: For ease of compatibility and ease of use it would be prudent to select an industry standard for this function. A commonly used interface is USB. This is extremely widely supported and relativity easy to integrate. This adds a USB connection to the electronics system.
- payload interface: For the payload, power, and data needs to be available, as the payload can use the onboard data handling and communications system to store and transmit data. To fulfil the requirements, this would combine into a connector with data-lines for interaction with the main system and power lines for 12V and 5V at 2W.
- system interface: Because the electronics and battery pack can be disconnected from the vehicle for calibration and data recovery, a connector interface is required. This connector carries the control lines for the servos and light. And a separate connector caries the antenna signals.
- Human interface: This interface is a bit more diverse. First off, a power switch is needed to turn the entire craft on. Second is some more interaction. The operator needs to be able to turn the craft on, make it go through a startup routine where it checks some internal functions. The craft needs to communicate to the operator that everything is fine. These functions can be partially served by the USB interface, however just for launch when everything is installed and secured the operator may still want this information and interaction. To serve that, short range communications can be added.

9.2.5. Communications

For communications, there are a few important considerations. First, an active continual downlink is required as it is important that the data is collected in a timely manner for reporting as weather models depend on it. It is however possible to post process a large set of collected data for use in later model runs. But this does not negate the need for a continual downlink. Use of the Radio spectrum is regulated. For the use of meteorological aid devices, the frequency band from 400.15 to 406MHz is appointed and regulated by the ECC and FCC. These aids are allowed to transmit with a maximum power of 200 mW and should be designed such that a channel separation of 200KHz between two devices is sufficient. The current radiosondes, equipped with a quarter-wave monopole antenna and transmission power of 60mW, achieve a data downlink of 4800 bit/s over a range of up to 350km. They transmit measurement

messages once per second. Considering that most sensors on board can perform measurements at a higher rate and allocating additional bandwidth for vehicle telemetry is desirable, it is necessary to increase the downlink capacity by a margin between two and 50. This will be further elaborated in subsection 9.3.3.

To have increased control over the vehicle, the addition of bidirectional communication was examined. This does however have a couple of drawbacks. First off, adding receive capabilities to the glider would complicate the communications system and require more energy. In addition, allowing the glider to accept command introduces the risk of it getting erroneous or malicious inputs. This results in the decision to keep communication unidirectional for the prototype and investigate bidirectional communications in the future.

In addition to the main data down-link, a secondary small local link can be integrated to perform final pre-flight checks and transmit some commands to the craft. This was generated from subsection 9.2.4. This adds another small communications subsystem, but considering the very small range required to perform this, it is possible to use a well-defined standard such as BLE (Bluetooth Low Energy) with commonly available off-the-shelf parts and great documentation on integration.

9.2.6. safety lights

Both EASA and the FAA require any UAV to have anti-collision lights on during nighttime operations. This is specified in CS-UAS for EASA. These lights must be visible from 5km or 3 miles and need to blink with a frequency of 40-60 times per minute. In addition to this, navigation lights need to be added such that direction of travel can be inferred. This takes the form of a green right on the right, a red light on the left and a white light on the rear. All combined, the lighting diagram is show in Figure 9.9.

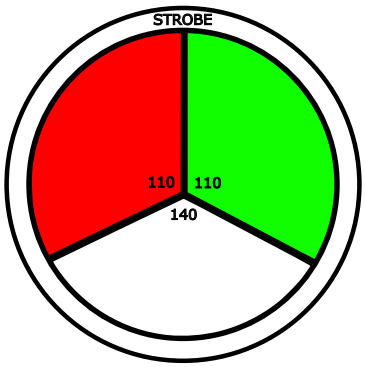

Figure 9.9: the required lights for the vehicles in this system

9.2.7. actuators

All static electrical components aside, the flight control system also requires mechanical movements to be actuated by the electrical system. Specifically, the ailerons and elevator must be actuated in accordance with the flight control system. To achieve this, appropriate actuators need to be selected. In order to minimize development and unit costs, off-the-shelf servos were chosen as the actuator solution. Sizing the actuator involves considering the maximum moments applied to the control surfaces which can be calculated using the coefficients from subsection 5.5.3 and subsection 5.6.2. The relevant limiting moments can be found in Table 9.4, which provides specific values for proper actuator sizing.

Table 9.4: Maximum hinge moment generated by control surface in mNm

	BRAVO Mini	BRAVO Max
Ailerons	60	220
Elevator	370	670

9.2.8. Icing Protection System

As described in section 5.2, icing poses a significant challenge that requires mitigation in the flight control system. This mitigation strategy will be partially performed by electronics. However, due to the size of both the small and large glider systems, certain methods, such as an inflatable leading edge or freezing point depressing fluid system (weeping wing) are impractical. Consequently, the most feasible solution would involve an electrically heated leading edge. Nonetheless, complete anti-icing consumes a substantial amount of energy. Therefore, a more practical approach would be de-icing, which allows for some performance degradation while periodically removing ice from the leading edge[41]. Furthermore, by continuously monitoring flight performance parameters such as glide slope, it is possible to assess the impact of icing. De-icing measures can then be applied when these parameters degrade beyond the acceptable performance envelope. This approach significantly enhances the system's efficiency. This is especially feasible since a lot of the manoeuvring is already done before the craft enters regions with an increased risk of icing, as is described in section 10.5. Therefore, the performance impact of icing can be more tolerable. On the way up icing is less of a concern, but in case of any build up, before release of the vehicle de-icing procedures are applied to mitigate risks.

Icing poses challenges not only to aerodynamic performance but also to control surfaces and airspeed measurements, which also necessitate mitigation. During ascent, small jitter movements can be employed to disrupt the formation of ice layers on control surfaces and ensure their usability. When in flight, the control surface will be moving, reducing the risk of icing, but then still small jitters can be utilised to disrupt ice formation when little movement has been required for a while. For the airspeed measurement, continuous anti-icing will be applied in regions where icing is a problem. This is done in the form of an added heating element to the pitot tube, such that this part remains above freezing and thereby ice free.

9.2.9. Internal temperature control

A final component the electrical systems needs to provide is internal temperature control. This is especially required for BRAVO Max, because its payloads may need to be within a specific temperature range. But for the BRAVO Mini, it is still important to keep the battery within it's operational limits.

Because the electronic components generate heat, a solution could be to simply add insulation thick enough such that the electronics can keep themselves warm enough. This is however hard as there is an interplay between the insulation thickness and the size of the fuselage and therefore drag. Finally, an insulation thickness of 15 mm was decided upon as a good balance between these design goals. This is however insufficient to keep the internal temperature up, resulting in the need for some internal heating. This heating can be calculated under the following assumptions: the skin is always the temperature of the surrounding air; the thickness is constant; and the loss can be calculated purely by heat conducted through the insulation material. With these assumptions and the heat conduction equation, this subsystem can be integrated into the power budget and the rest of the system.

9.3. Design implementation

In the following section, the design requirements and choices made in section 9.2 are implemented and used to create a final prototype design that would satisfy the design requirements.

In summary, for the design of the complete electrical system the following list of subcomponents are needed.

- sensors: temperature, relative humidity, absolute pressure, differential pressure, acceleration, gyroscope, e-compass, GNSS
- Processor
- Communications: Long range Downlink, BLE
- Antenna: GNSS, VHF
- Actuators: elevator, ailerons
- Battery: Bravo Mini, Bravo Max
- Power conversion: 12V, 5V, 3.3V
- Safety lights: Navigation lighting, Strobe anti collision light
- De-icing

- Heating
- Interface: power switch, interactive button
- connectors: USB, Airframe, charging, payload, antenna

In subsection 9.3.1 the exact sensor choices and the placement of these sensors will be discussed. Furthermore, in subsection 9.3.2 the placement of the processor is explained. In subsection 9.3.3 the placement of the communication system is elaborated. In subsection 9.3.4 the placement of the actuators is introduced. Furthermore, the power budget and battery sizing is presented in subsection 9.3.5, after which finally the software is presented in subsection 9.3.6.

9.3.1. Sensor choices and placement

For the sensor design requirements, which were stated in subsection 9.2.1 and subsection 9.2.3, a component selection was made. While it has to be noted that this does not necessarily reflect the optimal choice from a cost or supply chain perspective, it does fulfil all the requirements and can be implemented as a prototype. These choices with cost and explanation are shown in Table 9.5.

Table 9.5: Sensor choices with some reasoning

	Selected Component	Cost [€]	Explanation
Temperature	Platinum RTD	20	Many available in the market as they are commonly used
Relative Humidity	E+E HMCO3M, IST P14 RAPID-2	20	Fast response relative humidity sensors designed for use in radiosondes, with integrated heating element to prevent condensation.
Differential Pressure	Amphenol ELVH-M050D	30	Sufficient range and precision for measuring airspeed with <0.5m/s accuracy over the entire altitude range.
Absolute Pressure	ST LPS22HH	2	High-performance absolute digital barometer for 260-1100hPa. Best-in-class accuracy and better accuracy within the range compared to current methods.
Acceleration	ST LSM6DSL, many others	3	Good range, good accuracy, acceleration and gyroscope integrated in one package. There are many other options, but this part is selected for budgeting.
Gyroscope	ST LSM6DSL, many others		See acceleration sensor.
E-compass	ST LIS3MDL, many others	3	Many options available.
GNSS	u-blox MAX-M10S	20	High-performance multi-constellation GNSS receiver. Other options from u-blox or Quectel will also work.

Some of these sensors need some special consideration when placed. The humidity sensor needs to be exposed to airflow to function properly, but it's also very sensitive to handling and touch. Ideally, you want it to be protected and housed internally. In addition to this, it can also get damaged by contaminants such as dust in the atmosphere, therefore having it be replaceable is desirable. The temperature sensor also needs to be exposed to the outside temperature. All this was combined into a replaceable assembly which has a duct for airflow to the sensor to protect it. The placement of the humidity and temperature assembly is shown in Figure 9.10a. Attached to this assembly is a cable which is fed through the foam nose cone and subsequently plugged into the electronics board.

The differential pressure sensor is attached to the pitot tube with 2 pressure tubes as depicted in Figure 9.10b. Besides this connection are also 2 wires for heating the pitot tube.

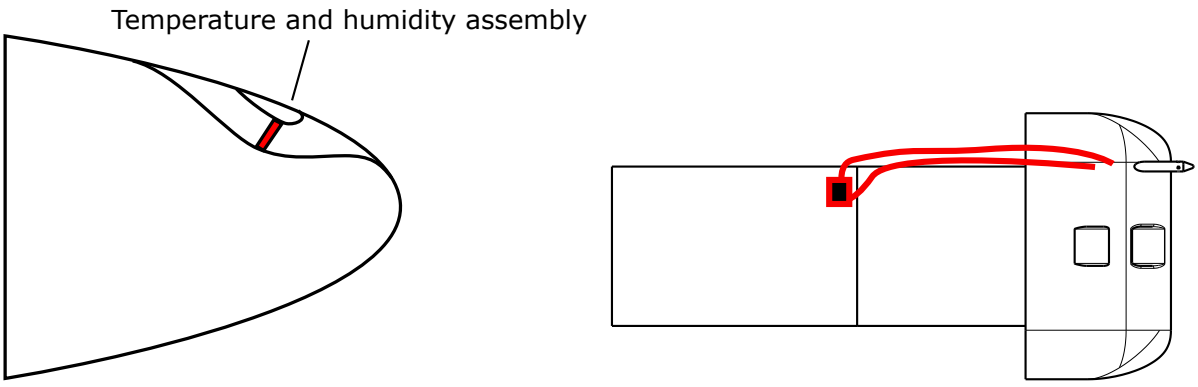

(a) Placement of the humidity temperature assembly

(b) Pitot tube attachment diagram

Figure 9.10: Sensor placement diagrams

9.3.2. Processor

As stated in sections before the processor, main tasks the processor needs to handle are: processing of sensor measurements, flight control, flight path planning, communications. Of these tasks, flight control places stringent requirements on the timing of the algorithm as this needs to be updated multiple times a second (order of 50-100Hz) and needs to have a little delay as possible. All these requirements could be satisfied with an arm cortex-m7 with floating point unit. But for more reliably real-time design, it can be desirable to have the flight control algorithm running on a separate core in real time. What is meant by this is that a core uses interrupts and the software is written such that it performs deterministically and within a certain time. This can also be achieved using a single core. But since there is a pretty diverse range of tasks to be handled which don't need to be real-time, using a processor such as the STM32H747 series dual-core to split real-time and non-real-time code is a good solution.

For this initial design, the STM32H747 is chosen with a budgetary cost of 18 euro.

9.3.3. Communications systems

In order to let the long range communications system perform all required functions, a fitting solution must be chosen. Here, two main aspects are of concern. Firstly, the antenna must be able to handle the required data rate. Secondly, it must be able to provide a sufficient link budget such that it can both receive and transmit with sufficient strength to receive said data.

As discussed in subsection 9.2.5, A maximum transfer power of 200mW along with a maximum channel separation of 200KHz is required. Furthermore, a small mass and size is strongly desired for integration purposes.

With these considerations in mind, two options were determined. The first option presented was a quarter-wave monopole antenna, while the second option was a half-wave dipole antenna. Directional antennae were omitted, as a sufficient data rate needs to be possible in most orientations of the craft. While the quarter wave monopole is smaller and lighter, its radiation pattern is a drawback, as it radiates only in a hemisphere. This would be fine for something that has a constant orientation, such as the current sondes. But because the craft changes orientation, it is not the most ideal option. A dipole solves this problem nicely and additionally has a slightly increased gain. The placement of the dipole would be ideal if it is orthogonal to the receiver. Therefore, integrating it in the wing ensures that it will be mostly orthogonal during the mission, especially on the way back down.

The dipole antenna was then sized for the 403MHz application as mentioned in subsection 9.2.5. Utilizing the formula for the length of a half-wave antenna, Equation 9.1

$$l = \frac{1}{2} k \frac{c}{f} \tag{9.1}$$

$$FSPL = 20log_{10}\left(\frac{4\pi df}{c}\right) \tag{9.2}$$

Using a typical adjustment factor k of 0.95, an antenna length of 0.354m is found. An illustration of this

antenna is shown in Figure 9.11.

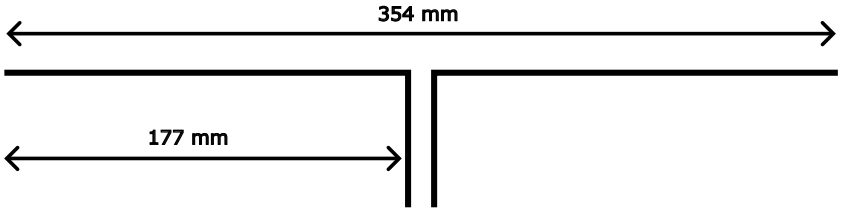

Figure 9.11: Illustration of the dipole antenna sized for the 403 MHz application.

The next part to consider was the orientation of the antenna on the aircraft. Here, two possible orientations were found. The first option places the antenna spanwise in the wing, while the second option places the antenna along the symmetry line oriented nose-to-tail.

To determine the preferred orientation, coverage analysis was conducted. The first option's dead zone posed a higher risk of blocking data flow during early ascent due to potential wind-induced orientation changes. However, as the system climbs, this issue is expected to resolve. The antenna provides nearly perfect coverage during descent as the aircraft consistently points towards the ground station. On the other hand, the second option has good ascent coverage but poor descent coverage due to the dead zone facing the ground station. Considering the risk of data loss during early ascent, the first configuration was chosen.

The free-space path loss is determined using a rewritten Friis transmission formula, which can be seen in Equation 9.2

The receiving antenna was assumed to be an umbrella antenna due to its correspondence to the current standard and its relatively low cost in case an upgrade is required. This antenna type has an approximate gain of 3.52dBi. Because of this, a worst-case gain of 3dB is used. The last step for determining the maximum communication range is setting the sensitivity of the receiver. Two transceivers were analysed here, one with a data rate of 9600bps to provide an insight into the current baseline, while the other has a data rate of 200kbps with GFSK modulation to meet the set requirements. From off-the-shelf transceiver modules, it is found that the first transceiver has a sensitivity of -110dBm while the second transceiver has a sensitivity of -96dBm. The resultant plot can be seen in Figure 9.12. From this, a maximum communications range of 100km for a high bitrate and 400km for the minimum bitrate is found.

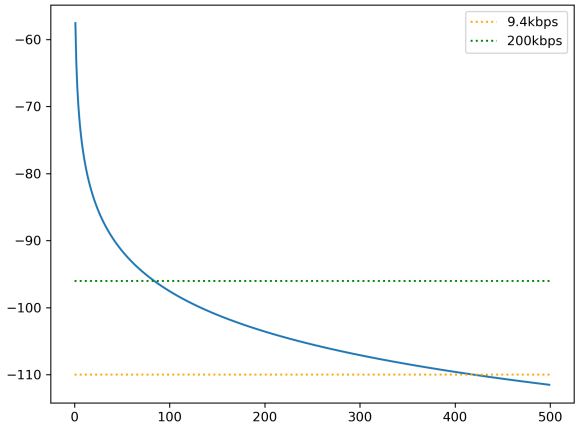

Figure 9.12: Plot of the signal power over distance compared to the antenna sensitivity.

9.3.4. actuator choice and placement

Each of the gliders needs three servos of two different types.

For the BRAVO mini, the moment required for the ailerons is relatively tiny. There are a lot of off the

shelf servo's available which are capable of handling this force. What was far more limiting on this scale is the size and weight of the actuator. Finally, a tiny 5gram servo was selected, as even smaller servos would require custom parts. An example of such a servo is the Hitec HS-40 with 73.5mNm of torque, plenty for the 60mNm required. For the elevator, finding an appropriately sized servo turned out to be even harder again due to the tight space constraints. A small servo with some added mechanical advantage seems to be a good balance between size weight and performance. A choice for this could be the HS-70MG with 290mNm of torque, which is sufficient if a mechanical advantage of 1.3 is used. It would come out to be 377mNm for the required 370mNm. This mechanical advantaged could be achieved by using a bigger lever arm at the elevator servo as opposed to the arm on the servo. The only consideration is the range of the servo compared to the elevator. Since the servo can achieve ±90deg and elevator needs to ±20deg an advantage of 4 would be achievable, but to keep it within the range of 2 would be'desirable as that would be easier to integrate into the vehicle.

For BRAVO Max, the same servo used for the elevator of the BRAVO mini can directly be used for the ailerons, as these require 220mNm. This would be a good consideration as it is tricky to find lighter servos within the performance range required for the design, and it would cut down on the BOM. For the elevator however a larger servo is required as it the elevator calls for 670mNm at maximum. This can be achieved using a 30gram servo and again a mechanical advantage of 1.3, for example the Futaba BLA6HB which can provide 530mNm of torque and 690mNm with advantage. This could work with the same design as the elevator for the mini.

9.3.5. Power budget and battery sizing

With a more clear picture of the internal components and an initial trade-off on the battery design, the actual battery can be designed. For sizing the battery, the worst case mission is chosen. Such a mission can be split into 3 parts: ascend, descend and time on the ground. Ascend, with a speed of 5 m/s, takes approximately 1.5 hours. Descend with an average descend rate of 3.4 m/s take a little over 2.5 hours. And finally, some time both before and after the flight will be spent on the ground, either to prepare for the flight or to aid in locating the vehicle in case it couldn't return. This time is set at 1.5 hours. During these stages, various systems can require more or less power. These systems are: internal temperature control, sensors, flight processor, actuators, communications, de-icing, pitot heating, safety lighting. The bravo max then subsequently adds the payload to this list. These systems don't have a constant power draw over time, as they may be used more intensive during certain parts of the mission and may be entirely switched off during other parts. In addition, the heater system can be controlled such that it only uses as much power as is being lost to the environment. In Figure 9.13a these systems and the power they draw at each moment throughout a mission is plotted for the bravo mini. For BRAVO Max, this is plotted in Figure 9.13b. The power draw of all these various subsystems then combine to the total power draw over time, which is shown in Figure 9.14.

With this information, the total required energy storage of the system can be determined. Exact design values are shown in Table 9.6. The design energy is the required energy for the worst case mission with a safety factor of 10%. This safety factor is there to account for battery wear with charge discharge cycles as the craft needs to perform for at least 200 cycles and a lot of current cells have only 80% of their initial capacity left after about 500–1000 cycles. Besides the design energy, the peak power drawn from the battery is also a concern as this may also limit the battery design. In addition to the design values shown in Figure 9.15 is the breakdown of energy use per the various electrical subsystems for both gliders.

Table 9.6: battery energy design

	Energy required	Design energy	Peak power
BRAVO mini	45.3 Wh	49.8 Wh	33.1 W
BRAVO max	89.9 Wh	98.9 Wh	44.1 W

To design the battery, various lithium-ion cells were looked up and the top performing in terms of energy density were compiled in to a list, shown in Table 9.7. Because a battery can only be build with discrete cells, it can be beneficial for weight to use less large cells or smaller cells.

This all combines into the finished battery pack design in Table 9.8. Coincidentally, the number off cells

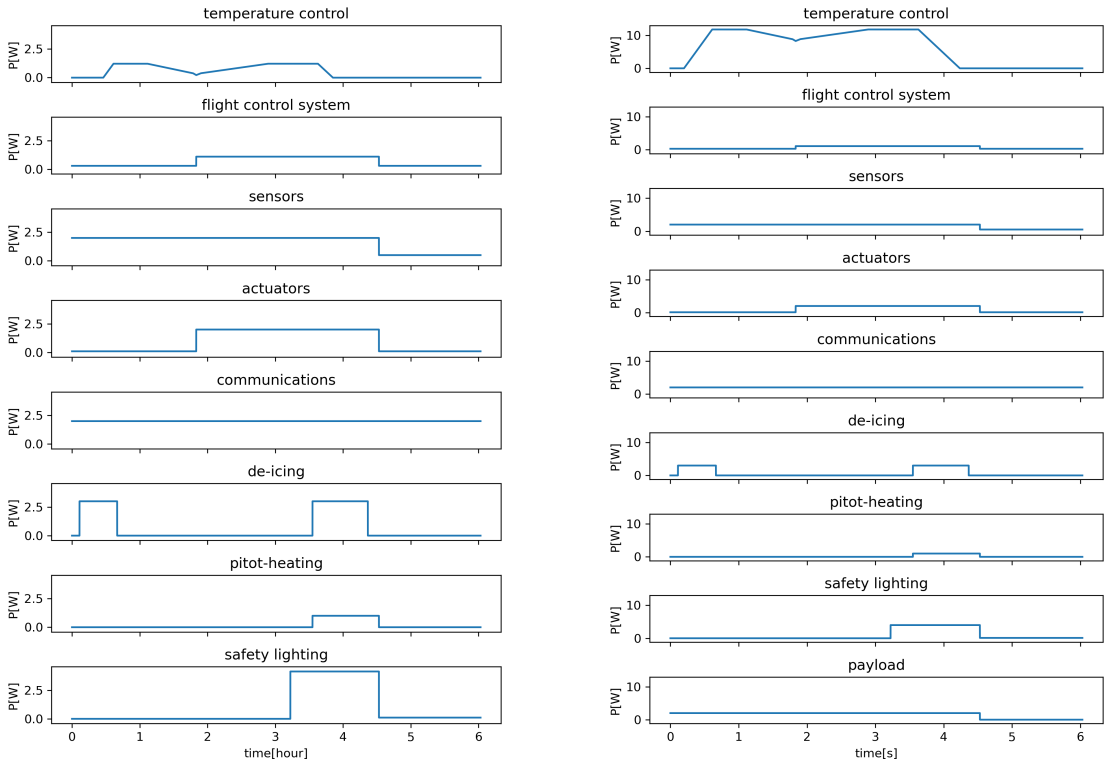

(a) BRAVO Mini

(b) BRAVO Max

Figure 9.13: Split up power draw for various electrical subsystems over mission time

Table 9.7: Battery cells for battery design

model	mAh	mass [kg]	$V_{nominal}$	package	length [mm]	diameter [mm]	manufacturer	cost [
NCA21700-52EM	5200	0.068	3.6	21700	69.7	21.4	Sony / Murata	8.75
INR21700-50E	4900	0.069	3.6	21700	70.6	21.1	Samsung	4.45
UH2655	5500	0.094	3.6	26650	67.4	26.2	Keeppower	10.45
P1835J	3500	0.0493	3.6	18650	68.6	18.6	Keeppower	11.45

for the Mini and the Max line up nicely. While in the design of the battery pack the weight was deemed to be more important, this makes it possible to configure the bravo mini with 4 cells in series and the max also with 4 in series and 2 in parallel. This simplifies the hardware and means it is easier to share designs between the 2 glider designs.

Table 9.8: final battery pack designs

	Pack Energy [Wh]	n cells	Cell type	pack mass [g]
BRAVO mini	50.4	4	P1835J	197
BRAVO max	100.8	8	P1835J	394

9.3.6. Software

In selecting the processor, some mention of the main tasks that need to be performed were already mentioned. To give a clearer overview of all that actually need to happen, the various tasks are shown in Figure 9.16. Some tasks have a hard real time requirement, as temporal stability of this tasks if important for stability of the control algorithm. These tasks are: data acquisition of the sensor required for flight control, parsing and filtering the sensor data, and finally performing the flight control functions. Besides the real time functions, there are several tasks which need to be performed but have less strict timing requirements. These are sensor data acquisition, sensor data filtering, data handling, communications, housekeeping tasks, flight navigation, and ground operations control. Data handling

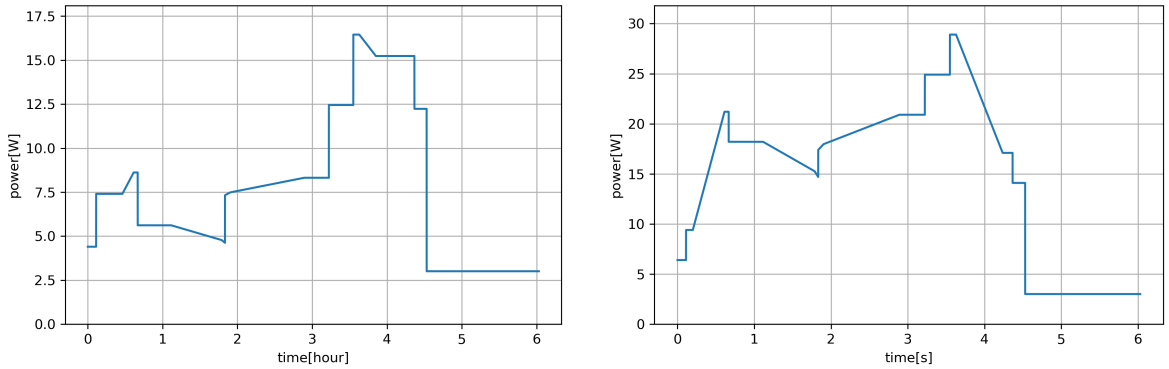

(a) BRAVO Mini **(b)** BRAVO Max

Figure 9.14: Total power draw of all electrical components combined over mission time

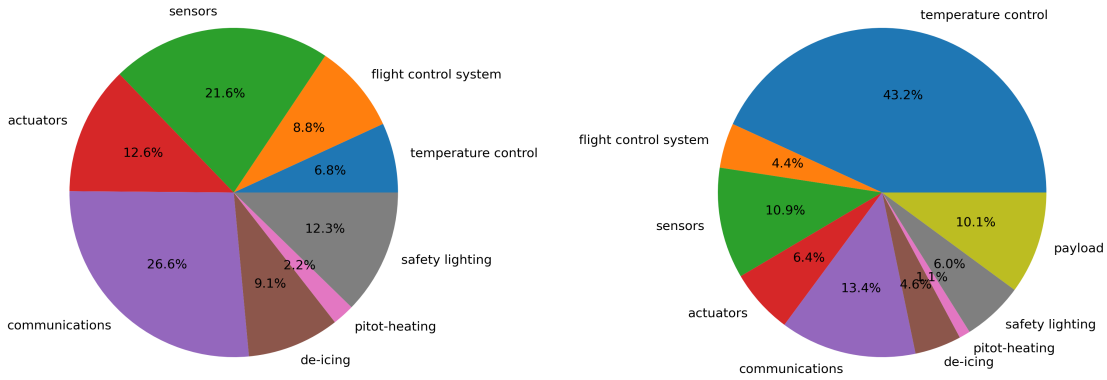

(a) BRAVO Mini **(b)** BRAVO Max

Figure 9.15: Total power draw of all electrical components combined over mission time

refers to compiling sensor data and telemetry information from all the various sources and storing this locally onboard, as well as compiling the messages to be sent by communications. Housekeeping tasks refer to managing functions such as internal temperature control, de-icing and controlling the lights.

9.4. Final design diagrams

To conclude, in the following diagrams the complete electrical system and wiring diagram is shown. In Figure 9.17 the cable harness and antenna is shown. And finally, the complete diagram of the electrical system is shown in Figure 9.18. This diagram includes every sensor and the used data bus for the sensors.

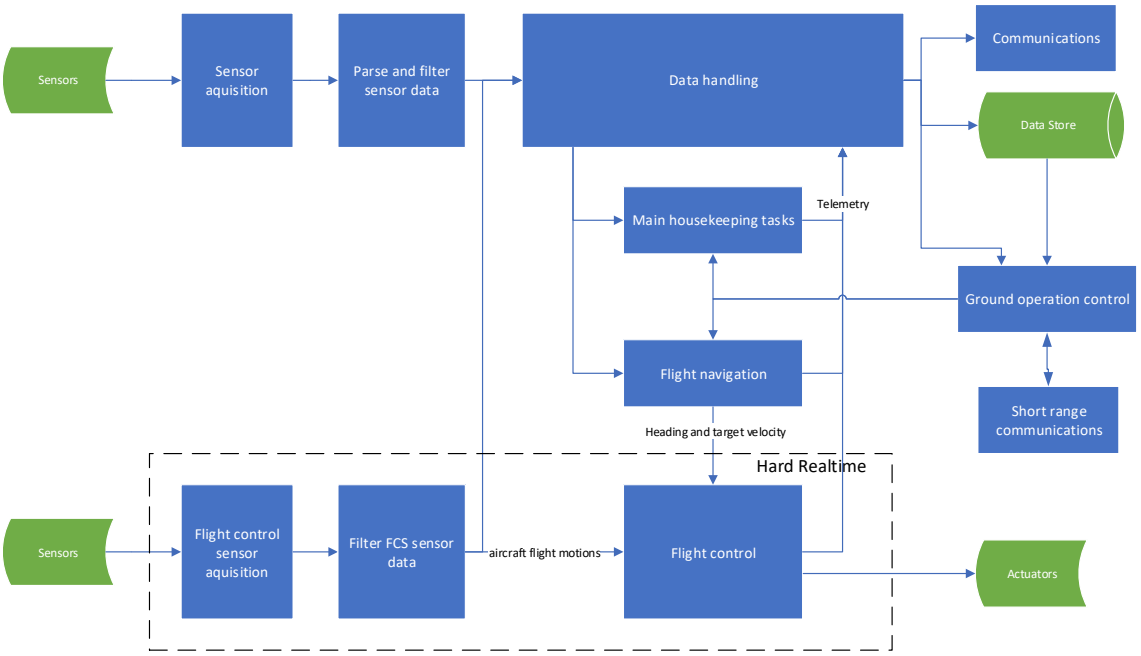

Figure 9.16: Software diagram for both gliders

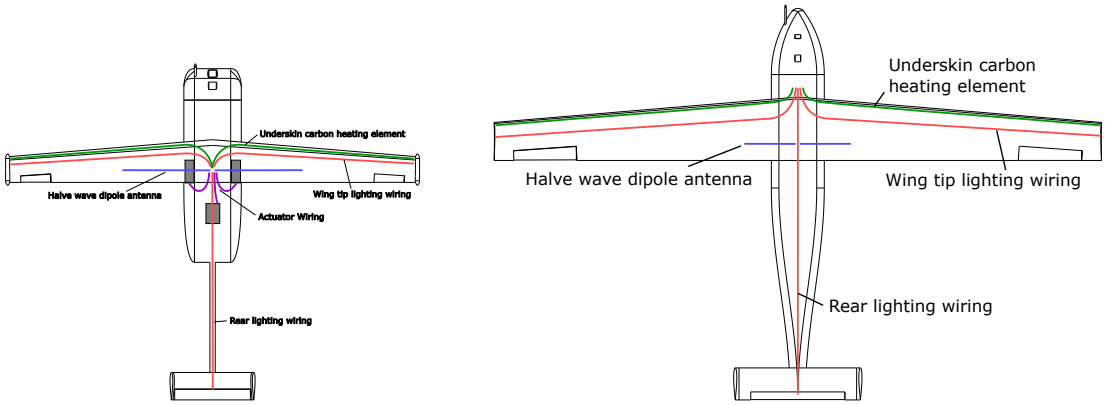

(a) Wiring diagram for BRAVO Mini

(b) Wiring diagram for BRAVO Max

Figure 9.17: Wiring diagrams for BRAVO Max and Mini

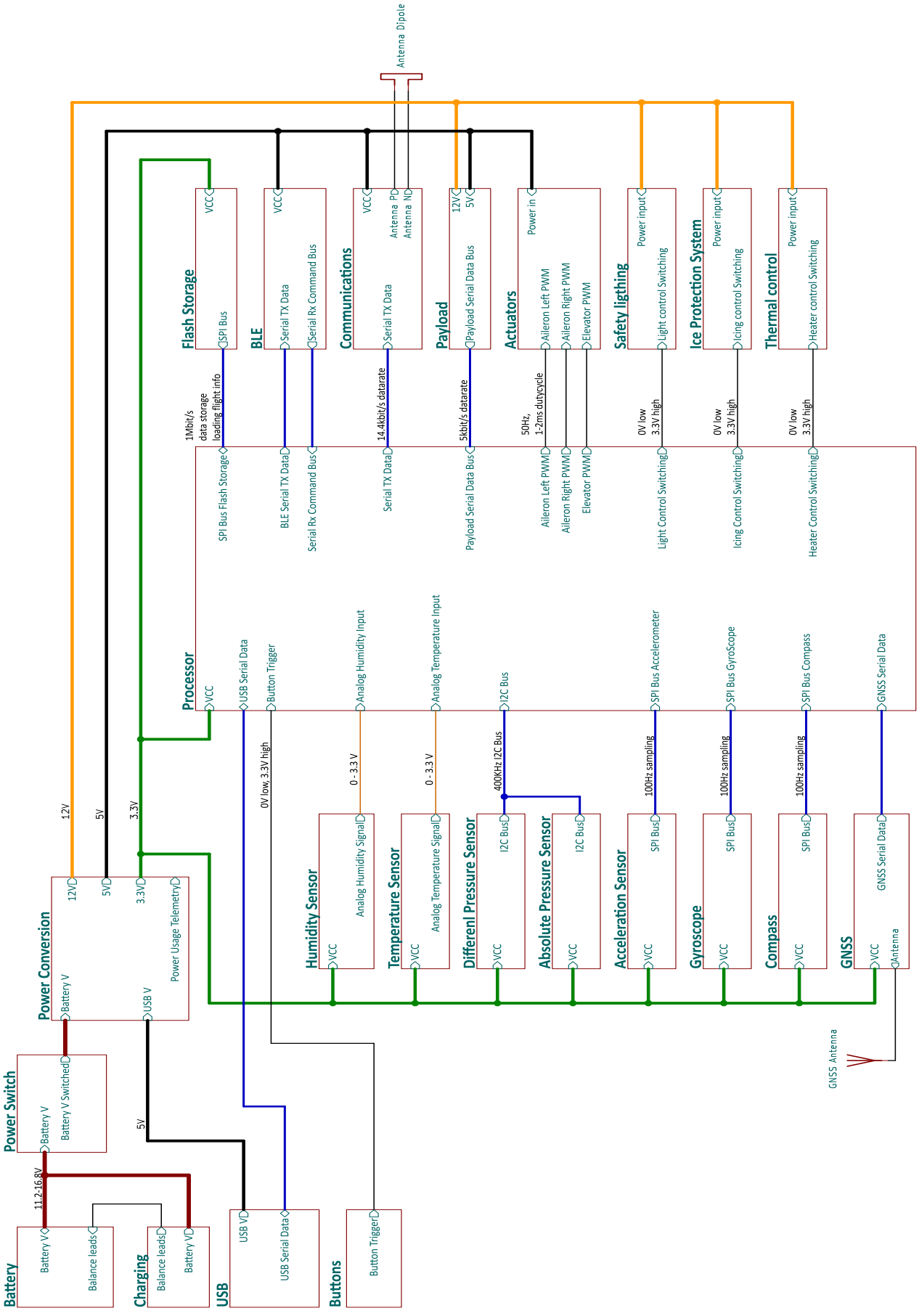

Figure 9.18: A diagram of the electrical system

10 Flight Navigation & Guidance

This chapter concerns the navigation and guidance logic of the glider systems. In section 10.1 the requirements on the flight control system are discussed. After this, in section 10.2 the air traffic management is discussed, followed by the guidance navigation and control in section 10.3. It is important for the glider to be able to estimate its ability to return to the launch site, therefore, in section 10.4 the estimation of the range is done. Finally, it is possible for a system to get out of range of the original location, therefore, in section 10.5 the return trajectory logic is elaborated upon.

10.1. Requirements

In order to begin the design of the flight navigation and control sub-system, requirements must be generated. Some of these requirements will flow from user requirements, while others have been uniquely generated in order to further constrain the design.

The first requirements have been drawn from system requirements and are namely: the flight control system shall communicate with onboard ADS-B transponder, the flight control system shall be capable of adapting the flight path based on TCAS information on descent, the flight control system shall be capable of adapting the flight path in order to avoid restricted airspace on descent and the flight control system shall have a user-friendly interface. Next, a number of unique requirements were generated, they are: the flight control system shall be capable of determining the landing site from a suite of predetermined sites and the flight control system shall be capable of landing the aircraft at the designated landing site.

These requirements will be the base for the design of the flight control system along with other necessities which will flow from the other subsystems.

10.2. Air traffic management

For the vast majority of the trajectory, the glider will not encounter controlled airspace. For now, it is assumed that general controlled airspace is not a problem for Air Traffic Control (ATC) authorities. There are a few prohibited airspace zones in The Netherlands, around governmental buildings and military complexes, but these are small and have low upper limits of 600 [m] to 1500 [m]. Additionally, some control zones (CTR) exist around airports. However, these zones have a low upper limit of up to 1000 [m] and none of them are significantly close to De Bilt to be an issue, except for Hilversum airport, which will be discussed later. Lastly, parts of the Dutch airspace can get closed temporarily as restricted airspace. These can be large areas and have a high upper limit of up to 8.7 [km]. However, these rarely occur during nighttime, when the majority of the balloon launches take place. [42]

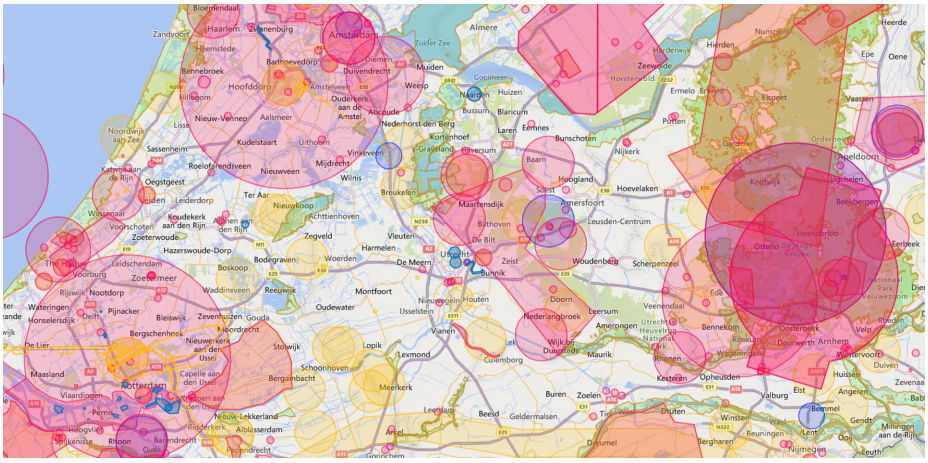

Figure 10.1: Restricted Airspace Regions around De Bilt, the Netherlands

Notably, De Bilt is situated in a PJE (Parachute Jumping Exercise) area. This is not a restricted airspace, but it is an area where low-flying general aviation aircraft and parachute jumpers are prevalent. It is worth considering to avoid the specific PJE drop zones around De Bilt. These airspaces have an upper limit of 1862 [m] to 3962 [m]. They have a radius of 3.5 [km]. Hence, taking half of the circumference and subtracting the diameter as a worst-case diversion, the maximum diversion is 4.0 [km]. One important thing to note is that this zone is only active from 7:00 to 19:00. Since a large part of the launches happen at midnight, the impact is limited. Additionally, there is a no-fly zone around Hilversum airport, approximately 10 km from the KNMI. This no-fly zone has an upper limit of 700 [m] and a radius of 3 [km]. Hence, the maximum diversion for this is 3.42 [km]. [43]

10.3. Guidance, Navigation and Control

The guidance, navigation, and control (GNC) system of BRAVO is responsible for autonomously steering the glider back to the launch site after it is released from the balloon. The glider first sends a signal to the ground station to indicate that it has initiated autonomous flight. The glider then retrieves its position, attitude, and speed from the navigation system. The guidance system uses this information to determine the path to be followed by the glider. Using the output of the guidance system, the control system determines the magnitude and direction of deflection of the control surfaces. The state of the glider is updated until the mission is completed. This logic is outlined in Figure 10.2.

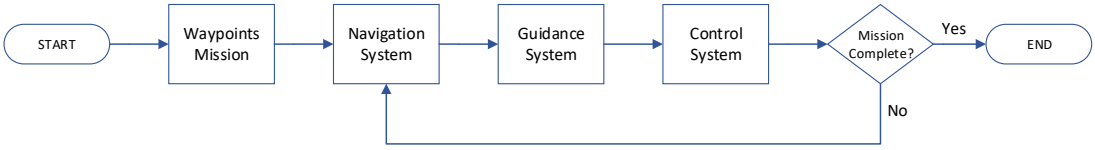

Figure 10.2: GNC Flow Diagram

The control will be handled by an autopilot system. The autopilot uses a planned trajectory as input to deflect the control surfaces and stay on the trajectory. To determine the trajectory computed by the guidance system, several optimisation methods were considered. However, with only one-way communication from the glider to ground station and to limit the onboard computing power, most methods were infeasible. The chosen method to determine the trajectory is described in the following section.

10.4. Range Estimation

A computer program was developed in order to evaluate the descent performance of the glider. Since returning to the launch site is the main priority, the ground-velocity to sink-rate (or rate of descent, RoD)

ratio was used as a performance indicator instead of only the lift-to-drag-ratio. The RoD ratio was calculated as shown in Equation 10.1. Unlike conventional gliders which are optimised for endurance, the BRAVO Mini and Max are optimised for range.

$$\frac{V_{gnd}}{RoD} = \frac{V_{TAS} - V_{Wind}}{V_{TAS} \cdot \frac{C_D}{C_L}} \tag{10.1}$$

C_D and V_{TAS} were calculated as shown in Equation 10.2 and Equation 10.3, respectively.

$$C_D = C_{D_0} + \frac{C_L^2}{\pi \cdot AR \cdot e} \tag{10.2}$$

$$V_{TAS} = \sqrt{\frac{2 \cdot m \cdot g}{\rho \cdot S \cdot C_L}} \tag{10.3}$$

The wind speed was extracted from the Integrated Global Radiosonde Archive (IGRA) [44] and the Network for the Detection of Atmospheric Composition Change (NDACC) [45]. The wind speeds within two standard deviations from the mean were used to calculate the range, implying that the glider range was determined so that it could return to the main launch site over 95% of the time. For the approximately 5 % of wind conditions in which the glider's range is not high enough, a diversion to the next closest launch site will be necessary, as shown in Figure 10.3.

The optimal flight path was determined by finding the C_L for which the ground-velocity to sink-rate ratio was the highest. This was the optimum C_L The corrected lift-drag ratio to optimise for range was thus calculated as shown in Equation 10.4.

$$\left(\frac{L}{D}\right)_{opt} = \frac{C_{L_{opt}} \cdot \pi \cdot AR \cdot e}{C_{D_0} + C_{L_{opt}}^2} \tag{10.4}$$

$$V_{TAS_{opt}} = \sqrt{\frac{2m \cdot g}{\rho \cdot S \cdot C_{L_{opt}}}} \tag{10.5}$$

The calculated parameters were used to calculate the optimal glide path to obtain the maximum range. To return to the main launch site in 95% of the wind conditions, the calculated required range of the glider from release altitude was 150 km.

10.5. Return Trajectory Logic

Once the glider is released from the balloon, it must determine a path to follow. Based on the optimal glide path for the worst-case wind conditions, cones are generated for each landing site to indicate the region in which the glider can return to those sites.

Pre-flight parameters are used as an input to determine the cone boundaries. These parameters include the coordinates of landing sites, restricted airspace boundaries, release altitude, historical wind data and the wind forecast. The cones originate from the landing sites. The landing sites are chosen such that at the release altitude, the glider is within the boundaries of at least one cone. Figure 10.3 shows the input data, methods, and decisions required during the descent and landing procedure. Under ideal conditions, the glider always stays in the cone of De Bilt, thus allowing for complete return to base functionality. In the case of unexpected wind levels during ascend, the onboard stored data is used in the decision-making for the optimal path of action. This decision-making process has to be optimized for the low amount of computing power available onboard, as there is no two-way communication system available.

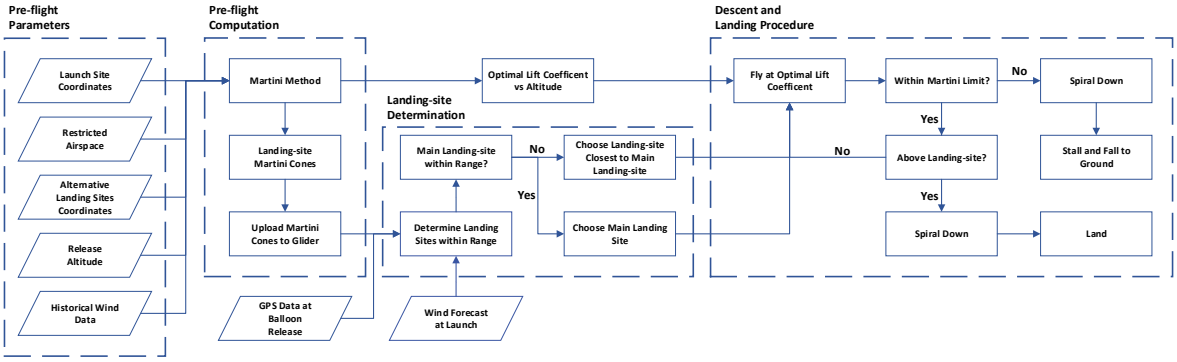

Figure 10.3: Return Trajectory Logic

The 'Martini Method' described in Figure 10.3 refers to the process of determining the cone boundaries for each landing site. The optimal trajectories for the maximum range are used as the cone boundaries. Each cone is centred around its respective landing site. Figure 10.4 shows a top view of the regions covered by the cones of each landing site such as the Bilt (in red), alternatives in the Netherlands (in orange), Belgium and Germany (in grey).

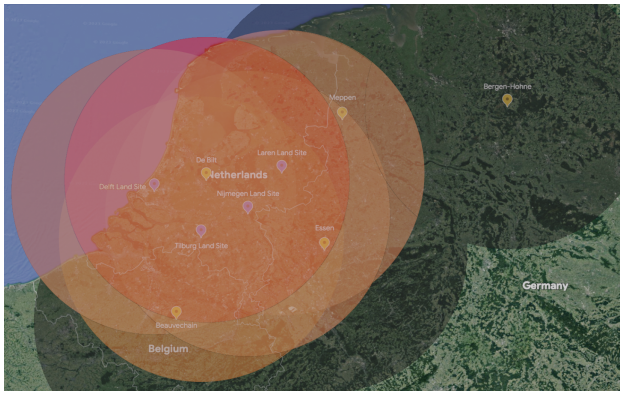

Figure 10.4: Top View of Martini Cones

Figure 10.5 shows a 3D view of the 'Martini cones' of landing sites in the Netherlands (in orange) and one landing site in Germany (in grey). The top of the cones are at the release altitude, and several landing sites are chosen in case landing in De Bilt is not possible. While these images represent the Netherlands, the same method can be applied to countries globally.

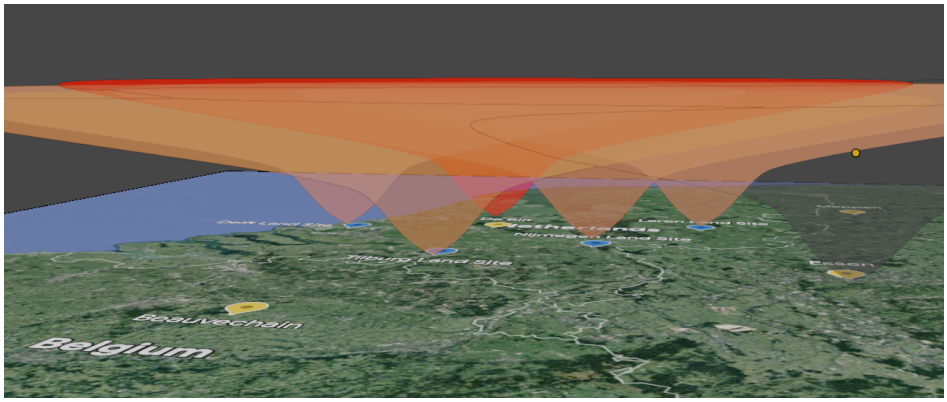

Figure 10.5: 3D View of Martini Cones

11 Balloon

During ascent, BRAVO min and BRAVO max will be lifted to the release altitude with a balloon. In this chapter, the lifting gas is first discussed in section 11.1. Following this, in section 11.2 the balloon sizing is explained. Attaching the balloon to the glider safely is explained in section 11.3, after which finally in section 11.4 the separation of the balloon is explained.

11.1. Lifting Gas

The two lifting gasses commonly used for weather balloons are hydrogen and helium. For the BRAVO family, hydrogen will be used, since the increasing cost and lack of renewability of helium makes the system less sustainable. In addition, hydrogen has better lifting performance. The handling of hydrogen by the personnel will be evaluated in section 15.3.

11.2. Balloon Sizing

After determining the take-off mass of the two gliders, the balloon system can be sized. Since the balloon is a significant source of cost, using the smallest size possible is important to keep the system economically feasible. There are three main cases: launching the small glider, launching the big glider with an ozone sonde, and launching the big glider with the full 2 kg payload. In this section, the method of how sizing the balloon was approached is discussed in subsection 11.2.1 and the results presented in subsection 11.2.2.

11.2.1. Method

It was decided that given the limited amount of commercially available balloon sizes, that calculating the burst altitude for each of these sizes and each payload would be the best approach. To calculate the burst altitude, the amount of lifting gas filled into the balloon is needed, for which in turn the positive lift to achieve the required ascent speed of 5 m/s is needed. For the calculations, the balloon is assumed to be a sphere. Equation 11.1 is the formula for drag rewritten to the surface area, which in this case is the cross-section of the balloon. The drag is equal to the buoyancy force, which is equal to $m_{lift} \cdot g$, the positive lift times the gravitational constant. v_{asc} is the ascent velocity and c_d the drag coefficient. Equation 11.2 is the volume of the balloon at launch, where m_{pl} is the mass of the payload, and m_b the mass of the balloon. Equation 11.3 gives the cross-section of a sphere given its volume. These can then be combined into Equation 11.4.

$$A = \frac{2\,g\,m_{lift}}{\rho {v_{asc}}^2 c_d} \quad (11.1) \qquad V_{launch} = \frac{m_{pl} + m_b + m_{lift}}{\rho_{air} - \rho_{H_2}} \quad (11.2) \qquad A = \pi r^2 = \pi \left(\frac{3V_{launch}}{4\pi} \right)^{\frac{2}{3}} \quad (11.3)$$

$$\frac{m_{pl} + m_b + m_{lift}}{\rho_{air} - \rho_{H_2}} = \frac{4}{3} \sqrt{\frac{2{m_{lift}}^3 g^3}{\pi {\rho_{air}}^3 {v_{asc}}^6 {c_d}^3}} \quad (11.4)$$

Determining the drag coefficient: One thing that still needs to be determined is the drag coefficient. Even approximating the balloon to be a sphere, it still depends on the Reynolds number. This relationship is shown in Figure 11.1 [46]. The Reynolds number is defined as $Re = \frac{\rho v l}{\mu}$, and all of these parameters vary with altitude. However, the dominant factor is the density, which decreases by a factor of over 100. For the three launch cases discussed here, the Reynolds number is mainly in the range

between 10^5 and 10^6, however at high altitudes for the small glider goes below that.

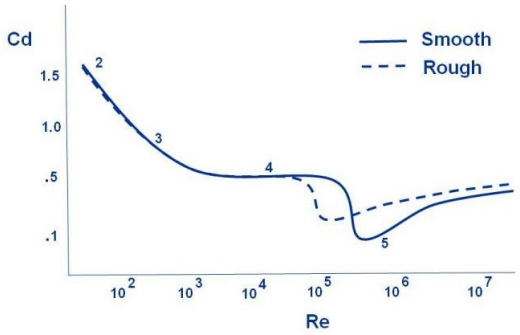

Figure 11.1: Drag on a sphere depending on Reynolds number

Finally, from Figure 11.1, as well as literature [47] the drag coefficient was determined to be 0.275.

Finding the burst altitude: Equation 11.4 can then be rewritten to Equation 11.5, which is a polynomial where only m_{lift} is unknown, and can therefore be solved. This gives the total amount of lift that needs to be provided. Utilising the ideal gas law, the required amount of hydrogen can be calculated, as well as its volume at each altitude. Still assuming a spherical balloon, its radius at each altitude can be computed. The altitude where the radius becomes greater than the burst radius of the balloon is then the burst altitude.

$$\frac{128g^3}{9\pi g^3 {v_{asc}}^6 {c_d}^3} \cdot {m_{lift}}^3 - \frac{1}{\left(\rho_{air} - \rho_{H_2}\right)^2} \cdot {m_{lift}}^2 - \frac{2(m_b + m_{pl})}{\left(\rho_{air} - \rho_{H_2}\right)^2} \cdot m_{lift} - \frac{\left(m_b + m_{pl}\right)^2}{\left(\rho_{air} - \rho_{H_2}\right)^2} = 0 \tag{11.5}$$

11.2.2. Results

Utilising this approach, a table was compiled showing the burst altitude for different commercially available balloon sizes with the three different payload weights. This is found in Table 11.1. Combinations that do not reach the required altitude of 33 km are marked red, while those clearing that height being marked green. Those combinations that are just under 33 km are marked yellow, as they can still reach the required altitude if the ascent speed is lowered slightly. That however means that the ascent time is longer and the drift away from the launch site greater. Therefore, on days with windy conditions where the range is limiting, these can not be used. Since they can still be used on most days, they provide significant cost savings. Finally, it needs to be noted, that the exact burst altitude can differ a fair amount from the value in the table. The value in the table assumes ISA standard conditions, which of course are not representative for individual days. Additionally, the balloons themselves will burst at different pressure differentials due to small material imperfections and differences. Therefore, a safety factor needs to be taken into account while choosing the balloon.

Table 11.1: Balloon burst altitude in metres given balloon size and payload mass

	Small glider (750g)	Big glider with ozonesonde (2650g)	Big glider with 2 kg payload (4000g)
600g balloon	28990	24160	22215
800g balloon	31180	26700	24825
1000g balloon	32760	28615	26810
1200g balloon	33970	30150	28405
1500g balloon	34885	31450	29800
2000g balloon	35900	32915	31445
3000g balloon	38265	35830	34570

Concluding, we can see that for launching the small glider a 1000g balloon can be used for most days, while in windy conditions a 1200g balloon is necessary. For launching the big glider with the ozonesonde only, a 2000g balloon is sufficient most days, while in windy conditions a 3000g balloon is required. For the big glider with full 2 kg payload a 3000g balloon is always sufficient. A summary table is given in Table 11.2. Balloon prices are from websites for private sales [1] and actual prices for large quantities or government institutions might be lower.

Table 11.2: Final choice of balloons for launch

	Balloon size	**Burst altitude**	**Positive lift**	**Required Hydrogen**	**Cost balloon**
Small glider (750g)	1000 g	32780 m	915 g	211 g	~€88
	1200 g	33990 m	973 g	232 g	~€107
Big glider with ozonesonde (2600g)	2000 g	32975 m	1611 g	493 g	~€279
	3000 g	35885 m	1813 g	588 g	~€419
Big glider with 2 kg payload (4000g)	3000 g	34570 m	2075 g	720 g	~€419

11.3. Attaching the balloon to the glider

For attaching the balloon to BRAVO, a few things have to be taken into account. The line connecting the two needs to be strong enough to ensure it is not severed inadvertently, yet must not pose a safety risk when it lands at a random location after the balloon burst. Because it is not retrieved, it also needs to be biodegradable. Finally, it needs to maintain enough distance between BRAVO and the balloon to make sure, that the measurements are not disrupted by the balloon. This is especially true if BRAVO is carrying an ozonesonde payload, which can be affected by the latex of the balloon. The sizing for the line was based on historical data. Since the balloons needed for launching BRAVO are bigger than for traditional radio- and ozonesonde launches, the line length was scaled linearly with the balloon radius. The final values are presented in Table 11.3. The material was chosen to be cotton, as it fulfils the remaining requirements.

Table 11.3: Line lengths for BRAVO and radiosondes

	Radiosonde	Ozonesonde
Traditional launch method	25 m	30 m
BRAVO	33 m	40 m

[1] https://www.kaymont.com/shop

11.4. Balloon Separation

For the reliability and the accuracy of the BRAVO glider, having a functional separation mechanism for the hydrogen balloon is crucial. There are several methods of achieving this; having redundant systems or having a fail-safe design are options that need evaluation. This section will analyse and trade off the different separation mechanism that satisfy the mission. In subsection 11.4.1 the bursting of the balloon is analysed. After this, different techniques are discussed like a hot wire in subsection 11.4.2, pyrotechnics in subsection 11.4.3, a 3-ring mechanism in subsection 11.4.4 and finally a quick release snap shackle in subsection 11.4.5. All of these options are proven technologies already in use to ensure safety of this critical system. This section is rounded off by doing a trade-off in subsection 11.4.6 and then elaborating on the secondary alternative in subsection 11.4.7.

11.4.1. Balloon Bursting

The current weather balloon solution implemented by KNMI does not involve any kind of separation mechanism. It solely relies on the burst of the balloon at a pre-determined altitude range. This low level of control, while sufficient to adjust the vertical climbing profile with max ceiling, is not enough to prematurely start the descent for various reasons. Given the payload capabilities of BRAVO, it is expected that there will be payloads that won't have to reach the maximum altitude the balloons can, and not being able to deploy before the balloon bursts is a substantial disadvantage of the current layout. In addition, being able to release the balloon at any stage of the flight also increases the safety standards of the system, as if the drift of the balloon create a potential hazard to nearby no-flying zones such as airports or hospitals, the system should have the ability to be able to release the balloon and glide to a safe zone.

11.4.2. Hot-Wire

The hot wire cut-down system exploits the material properties of the lines used in between the glider and the balloon. The 100% cotton used for the lines have a rapid deterioration temperature of 246 C° [48]. Using a high resistance nickel-chromium wire, and sending a current of 2.2A will generate sufficient heat to cut through the wire. An important design aspect of this method is the contact between the wire and the cotton line. Traditional designs of this method have the hot wire wrapped around the line that wants to melt, this ensures that the heat is conducted through from the wire to the line. Since reusability and turn-around times are important aspects, an alternative solution where the wire is directly placed on the inner surface of the attachment hook of the line as shown in Figure 11.2a. This ensures that despite the cold and low density environment, sufficient heat is transferred into the line with conduction. To minimize the current required, a 30 gauge wire with a length of 2cm has been chosen. With this, the 1.35W at 2.2A can be provided from the system power using a current controller.

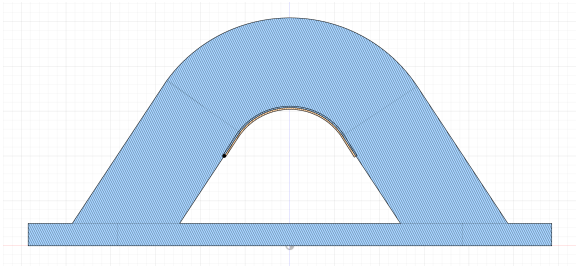

(a) Attachment hook with Ni-Chromium wire)

SWG	Diameter		Nickel–chromium		
	(mm)	*(in)*	*(ohm/m)*	Current *(A)* to maintain temperature rise	
				500 °C	*1000 °C*
12	2.642	0.104	0.197	38	78
14	2.032	0.080	0.333	26	53
16	1.626	0.064	0.520	19	40
18	1.219	0.048	0.92	13	27
20	0.914	0.036	1.65	8.5	18
22	0.711	0.028	2.72	6.3	13
24	0.559	0.022	4.40	4.5	9.5
26	0.457	0.018	6.60	3.5	7.0
28	0.376	0.0148	9.7	2.7	5.5
30	0.315	0.0124	13.9	2.2	4.5
32	0.274	0.0108	18.3	1.9	3.5
34	0.234	0.0092	25.2	1.6	3.0
36	0.193	0.0076	37.0	1.3	2.3

(b) Ni-Chromium Temperature Rise vs. Amps

Figure 11.2: Hot-Wire Cut-Off Design

11.4.3. Pyrotechnics

Similar to the hot-wire concept, pyrotechnics can also be used to melt away the cotton lines that carry the glider. To do this, a capsule including explosive powder and an igniter is attached to the cotton line. The spark igniter can be supplied using the system power. Main drawbacks of this system are the lack of reusability for the explosives and the operational hazards that arise from using combustible powder

close to a hydrogen balloon.

11.4.4. 3-Ring

The 3-ring detachment system is a method widely used in skydiving and paragliding activities, and therefore is a proven method of separation especially for high load/reliability situation. Traditionally, the 3-ring from large to small are used in a chain configuration to distribute the load evenly to the line, similarly to how pulleys work. By letting go of the string attached to the smallest ring, the entire line escapes through the other two rings and the load is separated. In the case of BRAVO, where unit weight is critical, the system can be implemented with loop knots instead of metal rings. For the loads that the line will experience, this setup will be sufficient, and using knots will also make the system have a lower environmental impact as in the standard configuration, the large ring has to be attached to the released part. To integrate this setup in BRAVO, a small 9g servo is necessary. The servo can be powered with the onboard battery, but an additional controller circuit will be necessary.

11.4.5. Quick Release Snap Shackle

The snap shackle is another high load capable detachment mechanism. It consists of a spring-loaded hook attached to a freely rotating body. This system is commonly used in sailing as it offers reliability and performance even under very high loads, however, the low temperatures at high altitude could bring icing issues to this mechanism. To compensate, the pin that has to be pulled to release the system might require high amounts of force. This means that a stronger and therefore heavier servo has to be used. The advantage of this mechanism is that it is fully reusable; no hardware is ejected with the balloon.

11.4.6. Trade-off

To ensure the selection of the most fitting solution, a trade-off of the release mechanism is necessary. The trade-off criteria are chosen to be: reliability, operational safety, system integration, weigh, cost and reusability. Reliability is the most important criteria, as the release mechanisms has to work under operational conditions and using a proven, fail-safe technology has to be rewarded highly. Operational safety quantifies the dangers that arise with the human interactions and possible flight path collisions. For example, having energetic powder on board is both a safety risk for the ground crew launching the vehicle and aircraft flying, as a misfire near a hydrogen balloon can result in an explosion. System integration evaluates how well the chosen mechanism is implemented into the power and control systems of the BRAVO family, as well as the physical space inside the gliders. For example, the power of the hot-wire separation system can be powered from the onboard power system of the glider. Weight, cost and reusability are self-explanatory. The system should be as light, cheap and reusable as possible. All the criteria are given a weight between 1 and 5 and the designs are scored also on a scale of 1 to 5.

Table 11.4: Trade-off table for the balloon release mechanism

Criteria	**Weight**	Hot-wire	Pyrotechnics	3 Ring	Release Hook
Reliability	5	4	5	4	3
Operational Safety	3	3	1	5	5
System Integration	2	4	4	2	2
Weight	4	5	5	3	1
Cost	3	3	2	2	3
Reusability	4	4	1	4	5
Total		82	66	73	67

As a result of the trade-off in Table 11.4, the hot wire system will be implemented.

11.4.7. Passive System

Despite the reliability of the chosen hot-wire system, it will be controlled and powered by the gliders systems. This means that any failure in the power system or the control computers will result in no release of the balloon. If the balloon then does not pop (which happens in some cases) the system could stay afloat in the stratosphere. It is for this reason that a passive system will also be integrated into the design of BRAVO. There are currently no commercial solution that fit the criteria given in Table 11.4 therefore a novel solution has to be designed. The design is based on the pressure differential between the launching altitude and the mission ceiling. A canister with a pressure sealed piston is filled with non pressurised sea level air before launch. The glider is then launched, and the outside pressure starts decreasing. Once the maximum altitude of 33.5km, or outside pressure of 700Pa is reached, the pressure difference between the internal piston and outside becomes sufficient to break the string restricting the expansion of the piston. Once this happens, the piston expands rapidly and the blade attached to the piston cuts off the line. This contraption is shown in Figure 11.3.

(a) Launch state **(b)** After expansion

Figure 11.3: Passive Pressure Cut-Off Mechanism

12
Ground Systems

Another important part of the full system is the design and sizing of the ground systems used for launching, recovering, and communicating with the vehicle. The first part is the launching system, the design of which is described in section 12.1. Secondly, a tradeoff and sizing is performed for the landing and recovery system in section 12.2.

12.1. Launch System

The launch system offers two main options for consideration. Since the launch employs a balloon, similar to current radiosonde launches, the first option involves retaining the existing manual procedures. These procedures would remain largely unchanged, except for attaching a glider to the balloon instead of a radiosonde. However, this approach would necessitate the presence of staff working at 2 am during launches, resulting in substantial associated costs.

To address this challenge, an alternative solution is to develop a semi-automatic launcher. This launcher can be prepared with minimal effort during the day and then autonomously conduct launches throughout the night. Although the development of this launcher was deemed beyond the scope of the initial product development, it has been identified as a future opportunity with the potential to significantly enhance the economics of the BRAVO platform.

While the detailed implementation of the semi-automatic launcher will not be explored in depth at this time, it is important to understand its fundamental idea and working principle. In the following section, we will provide a more detailed explanation of this concept, highlighting the potential benefits it offers.

12.1.1. Semi-automatic launcher

The semi-automatic launcher incorporates several key components to streamline the launch process and minimise the need for manual labour. During the workday, the launcher is prepared by attaching the line to the calibrated glider and placing it in the launcher. The balloon is placed securely on the launcher's nozzle. Automated clamping or fastening mechanisms are utilized for reliable and controlled attachment of the line pre-attached to the glider and the balloon after filling.

Another essential component is the automatic hydrogen generator, which produces the required hydrogen through electrolysis after the glider and balloon are placed in the launcher. This eliminates the need for workers to be in close proximity to hydrogen, a hazardous material. Additionally, since the quantities of hydrogen are relatively low, being mainly in the range between 200 and 700 grams, no high pressure storage tanks are required. However, due to the electricity requirement of about 50 kWh per kg of hydrogen[49], a sufficiently powerful connection needs to be established, or the hydrogen generation needs to take place over a longer time period.

Before the launch, relevant pre-flight checks will be performed automatically and a communication link is established. During the launch, the generated and stored hydrogen is pumped into the balloon. After the required fill level is reached, the balloon is tied off and attached to the payload. The hatch is then opened, and the balloon is ready to be released. The release can be scheduled for a specific time or a launch window can be designated, in which case the launcher picks the time for when weather conditions allow for the best performance of BRAVO, and the highest likelihood of returning to the launch site.

It needs to be noted, that a lot of rigorous design and testing needs to be performed. For the automatic

launcher, a very high reliability is required, as finding out the next morning that the launch did not happen is not acceptable.

In summary, the semi-automatic launcher system can streamline the launch process by reducing manual effort and enabling automated and reliable nighttime launches. Since it is capable of launching balloons with any payload, the semi-automatic launcher could be sold as a standalone system separate from BRAVO.

12.2. Landing System

Another essential ground system is the landing system. To ensure reusability, the ground system needs to recover the vehicle safely and reliably. This would preferably be at the launch location, where limited space may be available. To find a design solution that best fulfils all the requirements, a trade-off was performed in subsection 12.2.1, after which the landing net was sized in subsection 12.2.2.

12.2.1. Trade-Off

Criteria

For the trade-off, the following criteria were used.

- **Cost (2):** While the cost of the entire landing system is an important factor, since it is a one time expense used for many landings, its importance in this trade-off is relatively low.
- **Space (5):** One of the most important criteria is the space required on the ground, as in De Bilt there is only a 60mx60m field is available with obstacles surrounding it. This puts traditional landing methods at a significant disadvantage.
- **Mass added to aircraft (5):** As the balloon size is a significant cost driver, which directly depends on the glider mass, it is of the essence that the landing system adds as little mass as possible to the vehicle.
- **Complexity (3):** The more complex a system is, the more prone it is to failure. This needs to be taken into account.
- **Weather handling (4):** Another important aspect of the landing system is fulfilling the requirements to land in strong winds.
- **Ease of retrieval (2):** Minimising required man-hours is crucial, and therefore it is important that the vehicle can be easily retrieved and made ready again for the next flight.
- **Effect of failure (2):** Finally, the potential consequences of a landing mechanism failure need to be considered. A parachute failure for example would result in a high speed impact with the ground and potential significant damage to the vehicle. For a conventional landing, a failure could be an overrun and collision with obstacles.

Design Options

The following design options for the landing system were evaluated based on the aforementioned criteria to determine the most suitable approach.

- **Parachute:** In this option, a small parachute is deployed at low altitude, followed by a soft touchdown in the landing zone. Its advantages are the little space required on the ground as well as its ease of retrieval, as it can be simply picked up from the ground the next morning. However, it adds a fair bit of mass to the vehicle, does very poorly in strong winds, and adds a lot of complexity.
- **Parachute with vertical net:** Similar to the previous option with the difference, that the parachute is deployed in the last second mainly to slow down the vehicle shortly before impacting a vertical net. This improves the wind capability, however it makes retrieval more difficult, as it has to be removed from the net. There is also the risk of the parachute getting tangled in the net. In addition to the drawbacks of the previous option, this one increases the cost significantly.
- **Horizontal net:** In this option a big horizontal net is installed hanging above the ground into which the aircraft nose dives. While this is expensive and retrieval from the net adds work, it needs very little space, adds no weight to the aircraft and is able to handle strong winds.
- **Arresting Hook:** The idea here is to catch an arresting wire with a hook installed on the aircraft, akin to landing on an aircraft carrier. While being space efficient, needing little additional mass on the aircraft, and easy retrieval, catching the arresting wire in bad weather would be very difficult.

- **Wheels:** This option is essentially a conventional aircraft landing utilising wheels. The main drawback here is the large require area for the landing, as for best wind handling it would be required to always be able to land into the wind.
- **Skis:** Very similar to the previous concept, but using skis instead of wheels. Since no breaking can be applied to the skis, even more space is required.

Conclusion

After conducting a comprehensive trade-off, shown in Table 12.1, analysis of various landing system design options, it is evident that the horizontal net option emerges as the most favourable choice. The horizontal net excels in multiple criteria, scoring the highest among all options in the majority of factors considered. It addresses the crucial requirement of limited ground space, eliminates the need for additional mass on the aircraft, and exhibits superior performance in handling strong winds. Although it requires additional effort for retrieval and involves higher costs, these drawbacks are outweighed by its overall effectiveness and efficiency. Therefore, the horizontal net design is the recommended landing system solution, ensuring the safe and repeated recovery of the vehicle with minimal limitations and optimal performance.

Table 12.1: Trade-off on landing design options

Criteria	**Weight**	Parachute	Net	Arresting hook	Wheels	Skis	Parachute & vertical net
Cost	2	2	1	2	3	3	1
Space	5	4	4	2	1	1	4
Mass added to a/c	5	1	4	3	4	4	1
Complexity	3	2	4	2	4	4	2
Weather handling	4	2	4	1	2	3	4
Ease of retrival	2	4	2	4	4	4	1
Effect of failure	2	2	2	3	3	3	2
Total score		55	78	53	60	60	55

12.2.2. Landing net design

After selecting a horizontal net for the landing system, several parameters needed to be determined for its design. These parameters included the size of the net, the height above the ground, the material, strength of the net, the mesh size, as well as the method of retrieving the landed gliders. In order to keep costs low, the decision was made to utilize commercial off-the-shelf components. This approach allowed for cost-effective solutions without compromising the performance and safety of the landing system.

For the material choice of the nets, polypropylene was selected due to it being lightweight and cost-effective. Its excellent chemical resistance and water absorption resistance make it well suited for outdoor use. It is not as strong as nylon or polyamide, however, this can be easily mitigated by using a slightly thicker netting. Polypropylene nets have a UV resistance of 300 kLy, which is slightly higher than alternate materials. Given a yearly UV radiation dose of about 80-100 kLy in the Netherlands means that the nets need to be replaced every three years.

To identify the most suitable net type and size, a comprehensive simulation was conducted, considering three different load cases of BRAVO mini and BRAVO max landing with different payloads. The simulation analysis played a key role in determining the net configuration that performed best in terms of important factors such as minimising the g-forces experienced by the glider upon landing, minimal maximum deflection, allowing the net to be mounted lower to the ground, as well as making sure the net does not exceed its maximum strength capabilities, taking into account a safety factor.

The input for the simulation were the strength parameters of the available nets, the net size, the payload weights of 0.75, 2.65 and 4 kg, a landing speed of 18 metres per second, and the CEP (Circular error probable) positioning error of the navigation system, which was set to 2 m. The simulation then for each

combination of glider, net strength, and net size yielded the maximum deflection, maximum strain, and maximum experienced deceleration.

The acceptable bounds were determined from material properties, historical data, as well practical considerations. The polypropylene nets have a breaking elongation of 15% and given a safety of 2, a maximum elongation of 7.5% was deemed acceptable. For the maximum deflection 4.5 m was selected to make sure, that the landing system is not taller than 5m, as to not obstruct launching operations.

From this evaluation, it became clear that two separate nets were needed to accommodate the specific landing requirements of the BRAVO mini and BRAVO max configurations, as a stronger net was needed to safely catch the up to five times heavier BRAVO max. This net would have stopped BRAVO mini too fast, introducing excessive g-forces. The net for BRAVO mini was positioned above the one for BRAVO max. For the max landing, the upper net contributes minimally to stopping the glider, while the lower net does most of the work. For the landing of BRAVO mini, the lower net is lowered to the ground to ensure a soft landing. Both nets can be lowered as necessary to retrieve of the gliders after landing.

Table 12.2: Landing simulation results

	Maximum deceleration	Maximum strain	Maximum deflection
BRAVO mini	79.9 m/s	5.62 %	3.85 m
BRAVO max with ozonesonde	90.0 m/s	4.48 %	3.42 m
BRAVO max with 2 kg payload	78.5 m/s	5.82 %	3.92 m

The results of the simulation for the selected nets can be found in Table 12.2. For the poles, street light poles were selected, as they are cheap and readily available. The maximum deflection for the selected nets in the simulation is 3.85m and 3.92m respectively. To account for potentially faster landings and therefore higher maximum net deflection, it was decided to mount the net five metres above the ground.

Final Design:
An artists' impression of how the landing system looks like is provided in Figure 12.1. It consists of four five metre high poles, between which 2 nets of 16 by 16 metres each are spanned.The nets can be both lowered to provide access to remove the landed gliders and to configure the landing system for the two different gliders. From the simulation, two commercially available nets were selected, whose properties are shown in Table 12.3

Table 12.3: Net properties

	Material	Max Tensile Strength	Max Elongation	Material Diameter	Mass per Area	Mesh size
BRAVO Mini net	Poly-propylene	250 N	15%	1.5 mm	15 g/m²	100 x 100 mm
BRAVO Max Net	Poly-propylene	1250 N	15%	3.0 mm	65 g/m²	120 x 120 mm

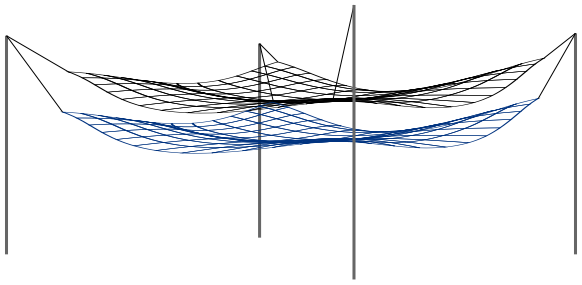

Figure 12.1: Illustration of landing net

13 Design Overview

After finishing the subsystem design, the performance of the system must be analysed. This is done to evaluate the design and see if it complies with all performance-related requirements, as well as to generate needed data for a thorough market analysis. First, in section 13.1 the range for De Bilt is analysed along with the sensitivity of the system to changes in certain inputs, followed by an analysis for different locations in section 13.2. Then, an overview of the system design is given by providing the technical drawings in section 13.3, and finally, the compliance is analysed in section 13.4.

13.1. Analysis of System Performance and Sensitivity

This section will be dedicated to summarizing the capability and performance of the system. Of course, the exact range and flight profile of the BRAVO family depends on the vehicle's mass, wind speeds and maximum altitude. As described in chapter 10, the Martini Method is used in order to determine the landing site of the vehicle. Using the Flight Performance tool, a number of mission scenarios can be compiled for a number of different conditions. Table 13.1 displays the capability of the BRAVO family based on wind speed data taken from [6] for KNMI's De Bilt location. Furthermore, Table 13.1 shows how the system reacts to different wind conditions and different wing loading ($\frac{W}{S}$) which are the two primary factors which influence the performance of the system. Drawing conclusions from this, it can be seen that for higher winds a higher wing loading is advantageous, as it allows the glider to fly at a higher true airspeed, resulting in a higher fraction of that true airspeed going to the ground speed. Farther solidifying this is the fact that the range in zero wind conditions actually suffers with a higher wing loading, meaning that there is a balance to be had.

Table 13.1: Range of the BRAVO system based on a maximum altitude of 33 km, spiral altitude of 1.5 km and different wind speeds.

Vehicle type	MTOM [kg]	Range [km] no wind	Range [km] avg wind	Range [km] +1 SSD wind	Range [km] +2 SSD wind
BRAVO Mini	0.750	463	270	195	142
BRAVO Max	2.6 (0.6kg payload)	478	267	188	133
	3 (1kg payload)	477	276	199	143
	3.5 (1.5kg payload)	475	286	209	154
	4 (2kg payload)	474	294	218	163

13.2. Performance from selected locations

As it is the ambition to use the system not only in De Bilt but worldwide, it needs to be ensured that the system's performance is sufficient in the highest number of locations possible. To analyse how the system would perform in these cases, a number of locations were picked scattered around the world to represent as diverse set of different weather patterns. The locations besides De Bilt were: Broadmeadow in Australia, Boulder in the USA, Macquarie Island in Australia, Paramaribo in Suriname, as well as the South Pole in Antarctica. For analyse performance, past ozonesonde data [6] from these locations was used, and the system performance was calculated for each data point. From the GNSS locations in the data, the drift from launch to burst can be calculated. From the wind data, a wind profile can be generated and put into the flight performance tool to get the range. By subtracting the drift from the excess-range can be calculated. This was done three time for each data point for BRAVO mini, as

well as BRAVO max with ozonesonde and 2 kg payload respectively. It should be noted, however, that the data was taken from past ozonesonde launches, which are only launched once a week for most locations and therefore also have some flexibility for the launch time. Consequently, they may not be completely representative of everyday conditions, as for adverse weather conditions the launches can be moved by some time. Furthermore, the ozonesondes don't always reach an altitude of 33 kilometres. This was taken into account in the performance calculation and leads to degraded performance on those days.

The most important metric is the percentage of returns to the launch site, so in how many percent of days the excess range is above 0. A histogram of the excess-range of BRAVO mini for the six stations is provided in Figure 13.1. The diagrams for BRAVO max are very similar with only minor differences and are therefore not shown here. From the histogram it can be seen, that for all but one station, Macquarie Island in Australia, the glider manages to return to the launch site in at least 90% of cases. A table including the return percentages for BRAVO mini and BRAVO max in two configurations is given in Table 13.2 to give an indication of how well the system will perform for other potential customers. It needs to be noted that performance calculations based on wind forecasts will be done, allowing to know in advance if BRAVO is at risk of not returning to the launch site. In these cases it can be decided to launch traditional radiosondes instead to avoid a loss of the system. Therefore, BRAVO can still be viable in locations where wind conditions sometimes prevent the return to the launch site, as long as good wind forecasts are available.

Table 13.2: The probability of returning to the launch site for BRAVO mini and BRAVO max

	BRAVO mini	BRAVO max + ozonesonde	BRAVO max + 2 kg payload
Broadmeadows, AU	96.5%	96.5%	98.2%
Boulder, US	99.0%	99.0%	99.2%
De Bilt, NL	90.9%	90.6%	92.5%
Macquarie, AU	63.9%	63.4%	67.4%
Paramaribo, SR	100.0%	100.0%	100.0%
South Pole, AQ	99.0%	99.0%	99.4%

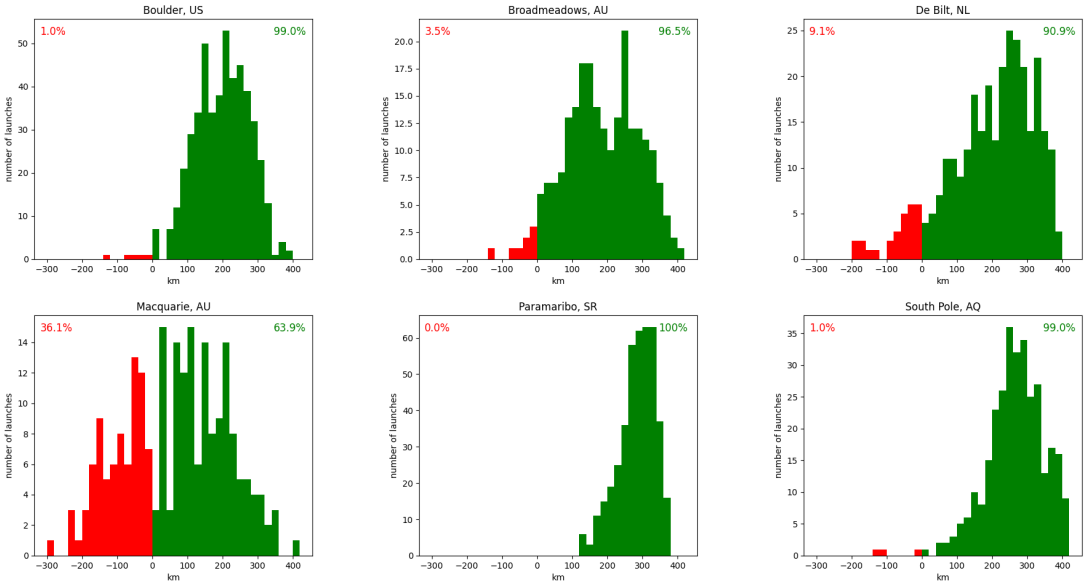

Figure 13.1: BRAVO mini excess-range for different stations

13.3. Technical Drawings

Below, technical drawings of both BRAVO Mini and Max can be seen. These technical drawings provide a top-level overview of the different aircraft, covering some of the more critical dimensions, aerodynamic characteristics and key features that the vehicles contain. Note that the weight for BRAVO Max is given as a range from 2.021 to 4.021 kg as this depends on the payload mass (ranging from 0 to 2 kg).

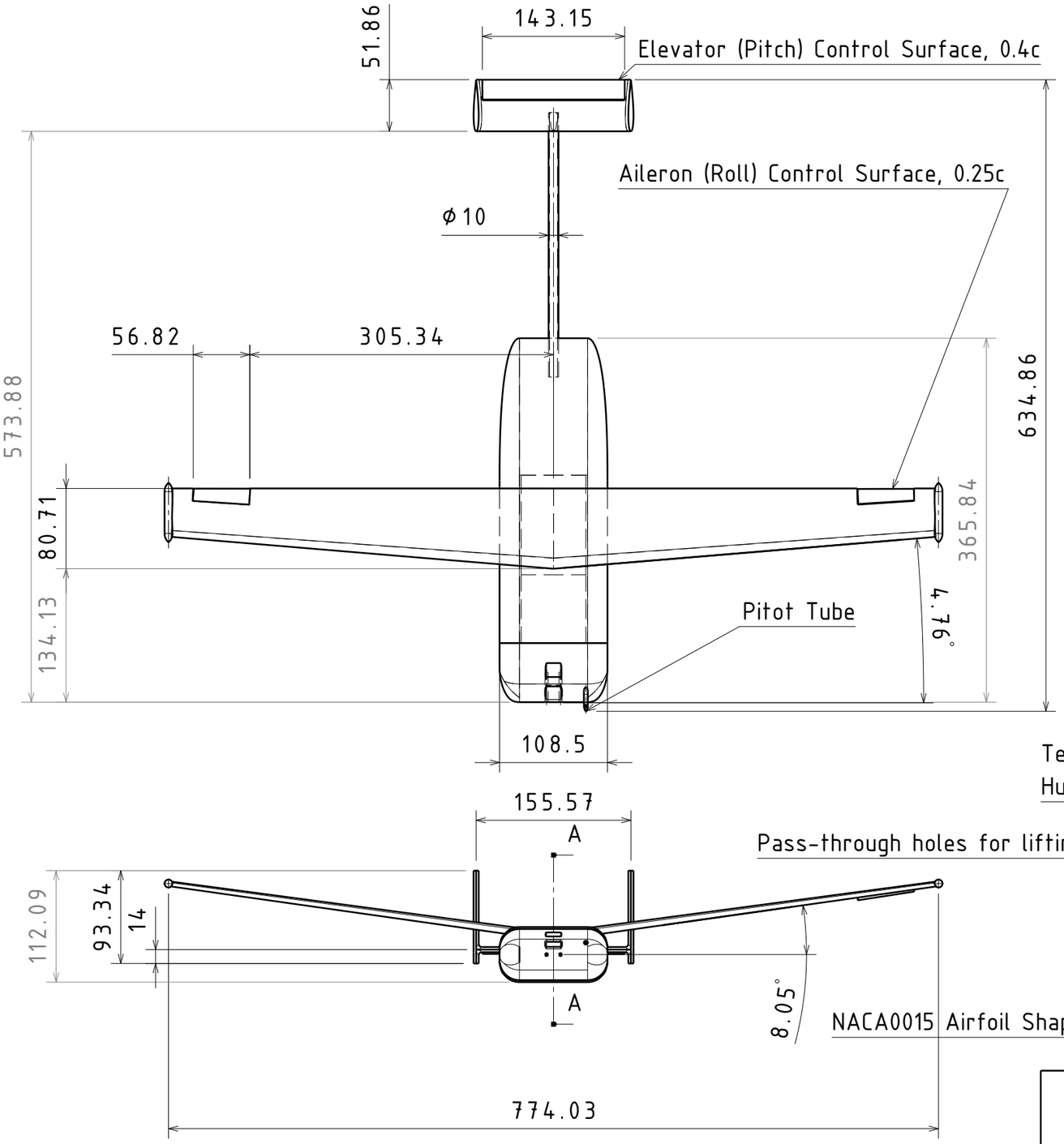

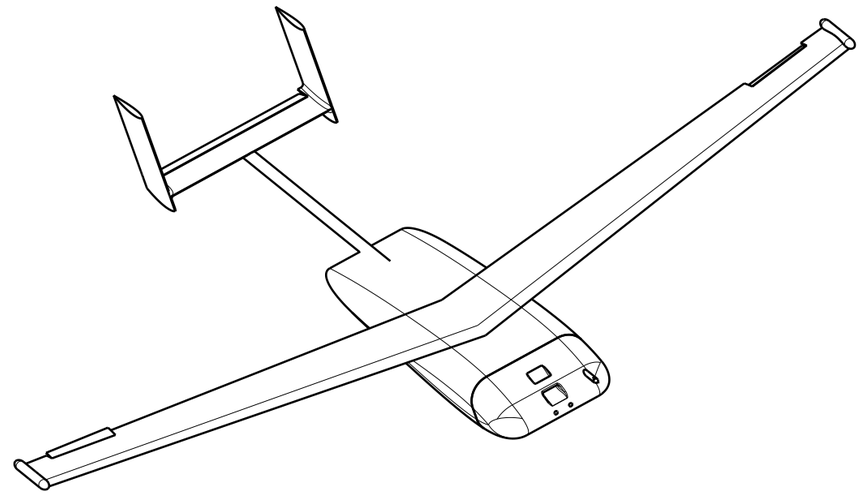

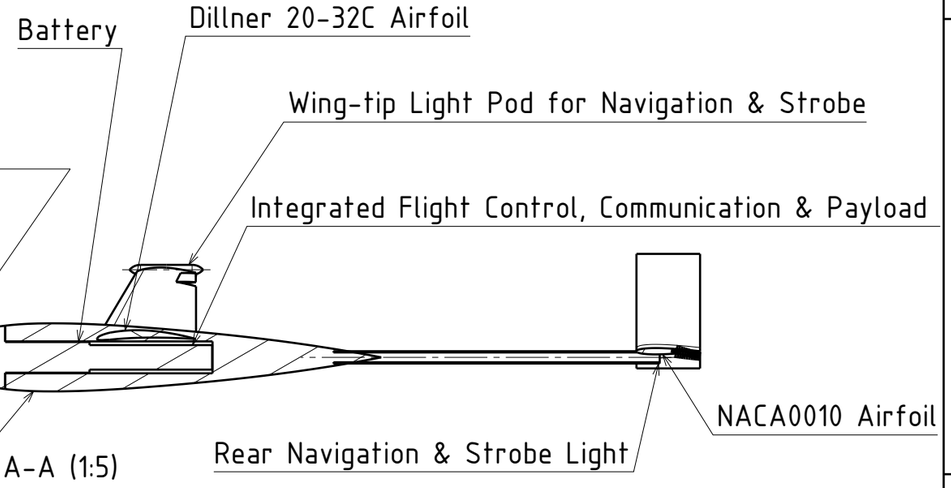

A-A (1:5)

Please note that this drawing is for informative purposes only and does not comply with the TUDelft standards for technical drawings.

DRAWN BY: Rafael Milla-Koch	DATE: 15-06-2023
CHECKED BY: Varun Gottumukkala	DATE: 20-06-2023
DESIGNED BY: 2023 DSE Group 01	DATE: 15-06-2023

DASSAULT SYSTEMES

DRAWING TITLE: BRAVO Mini Glider

SIZE	DRAWING NUMBER	REV
A3	01	14

SCALE	WEIGHT(kg)		SHEET
1:5	0.750		1/1

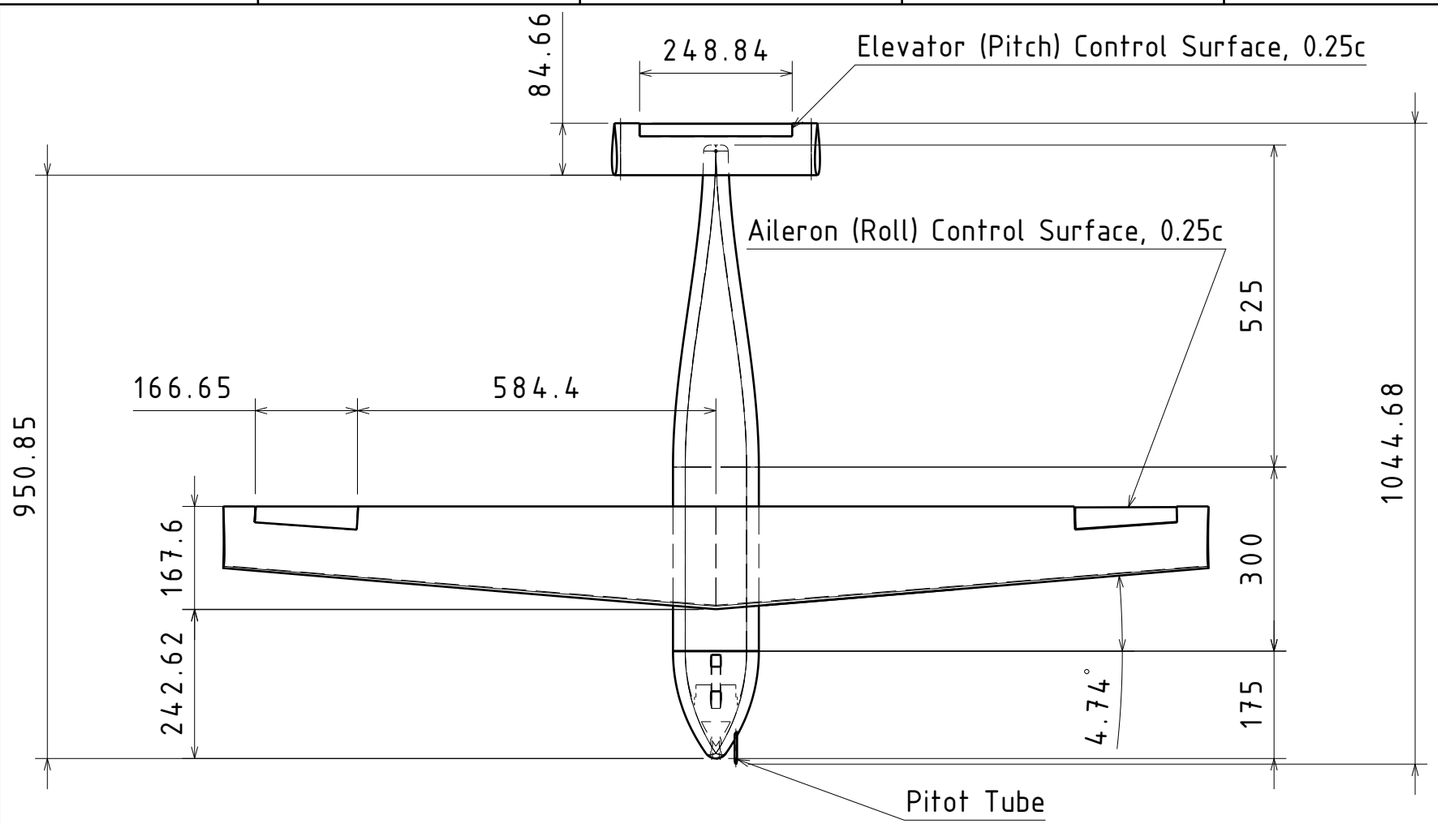

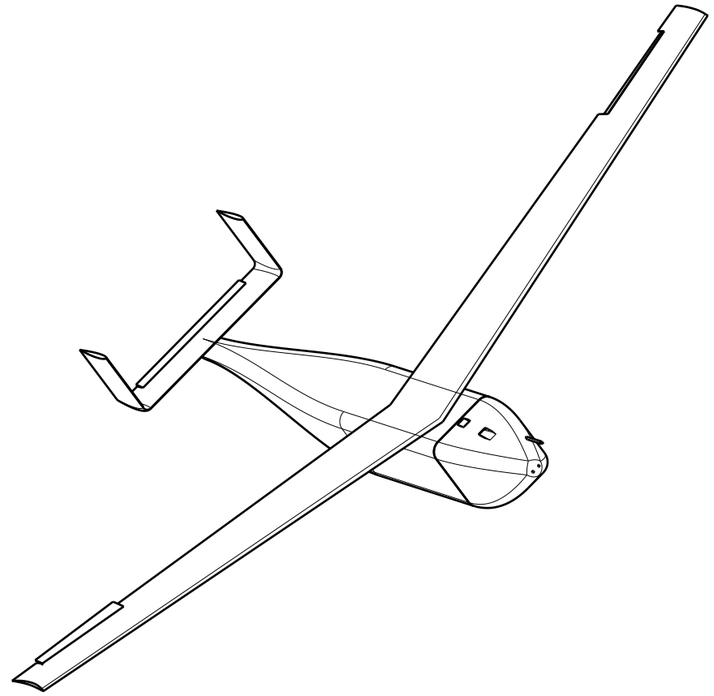

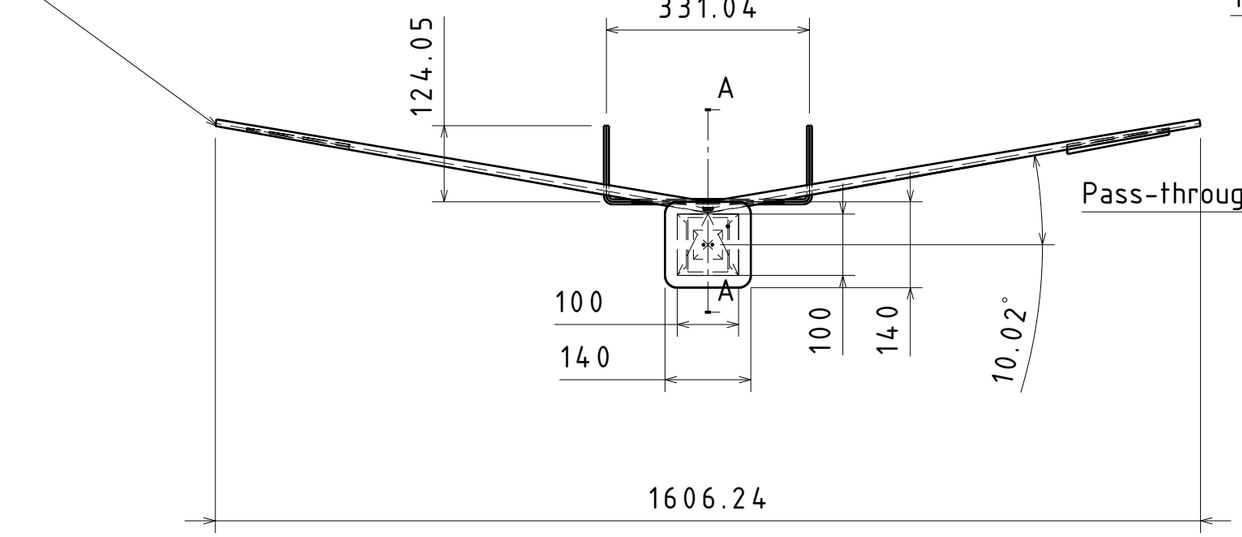

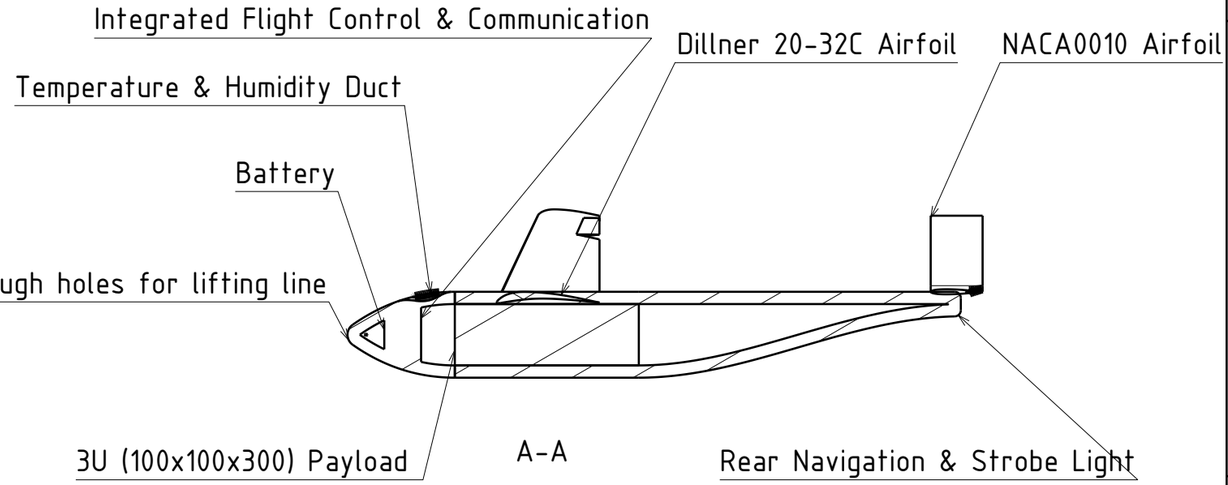

DASSAULT SYSTEMES

DRAWN BY: Rafael Milla-Koch	DATE: 16-06-2023	DRAWING TITLE: BRAVO Max Glider	
CHECKED BY: Varun Gottumukkala	DATE: 20-06-2023	SIZE: A3	DRAWING NUMBER: 01 / REV: 15
DESIGNED BY: 2023 DSE Group 01	DATE: 16-06-2023	SCALE: 1:10	WEIGHT(kg): 2.021-4.021 / SHEET: 1/1

Please note that this drawing is for informative purposes only and does not comply with the TUDelft standards for technical drawings.

13.4. Compliance Matrix

Given the finalisation of the design, the compliance of the design with previously set-up requirements needs to be checked. Several requirements have not been met due to them being infeasible and in order to achieve the best possible system overall. The requirements used are listed below in Table 13.3, which also states whether they have been satisfied.

Table 13.3: Compliance matrix for the BRAVO system

Operations	Requirement	Compliance
WBA-OP-001	The system shall be launchable twice a day	Yes
WBA-OP-002	The system shall be able to operate in day- and nighttime conditions	Yes
WBA-OP-003	The system shall be able to be made ready for transport in 8 [hr]	Yes
WBA-OP-004	The system shall be able to be transported by road	Yes
WBA-OP-005	The system shall be able to be transported by sea	Yes
WBA-OP-006	The system shall be transportable in at most a 20 [ft] container	Yes
WBA-OP-007	The system shall have an expected operational lifetime of 5 [years]	Yes
WBA-OP-008	The system shall have a transport mass of at most 24000 [kg] including container	Yes
WBA-OP-SCH-001	The system shall be designed in 10 weeks	Yes
WBA-OP-SCH-002	The system shall be designed by 10 people	Yes
WBA-OP-SCH-003	The system shall be designed with 2.05Fte	Yes
WBA-OP-ENV-001	The system shall be carbon-neutral during operations	No
WBA-OP-ENV-002	The system shall only use renewable energy	Yes
WBA-OP-ENV-003	The system shall not release non-renewable resources into the atmosphere	Yes
WBA-OP-RES-001	The flying component of the system shall not exceed a unit cost of 75[k€]	Yes
WBA-OP-RES-002	The system shall require a maximum of 1 active personnel for operation	Yes
WBA-OP-RES-003	The system shall be storable in a 20 [ft] container	Yes
WBA-OP-RES-004	The system shall only rely on renewable consumables	Yes
WBA-OP-RES-005	The system shall be operable by trained personnel	Yes
WBA-OP-RES-006	The system shall be able to attain an altitude change of 15 [m] within a horizontal distance of 200 [m] during take-off and landing	Yes
WBA-OP-RES-007	The individual parts of the system when disassembled shall weigh less than 25 [kg]	Yes
WBA-OP-REG-001	The system shall have a fault rate less than 10^-6 per year	Yes
WBA-OP-REG-002	The system shall have an ADS-B transponder	No
WBA-OP-REG-003	The system shall remain within a pre-defined operating area	Yes
WBA-OP-REG-004	The system shall be able to avoid other aircraft in flight	No
WBA-OP-REG-005	The flight path of the system shall be known and sent 12 [hr] in advance to ATC	No
WBA-OP-REG-006	The system shall be able to avoid prohibited flight zones in the Netherlands	Yes
WBA-OP-REG-007	The system shall comply with regulations for transport	Yes
Mission	**Requirement**	**Compliance**
WBA-MIS-001	The system shall be able to reach any specified horizontal position within the Netherlands mainland	No
WBA-MIS-002	The system shall be operated and stored in De Bilt	Yes
WBA-MIS-003	The system shall be reusable during its operational lifetime	Yes
WBA-MIS-ASC-001	The system shall be able to ascend in weather conditions as defined in requirement subset WBA-MIS-WEAT	Yes
WBA-MIS-ASC-002	The system shall be able to reach an altitude of 33 [km] in 1.5 [hr]	No
WBA-MIS-DES-001	The system shall be able to descend back to the launch site from its maximum mission radius	Yes
WBA-MIS-DES-002	The system shall remain vertically controllable during the entire descent	No
WBA-MIS-DES-003	The system shall be able to follow a flight path	Yes
WBA-MIS-DES-004	The system shall remain horizontally controllable during the entire descent	Yes
WBA-MIS-DES-005	The system shall be able to descend in weather conditions as defined in requirement subset WBA-MIS-WEAT	Yes
WBA-MIS-DES-006	The System shall be able to determine its position to within 2 [m]	Yes
WBA-MIS-TA-001	The system shall be able to be transport from the launch site to a storage site	Yes
WBA-MIS-TA-002	The system shall be able to be transport from the storage site to the launch site by the operating personnel	Yes
WBA-MIS-TA-003	The system shall be maintainable by trained individual	Yes
WBA-MIS-TA-004	The system shall carry a payload which can be replaced	Yes
WBA-MIS-TA-005	The system shall have a turn around time at most 8 hours	Yes
WBA-MIS-TA-006	The system shall be able to receive regular maintenance in less than 12 [hr]	Yes

WBA-MIS-WEAT-001	The system shall operate with wind speeds of up to 30 [m/s] at 10 [m] above ground level	Yes
WBA-MIS-WEAT-002	The system shall operate during wind speeds of 60 [m/s] at 10 [km]	Yes
WBA-MIS-WEAT-003	The system shall operate within a temperature range of 200 [K] to 320 [K]	Yes
WBA-MIS-WEAT-004	The system shall be able to withstand a rainfall of 10 [mm/h]	Yes
WBA-MIS-WEAT-005	The system shall be able to withstand snow fall	ND
WBA-MIS-WEAT-006	The system shall be able to withstand hailstones up to 4 [mm]	ND
WBA-MIS-WEAT-007	The system shall be able to withstand ice formation	Yes
WBA-MIS-PAY-001	The system shall be able to carry a payload of 2[kg]	Yes
WBA-MIS-PAY-002	The payload shall be replaceable by an operator	Yes
WBA-MIS-PAY-003	The system shall have 22[W] available for the payload	Yes
WBA-MIS-PAY-004	the system shall be able to measure every 50[m] of vertical displacement	Yes
WBA-MIS-PAY-005	The system shall be able to measure with an interval of at most 10[s]	Yes
WBA-MIS-PAY-MEAS-001	The system shall be able to measure temperature in the range of 200 [K] up to 350 [K]	Yes
WBA-MIS-PAY-MEAS-002	The system shall be able to measure temperature with a resolution of 0.1[K]	Yes
WBA-MIS-PAY-MEAS-003	The system shall be able to measure temperature with a min. accuracy of 0.5[K]	Yes
WBA-MIS-PAY-MEAS-004	The system shall be able to measure magnitude of the wind speed with an accuracy of 0.15 [m/s]	Yes
WBA-MIS-PAY-MEAS-005	The system shall be able to measure direction of the wind speed with an accuracy of 2 [degrees]	Yes
WBA-MIS-PAY-MEAS-006	The system shall be able to measure relative humidity in the range of 0-100 [%]	Yes
WBA-MIS-PAY-MEAS-007	The system shall be able to measure RH with a resolution of 1 [%]	Yes
WBA-MIS-PAY-MEAS-008	The system shall be able to measure RH with an accuracy of 5 [%]	Yes
WBA-MIS-PAY-MEAS-009	The system shall measure ozone levels with a resolution of parts per billion(PPB)	ND
WBA-MIS-PAY-MEAS-010	The system shall be able to measure ozone levels in the range of 0 to 10 parts per million (PPM)	ND
WBA-MIS-PAY-MEAS-011	The system shall be able to measure static pressure in the range of 1080 [hPa] to 3 [hPa]	Yes
WBA-MIS-PAY-MEAS-012	The system shall be able to measure static pressure with a resolution of 0.1 [hPa]	No
WBA-MIS-PAY-MEAS-013	The system shall be able to measure static pressure with an accuracy of 1 [hPa] above 100 [hPa] and 0.6 [hPa] below	Yes
WBA-MIS-PAY-MEAS-014	The system shall be able to measure NOx concentration	ND
WBA-MIS-PAY-MEAS-015	The system shall be able to measure NOx concentration with a resolution of 10 PPB	ND
WBA-MIS-PAY-MEAS-016	The system shall be able to measure NOx concentration with a range of 0 to 2.0 PPM	ND
WBA-MIS-PAY-MEAS-017	The system shall be able to measure CO2 concentration	ND
WBA-MIS-PAY-MEAS-018	The system shall be able to measure CO2 concentration with a resolution of 0.1ppm	ND
WBA-MIS-PAY-MEAS-019	The system shall be able to measure CO2 concentration with a range of 250 to 520 PPM	ND
WBA-MIS-PAY-MEAS-020	The system shall be able to measure particulate matter density	ND

14

Production Plan

This chapter provides the production plan for the BRAVO Mini and Max aircraft. The thought process of developing a production plan can aid in determining the manufacturability of the system and associated challenges. This is critical, as a system which cannot be manufactured is of no use. The main production steps are first briefly described in section 14.1, and a flow-chart outlining the production tasks and sequence is presented in section 14.2.

14.1. Production steps

The production steps for BRAVO Mini and Max are very similar. Both gliders differ in shape and size but are comprised of the same sections and electronics and materials. The difference in shape and size do not result in very different manufacturing processes, so the steps discussed and shown in Figure 14.1 apply for both the BRAVO Mini and Max.

The fuselage, wing, and tail sections will be manufactured separately. The electronics that need to be placed within the sections will first be installed, and then the fuselage, wing, and tail sections will be assembled. The fuselage of the Bravo Mini and Max will be assembled in two halves along the x-y plane. This is to allow for a feasible manufacturing process to create the hollow interior of the fuselage. The manufacturing processes used are CNC routing, Wire-cutting, laser-cutting and composite laminating. The primary joining method used is glueing.

The ascent and landing phases involve components other than the glider. The balloons used for ascent will and the net used for landing are both commercially available and can be purchased. Therefore, they are not included in the production plan. Furthermore, certain subcomponents manufacturing such as PCB printing and assembly of circuitry is not described in Figure 14.1 as these processes can easily be outsourced at a lower cost.

14.2. Flow-chart

A flow-chart of the production plan is provided in Figure 14.1. The production steps of each glider section and their assembly to form the final product is shown. Tasks that are unique to the BRAVO Mini and Max are accordingly indicated. Section-specific tasks are stated in orange boxes, and green boxes indicate the completion of section or assembly phases.

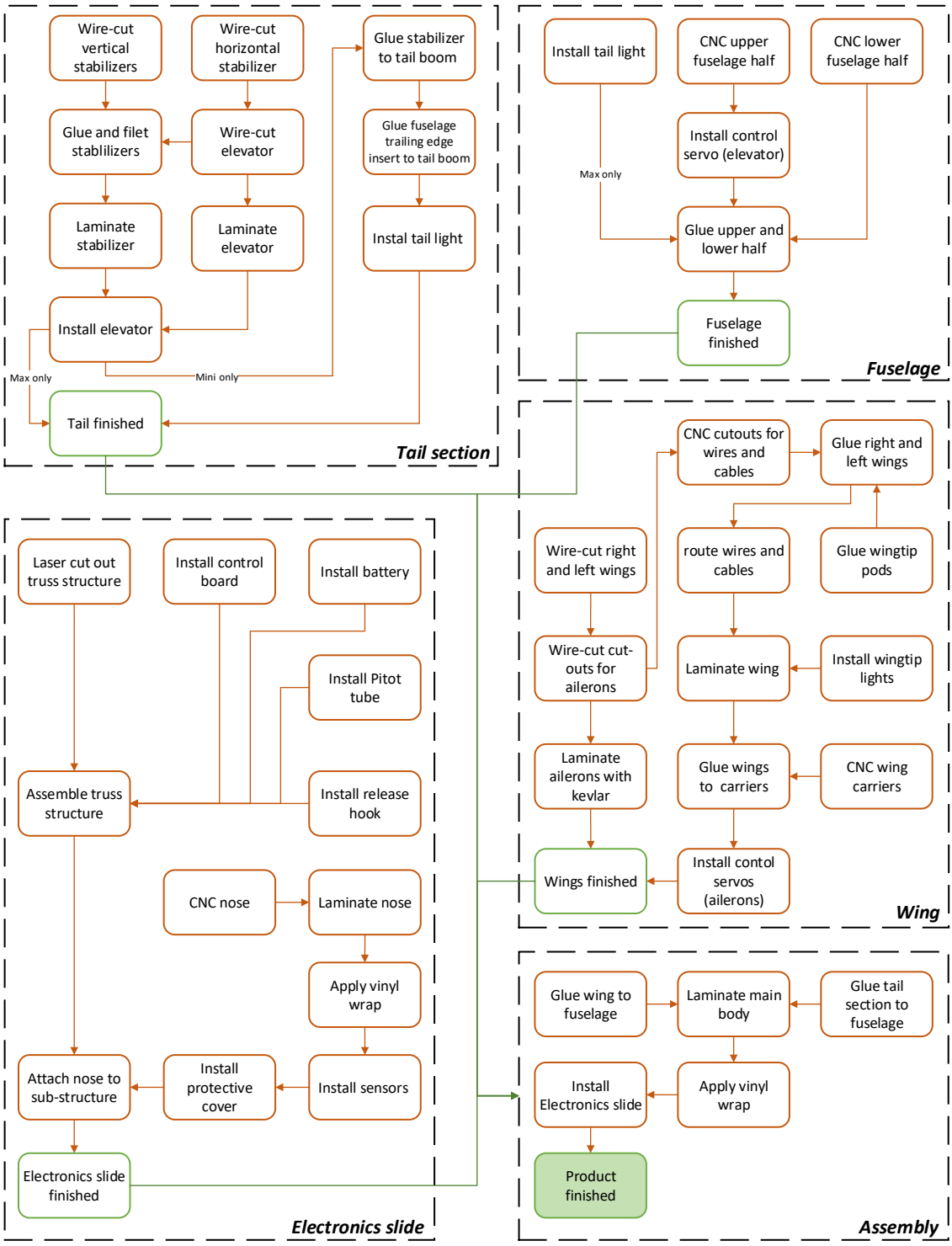

Figure 14.1: Flow-chart outlining Production Steps

15 Logistics & Operations

The logistics and operations of handling weather balloon launches with the drone system are not trivial. There are certain aspects in the operation of this new system that require specific new protocols. In this chapter, the most significant operational challenges and protocols will be elaborated upon. The first integration step is the selection and return protocols of the landing sites, which will be explained in section 15.1. Since the vehicle can actively control itself, it must comply with the UAV regulations. The specific rules that are of importance will be explained in section 15.2. Since the operations of the system have significantly changed, a change in launch preparation procedures is also required. How this change is going to affect the procedures is described in section 15.3. Furthermore, the calibration of the onboard sensors will differ from that of the original sonde systems currently used. The new calibration procedure and how it differs from the old calibration procedure will be explained in section 15.4. Since the system must attain a very high return rate, regular inspection of the system is required, which will be described in section 15.5, and regular maintenance which will be described in section 15.6 must be performed. A description of how to set up the glider is beyond the scope of this report, as the design of the system is not yet finalized.

15.1. Landing Sites

In order to ensure the safe return of the aircraft, a number of landing sites must be established. This section will explain how the ideal landing sites are selected and, further, what infrastructure these sites will require. To get a better understanding of the return procedure, Figure 15.1 has been generated. This flow chart shows how the vehicle will determine the landing site based on its position and the predetermined flight profile, described in chapter 10.

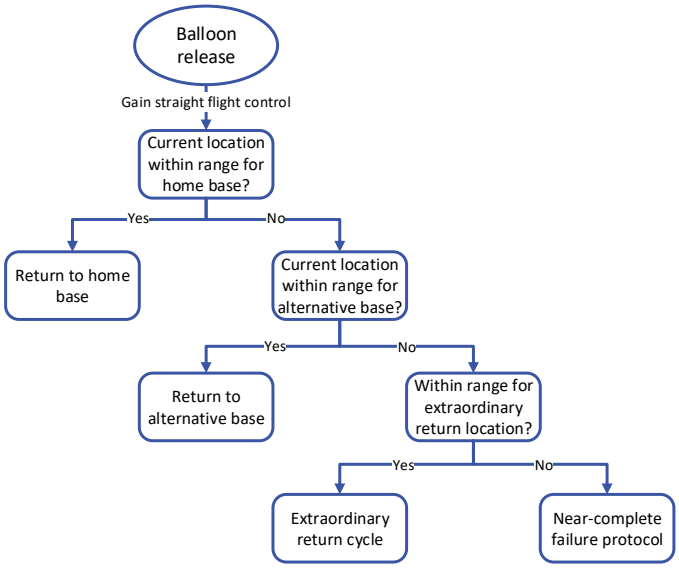

Figure 15.1: Return protocol

In this section, all the possible outcomes of the flowchart are analysed. First, the regular return cycle will be explained in subsection 15.1.1. After this, the secondary return cycle will be explained in subsection 15.1.2. Finally, the return cycle for a near complete failure scenario will be explained in subsection 15.1.4.

15.1.1. Regular return cycle

In case the aircraft has stable, steady control and is within the ”martini glasses” as defined in section 10.4. The vehicle will fly the optimal flight trajectory back to the launch site. The ”martini method” has been developed so that, if no unexpected conditions occur, the glider can simply return to the launch site. This is the condition that the vehicle has been designed for.

15.1.2. Secondary return cycle

In some cases, it is possible that the aircraft gets out of bounds of the ”martini glasses”. In this case, the system is set up such that it will return to these secondary bases if the release altitude is outside the main landing range but inside the range of another landing site. This landing can be considered a normal landing, meaning that the system is expected to show the same wear due to landing as in the case of landing back at the original base. The system can then be retrieved at this alternative landing site for re-use at the original base. The regular and secondary return cycle should account for over 99 percent of all launches. It can be considered that the two cases below are true emergency cases, in which, it is likely that a serious failure has already occurred.

15.1.3. Extraordinary return cycle

In case of an extraordinary return cycle, numerous landing spots are selected, roughly on an interval of 10 km radially, where the system can relatively safely return with the expectation that the fatality rate due to the selection of these landing spots will be zero. A practical example of this would be a farmer’s field or an abandoned airport. In this case, the aim is to keep the fatality rate as low as possible, it is not the primary aim any more to keep the vehicle intact.

15.1.4. Near-complete failure

The final scenario is truly the worst-case scenario: the system is not able to return to any of the primary or secondary landing sites, therefore, in this case, the system circles down from the altitude at which it identifies that there is no possibility for landing at an extraordinary landing location. 100m above the ground, the system starts to fly straight again with the aim to allow for flight path predictability of anyone observing this event from the ground and aims to reduce velocity to 1.5 times the landing speed. 10m above the ground, the system starts to flare until stall occurs. The reason for flying at this relatively high speed until just before landing is that the most likely scenario in which this occurs is when ice formation has occurred on the wing, therefore the true stall speed might in fact at a higher speed than expected. Due to the severity of the consequences of this scenario, further research can be done to make sure that in this scenario the flight computer can autonomously search for the location with statistically the lowest likelihood of hitting any person. This is however out of the scope of this report.

15.2. UAV Regulations

Regulations for UAVs in the EU are maintained by the European Union Aviation Safety Agency (EASA). There are three categories of drones specified by EASA: open, specific, and certified, which correspond to low, medium and high risk categories, respectively.

A distinction is made between autonomous and automatic drones. Autonomous drones are capable of intelligent flight, enabling them to cope with unforeseen and unpredictable emergency situations. On the other hand, an automatic drone follows a pre-determined path defined by the drone operator before the flight. It is essential that the drone operator remotely takes control of the drone to intervene in unforeseen events for the which the drone has not been programmed. BRAVO falls within the autonomous drone category, as the glider is designed to return to the launch site without any human intervention.

While there is no available regulation for autonomous UAVs specifically, according to EASA, ”*‘Unmanned Aircraft’ means any aircraft operating or designed to operate autonomously or to be piloted*

remotely without a pilot on board" [50]. Thus, all regulations for 'Unmanned Aircraft' were deemed applicable for autonomous gliders. Autonomous drones are not permitted in the open category, as they require certain levels of verification and compliance with technical requirements. Autonomous drones are allowed in the 'specific' and 'certified' categories, but only up to an altitude of 120 m above ground or water. Thus, the aircraft would need to fly in the 'certified' category, in which flights are currently not permitted in the Netherlands. It is highly likely that new regulation is required for operating the glider, but since KNMI is a government organisation and the drone flights have a social and economic purpose, obtaining permission is a process that should not be underestimated, but will likely not be limiting for the integration of the system. The actual integration and the interaction between the weather institutes, the legislator and the governing air traffic control body is outside of the scope of this report.

15.3. Launch Preparation

This section describes the preparations required to launch a BRAVO glider. The ability of the glider to return to the launch site and carry custom payloads introduces certain risks and considerations. In particular, the payload mass and wind conditions affect the range of the glider and the kind of balloon used. The pre-launch user inputs and outputs are shown in Figure 15.2.

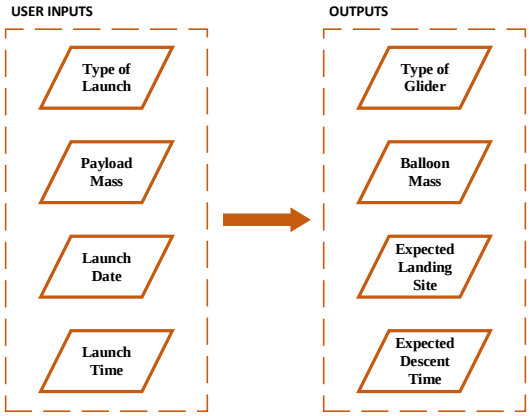

Figure 15.2: Pre-launch User Inputs and Outputs

The types of launch can either be the BRAVO Mini with a sounding payload of the BRAVO Max with an ozonesonde or custom payload. The custom payload can have a mass up to two kilograms. It is important to note that for very light payloads it may be beneficial to add additional mass, especially in high wind conditions, as this increases the range of the glider. This does add more weight and may require a larger balloon and volume of the filling gas, thus driving up the operational costs.

The launch data and time will be used to determine the corresponding wind forecast. This wind forecast data will be used to update the range prediction. However, at the time of writing the report, it was out of the scope to assimilate wind forecast data into the existing historical wind dataset. With the addition of wind forecast data, the accuracy of the expected range will be greatly improved.

Once the payload is secured in the glider and the balloon size is chosen, the balloon can be inflated, and the winding can be attached to the glider. Then, the glider can be treated as a regular radiosonde or ozonesonde payload, but it must be noted that the weight will be significantly larger. The BRAVO Mini weighs 0.750 kg and the BRAVO Max can weight up to 4.021 kg. The weights of the gliders are however low enough to be comfortably handled and launched by operators.

An example of potential user inputs and the corresponding outputs is provided in Figure 15.3a and Figure 15.3b. The launch site and date inputs are omitted, as the current program does not include the effects of wind forecasts.

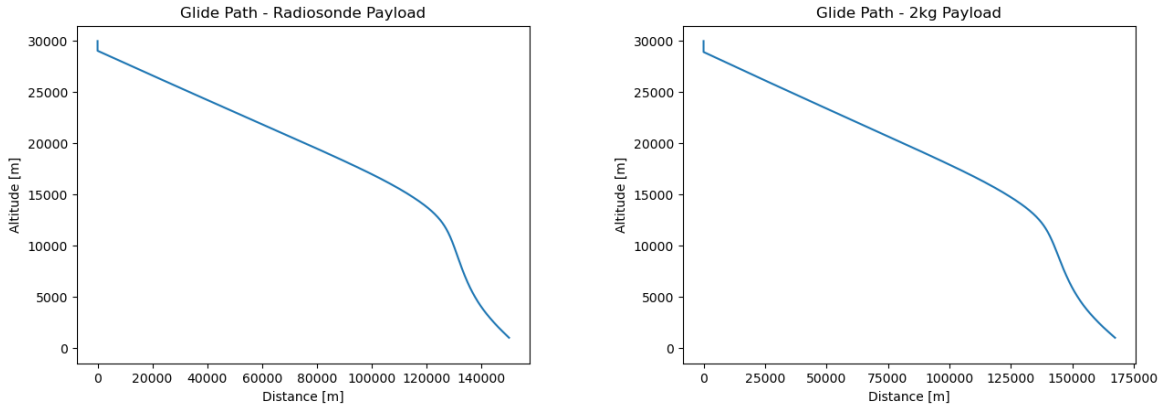

(a) Glide path of BRAVO Mini for a radiosonde payload

(b) Glide path of BRAVO Max for a 2 kg payload

Figure 15.3: Glide paths for different payloads

Figure 15.3a shows the glide path for the worst-case wind conditions for a radiosonde payload being launched on the BRAVO Mini, while Figure 15.3b shows the same for a maximum payload of 2kg launched on the BRAVO Max. Both glide paths are very similar in shape because they both represent the optimal descent trajectory to ensure maximum range.

15.3.1. Using hydrogen as a filling gas

KNMI has already used hydrogen as a filling gas in the past. It is advised that the KNMI takes the already existing procedures and updates them based on the new, to-be regulations of the ”Rijksdienst voor ondernemend Nederland” which are described in the Generic guidelines for hydrogen safety (”Generieke richtsnoer waterstofveiligheid”[51]). The superposition of both the existing procedures and the guidelines should provide a method that allows the KNMI to use hydrogen as a filling gas.

15.4. Calibration

System calibration for the BRAVO mini and BRAVO Max is slightly different, but they rely on the same principle. For both systems, the payload including the sensor package can be removed from the system for calibration, and the sensor package, including the flight computer, has a docking station which supports the three required tasks. Those are: storing the sensor package, charging the battery and calibration of the sensor package. There is two-way communication between the docking station’s calibration device and the sensor package, allowing the system calibration to be updated in the sensor package as well, instead of in post-processing.

15.5. Inspection

In order to ensure the desired return rate of the aircraft, it is of the utmost importance that the glider itself is in the best condition that can be achieved. Therefore, after every landing, the system must be checked for damages. In case significant damage is found, it is advised to replace the part in question. Furthermore, it is important to validate that the control surfaces are intact and that they are all operative. Another significant factor that needs to be considered is the functionality of the lighting. For this, it is important that: first, the navigation lighting is functioning and second, that the anti-collision lighting is functioning. In case any of these electronics are not functioning properly, they need to be replaced via the procedures laid out in section 15.6.

15.6. Maintenance

The maintenance procedures of BRAVO Mini and BRAVO Max are mostly similar but differ slightly. Therefore, they are explained separately in subsection 15.6.1 and subsection 15.6.2.

15.6.1. BRAVO Mini maintenance

The maintenance capabilities of the BRAVO mini are limited to replacing the lights as well as the nose, Pitot tube, and temperature plus humidity sensor. Along with this, the entire airframe or electronics slide may be replaced. The lights on the wings and tail are protected by a fairing that can be removed by removing two screws. After this, the lights can be removed and replaced. For the wings, the most forward light is the navigation light, the most aft light the anti-collision light, for the rear light there is only one light present.

Unfortunately, certain components of Bravo Mini are not replaceable, namely, the elevator and the aileron control servos, as well as the wing section. This means that the entire airframe must be replaced, but the electronics slide may be reused.

15.6.2. BRAVO Max maintenance

The maintenance capabilities of the BRAVO Max include all the same replaceability as the BRAVO Mini, along with the ability to replace the entire wing section as well as the aileron servos.

The lights can be replaced in the same fashion as on the BRAVO Mini. In case a servo from the ailerons ceases to function, it can be replaced by removing the wing section and replacing the entire servo along with the associated wiring and connector.

Unfortunately, certain components of Bravo Max are not replaceable, namely, the elevator control servo. This means that the entire airframe must be replaced.

16
Sustainability

This chapter discusses the sustainability of the BRAVO Mini and Max. The inclusion of sustainability in the design approach is first discussed in section 16.1. The sustainability of the entire life-cycle of the gliders is considered, from manufacturing to operation to end-of-life, which is discussed in section section 16.2 through section 16.4. The impact of the mission itself with regard to broader sustainability issues is discussed section 16.5.

16.1. Design Approach

The design phase of the glider began with a thorough understanding of the sustainability of conventional weather balloons. The biggest improvement in sustainability is the recovery of payloads after launching and the lack of a propulsion system. The glider itself has zero emissions, as, by definition, it does not utilise any propulsion method. During the design of the glider, the sustainability of the glider itself and its contribution to sustainability during the operation was accounted for.

The initial sustainability requirements included a requirement of the system being carbon-neutral and causing zero emissions. However, these two requirements were deemed to be killer requirements, as there were no feasible design options that satisfied the requirements. Based on preliminary calculations, it was impossible to reach the required altitudes with a sustainably-powered vehicle. Using a balloon for ascent was one of the few feasible options. The possibility of retrieving the balloon and gas upon return was considered, but the extra weight and space occupied by the balloon, gas, and associated mechanisms would lead to an infeasible design. These considerations, along with several other technical, operational and logistical factors, lead to the selection of the glider and balloon concept.

The driving performance indicator was the range of the gliders, which was positively correlated with the mass of the gliders. However, a larger mass requires a larger balloon, and consequently, more hydrogen, to lift the mass to the required altitude. These negatively affect the sustainability of a mission, and therefore the range of the glider was limited to ensure it meets performance requirements but does not use an unnecessarily large balloon or excess hydrogen.

The logistics of the missions were also planned keeping sustainability in mind. For the De Bilt case study, a network of alternative landing sites was determined to allow for diverted landings in unforeseen scenarios such as extreme winds. Landing sites were strategically chosen based on statistical data of historic burst and land locations. However, due to the large ranges, the initially determined landing sites were very far apart, with an average distance between launch sites being over 200 km. This would lead to emissions caused by the transport of the glider back to the main launch site. It was therefore decided to include landing sites closer to the launch site, in order to limit the distances required to for transport. This can be avoided if each alternative landing site also has the capability to launch the BRAVO Mini and Max. A collaboration between launch/land sites in different countries would then be required.

16.2. Manufacturing Emissions

The manufacturing emissions comprise a significant fraction of the life-cycle emissions; the operational emissions are limited to the release of hydrogen when the balloon bursts. The BRAVO Mini and Max both have the same material composition: EPP (Expanded Polypropylene) foam for the core and aramid fibres for the outer skin. EPP foam can either be produced using an autoclave or an extrusion process. Both are very energy-intensive processes, but the amount of foam required is very small. To keep the

aramid fibres in solution while spinning, sulphuric acid is used. If disposed of, the sulphuric acid can cause significant harm to plants and animals.

Apart from the emissions associated with the production of the glider structure, there are also emissions caused due to the production of the internal electronics. In particular, amongst the several sensors, processors, and actuators onboard the gliders, the battery itself is the most energy and resource intensive. Mining lithium requires huge amounts of fresh water, and the remains are toxic and take centuries to be cleared up by nature. Further, most lithium mines are in drought-stricken areas. The mining results in the contamination of water bodies, making the consumption of water for the local population and wildlife very harmful. The heavy machinery used for extraction and long transport distances also cause increased CO_2 emissions. However, the battery being used is relatively small and is only used to power electronics and sensors. In comparison to batteries used to power motors, the environmental impact is orders of magnitude smaller [52].

The actual extent of the manufacturing emissions depends on the nature of the energy used during the manufacturing processes. It is desirable to use 100% green energy, generated entirely by renewable sources. However, evaluating the source of energy used for production is out of the scope of this report.

16.3. Operational Emissions

For powered aircraft flying on liquid hydrogen, the environmental impact is especially harmful due to the emission of water vapour when liquid hydrogen is burned in a combustion engine. When released at altitudes of 25-35 km, the climate impact is 10-20 times worse than conventional aircraft flying at 10 km [53]. However, the BRAVO system only involves the release of pure hydrogen at an altitude of around 30 km. One adverse effect of hydrogen emissions is that it could cause as much as a 10% decrease in atmospheric ozone.

The loss of the balloon material itself is not considered a threat to the environment, as the Totex balloons used are 100% biodegradable. However, a larger balloon is still undesirable as it would require more hydrogen to be inflated. The additional energy and resources used to produce a larger balloon is also not desired. The low-density EPP foam used allows for a very lightweight structural design, thus saving on the size of the balloon and the amount of hydrogen required to lift the gliders

The amount of hydrogen expelled into the atmosphere can be controlled to an extent. In chapter 11, the sizes of balloons needed to provide sufficient lift to reach the required altitudes and the corresponding amount of hydrogen required is discussed. In the interest of limiting operating emissions, it is desired to limit the size of the balloon and hence the amount of hydrogen released upon bursting. Figure 16.1 shows the required amount of hydrogen for lifting different payloads with different balloons.

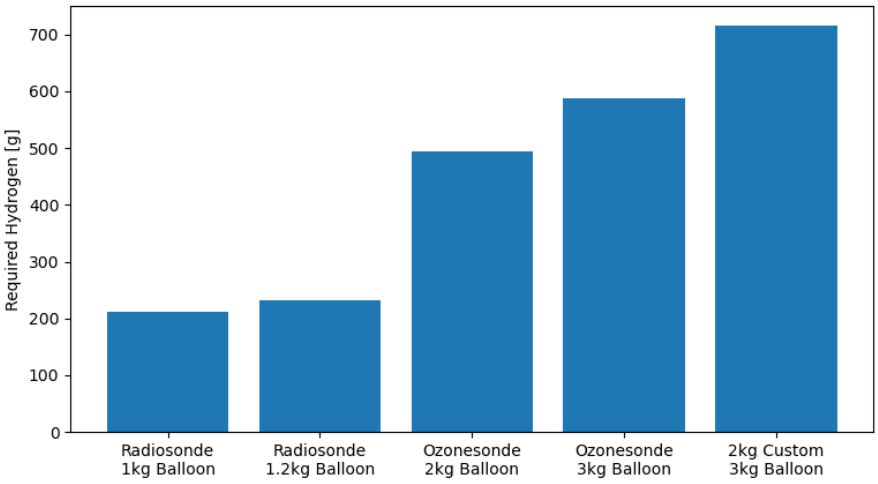

Figure 16.1: Mass of hydrogen required to lift different payloads with different balloons

As shown in Figure 16.1, the amount of hydrogen used varies significantly depending on the kind of launch. A 1kg balloon for radiosonde launches emits almost 3 times less hydrogen than a 3kg balloon for ozonesonde launches. The different balloon sizes for each type of launch determine the ascent rate of each launch, with larger balloons ascending faster. The significantly lower amount of hydrogen emitted during radiosonde launches justifies the decision to design a glider optimised for a radiosonde-only payload. The radiosonde payload on the BRAVO Mini will also be the most common mission, launching at least once a day. Launches with ozonesonde or custom payloads should be limited, as they require much more resources. This is not problematic, as the frequency of measurements for greenhouse gases is not critical, as they do not vary as quickly as meteorological variables. The testing of custom payloads and sensors is also not expected to be as frequent as radiosonde launches.

The choice of using hydrogen as a filling gas has a major advantage over helium in that it is a renewable resource. Unlike Helium, which is extracted from underground natural gas reserves, hydrogen can be reproduced via methods such as electrolysis. While some hydrogen reacts with oxygen to create water vapour, most escapes into space, thus not posing a significant threat to warming. Three factors influence the ability of a gas to escape Earth's atmosphere into space: the mass of the molecule, the escape velocity of the planet, and the heating of the upper atmosphere. As hydrogen is the lightest gas, it can easily escape Earth's atmosphere when released at altitudes of around 30 km [54].

16.4. End-of-Life

EPP foam is made from a single material: polypropylene, which makes it easy to recycle [55]. EPP consists of up to 98% air, making it very resource-efficient [56]. The remaining 2% is a thermoplastic material which can be reheated without structural damage; this means that EPP is 100% recyclable. Defective parts can be ground down and used as material for production [57]. AFRP is not biodegradable, and if left in nature, it will not decompose for centuries. However, it is 100% recyclable. It is chopped into 3-6 mm fibres and re-spun to form fibres for new products [58].

Lithium-ion batteries are made of several metals that are rare and extremely valuable. Most of the materials used in the batteries are recyclable [59]. When not disposed of correctly, metals such as manganese, cobalt and nickel can leak out and contaminate waters [60].

While recycling is the most sustainable option once a product is no longer functional, it is important to first ensure that the material needed to be recycled is limited as much as possible, as energy is required for any recycling process. Thus, the minimum amount of material was used to prevent unnecessary energy and resource consumption.

16.5. Mission Impact

The mission of collecting meteorological and climate data on a regular basis has a significant positive impact on sustainability. Sustainability is not only affected by life-cycle emissions but by several other factors, as outlined in the United Nation's 17 Sustainable Development Goals [61]. One of the goals, Climate Action, can be driven by the data collected by payloads onboard the BRAVO vehicles.

With the accelerating climate crisis, the importance of accurate weather and climate models is higher than ever. To improve the accuracy of numerical weather forecasts and climate models, comprehensive and accurate data is required. The BRAVO family can allow for more frequent soundings as the cost per launch is reduced and gliders return to the launch site with the payload within 3 hours of launching. Not only will frequent soundings gather more meteorological and climate data than before, the accuracy of the soundings will also be maintained. In-situ measurements using radiosondes on weather balloons are still unparalleled in terms of the accuracy of the collected data. While ground-based sensors and remote-sensing satellites are becoming increasingly prevalent, the importance of in-situ measurements for validation of other measurement techniques remains. Extreme weather events require frequent measurements to monitor their development. Planning of disaster response and assessing the impact of extreme weather events can be aided by a greater abundance of data. The data gathered from soundings with the BRAVO family will lead to economic and societal benefits.

17

Cost & Resource Allocation

In this chapter, the cost of the BRAVO system is estimated and mass and power budgets are generated to track the distribution of these resources, In section 17.1, the cost is broken down in a cost breakdown structure and budgets are generated for both BRAVO Mini and BRAVO Max. Additionally, the important resources of mass and electrical power are distributed in section 17.2.

17.1. Cost breakdown

To estimate the cost of the BRAVO system, the system is broken down into pieces of which the cost is known or can be estimated. The cost is broken down per vehicle, per launch and for the whole project in Figure 17.1. This breakdown is applicable to both BRAVO Mini and BRAVO Max, but the quantities are different. Therefore, separate quantitative cost breakdowns can be found in Table 17.5 (BRAVO Mini) and Table 17.6 (BRAVO Max).

The cost for both gliders is dominated by operational costs and especially the cost of the balloons. In fact, the cost per launch excluding the balloon is only around €13.50 for Mini and €16.50 for Max. Hence, finding ways to reduce the cost of the balloon would result in a much lower launch cost. However, this was deemed out of the scope of this project as this is mainly a matter of materials science. For this cost analysis, the lifetime of a vehicle is assumed to be 200 flights. This is a simplification, since the components will all have different lifetimes. For example, the humidity sensor is likely to be the first components to fail. Thus, it is designed to be easily replaceable. Much of the electronics can be replaced, but a crack in the foam or composite structure would mean that part of the airframe fails entirely. Composite gliders have a lifetime of around 3000 hours,[62] but they do not nearly experience the same load factor on landing. Additionally, model aircraft constructed out of foam usually only last about 30 flights. Hence, also taking into account the lifetimes of the electronics, the number used for now is 200 flights.

Without the balloon, operational costs form around 30% of the remaining costs. This is not extraordinary considering the relatively simple system and components, except for the composite skin. One important note is that most of the operations will be carried out by employees of KNMI or other institutes as an addition to their usual responsibilities. Thus, it will likely not be as clear of an extra labour cost as estimated. Even still, it can be considered a conservative estimate.

17.2. Resource allocation

In any aircraft design process, mass and power are scarce resources that need to be carefully managed. Budgets for both resources are made in order to track which components or subsystems draw the most resources and if that is justified. The mass budgets can be found in Table 17.2 (BRAVO Mini) and Table 17.1 (BRAVO Max). The power budgets can be found in Table 17.3 (BRAVO Mini) and Table 17.4 (BRAVO Max).

Table 17.1: The mass budget for BRAVO Mini

Component	Mass (kg)	Percentage (%)
Fuselage foam	0.057	8.30
Fuselage skin	0.041	5.95
Main wing foam	0.011	1.59
Main wing skin	0.055	7.89
Tail boom	0.017	2.51
Empennage foam	0.002	0.29
Empennage skin	0.028	4.07
Battery	0.250	36.14
Electronics package	0.230	33.25
Anti-collision lights	0.010	1.45
Total	0.692	100.00

Table 17.2: The mass budget for BRAVO Max

Component	Mass (kg)	Percentage (%)
Fuselage foam	0.34	9.56
Fuselage skin	0.11	3.04
Main wing foam	0.08	2.39
Main wing skin	0.23	6.63
Empennage foam	0.02	0.69
Empennage skin	0.08	2.33
Battery	0.40	11.29
Electronics package	0.18	4.94
Payload	2.00	56.46
2 servos in wing	0.05	1.41
1 servo in tail	0.03	0.71
Antenna	0.02	0.56
Total	3.54	100.00

For BRAVO Mini, the battery and electronics package take up more than two-thirds of the mass budget. One important thing to note is that this includes the payload for Mini. For Max, it is not, but when including the payload here too, it makes up a similar part of the budget. Apart from that, the structural foam and composite elements comprise most of the remaining mass. This is a positive result, as it means that we are not in the realm of diminishing returns, and the payload capability of the airframe is quite high.

Table 17.3: Power budget for the BRAVO Mini

Component	Power draw at peak (W)	Power draw percentage (%)	Total energy draw (Wh)	Total energy percentage (%)
Temperature control	1.3	7.8	3.1	6.8
Flight control	1.4	8.4	4.0	8.8
Sensors	2.3	13.8	9.8	21.6
Actuators	2.1	12.6	5.7	12.6
Communications	2.2	13.2	12.0	26.6
De-icing	2.6	15.6	4.1	9.1
Pitot heating	0.8	4.8	1.0	2.2
Safety lighting	4.0	24.0	5.6	12.3
Total	16.7	100.0	45.3	100.0

Table 17.4: Power budget for BRAVO Max

Component	Power draw at peak (W)	Power draw percentage (%)	Total energy draw (Wh)	Total energy percentage (%)
Temperature control	11.2	38.8	38.8	43.2
Flight control	1.4	4.8	4.0	4.4
Sensors	2.3	8.0	9.8	10.9
Actuators	2.1	7.3	5.8	6.4
Communications	2.2	7.6	12.0	13.4
De-icing	2.6	9.0	4.1	4.6
Pitot heating	0.8	2.8	1.0	1.1
Safety lighting	4.0	13.8	5.4	6.0
Payload	2.3	8.0	9.1	10.1
Total	28.9	100.0	89.9	100.0

For the BRAVO Mini, the biggest power draw are the anti-collision lights, which are required by regulation. Apart from that, the power is distributed relatively equally among the major subsystems. For BRAVO Max, the temperature control has by far the highest power draw, much higher than BRAVO Mini. This is due to the ozonesonde, which needs to be kept in its operational temperature range. After that, the anti-collision lights draw a lot of power again. The rest of the power is distributed similarly to BRAVO Mini.

As for the total energy draws, communications and sensors are major energy draws for both Mini and Max. This is due mainly to the fact that their power draw is relatively constant throughout the mission. For BRAVO Max, only the temperature control has a much higher energy draw. This subsystem too operates at a high, relatively constant power throughout the majority of the mission.

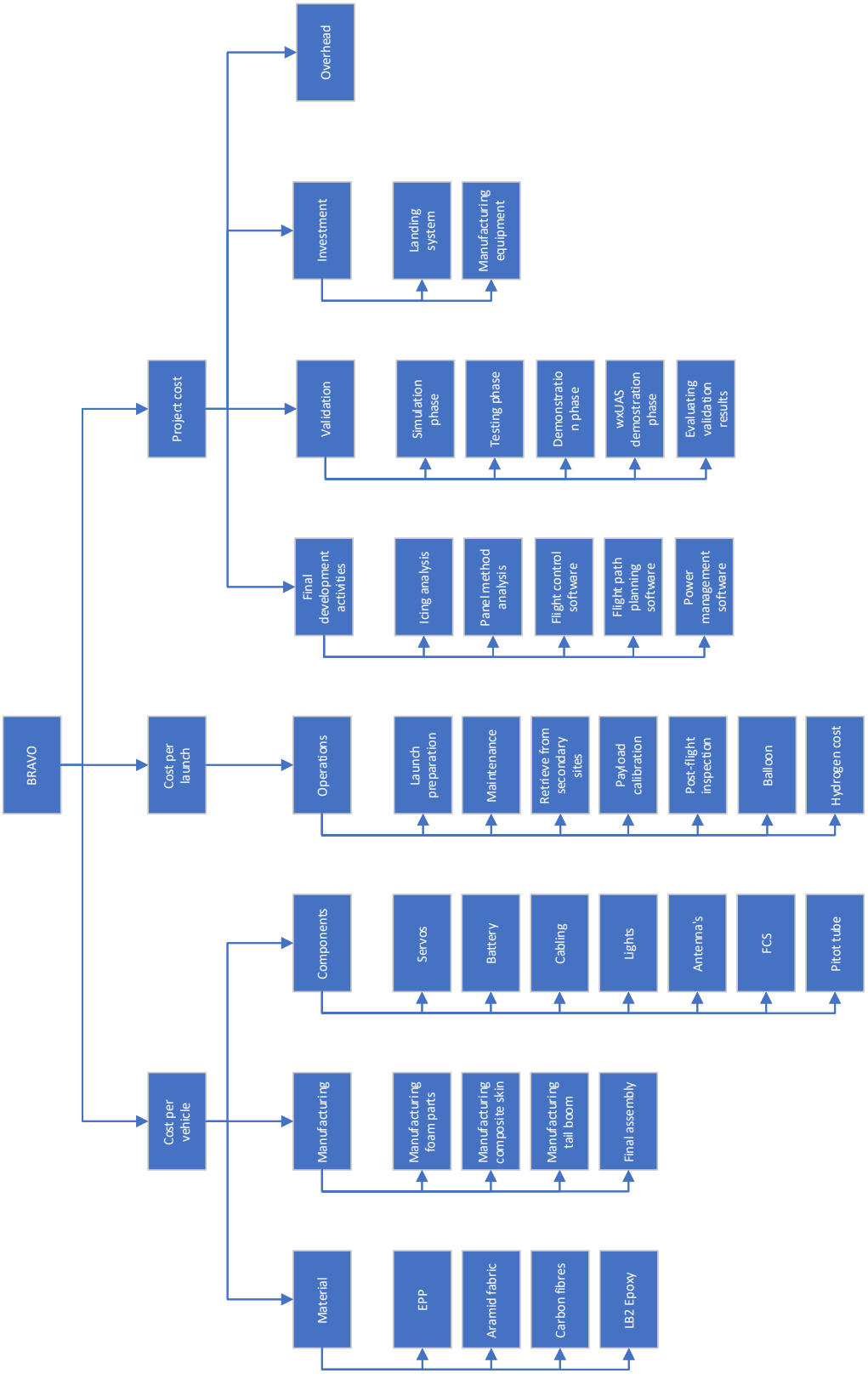

Figure 17.1: Cost breakdown structure

Table 17.5: Cost breakdown of BRAVO Mini

Header	Amount	Cost per piece [€]	Total cost [€]	Notes
Material				
Foam	0.4	1.0	0.4	kg, material efficiency 5
Aramid fabric	0.7	40.5	27.0	$/m^2$, material efficiency 1.5
Carbon fibres	0.0	20.0	0.6	/kg, material efficiency 1.5
LB2 Epoxy	0.1	22.9	1.2	/kg, material efficiency 2
Total material			29.1	
Manufacturing labor				
Manufacturing foam parts	2	15	30	man-hours
Manufacturing composite skin	8	15	120	man-hours
Tailboom Manufacturing	4	15	60	man-hours
Assembly	8	15	120	man-hours
Total manufacturing			330	
Operations				Expected lifetime 200 flights
Launch preparation	33.4	15.0	501	man-hours
post-flight inspection	66.6	15.0	999	man-hours
Maintenance	10.0	15.0	150	man-hours
Retrieval secondary sites	20.0	15.0	300	man-hours
Balloon	200	107	21400	per 200 launches
Hydrogen cost	46.4	2.73	127	per 200 launches
Total Operations			23500	
Components				
Servos	3	10	30	
Battery	1	50	50	
Cabling	1	2	2	
Anti-collision lights	1	30	30	
Antenna's	1	10	10	
FCS	1	62.5	62.5	
Pitot tube	1	13.7	13.7	
Payload	1	85	85	
Total components			283	
Investment costs				
landing system	1	1675	1675	€1200 replacement every 3 years
Manufacturing equipment	1	56695	56695	Autoclave + Foam CNC
Total investment cost			58400	
Total cost per vehicle (excl. operations)			642	
Total cost per vehicle			24100	
Total cost per vehicle per launch			121	
Total cost per vehicle per launch			436	

Table 17.6: Cost breakdown of BRAVO Max

Header	Amount	Cost per piece [€]	Total cost [€]	Notes
Material				
Foam	2.24	1.01	2.27	/kg, material efficiency 5
Kevlar fibres	3.36	40.5	136	$/m^2$, material efficiency 1.5
Carbon fibres	0.08	20.0	1.62	/kg, material efficiency 1.5
LB2 Epoxy	0.26	22.9	5.96	/kg, material efficiency 2
Total material			146	
Manufacturing				
Manufacturing foam parts	3	15	45	man-hours
Manufacturing composite skin	12	15	180	man-hours
Tailboom Manufacturing	6	15	90	man-hours
Assembly	8	15	120	man-hours
Total manufacturing			435	
Operations				Expected lifetime 200 flights
Launch preparation	33	15	501	man-hours
post-flight inspection	67	15	999	man-hours
Maintenance	10	15	150	man-hours
Retrieval secondary sites	20	15	300	man-hours
Balloon	200	419	83800	per 200 launches
Hydrogen cost	144	2.73	393	per 200 launches
Total Operations			86100	
Components				
Servos	1.00	42.0	42.0	
Battery	1.00	100	100	
Cabling	1.00	3.00	3.00	
Anti-collision lights	1.00	30.0	30.0	
Communications	1.00	10.0	10.0	
FCS	1.00	62.5	62.5	
Pitot tube	1.00	13.7	13.7	
Payload	1.00	200	200	
Total components			461	
Investment cost				
landing system	1.00	1675	1675	€1200 replacement every 3 years
Manufacturing equipment	1.00	56695	56695	Composite oven + Foam CNC
Total Investment cost			58400	
Total cost per vehicle (excl. operations)			1040	
Total cost per vehicle			87100	
Total cost per vehicle per launch			436	

18 Market analysis

In this chapter, the market analysis will be presented. The market analysis consists of four parts, in the first part the market is divided up into segments, and an explanation is given about the possible implementations of the BRAVO and its comparative performance with respect to potential competitors, this is presented in section 18.1. Following this, an analysis of the market's size and the expected market share is presented in section 18.2. Next, the target cost based on the current market is estimated and the return on investment is extrapolated in section 18.3. To further understand the potential of the market, it is important to know the performance of the developed system, therefore a short elaboration will be done in section 18.4, specifically of interest here is the performance in other regions than de Bilt with vastly different climates. Finally, to elaborate on the performance of the performance of the system within the currently established climate, a SWOT analysis is performed in section 18.5.

18.1. Market segmentation

Now that the final configuration of the solution and its performance parameters are known, the market segments that were identified to potentially be of interest in the baseline report [4] can be re-evaluated, which is done in subsection 18.1.1. Additionally, some newly or more specifically identified market segments are discussed in subsection 18.1.2. A final important point in the market analysis is the identification of competition, this will be elaborated on in subsection 18.1.3.

18.1.1. Market segments re-evaluation

The market segments previously identified to be of interest were the markets for high-altitude balloons (HAB), high-altitude pseudo satellites (HAPS) and satellite testing. Firstly, the high-altitude balloon market has been the main aim of this project and is where the majority of requirements came from. Hence, it is logical that this market is still very much relevant. The altitude required to satisfy the meteorological institutes and the low prices they need to achieve this with make suit well with the BRAVO concept. The final solution is still a weather balloon and is designed to carry the same instruments as current weather balloons do. The unique selling points (USP) of BRAVO in this market are the return-to-base capability of the glider and the second vertical atmospheric profile that can be obtained from the descent. Other scientific missions can also be done using the final solution, but that is expanded upon in subsection 18.1.2.

Conversely, the HAPS market is no longer attractive. This is mainly due to the high flight endurance that this market necessitates. Some design options considered in the baseline report, like the blimp and the powered aircraft, would have been able to achieve higher endurance. [5]

Lastly, stratospheric testing of nano-satellites has been identified as a possible market. These customers require their payloads to reach similar altitudes as ozonesondes as the conditions at these altitudes are quite close to conditions in space. Therefore, launching satellites using weather balloons is a relatively cheap way to validate their design. However, the satellites must be recovered by chase cars and are at risk of being damaged during landing. Therefore, the return-to-base capability is a USP in this market as well.

18.1.2. New market segments

After the previously known markets were re-analysed, some new segments could be identified. Some of these are segments that were mentioned earlier, but can now be narrowed down more with the final

design in mind.

Firstly, BRAVO Max can be used for scientific missions in fields like earth observation and atmospheric science, other than regular meteorological launches. For example, the payload could simply be altered to perform measurements on greenhouse gases or particle matter. This application fits especially well with the vertical profiling capability of BRAVO Max. Additionally, earth observation payloads can be incorporated as well. At this altitude, the payload could provide a higher resolution and frequency at a lower cost for specific areas of interest compared to nano-satellites. Earth observation missions often need a longer endurance than BRAVO can offer. This need can be satisfied by (high-altitude) UAVs or super-pressure balloons. But the BRAVO's USP in this market is its low cost, which makes it more attractive than these when long endurance is not absolutely required.

Secondly, there are military applications that BRAVO could potentially fulfil. Similar to the earth observations, it could take on specific reconnaissance missions. Of course, it is limited as compared to UAVs due to limited range and windy conditions can render it inoperable. However, the low cost of the glider makes it an attractive alternative if the mission allows for it.

Lastly, in the same vein, the gliders could be employed in monitoring and surveillance applications, such as forest fire monitoring, crop monitoring or security surveillance. Yet again, deploying the glider might not be reasonable in all conditions. For instance, when wind conditions blow BRAVO too far away from the target area or make it impossible for the glider to return all together. However, given the range and excess range estimated in chapter 13, this should not occur too often. Additionally, BRAVO can be easily transported and launched from the most optimal location given its predicted trajectory while ascending with respect to the target area. Furthermore, the low cost makes BRAVO an attractive alternative even considering these limitations.

18.1.3. Competition

BRAVO is designed as an alternative to traditional weather balloons and should outcompete them on cost per launch and reusability. But there are other products and concepts in-development that can perform the same type of missions as BRAVO.

The closest product to BRAVO is the Stratodynamics HiDRON™[63] glider that is currently under development. This aircraft was designed with a similar objective of retrieving ozone- and radiosondes and other atmospheric sensors. The main difference between HiDRON and BRAVO is size. The HiDRON is designed for a payload mass of 5 kg, as opposed to BRAVO's lightweight Mini sonde or Max's 2 kilograms payload. Although it caters to very similar customers, the competition from this product on specific missions is limited. Stratodynamics plans to lease the HiDRON in order to mitigate the investment cost for institutions. No specific lease cost has been announced.

Another potential competitor for earth observation and monitoring missions is the Urban Sky Microballoon™. This is a reusable stratospheric balloon that reaches an altitude of 17 to 21 km. The Microballoon is aimed at earth observation and monitoring missions like wildfire monitoring.[64] It has an endurance of 4 to 7 hours, which is longer but comparable to BRAVO. Urban Sky is targeting a price of 6 $per square kilometre of coverage. [65]

Other competitors for the earth observation market are nano-satellites. These are now commonly used for earth observation missions. They can cover far larger areas, but with a lower resolution and frequency and at a higher price. Overall, BRAVO can be an addition to this market for specific situations where the area of interest is small and well-defined. The average nano-satellite costs $575.000 to launch. [66]

Lastly, superpressure balloons could also compete with BRAVO on specific missions. Superpressure balloons are similar to conventional weather balloons. However, instead of bursting in the stratosphere, it stays in intact and releases some lifting gas to maintain a constant altitude for up to 100 days.[67] Thus, similar to the Urban Sky Microballoon, these balloons are suitable for earth observation and monitoring missions. However, since they do reach the same altitude as conventional weather balloons, it can also be used to do vertical profiling of the atmosphere. One important difference is that he superpressure balloon can only be vertically controllable, while the glider is horizontally controllable during its descend.

18.2. Market size and share

The Earth observation (including monitoring and surveillance) market size will increase from 13.75 billion to 29.61 billion euros from 2020 to 2027. 69.1% of this market is covered by aerial vehicles and the remainder by satellites. The largest market segment is military and intelligence. The fastest growth is expected in disaster management. This segment includes monitoring of (natural) disasters like wildfires and volcano eruptions. North America is the largest market at 38.12 % of the global market. Asia Pacific is the fastest-growing market. Growing with over 12% a year until 2027 [68]. In the baseline report, the market for high-altitude balloons for meteorological institutes was estimated to be around 224 million €. [4].

In both of the aforementioned markets, it is expected that BRAVO Mini and BRAVO Max will achieve a significant market share. Of course, this will take time, as not all institutes and companies have interest or resources to invest in a relatively unproven solution. For the meteorological institutes, the target is to achieve 15% market share after 2 years of operation. This is similar to the goals Stratodynamics [63]. Since balloon launches are quite a homogeneous market, the market share can grow steadily in the years after that.

In the earth observation market, there is more competition with higher technology readiness. Additionally, BRAVO is not suitable for all subsegments of this market. Therefore, the expectation for this market is low. After 2 years of operation, the target is to have a 5% market share in the aerial vehicles segment of this market.

18.3. Target cost and return on investment

In order to determine the competitiveness of the BRAVO system, the target cost is estimated. This is done based on the cost of conventional radio and/or ozonesonde launches similarly to the baseline report [4], but with more certainty. To significantly undercut conventional sonde launching in price, the target cost is set 20% lower than the current cost. The target cost estimation is based on costs obtained in this report and the baseline report. [4] It is broken down in Table 18.1.

Table 18.1: The target cost per launch of the BRAVO system based on the cost per launch of conventional systems

	Radiosonde [€]	Ozonesonde [€]
Balloon	107	419
Payload	250	400
Hydrogen	0.23	0.72
Parachute	10	10
Total cost	367	830
Target cost	294	664

To give an indication of the profitability of BRAVO, the return of investment (ROI) can be calculated. The ROI is defined in Equation 18.1.

$$RoI = \frac{Value + Income - Investment}{Investment} \cdot 100\% \tag{18.1}$$

Here, the value is the target cost obtained from Equation 18.1. The income is the amount of money the product generates when still in possession of the company. In this analysis, only a traditional business model where the gliders are sold to and operated by KNMI and other customers. Service-based business models can be attractive as well, but there are too many unknowns at this point to estimate a target cost with reasonable confidence. Hence, the income is not relevant in this case and the return on investment is the profit margin relative to the cost. Lastly, the investment in this is the total cost of the product for the company, including indirect costs like overhead. Based on the cost estimations from section 17.1 and target costs from section 18.3, the return on investment is 147% for BRAVO Mini and 52% for BRAVO Max.

18.4. Performance evaluation

Until now, the majority of the design work has been done with KNMI's De Bilt location in mind. However, for the economic feasibility of the concept, it is vital that BRAVO can be used at other institutes as well. Therefore, a performance analysis was done in chapter 13 for selected balloon launch sites across the world. These sites were selected to have a varied combination of vertical wind profiles with different geographic locations from seaside to inland to island.

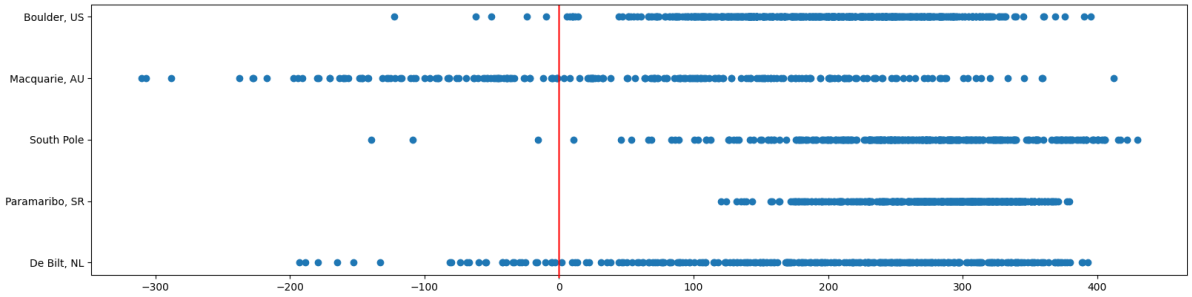

Figure 18.1: Excess range for BRAVO mini

As can be seen in Table 13.2, the performance varies across the different locations. Most strikingly, the probability of returning to Macquarie is significantly lower than the other locations. Macquarie is a small island in the Southern Ocean midway between Tasmania and Antarctica (about 1500 km from each). Due to a combination of the extreme temperatures in Antarctica, the steep elevation drop at its coast and the Antarctic polar vortex, the wind speeds are extremely varied [69]. This is also visible from the high variance in estimated excess range in Figure 18.1. Apart from Macquarie, the other locations all have probabilities of 90% or higher and, apart from De Bilt and Broadmeadows, the probability of return is 99% or higher at all other locations. The other locations also have more consistent excess range estimations with fewer outliers. This indicates that BRAVO can operate reliably through adverse wind conditions at most meteorological stations. However, at extreme locations such as Macquarie Island, operating the BRAVO is not reliable enough to be feasible. Furthermore, it should be noted that in locations like De Bilt, the fact that the balloon does not return to the launch station does not mean that the system cannot be re-used: in cases like the Bilt, not returning means that the glider will likely end up at another weather station. Therefore, these results still present the solution in a worse case than their actual performance.

18.5. SWOT analysis

To gain an overview on the position of BRAVO with respect to markets, a SWOT analysis is made. This brings up the strengths, weaknesses, opportunities, and threats of the concept. Thus, it points to where the BRAVO can best be applied and what to watch out for in the development and implementation phases. The result can be found in Table 18.2.

Table 18.2: SWOT analysis for BRAVO

	Helpful	Harmful
Internal	Strength: • Reliable operation • Low cost compared to UAV solutions • Compatible with most existing infrastructure	Weakness: • Not as controllable as UAVs • Lower endurance as UAVs • Not compatible with current regulations
External	Opportunity: • Reliable demand from meteorological institutes • Big growth expected in earth observations market	Threats: • Competitive concepts in development in earth observations market • Uncertainty with respect to regulation changes or special permission to operate

19 Technical Risk Assessment

During the design process, several potential risks were identified that could impact the performance of the system. The risks are first described in section 19.1 and after, in section 19.2, mitigation for the most severe risks are formulated and an updated risk map is shown.

19.1. Risk identification

Table 19.1 shows the identified technical risks for future development of the system. The description, consequence, and probability of occurrence are all listed per possible risk. The risks are also mapped in a risk matrix in Table 19.2, where the severity of the risk is shown by the colour of the cells.

Table 19.1: List of technical risks associated with the BRAVO system

ID	Description	Consequence	Probability of occurrence
TR-1	Balloon catches fire during launch	Critical, System potentially crashes and gets damaged	Improbable,
TR-2	System hits other air traffic	Catastrophic, System destroyed and potential collateral damage	Improbable, system is visible and air traffic is not dense
TR-3	Glider misses the landing net	Critical, glider gets damaged	Improbable, net is large and control is accurate
TR-4	Flight control system fails at max deflection	Catastrophic, system spirals down	Negligible, FC components are reliable
TR-5	Control surfaces ice up	Marginal, system glides down without control	Probable, icing is likely at lower altitudes
TR-6	Balloon bursts prematurely	Marginal, glider will still get back if popped above 10[km]	Probable, balloons can contain defects
TR-7	Scientific sensors get blocked by icing	Critical, No scientific data collected	Probable, icing is likely at lower altitudes
TR-8	System is struck by large bird	Critical, potential loss of flight	Negligible
TR-9	System is struck by hail	Marginal, surface will be less aerodynamic	Improbable, most flight is above clouds and severe hailstorms are rare.
TR-10	Disconnection from balloon fails	Catastrophic, uncontrollable free fall	Improbable,
TR-11	Communication is lost	Negligible, glider still returns to base	Improbable, communications is designed with margin.
TR-12	Electrical system fails	Critical Loss of control and test equipment	Improbable, an all out electrical system is rare but not impossible
TR-13	System drifts too far from launch site	Marginal, System cannot return to launch site	Improbable, glider designed for the worst case scenario
TR-14	low Reynolds numbers makes the glider unflyable at altitude	Critical, range severely hampered	Probable, lack of research of UAV's this size
TR-15	Insulation is not sufficient	Marginal, higher battery mass needed	Improbable, already oversized

TR-16	Meteorological companies not willing to implement	Critical, main customer	Probable, scientist unwilling to change methods
TR-17	Landing net too stiff	Marginal, easily adjusted	Probable, testing required
TR-18	Material fatigue causes damage in the structure	Catastrophic, Potential failure of the structure	Improbable, structure is over designed

Table 19.2: Heat map showing the pre-mitigation levels of risk for each event

Likelyhood / Concequence	Negligible	Improbable	Probable	Highly probable
Catastrophic	4	2, 10, 18		
Critical	8	1, 3, 12	7, 14, 16	
Marginal		9, 13, 15	5, 6, 17	
Negligible		11		

19.2. Risk mitigation

In Table 19.2 there are several risks in the dark-orange/red zone of the risk matrix. Therefore, a mitigation plan must be formulated to move them into the yellow and orange zones. Table 19.3 lists these mitigations per risk as deemed necessary. The updated risk matrix is shown in Table 19.4, where there are only 5 remaining in the orange zone, with the remaining located in the yellow zone.

Table 19.3: List of risk mitigation measures where applicable

ID	Mitigation
TR-1	Ensure a spark free environment during launch and a low altitude release procedure
TR-2	Include a transponder if likelihood is indeed too high
TR-3	Let grass grow high around the net
TR-5	Ensure control surfaces are moved to full positions regularly.
TR-6	Secondary flight plan for lower altitudes and/or secondary landing zone
TR-7	Add heating to measurement equipment to clear the ice.
TR-10	A passive automatic release mechanism is added to ensure release
TR-14	More research and testing needs to be performed to quantify effect. An additional landing sites would compensate for this loss of range.
TR-16	Prove method with tests in collaboration with KNMI, to prove capability
TR-17	With testing the net can be adjusted to perfect size and stiffness
TR-18	Routine inspections and ensure that components can be replaced

Table 19.4: Heat map showing the post-mitigation levels of risk for each event

Likelyhood / Concequence	Negligible	Improbable	Probable	Highly probable
Catastrophic	2, 4, 10, 18			
Critical	1, 8	3, 12, 16		
Marginal		5, 9, 13, 15	7, 14	
Negligible		11, 17	6	

20 RAMS

RAMS is concerned with the Reliability, availability, maintainability and safety of the system. This is a method generally used in large scale projects to assess the functioning of a continuously operating system. This whole chapter follows the RAMS method and setup as described in Guideline RAMS, aiming for system performance (”Leidraad RAMS, sturen op prestaties van systemen”[70]). In this guideline, it is advised to do three analyses: a serviceability analysis which will be described in section 20.1, then an analysis on the maintainability needs to be done in section 20.2. Finally, the safety is assessed in section 20.3

20.1. Serviceability analysis

Serviceability considers a few things, namely the reliability of the system: how large is the chance of failure? Which is described in subsection 20.1.1, but also the availability: what is the chance that you need the system but cannot use it properly in the case that you want to use it in. Availability itself is subdivided into planned unavailability, described in subsection 20.1.2, furthermore, there is also the unplanned unavailability, described in subsection 20.1.3 and finally there is the issue of availability being affected by external boundary conditions like the weather, which is discussed in subsection 20.1.4.

20.1.1. Reliability

There are three phases related to the reliability of a component that can be considered over time. These phases are:

1. Teething failure period
2. Random failure period
3. Wear out failure period

The goal of the test campaign is to identify and solve the teething failures, furthermore, if possible, the point at which wear-out failure starts to occur should be determined as soon as possible. Furthermore, the reliability has to properly consider the working and failure rate of the electronics or the combination of electronics used. Another consideration for reliability is the reliability of the system to return to base, but this is better suited and therefore as explained in more depth in subsection 20.1.4

20.1.2. Availability due to planned causes

Availability can be limited due to planned causes like maintenance and system tests. For example, the calibration that needs to be done for the sensors which is always done pre-flight, This on a very strict level limits the availability of the system, but is not limiting, as it is a system which does not inherently requires continuous availability. Furthermore, maintenance is of course also reducing availability, but this is again not limiting as all maintenance procedures and cycles are aimed to be done in less than eight hours of work. How maintenance will exactly fit into this concept, is considered in section 20.2.

20.1.3. availability due to unplanned causes

Availability due to unplanned causes has to do with unexpected system failure. Of course, all electrical components can naturally fail, furthermore wings can break off or other parts can be damaged beyond reasonable structural integrity. Furthermore, sensors on board the drone can fail, which prohibits the use. Finally, this condition is really on the edge of unplanned availability and external boundary conditions, but if the system has to fly to a diversion landing sight, the system will not be available immediately

after for re-launch. For all these unplanned causes, the solution is to have multiple drones of each size which can be used interchangeably.

20.1.4. Availability due to external boundary conditions

Availability is adversely influenced by mainly the wind conditions. The formation of ice is the other major external condition influencing the system, but since there is active de-icing available, this subsection will focus on only the takeoff and landing in strong wind conditions.

Takeoff There is no reason to assume that the launch availability will be any different from the availability of the current system. This practically means that if a person is physically able to step outside, the system can be launched. This comes down to an availability of over 99 percent.

Landing Landing availability strongly relates to the likelihood of early bursts.

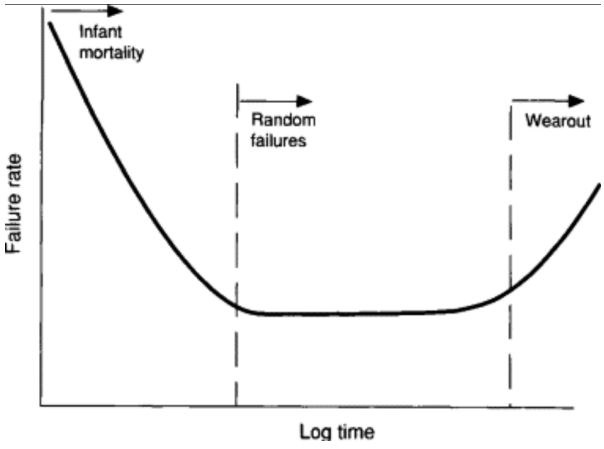

Figure 20.1: The bathtub curve of reliability[71]

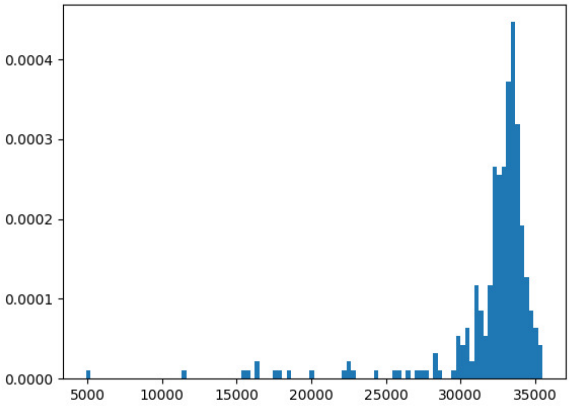

Figure 20.2: Balloon burst height

The martini method as described in section 10.4 is used to create cones for the return of the gliders. The landing availability can be defined as the percentage of the time that the system is not able to return to the Bilt multiplied with the percentage of bursts that occur under the height where the martini glasses of the complete coverage overlap, assuming that the wind speed and early bursts have no influence on one another. The chance of staying within range in the Bilt was calculated to be 90.9 percent. Furthermore, the height at which the balloon cannot return to the Bilt is conservatively estimated to be 10 [km]. The chance of a balloon popping before this is 0.01 percent. Therefore, the chance of a glider not being able to return to any base can be estimated to be $9 * 10^{-5}$. This scenario is however not considering the formation of ice. This is due to the fact that the electronics have the ability to reverse the formation of ice. It is beyond the scope of this analysis to consider the reliability of the de-icing system in combination with these other failures.

20.2. Maintenance analysis

Maintenance in this context has to do with being able to do maintenance without interfering in the operations that are desired by the customer. Therefore, this is subdivided into two parts: maintenance planning which will be introduced in subsection 20.2.1, and secondly the maintenance plan which is introduced in subsection 20.2.2.

20.2.1. Maintenance planning

The maintenance planning is concerned with planning maintenance such that the needs of the customers can be most accurately fulfilled; weather agencies generally desire to gather more data on days when the weather is unpredictable; circumstances that the weather models cannot accurately predict. Therefore, maintenance should be planned such that periods with “interesting” weather are avoided as maintenance periods and furthermore, the maintenance is scheduled with a margin to the

absolute maintenance limit such that the maintenance can be delayed such that more measurements can be taken.

20.2.2. System maintenance plan

The regular scheduled maintenance work packages should be sized such that they can easily be completed between two flights, which means that the work packages can take at most eight hours. Furthermore, there is “maintenance” that needs to be done before and after every launch, such as the calibration of the system and inspection of possible impact damage by landing.

20.3. Safety analysis

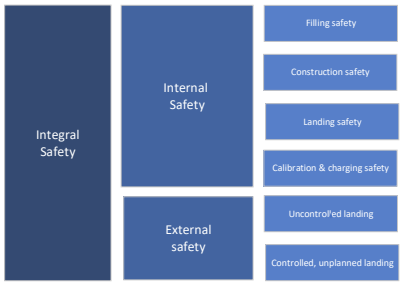

Figure 20.3: Safety theme breakdown

The safety analysis is concerned with the overall safety of the entire, integral system. This can be subdivided into two parts, namely the internal safety discussed in subsection 20.3.1, and the external safety, which is discussed in subsection 20.3.2.

20.3.1. Internal Safety

Balloon filling safety The new method of filling the balloon with hydrogen does introduce new safety concerns as hydrogen is flammable, but the KNMI has already shown in the past that handling hydrogen can be done safely. Simply adjusting these procedures based on what is now known about handling hydrogen should be sufficient to make this process safe for the operations envisioned by KNMI.

Construction safety Construction safety is concerned with the safety of the system for handling of the vehicle itself and the replacement of parts or subsystems of the construction. For this, it is necessary to ensure that there are no sharp edges and that the system has a user manual that allows for proper and safe maintenance.

Landing safety The landing site at the KNMI or at the alternative landing sites of course introduces risk. If the glider returns and misses the net, there is a possibility that it will hit someone observing the events, but the net has been designed to be very large, and the control accuracy should prevent the drone from exiting the net. Furthermore, the system envisioned by KNMI is more a “launch and forget”. Therefore, it can be safely assumed that no operator is present at landing, which therefore also means that the safety during landing is very high. Removing the glider from the net can be done by lowering the net, therefore, there is no reason to assume that this will introduce an issue.

Calibration & charging safety Calibration and charging should be an automated process, however, batteries can still go into thermal runaway and the calibration device itself can of course malfunction in a way that is causing danger, however, the KNMI has been doing these measurements long enough to take the proper precautions to make both charging and calibration safe for operations.

20.3.2. External safety

There are two types of external safety that have to be considered: uncontrolled landing, and controlled, but unplanned landing.

For both cases, it has to be considered that the fatality rate of this system must be lower than 10^{-6} fatalities per year. To quantify the exact fatality rate of the systems, a few metrics can be used, first, it has to be considered that an impact to the head with 2000 joules or 25600 joules per square meter is considered deadly[72].

Furthermore, for the analysis done here it is considered that landing in rural areas, by approximation, no people will be outside.

Uncontrolled landing In case of an uncontrolled landing, one can consider that the vehicle is able to recover itself from stall and is stable in all eigenmotions, therefore, when all electronics on board have died, the system is still able to fly in a straight line at a near-optimal lift coefficient. Therefore, the landing speed is going to be similar to the landing speed of the glider itself. It is important to realise that the only reason why this scenario would occur is either due to a fatal short circuit, or due to a software failure. Both scenarios are highly unlikely: properly produced systems do not short circuit without a cause, furthermore, good coding practices should prohibit any piece of software to fail in a manner such that flying back to a safe landing site is not possible. Therefore, the risk of this occurring can be classified as incredibly rare. It is therefore hard to quantify the failure rate from this. It is however possible to calculate the maximum allowed failure rate.

For this calculation, an upper bound on the likelihood of hitting a person to the head need to be found. For this, the approximation is made that a head is a sphere with a diameter of 30 centimeters. Furthermore, any hit by the vehicle to the head is considered deadly. On average, there live 508 people per square kilometer in the Netherlands.[73] In the Netherlands, roughly half the population spends less than one hour outside a day.[74] If we assume that these hours are uniformly divided over the day, which is a very harsh assumption since launching at 2 o'clock in the morning ensures very little people will be outside, this comes down to a likelihood of 4.17 percent of the time outside, or converted to people outside at any instantaneous time, it is 4.17 percent. This gives that there are 21.2 people outside at any time in any square kilometre. Therefore, the number of people per square meter is $2.12 \cdot 10^{-5}$. Assuming a rather high glide ratio: 15 to 1, which is likely not going to be attained, but still adheres to the conservative estimates. The area covered at the height of a head is therefore for the big glider 7.2 square meters and the area covered for the small glider is 3.5 square meters. This makes the likelihood of hitting a person for the large glider $1.53 \cdot 10^{-4}$ and for the small glider $7.42 \cdot 10^{-5}$. These values are per flight in which an incident occurs that will completely de-activate all electronics. Since the requirement (WBA-STK-KNMI-011) states a fatality rate per year, the assumption that normal operations are continued, one launch per day for the small glider, one per week for the large one. Assuming both use the same flight computer and basic hardware, it is easier to calculate the allowed failure rate per year. This failure rate is equivalent to:

$$F_{tot} = (1 + F_{MAX})^{52}(1 + F_{mini})^{365} - 1 \tag{20.1}$$

$$F_{tot} = 1.000153^{52} \cdot 1.0000742^{365} - 1 = 3.57 \cdot 10^{-2} \tag{20.2}$$

From this total failure rate, and the requirement that the system may have a maximum fatality rate of 10^{-6} per year, it can be concluded that the system may have a combined short circuit- and code failure rate of $2.8 \cdot 10^{-5}$ maximum.

controlled, unplanned landing In a case that a vehicle has to make an unplanned landing, that even in the case that ice has somehow formed on the vehicle, the vehicle is still likely able to steer clear of inhabited areas, meaning that by the approximations earlier made, this would never result in a fatal accident. This is a realistic assumption since the vehicle will try to aim for a landing location that is included in its flight management computer which is known to be a safe, crash landing alternative. In this case, you can think about a farmer's field or a forest. In this case, it is assumed that the vehicle is a write-off.

21

Verification & Validation

When developing new systems there is always the risk of the unknown: whether the tools that were used reflect reality properly enough to give an accurate result. This is what the first part of this chapter will focus on: the verification and validation of tools used and their corresponding confidence levels. This is worked out in section 21.2. In the second part of this chapter, it is acknowledged that the design is not finished: the products developed are not yet ready to be built completely. Therefore, a plan will be laid out that describes the efforts that need to be taken from the result of this report to the first fully integrated flight.

21.1. V&V Plan

In this product design it was chosen to go for the V-model which breaks down a system into subsystems and the subsystems into even smaller tasks until the whole system is separated into elementary tasks which can be checked by unit-tests. In the earlier phases of the design, requirements were made. These requirements create a task: a test must show compliance with this requirement. Based on the requirement in question this requirement itself will require individual unit tests in order to perform an integrated system test, or can be verified by performing a single unit test.

Before testing the design for meeting certain requirements, it is crucial to verify the mathematical and computational tools that will be used throughout the design process. This will be done in section 21.2.

After all unit tests have been completed, the parent subsystem test can take place. This should verify that the units are used in the combinations they are designed for. Finally, after all subsystems are verified, the complete systems' functionality can be tested in a validation procedure. In this report, the complete procedure happens on three levels: the first is verification and validation of code and coding tools. This checks whether the code actually calculates what it is expected to calculate. Secondly, the verification and validation of the design discussed in the report will be done to check that the design in theory fulfils all requirements that can be checked. Finally, the verification and validation for final integration is performed. This entails the complete integration, verification, and validation up to the point where the system can replace the original system.

21.2. Design Methods V&V

This section will verify and validate the computational models that were used in the design phase. It is important to note that proven simulation and design tools that were used in the project such as 3DEXPERIENCE and Open VSP will not be verified in local scale for their accuracy. The accuracy and validation of the OpenVSP methods have been briefly covered in chapter 5.

21.2.1. ISA Validation

The ISA model that has been used in the various stages of the design is the Ambiance Python module. Since the altitudes that will be dealt with are significantly high and above normal aircraft operating limits, the model used will be validated by the data that was historically collected by weather balloons themselves. Comparing the experimental data with the Ambiance atmospheric model will show whether the model is viable for the design of a high altitude system.

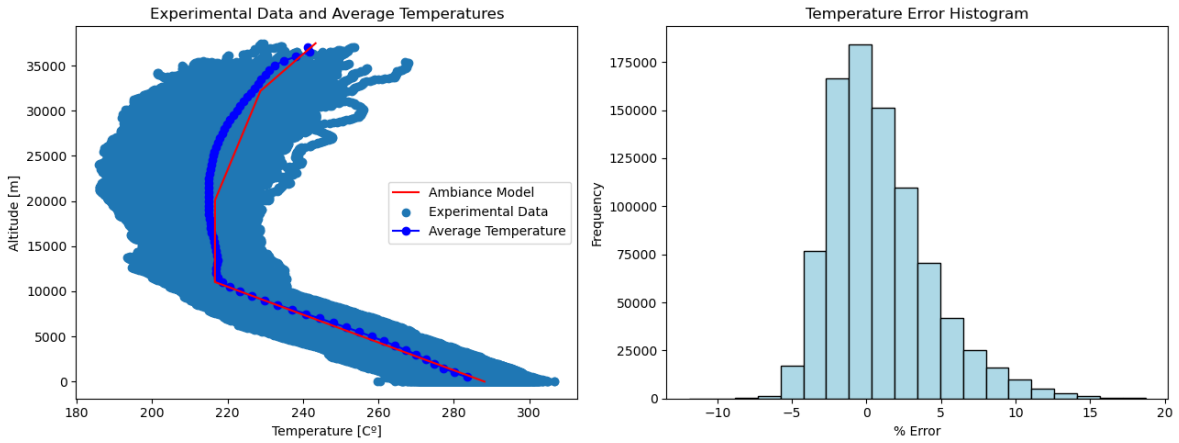

Figure 21.1: Ambiance ISA Model vs Experimental Data

In Figure 21.1, the atmospheric temperature is plotted against altitude. When compared to the ISA model, the experimental temperature values have only a difference of 0.89ºC on average. In addition, the average temperatures for every 500m of altitude (shown in dark blue) differ only by 0 - 2.5ºC. The major discrepancy between the model and the experimental values are between 20000m and 33000 m, where the difference spikes to 5ºC. While still low, this is a notable difference in the ISA model currently being used for calculations for flight at that altitude range.

21.2.2. Flight Performance Tool Verification

In this section, the verification of the flight performance/profile tool, explained in section 4.4, will be discussed. Note that validation of this tool was not possible as this would require either test data or historical data similar to this mission, with the knowledge of wind conditions during the flight and a number of other critical parameters. Therefore, verification is as far as this V&V can go.

This flight performance tool was used for both aircraft sizing, flight control and navigation as well as a final performance analysis, meaning that this tool must have a certain associated confidence that can only be gained through verification.

Alongside the basic unit tests, which tested the methods of the “FlightPerformance” class, some larger system tests were run. One of the major assumptions this tool uses is the small angle approximation. This was tested by comparing the simplified method “Vgnd_over_sink_variable” against a duplicate method which incorporated small angle approximation by using a number of other variables such as “gamma”, “Lift”, and “V_TAS”. After conducting a comparison over a number of different aircraft parameters and flight profiles, it was found that indeed small angle approximation remains valid, with less than a 1% difference between the two methods.

21.2.3. Stability & Control V&V

For the verification and validation of the methods used in the stability and control analysis, multiple tests were used.

Firstly, unit tests were used to make sure that all individual functions performed satisfactorily. For this, a hand-calculated example was worked out for each function, and the same example was then worked out by each respective function. If the function did not obtain the same result, it was investigated what the reason for this was. Nearly all functions performed as expected, except for the data loader, where a wrong coordinate transformation was discovered.

After this, degenerate tests were performed on the scissor plot function, the state-space systems and the control surface sizing function. Changes in function inputs gave the expected outputs, so this test was considered a pass for all tested functions.

Lastly, the state-space systems were tested using an eigenvalue test. Here, the eigenvalues of the system were compared to the approximated eigenvalues as described in section 6.4 and section 6.5. Since

there was a minimal difference between the approximated eigenvalues and the system eigenvalues, this test was considered passed as well.

The complete system was validated using historical data of the Cessna Citation[23]. Since all outputs, ranging from the scissor plot output to the control surface requirements, reasonably corresponded to the known values, the stability, and control system was considered to be validated to a reasonable standard. The major limitation to this validation is the issue of scale. Once test data is available, a better validation can be performed.

21.3. Structures

Unit tests were performed on the wing area moment calculations, where simple shapes such as square and circular tubes were used as input for the analysis method, and the results were checked against manually calculated values. The maximum calculated stress was also checked by hand in the same manner.

The deflection analysis code was also unit tested. This included using derived formulas for standard beams, and checking against the program result for the same input case. The standard beam formulas were also used to check the order of magnitude.

Because of the unique nature of the BRAVO structural design, no validation against existing data was performed, since this proved difficult to find for the construction method chosen. Due to lack of time, no FEM was performed either.

21.4. Integration V&V

Between the final design presented in this report and the final integration by weather prediction services, a rather extensive integration project needs to be completed. In this section, the preliminary plan to verify and validate the new replacement of the radiosonde is laid out. In correspondence with the KNMI it has come to light that the best scenario would be to do integrated test flights with this new vehicle during the wxUAS worldwide demonstration organized by the World Meteorological Organisation between the 1st of march and the 1st of September 2024. This chapter has therefore based the planning on being flight ready at the start of this test period. In order to do proper verification and validation of the product, the requirements that were developed in the previous reports were converted into tests on levels of: unit tests, subsystem tests and system tests. These tests were then divided into three phases:

1. Simulation
2. Test
3. Demonstration
4. wxUAS demonstration

Simulation
In the first phase, simulation, all simulation steps identified in the tests generated from the requirements are done. coincidentally, it can be identified that the summation of these simulations does a very well job at doing a verification of the design: if the design indeed capable of delivering upon the promise that has been made to truly replace the current system. Of course, this is still based on models, but if in the case it is identified that the vehicle has an irrevocable flaw, the integration activities can still be stopped. This is the exact aim of this phase: at the end of the simulation-phase, the milestone deciding on whether the system will actually be built is reached. If the green light is given that the system will be developed, the second phase will start: Tests. In the simulation phase, the V&V tests as described in Table 21.1 will be conducted.

Table 21.1: Simulation phase: verification and validation

Test identifier	Test description	Requirement parent	Completed	Test type	Verification method	When succeeded?
VV-WBA-ASC-002	simulate likelihood of early bursts	WBA-MIS-ASC-002	x	subsystem test	simulation	height attained must be reached at least 95 percent of the time
VV-WBA-ASC-003	simulate return performance in case of early bursts	WBA-MIS-ASC-002	x	subsystem test	simulation	return rate higher than 95 percent

VV-WBA-DES-001-01	Give the flight computer location inputs and read interpret the flight computer instructions, conclude the plan of the flight computer based on this	WBA-MIS-DES-001		unittest	simulation	expected behaviour based on the martini method
VV-WBA-DES-002	the complete range of flight conditions will be inputted to the stability matrix and the response will be monitored to prove vertical controllability	WBA-MIS-DES-002	x	unittest	simulation	controllability such that an input results in an output that is consistent with normal flying vehicles
VV-WBA-DES-003	simulate the flightpath inputs and monitor response	WBA-MIS-DES-003		unittest	simulation	monitor whether output response ensures return to the predefined flight path, check for noisy input data
VV-WBA-DES-004	The complete range of flight conditions will be inputted to the stability matrix and the response will be monitored to prove horizontal controllability	WBA-MIS-DES-004	x	unittest	simulation	controllability such that an input results in an output that is consistent with normal flying vehicles
VV-WBA-MEAS-004-03	convert pitot speed and GPS speed into actual wind speed	WBA-MIS-PAY-MEAS-004		unittest	simulation	conversion of 0.01 m/s
VV-WBA-MEAS-005-01	simulate compass and GPS heading wind direction conversion system	WBA-MIS-PAY-MEAS-005		unittest	simulation	less than 0.01 degrees
VV-WBA-OP-ENV-001	simulate carbon creation during operations	WBA-OP-ENV-001		system tests	simulation	carbon-neutral
VV-WBA-OP-ENV-003	simulate release of non-renewable sources into the atmosphere	WBA-OP-ENV-003	x	system tests	simulation	no renewable sources in the atmosphere
VV-WBA-OP-REG-001	simulate non-normal return rate based on burst and non-return conditions	WBA-OP-REG-001		unittest	simulation	95 percent confidence interval answer
VV-WBA-OP-REG-002	simulate fatality rate in case glider hits someone	WBA-OP-REG-001		unittest	simulation	95 percent confidence interval answer
VV-WBA-OP-REG-003	Simulate chance that person is hit in case of non-return conditions	WBA-OP-REG-001		unittest	simulation	95 percent confidence interval answer, multiplied with previous two below 10^{-6}
VV-WBA-PAY-001-01	simulate range with maximum payload	WBA-MIS-PAY-001	x	unittest	simulation	total range in 2 SSD conditions larger than 150 kilometres
VV-WBA-PAY-002-01	simulate range with minimum payload	WBA-MIS-PAY-001	x	unittest	simulation	total range in 2 SSD conditions larger than 150 kilometres
VV-WBA-PAY-005-02	Simulate constant discharge test of complete system	WBA-MIS-PAY-003	x	unittest	simulation	show compliance of discharge metrics with battery capacity
VV-WBA-PAY-006-02	simulate vertical mission profile	WBA-MIS-PAY-004, WBA-MIS-PAY-005	x	unittest	simulation	show no times with an ascent/descent speed over 10 m/s
VV-WBA-S&C-004	Simulate stability margins and showcase stabilities	WBA-S&C		system tests	simulation	all nodes in the positive quadrant
VV-WBA-WEAT-001-01	simulate glider behaviour during ascent in wind speeds of 30 [m/s] at 10 [m] and 60 [m/s] at 10[km]	WBA-MIS-WEAT-001, WBA-MIS-WEAT-002	x	unittest	simulation	glider shows no unexpected behaviour
VV-WBA-WEAT-001-02	simulate glider behaviour during descent in wind speeds of 30 [m/s] at 10 [m] and 60 [m/s] at 10[km]	WBA-MIS-WE, VV-WBA-WEAT-002	x	unittest	simulation	Glider is able to land safely at predicted position
VV-WBA-WEAT-002-01	simulate possible damage and adverse effects of the balloon in 10 [mm/h] rain	WBA-MIS-WEAT-004		subsystem test	simulation	Balloon still able to reach the release altitude and itself is able to continue past the height deck
VV-WBA-WEAT-002-02	simulate damage of downwards approach in 10 [mm/h] rain	WBA-MIS-WEAT-004		subsystem test	simulation	No permanent deformations influencing the handling characteristics of the glider
VV-WBA-WEAT-003-01	simulate balloon behaviour due to snow and ice forming on the wings	WBA-MIS-WEAT-005		subsystem test	simulation	Balloon still able to reach the release altitude and itself is able to continue past the height deck
VV-WBA-WEAT-003-02	simulate glider behaviour due to snow and ice during descent	WBA-MIS-WEAT-005		subsystem test	simulation	Glider is able to attain level flight at the expected altitude
VV-WBA-WEAT-004-01	simulate balloon impact damage by 4mm hailstones	WBA-MIS-WEAT-006		subsystem test	simulation	Simulation shows no significant effect on balloon burst altitude resulting in early burst

VV-WBA-WEAT-004-02	simulate glider damage profile due to 4mm hailstones	WBA-MIS-WEAT-006		subsystem test	simulation	No permanent deformations influencing the handling characteristics of the glider
VV-WBA-WEAT-005-02	showcase capability to reverse ice formation in finite element simulation for low cloud conditions	WBA-MIS-WEAT-007		subsystem test	simulation	No threat of significant ice build-up
VV-WBA-WEAT-006-02	showcase capability to reverse ice formation in finite element simulation for medium cloud conditions	WBA-MIS-WEAT-007		subsystem test	simulation	No threat of significant ice build-up
VV-WBA-WEAT-007-02	showcase capability to reverse ice formation in finite element simulation for high cloud conditions	WBA-MIS-WEAT-007		subsystem test	simulation	No threat of significant ice build-up

Test

The test phase entails a lot of highly controlled test setups like pressure chambers, climate chambers and wind tunnels. In this phase, sensors will first be tested while simultaneously starting the prototyping process. A lot of tests can actually already be done without flying the gliders. Once the prototypes are available, more integrated system tests and calibration will be done. This is because it is very important to properly understand the airflow around the bodies in order to get the calibration correct, especially since the significance of these measurements cannot be understated: a small calibration error can lead to completely different interpretations of the climate in a constantly changing world. The steps that need to be undertaken in the test phase are described in Table 21.2.

Table 21.2: Test phase: verification and validation

Test Identifier	Test Description	Requirement Parent	Completed	Test Type	Verification Method	When Succeeded?
V&V-WBA-DES-005	The GPS system shall be placed on a well-defined location for both height and horizontal placement	WBA-MIS-DES-006		unittest	test	measurements within 2 meters spherically
V&V-WBA-DES-006	The GPS system shall be placed on a vehicle traveling a well-defined path from which the exact location at any time is known very well	WBA-MIS-DES-006		unittest	test	measurements within 2 meters spherically
V&V-WBA-DES-007	The GPS system shall be fed very noisy data and the recovery from these inputs shall be monitored	WBA-MIS-DES-006		unittest	test	recovery to within 2 m spherically within 10 seconds
V&V-WBA-MEAS-001	Placing the sensor package into a room where it will be subjected to temperatures between 200 and 350 [k] and measure the output data	WBA-MIS-PAY-MEAS-001		subsystem test	test	
V&V-WBA-MEAS-002	The sensor will be placed in a highly controlled climate chamber and over the required temperature range the results stay within accuracy and resolution ranges	”WBA-MIS-PAY-MEAS-002, WBA-MIS-PAY-MEAS-003”		unittest	test	”resolution less than 0.1, accuracy below 0.5”
V&V-WBA-MEAS-004-01	Place glider in wind tunnel and compare measured wind speeds with actual wind speeds at different angles of attack	WBA-MIS-PAY-MEAS-004		unittest	test	speed within 0.1 m/s
V&V-WBA-MEAS-004-02	”mount GPS shield on top of vehicle, compare actual velocity with the reported velocity of the glider”	WBA-MIS-PAY-MEAS-004		unittest	test	speed within 0.1 m/s
V&V-WBA-MEAS-005	measure in situ compass speed by placing it on a vehicle travelling in a well-defined direction and concluding on the outcome.	WBA-MIS-PAY-MEAS-005		subsystem test	test	less than 2 degrees

V&V-WBA-MEAS-006	measure output data of sensor boom in a well-defined humidity chamber	"WBA-MIS-PAY-MEAS-006, WBA-MIS-PAY-MEAS-007, WBA-MIS-PAY-MEAS-008"		unittest	test	"humidity range from 0 to at least 100%, resolution of 1, accuracy of 5 percent"
V&V-WBA-MEAS-007	place glider in climate controlled ozone level fluctuating measurement setup.	"WBA-MIS-PAY-MEAS-009, WBA-MIS-PAY-MEAS-010"		unittest	test	"parts per billion resolution, measure quantity in order of max million parts per billion"
V&V-WBA-MEAS-008	place glider in vacuum chamber and relay data of pressure measurements	"WBA-MIS-PAY-MEAS-011, WBA-MIS-PAY-MEAS-012"		unittest	test	"measurements between 1080 hPa and 3 hPa, accuracy better than 0.1 hPa"
V&V-WBA-MEAS-009	"place glider in climate controlled chamber, report results"	"WBA-MIS-PAY-MEAS-014, WBA-MIS-PAY-MEAS-015, WBA-MIS-PAY-MEAS-016"		unittest	test	"resolution lower than 10 PPB, range between 0 and 2.0 PPM"
V&V-WBA-MEAS-010	"place glider in climate controlled chamber, report results"	"WBA-MIS-PAY-MEAS-017, WBA-MIS-PAY-MEAS-018, WBA-MIS-PAY-MEAS-019"		unittest	test	"resolution lower than 0.1 ppm, range 250 to 520"
V&V-WBA-MEAS-011	place glider in controlled vacuum chamber and relay density of particulate matter results	WBA-MIS-PAY-MEAS-020		unittest	test	"density resolution below 0.001 kg/m^3 and accuracy below 0.1 percent"
V&V-WBA-MEAS-012	Integral wind tunnel test calibrating sensors for wind speed conditions	WBA-MIS-PAY-MEAS		subsystem test	test	check calibration within predefined limits
V&V-WBA-PAY-005	Set up a constant discharge test in the payload hold of the glider with a required power of 2 watts. perform a mission with the constant draw	WBA-MIS-PAY-003		subsystem test	test	"if 5 hours after takeoff the system can still draw power, the test has succeeded."
V&V-WBA-PAY-005-01	Perform a constant discharge test with a 2W discharge and a representative equivalent discharge power of the rest of the flight control system	WBA-MIS-PAY-003		unittest	test	"if 5 hours after the start of the test the system can still draw sufficient power, the test has succeeded"
V&V-WBA-WEAT-005-01	Show capability to reverse ice formation at low cloud conditions in wind tunnel	WBA-MIS-WEAT-007		subsystem test	test	No threat of significant ice build-up
V&V-WBA-WEAT-006-01	Show capability to reverse ice formation in medium cloud conditions in wind tunnel	WBA-MIS-WEAT-007		subsystem test	test	No threat of significant ice build up
V&V-WBA-WEAT-007-01	show capability to reverse ice formation in high cloud conditions in wind tunnel	WBA-MIS-WEAT-007		subsystem test	test	No threat of significant ice build up

Demonstration

The final phase of the V&V has a very clear milestone in between: the system can be declared flight ready roughly halfway through demonstration. During the demonstration, a lot of safety and handling operations need to be demonstrated. After the system has been proven to be flight ready, further demonstrations can take place where the vehicle is actually placed underneath a balloon and flown to show final system integration before the end of the V&V. The tests that need to be completed in the demonstration period are shown in Table 21.3

Table 21.3: Demonstration phase: verification and validation

Test identifier	Test description	Requirement parent	Completed	Test type	Verification method	When succeeded?

V&V-WBA-MEAS-003	For upwards measurements fly a weather balloon with two payloads: the glider and the original sonde. Compare measurements on whether they are consistent.	WBA-MIS-PAY-MEAS-004		subsystem test	demo	speed within 0.15 m/s
V&V-WBA-MEAS-004	For downwards measurements launch two weather balloons at the same time: one with the radiosonde and one with the glider. Compare relay measurements. Compare outcomes while realizing influence of different exact location.	WBA-MIS-PAY-MEAS-004		subsystem test	demo	speed within 0.30 m/s
V&V-WBA-OP-001	Demonstrate a two-cycle a day campaign	WBA-OP-001		system tests	demo	two launches 12 hours apart, succeeded without any delays
V&V-WBA-OP-RES-004	Simulate balloon release in 30[m/s] winds	WBA-OP-RES-006		subsystem test	demo	balloon attains 15 m within 200 m horizontal range change
V&V-WBA-PAY-001	Perform mission with maximum payload and show compliance of flight model with expected speed and dive velocities of computer model	WBA-MIS-PAY-001		system test	demo	total range within 1 km of predicted range based on wind conditions, always within 1.5 m/s of predicted optimum
V&V-WBA-PAY-002	Perform mission with minimum payload and show compliance of flight model with expected speed and dive velocities of computer model	WBA-MIS-PAY-001		system test	demo	total range within 1 km of predicted range based on wind conditions, always within 1.5 m/s of predicted optimum
V&V-WBA-PAY-004	Let operator go through complete launch cycle without any external help	WBA-MIS-PAY-002		system test	demo	Operator successfully launches the glider without any external assistance
V&V-WBA-PAY-006-01	Let payload show measurement frequency	”WBA-MIS-PAY-004, WBA-MIS-PAY-005”		unittest	demo	measurement frequency of at least 0.2 Hz
V&V-WBA-TA-001	Show a single operation cycle in which the operator takes the glider from the landing site to the storage site.	WBA-MIS-TA-001		subsystem test	demo	This action can be performed within arbitrary requirements and by a single person
V&V-WBA-TA-002	Show a single operation cycle in which the operator gets the glider from the storage, performs the calibration, and continues to launch the glider	WBA-MIS-TA-002		subsystem test	demo	Launch successful, sensors performing as intended at launch.
V&V-WBA-TA-003	Showcase the servos of the main wing being replaced by a single person	WBA-MIS-TA-003		unittest	demo	successful replacement, normally operating vehicle
V&V-WBA-TA-004	Showcase the servos of the horizontal tail being replaced by a single person	WBA-MIS-TA-003		unittest	demo	successful replacement, normally operating vehicle
V&V-WBA-TA-005	Showcase the detachment system of the balloon can be replaced by a single person	WBA-MIS-TA-003		unittest	demo	successful replacement, normally operating vehicle
V&V-WBA-TA-006	Showcase the navigation lights being replaced by a single person	WBA-MIS-TA-003		unittest	demo	successful replacement, normally operating vehicle
V&V-WBA-TA-007	Showcase the replaceable sensors of the payload can be replaced by a single person	WBA-MIS-TA-003		unittest	demo	successful replacement, normally operating vehicle
V&V-WBA-TA-008	Showcase a single person can correctly check that the data cable to the cargo hold of the large glider still functions properly	WBA-MIS-TA-003		unittest	demo	tests successfully checked, both for operating and not operating right conclusion is drawn
V&V-WBA-TA-010	Go through a complete turnaround cycle including calibration	WBA-MIS-TA-005		subsystem test	demo	time below 8 hours
V&V-WBA-TA-011	Go through a maintenance cycle	WBA-MIS-TA-006		subsystem test	demo	total time below 12 hours
V&V-WBA-OP-ENV-002	Accumulate the use of non-renewable resources	WBA-OP-ENV-002	x	system tests	inspection	no non-renewable resources

V&V-WBA-OP-RES-001	Accumulate the production costs	WBA-OP-RES-001	x	system tests	inspection	below 75 k per unit
V&V-WBA-OP-RES-002	Pack the system ready for transport	WBA-OP-RES-003		system tests	inspection	fits inside 20 ft container
V&V-WBA-OP-RES-003	Accumulate data on consumables	WBA-OP-RES-004	x	system tests	inspection	no consumables from non-renewable sources
V&V-WBA-OP-RES-005	Weigh the complete system or individual parts depending on what is available	WBA-OP-RES-007	x	system tests	inspection	all parts less than 25 kg
V&V-WBA-PAY-004-01	Show procedures that allow the operator to work alone with the filling gas	WBA-MIS-PAY-002		subsystem test	inspection	Operator manual does not prevent compliance by a single person
V&V-WBA-PAY-004-02	Show the manual does not have any steps that require more than one operator	WBA-MIS-PAY-002	x	unittest	inspection	User manual does not specify multiple person operations
V&V-WBA-TA-009	Show there is a payload bay with a swappable payload capability	WBA-MIS-TA-004		unittest	inspection	there is a payload bay for a payload
V&V-WBA-S&C-001	Showcase the capability of the system to operate without a rudder			system tests	demo	system can return to the launch site with the rudder disconnected
V&V-WBA-S&C-002	Showcase the capability of the system to operate with one aileron jammed			system tests	demo	system can return to the launch site with one aileron disconnected
V&V-WBA-S&C-003	Showcase the capability of providing sufficient torque for all servos at cruise speed			system tests	demo	system can actively deliver the expected outputs given a certain input as expected from the stability matrix
V&V-WBA-S&C-005	Showcase the capability of the system to naturally recover from a stall			system tests	demo	create inputs for stall condition at five uniformly distributed altitudes and see recovery from the glider
V&V-WBA-FC-001	Demonstrate a user-friendly interface			subsystem test	demo	complete simplified UX integration campaign
V&V-WBA-PE-001	Demonstrate the capability to provide 12V to the payload			unittest	demo	voltmeter measures 12±3V from completely full to completely empty conditions
V&V-WBA-PE-002	Demonstrate the capability to provide 5V to the actuators			unittest	demo	voltmeter measures 5±3V from completely full to completely empty conditions
V&V-WBA-PE-003	Demonstrate the capability to continuously provide <TBD> [W] to communications			unittest	demo	discharge test shows the capability of discharging continuously
V&V-WBA-PE-004	Demonstrate the capability to reliably provide <TBD> [W] for temperature regulation			unittest	demo	Full demo flight logs show compliance with the set requirement
V&V-WBA-PE-005	Demonstrate compatibility with EMC directive 2014/30/EU	Law		subsystem test	demo	All electronics are certified to the specs described in the directive
V&V-WBA-PE-006	Demonstrate compatibility with radio equipment directive 2014/53/EU	Law		subsystem test	demo	all radio equipment adheres to norms described in the directive
V&V-WBA-PE-007	Demonstrate compatibility with RoHS directive 2017/2102	Law		subsystem test	demo	all electronics must be certified in compliance with the regulation
V&V-WBA-PE-008	Demonstrate compatibility with REACH regulation EC No 1907/2006	Law		subsystem test	demo	none of the substances used in the construction are forbidden
V&V-WBA-PE-009	Demonstrate that there are no known hazardous substances present on the glider	Law		unittest	demo	no substances of concern present
V&V-WBA-PE-010	Demonstrate that all necessary symbols, labels, and markings are present on the glider	Law		subsystem test	demo	complete label and marking set
V&V-WBA-PE-011	Demonstrate compliance with EN ISO 9001:2015	Law		system tests	inspection	system fulfils all requirements of the standard

wxUAS Demonstration

The final integration step is taking part in the worldwide WMO wxUAS demonstration. Over a period of six months, measurements are done in parallel to the original radiosondes to allow for the international scientific community to validate that the conducted measurements. This part of the test campaign still has some final integration tests that can be completed, but the most important is that the measurements

are now done as planned by the worldwide demonstration. There might however be validation tests that cannot take place: there is no guarantee that there will be snow or hail during this period. These final validation tests might have to be done at a later time. The tests that are ideally completed within this test period are shown in Table 21.4.

Table 21.4: wxUAS demonstration phase: verification and validation

Test Identifier	Test Description	Requirement Parent	Completed	Test Type	Verification Method	When Succeeded?
V&V-WBA-ASC-001	Do a demonstration test showing the balloon can be burned off at least 33 km	WBA-MIS-ASC-002		Subsystem Test	wxUAS	Burst height at least 33 km
V&V-WBA-DES-001	Show proper functioning of return infrastructure by launching a weather balloon at the edge of the mission radius	WBA-MIS-DES-001		Subsystem Test	wxUAS	Safe return from within mission profile
V&V-WBA-MEAS-003-b	For upwards measurements fly a weather balloon with two payloads: the glider and the original sonde. Compare measurements on whether they are consistent.	WBA-MIS-PAY-MEAS-004		Subsystem Test	demo	Speed within 0.15 m/s
V&V-WBA-MEAS-004	For downwards measurements launch two weather balloons at the same time: one with the radiosonde and one with the glider. Compare relay measurements. Compare outcomes while realizing influence of different exact location.	WBA-MIS-PAY-MEAS-004		Subsystem Test	demo	Speed within 0.30 m/s
V&V-WBA-MEAS-013	In situ comparison of performance test with glider and original radiosonde by running obtained data in weather model	WBA-MIS-PAY-MEAS		Subsystem Test	wxUAS	Weather predictions accurate within predefined limits
V&V-WBA-OP-RES-004	Simulate balloon release in 30 [m/s] winds	WBA-OP-RES-006		Subsystem Test	demo	Balloon attains 15 m within 200 m horizontal range change
V&V-WBA-PAY-006	Perform mission from minimum possible wind conditions to 2SSD wind conditions and show compliance of measurement resolution.	WBA-MIS-PAY-004, WBA-MIS-PAY-005		Subsystem Test	wxUAS	Measurement accuracy in all tests during campaign showed a resolution higher than once every 50 m both up- and down going
V&V-WBA-WEAT-001	Launch and retrieve glider in wind speeds of up to 30 [m/s] at 10 [m] and 60 [m/s] at 10 [km].	WBA-MIS-WEAT-001, WBA-MIS-WEAT-002		System Test	wxUAS	Glider lands at expected landing spot and can be re-used without any pre-occupations
V&V-WBA-WEAT-002	Launch and retrieve glider in 10 mm/h rain	WBA-MIS-WEAT-004		System Test	wxUAS	No visible damage on the glider, the balloon attained no damage impacting the release altitude
V&V-WBA-WEAT-003	Launch and retrieve glider in snow conditions	WBA-MIS-WEAT-005		System Test	wxUAS	Glider is able to attain level flight at expected altitude. The balloon attained no damage or weight impacting the release altitude
V&V-WBA-WEAT-004	Launch and retrieve glider in hail conditions of 4 mm hailstones	WBA-MIS-WEAT-006		System Test	wxUAS	No visible damage to the glider, balloon not impacted in a fashion that it will cause an early burst
V&V-WBA-WEAT-005	Show capability to reverse ice formation in low clouds	WBA-MIS-WEAT-007		System Test	wxUAS	No threat of uncontrollable descent or significant decreases in range
V&V-WBA-WEAT-006	Show capability to reverse ice formation in medium clouds	WBA-MIS-WEAT-007		System Test	wxUAS	No threat of uncontrollable descent or significant decreases in range
V&V-WBA-WEAT-007	Show capability to reverse ice formation in high clouds	WBA-MIS-WEAT-007		System Test	wxUAS	No threat of uncontrollable descent or significant decreases in range

21.5. Project Gantt Chart

The steps discussed in this chapter are shown in the Gantt chart below.

ID	Task Name	Duration	Start
1	**GLOBAL PLANNING**	**264 days**	**Fri 01/09/23**
3	GO/NO GO for wx UAS campaign	0 days	Mon 02/10/23
8	BRAVO XL & BRAVO mini flight certified	0 days	Wed 07/02/24
9	Demonstration phase	44 days	Wed 03/01/2
2	Simulation phase	22 days	Fri 01/09/23
4	Testing phase	67 days	Mon 02/10/2
5	**Building gliders**	**30 days**	**Mon 02/10/2**
10	wxUAS campaign	132 days	Tue 05/03/24
11	**V&V-WBA-MEAS**	**264 days**	**Fri 01/09/23**
16	**V&V-WBA-MEAS-004**	**264 days**	**Fri 01/09/23**
17	V&V-WBA-MEAS-004-a	3 days	
21	V&V-WBA-MEAS-004-03	1 day	Fri 01/09/23
19	V&V-WBA-MEAS-004-01	3 days	Sun 12/11/23
20	V&V-WBA-MEAS-004-02	2 days	Wed 04/10/2
18	V&V-WBA-MEAS-004	132 days	Tue 05/03/24
22	**V&V-WBA-MEAS-005**	**88 days**	**Fri 01/09/23**
24	V&V-WBA-MEAS-005-01	1 day	Fri 01/09/23
23	V&V-WBA-MEAS-005	3 days	Fri 29/12/23
14	V&V-WBA_MEAS-003-a	3 days	
12	V&V-WBA-MEAS-001	1 day	Sat 07/10/23
13	V&V-WBA-MEAS-002	1 day	Tue 10/10/23
25	V&V-WBA-MEAS-006	3 days	Wed 15/11/2
26	V&V-WBA-MEAS-007	3 days	Sat 18/11/23
27	V&V-WBA-MEAS-008	3 days	Fri 24/11/23
28	V&V-WBA-MEAS-009	3 days	Thu 30/11/23
29	V&V-WBA-MEAS-010	3 days	Wed 06/12/2
30	V&V-WBA-MEAS-011	3 days	Sat 09/12/23
31	V&V-WBA-MEAS-012	10 days	Fri 15/12/23
15	V&V-WBA-MEAS-003-b	132 days	Tue 05/03/24
32	V&V-WBA-MEAS-013	132 days	Tue 05/03/24
33	**V&V-WBA-PAY**	**251 days**	**Mon 12/06/2**
34	**V&V-WBA-PAY-001**	**98 days**	**Mon 04/09/2**
35	V&V-WBA-PAY-001	10 days	Thu 04/01/24
36	V&V-WBA-PAY-001-01	1 day	Mon 04/09/2
37	**V&V-WBA-PAY-002**	**108 days**	**Mon 04/09/2**
38	V&V-WBA-PAY-002	10 days	Thu 18/01/24
39	V&V-WBA-PAY-002-01	1 day	Mon 04/09/2
40	**V&V-WBA-PAY-004**	**1 day**	**Mon 12/06/2**
41	V&V-WBA-PAY-004	1 day	
42	V&V-WBA-PAY-004-01	1 day	
43	V&V-WBA-PAY-004-02	1 day	
44	**V&V-WBA-PAY-005**	**87 days**	**Fri 01/09/23**
47	V&V-WBA-PAY-005-02	1 day	Fri 01/09/23
45	V&V-WBA-PAY-005	1 day	Mon 01/01/2
46	V&V-WBA-PAY-005-01	1 day	Fri 13/10/23
48	**V&V-WBA-PAY-006**	**103 days**	**Thu 04/01/24**
50	V&V-WBA-PAY-006-01	20 days	Thu 04/01/24
51	V&V-WBA-PAY-006-02	3 days	Fri 01/03/24
49	V&V-WBA-PAY-006	60 days	Tue 05/03/24
52	**V&V-WBA-TA**	**26 days**	**Tue 02/01/24**
53	V&V-WBA-TA-001	1 day	Tue 02/01/24
54	V&V-WBA-TA-002	1 day	Wed 03/01/2
55	V&V-WBA-TA-003	1 day	Thu 01/02/24
56	V&V-WBA-TA-004	1 day	Thu 01/02/24
57	V&V-WBA-TA-005	1 day	Thu 01/02/24
58	V&V-WBA-TA-006	1 day	Thu 01/02/24
59	V&V-WBA-TA-007	2 days	Fri 02/02/24
60	V&V-WBA-TA-008	1 day	Thu 01/02/24
61	V&V-WBA-TA-009	1 day	Thu 01/02/24
62	V&V-WBA-TA-010	1 day	Thu 01/02/24
63	V&V-WBA-TA-011	1 day	Tue 06/02/24
64	**V&V-WBA-WEAT**	**262 days**	**Tue 05/09/23**
65	**V&V-WBA-WEAT-001**	**262 days**	**Tue 05/09/23**
67	V&V-WBA-WEAT-001-01	3 days	Tue 05/09/23
68	V&V-WBA-WEAT-001-02	3 days	Tue 05/09/23
66	V&V-WBA-WEAT-001	132 days	Tue 05/03/24
69	**V&V-WBA-WEAT-002**	**261 days**	**Wed 06/09/2**
71	V&V-WBA-WEAT-002-01	2 days	Wed 06/09/2
72	V&V-WBA-WEAT-002-02	2 days	Fri 08/09/23
70	V&V-WBA-WEAT-002	132 days	Tue 05/03/24
73	**V&V-WBA-WEAT-003**	**259 days**	**Fri 08/09/23**
75	V&V-WBA-WEAT-003-01	1 day	Fri 08/09/23
76	V&V-WBA-WEAT-003-02	1 day	Mon 11/09/2
74	V&V-WBA-WEAT-003	132 days	Tue 05/03/24
77	**V&V-WBA-WEAT-004**	**257 days**	**Tue 12/09/23**
79	V&V-WBA-WEAT-004-01	1 day	Tue 12/09/23
80	V&V-WBA-WEAT-004-02	1 day	Wed 13/09/2
78	V&V-WBA-WEAT-004	132 days	Tue 05/03/24
81	**V&V-WBA-WEAT-005**	**255 days**	**Thu 14/09/23**
84	V&V-WBA-WEAT-005-02	1 day	Thu 14/09/23
83	V&V-WBA-WEAT-005-01	3 days	Mon 13/11/2
82	V&V-WBA-WEAT-005	132 days	Tue 05/03/24
85	**V&V-WBA-WEAT-006**	**255 days**	**Thu 14/09/23**
88	V&V-WBA-WEAT-006-02	1 day	Thu 14/09/23
87	V&V-WBA-WEAT-006-01	3 days	Thu 16/11/23
86	V&V-WBA-WEAT-006	132 days	Tue 05/03/24
89	**V&V-WBA-WEAT-007**	**255 days**	**Thu 14/09/23**
92	V&V-WBA-WEAT-007-02	1 day	Thu 14/09/23
91	V&V-WBA-WEAT-007-01	3 days	Tue 21/11/23
90	V&V-WBA-WEAT-007	132 days	Tue 05/03/24
93	**V&V-WBA-DES**	**254 days**	**Fri 15/09/23**
94	**V&V-WBA-DES-001**	**254 days**	**Fri 15/09/23**
96	V&V-WBA-DES-001-01	3 days	Fri 15/09/23
95	V&V-WBA-DES-001	132 days	Tue 05/03/24
97	V&V-WBA-DES-002	3 days	Fri 15/09/23
98	V&V-WBA-DES-003	3 days	Mon 18/09/2
99	V&V-WBA-DES-004	3 days	Mon 18/09/2
100	V&V-WBA-DES-005	2 days	Thu 19/10/23
101	V&V-WBA-DES-006	5 days	Mon 23/10/2
102	V&V-WBA-DES-007	1 day	Mon 16/10/2
103	**V&V-WBA-ASC**	**251 days**	**Wed 20/09/2**
105	V&V-WBA-ASC-002	3 days	Wed 20/09/2
106	V&V-WBA-ASC-003	2 days	Thu 21/09/23
104	V&V-WBA-ASC-001	132 days	Tue 05/03/24
107	**V&V-WBA-OP-REG**	**4 days**	**Mon 25/09/2**
108	V&V-WBA-OP-REG-001	3 days	Mon 25/09/2
109	V&V-WBA-OP-REG-002	4 days	Mon 25/09/2
110	V&V-WBA-OP-REG-003	4 days	Mon 25/09/2
111	**V&V-WBA-OP**	**244 days**	**Fri 29/09/23**
112	**V&V-WBA-OP-RES**	**150 days**	**Thu 08/02/24**
113	V&V-WBA-OP-RES-001	1 day	Thu 08/02/24
114	V&V-WBA-OP-RES-002	2 days	Fri 09/02/24
115	V&V-WBA-OP-RES-003	2 days	Fri 09/02/24
117	V&V-WBA-OP-RES-005	1 day	
116	V&V-WBA-OP-RES-004	132 days	Tue 05/03/24
118	**V&V-WBA-OP-ENV**	**94 days**	**Fri 29/09/23**
120	V&V-WBA-OP-ENV-002	1 day	Wed 07/02/2
119	V&V-WBA-OP-ENV-001	1 day	Fri 29/09/23
121	V&V-WBA-OP-ENV-003	1 day	Fri 29/09/23
122	V&V-WBA-OP-001	10 days	Wed 07/02/2
123	**V&V-WBA-S&C**	**105 days**	**Tue 19/09/23**
124	V&V-WBA-S&C-001	2 days	Wed 07/02/2
125	V&V-WBA-S&C-002	2 days	Wed 07/02/2
126	V&V-WBA-S&C-003	2 days	Wed 07/02/2
128	V&V-WBA-S&C-005	2 days	Fri 09/02/24
127	V&V-WBA-S&C-004	2 days	Tue 19/09/23
129	**V&V-WBA-FC**	**0 days**	**Sun 04/02/24**
130	V&V-WBA-FC-001	1 day	Sun 04/02/24
131	**V&V-WBA-PE**	**6 days**	**Tue 02/01/24**
132	V&V-WBA-PE-001	1 day	Tue 02/01/24
133	V&V-WBA-PE-002	1 day	Tue 02/01/24
134	V&V-WBA-PE-003	2 days	Fri 05/01/24
135	V&V-WBA-PE-004	2 days	Fri 05/01/24
136	V&V-WBA-PE-005	1 day	Tue 09/01/24
137	V&V-WBA-PE-006	1 day	Tue 09/01/24
138	V&V-WBA-PE-007	1 day	Tue 09/01/24
139	**V&V-WBA-STRUCT**	**8 days**	**Mon 19/02/2**
140	V&V-WBA-STRUCT-001	3 days	Mon 19/02/2
141	V&V-WBA-STRUCT-002	5 days	Thu 22/02/24
142	**V&V-WBA-L&L**	**37 days**	**Wed 10/01/2**
143	V&V-WBA-L&L-001	2 days	Wed 10/01/2
144	V&V-WBA-L&L-002	3 days	Thu 22/02/24
145	V&V-WBA-L&L-003	1 day	Fri 12/01/24
146	V&V-WBA-L&L-004	3 days	Tue 27/02/24
147	**V&V-WBA-GI**	**156 days**	**Fri 16/06/23**
149	V&V-WBA-GI-002	1 day	Fri 16/06/23
148	V&V-WBA-GI-001	5 days	Mon 15/01/2

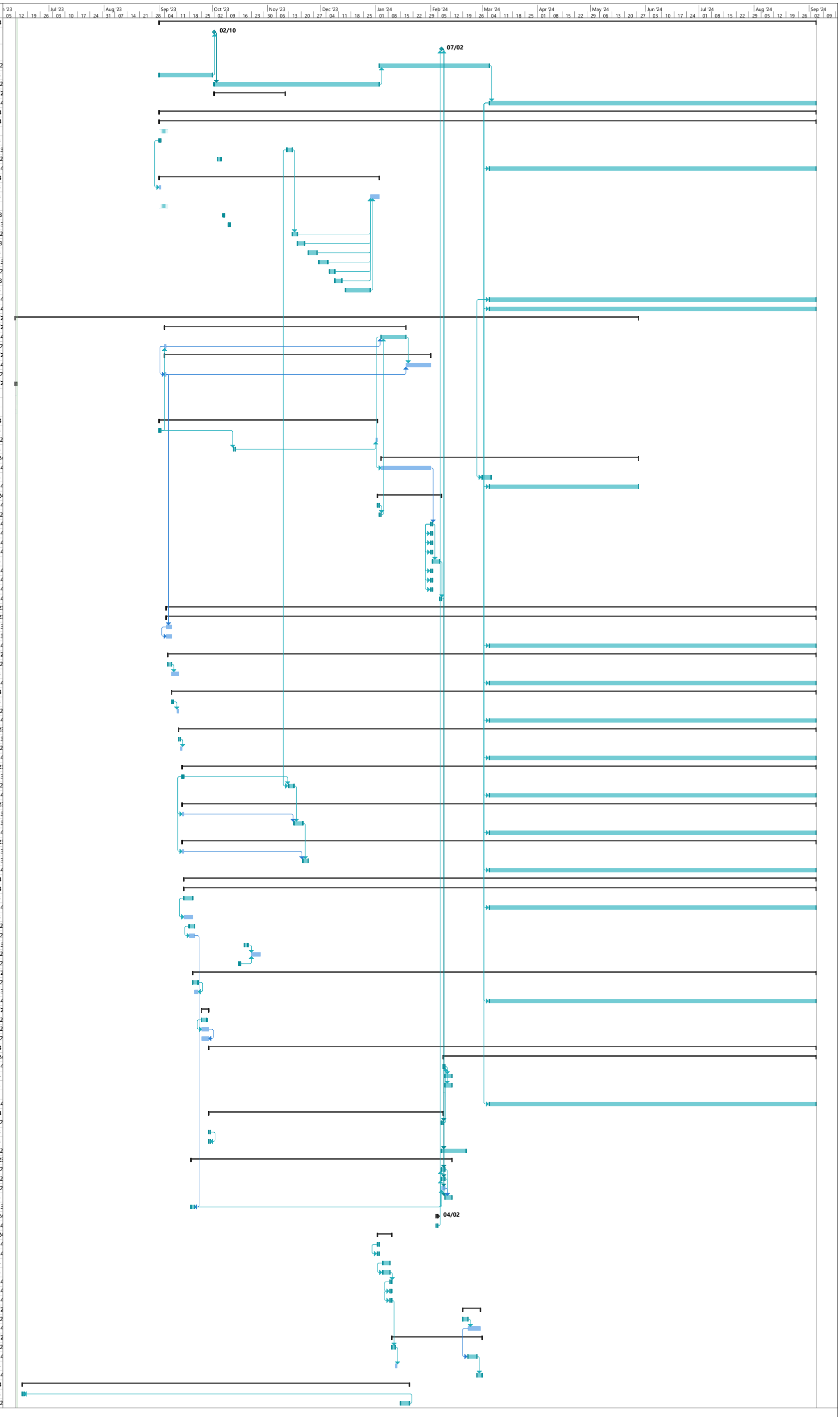

Project: Future_planning
Date: Tue 13/06/23

Task | Split | Milestone | Summary | Project Summary | Inactive Task | Inactive Milestone | Inactive Summary | Manual Task | Duration-only | Manual Summary Rollup | Manual Summary | Start-only | Finish-only | External Tasks | External Milestone | Deadline | Progress | Manual Progress

22

Conclusion and Recommendations

The mission objective of this DSE project was *"To design a sustainable and reusable system to replace the current high altitude meteorological measurement devices at a lower cost per launch."*. This report specifically concerns the detailed sub-system level design of the concept that resulted from previous development stages. On top of the subsystem level design, external analyses such as market, safety, and risk were performed to assess the effectiveness of the final design.

The final design of the system consists of two sizes of gliders, a small one optimised for basic radiosonde missions, and a larger one with a customisable payload. Using a hydrogen balloon, the glider is then lifted to up to 33km altitude, where it is released. The glider then autonomously glides down and returns to the launch site in a net, ready to be reused. Launching from de Bilt, both models can return in over 90% of wind conditions, while in other cases the flight navigation can divert to contingency landing sites. In many of the other possible launch sites investigated, the return rate was even higher.

The design presented successfully achieves the mission objective. It allows for reuse of the most carbon-intensive and non-degradable components, making the system much more sustainable than the current disposable radiosondes. This reusability also makes the system more cost-effective; the higher weight resulting from the glider is offset by reusing the sensors and electronics. In addition, the lifting gas in the balloon is switched from helium, which is non-renewable, to hydrogen, contributing to the sustainability.

Recommendations
To develop the design presented in this report into an operational system, the following recommendations are made. First, a more detailed analysis of the aerodynamics with more advanced computational fluid dynamics software is recommended. This would allow taking effects into account that were not with the current approach (openVSP panel method), specifically flight at low Reynolds numbers. Similarly, finite element methods could be applied to the structural analysis, with which factors that were discarded in the analysis performed in this project. Ultimately, flight tests of prototypes would likely be the best way of testing the various glider subsystems and the system as a whole.

In addition to the glider, more development could be focused on ground systems. This includes for instance a more detailed analysis of switching from helium to hydrogen infrastructure. Also, as was briefly discussed in this rapport, an automatic launcher could be developed to significantly decrease the labour costs of launching the gliders. Applying these recommendations would make the system even more effective.

References

[1] "Helium and fusion energy: Richard h. clarke and zhiming cai," *The Future of Helium as a Natural Resource*, pp. 273–302, 2012. DOI: 10.4324/9780203120675-24.

[2] "Weather balloons are important part of global observing system," World Meteorological Organization. (Feb. 17, 2023), [Online]. Available: https://public.wmo.int/en/media/news/weather-balloons-are-important-part-of-global-observing-system#:~:text=Radiosondes%5C%2C%5C%20which%5C%20act%5C%20as%5C%20upper,observations%5C%20at%5C%200000UTC%5C%20and%5C%201200UTC. (visited on 05/01/2023).

[3] D. G. 1, "Design of a weather balloon alternative - project plan: Design synthesis exercise," Apr. 28, 2023.

[4] D. G. 1, "Design of a weather balloon alternative - baseline report: Design synthesis exercise," Apr. 28, 2023.

[5] D. G. 1, "Design of a weather balloon alternative - midterm report: Design synthesis exercise," Jun. 12, 2023.

[6] "Sonde," Network for the Detection of Atmospheric Composition Change. (2023), [Online]. Available: https://ndacc.larc.nasa.gov/instruments/sonde (visited on 06/14/2023).

[7] B. C. Bernstein and C. L. Bot, "An inferred climatology of icing conditions aloft, including supercooled large drops. part ii: Europe, asia, and the globe," *Journal of Applied Meteorology and Climatology*, vol. 48, no. 8, pp. 1503–1526, 2009. DOI: https://doi.org/10.1175/2009JAMC2073.1. [Online]. Available: https://journals.ametsoc.org/view/journals/apme/48/8/2009jamc2073.1.xml.

[8] M. Bragg, A. Broeren, and L. Blumenthal, "Iced-airfoil aerodynamics," *Progress in Aerospace Sciences*, vol. 41, no. 5, pp. 323–362, 2005, ISSN: 0376-0421. DOI: https://doi.org/10.1016/j.paerosci.2005.07.001. [Online]. Available: https://www.sciencedirect.com/science/article/pii/S0376042105000801.

[9] R. Hann, "Atmospheric ice accretions, aerodynamic icing penalties, and ice protection systems on unmanned aerial vehicles," Ph.D. dissertation, 2020.

[10] N. Fajt, R. Hann, and T. Lutz, "The influence of meteorological conditions on the icing performance penalties on a uav airfoil," Jun. 2019. DOI: 10.13009/EUCASS2019-240.

[11] H. LI, Y. ZHANG, and H. CHEN, "Optimization design of airfoils under atmospheric icing conditions for uav," *Chinese Journal of Aeronautics*, vol. 35, no. 4, pp. 118–133, 2022, ISSN: 1000-9361. DOI: https://doi.org/10.1016/j.cja.2021.04.031. [Online]. Available: https://www.sciencedirect.com/science/article/pii/S1000936121001904.

[12] T. Ghisu, J. Jarrett, and G. Parks, "Robust design optimization of airfoils with respect to ice accretion," *Journal of Aircraft*, vol. 48, pp. 287–304, Jan. 2011. DOI: 10.2514/1.C031100.

[13] L. W. Traub and C. Coffman, "Efficient low-reynolds-number airfoils," *JOURNAL OF AIRCRAFT*, vol. 56, no. 5, 2019. [Online]. Available: https://doi.org/10.2514/1.C035515.

[14] "20-32c airfoil - dillner 20-32-c low reynolds number airfoil," Airfoil Tools. (), [Online]. Available: http://airfoiltools.com/airfoil/details?airfoil=2032c-il (visited on 06/08/2023).

[15] "Cr001sm - cody robertson cr 001 r/c hand-launch low reynolds number airfoil (smoothed)," Airfoil Tools. (), [Online]. Available: http://airfoiltools.com/airfoil/details?airfoil=cr001sm-il (visited on 06/08/2023).

[16] "Apex 16 (normalized using xfoil date021206) - drela apex 16 low reynolds number transonic research airfoil," Airfoil Tools. (), [Online]. Available: http://airfoiltools.com/airfoil/details?airfoil=apex16-il (visited on 06/08/2023).

[17] "Naca 2412 - naca 2412 airfoil," Airfoil Tools. (), [Online]. Available: http://airfoiltools.com/airfoil/details?airfoil=naca2412-il (visited on 06/08/2023).

[18] M. H. Sadraey, *Aircraft design a system engineering approach*. Wiley, 2013.

[19] F. Thomas and J. Milgram, *Fundamentals of sailplane design*. College Park Press, 1999.

[20] J. Taylor, *Jane's all the world's aircraft 1986-87*. Jane's Pub. Co., 1987.

[21] D. F. Oliviero, *Requirement analysis and design principles for a/c stability & control (part 1)*, Feb. 21, 2019.

[22] D. F. Oliviero, *Requirement analysis and design principles for a/c stability & control (part 2)*, Feb. 21, 2019.

[23] J. Mulder, W. van Staveren, J. van der Vaart, *et al.*, *Flight Dynamics: Lecture Notes*. Delft University of Technology, 2013.

[24] J. Kim and D. Cho, "Effects of waste expanded polypropylene as recycled matrix on the flexural, impact, and heat deflection temperature properties of kenaf fiber/polypropylene composites," *Polymers*, vol. 12, no. 11, 2020, ISSN: 2073-4360. DOI: 10.3390/polym12112578. [Online]. Available: https://www.mdpi.com/2073-4360/12/11/2578.

[25] M. MInus and S. Kumar, "The processing, properties, and structure of carbon fibers," *JOM*, vol. 57, no. 2, pp. 52–58, 2005. DOI: 10.1007/s11837-005-0217-8.
[26] PerformanceComposites, *Mechanical properties of fibre composite materials*, Jul. 2009. [Online]. Available: http://www.performance-composites.com/carbonfibre/mechanicalproperties_2.asp (visited on 06/18/2023).
[27] İ. Kartal and H. Demirer, "Wear properties of hybrid epoxy composites reinforced with carbon/kevlar/glass fabrics," *Acta Physica Polonica A*, vol. 131, pp. 559–562, Mar. 2017. DOI: 10.12693/APhysPolA.131.559.
[28] S. Kulkarni, J. Rice, and B. Rosen, "An investigation of the compressive strength of kevlar 49/epoxy composites," *Composites*, vol. 6, no. 5, pp. 217–225, 1975, ISSN: 0010-4361. DOI: https://doi.org/10.1016/0010-4361(75)90417-6. [Online]. Available: https://www.sciencedirect.com/science/article/pii/0010436175904176.
[29] EASA. "Cs-23 initial issue." (2003), [Online]. Available: https://www.easa.europa.eu/en/document-library/certification-specifications/cs-23-initial-issue (visited on 06/19/2023).
[30] M. C.-Y. Niu, *Airframe structural design: Practical design information and data on Aircraft Structures*. Conmilit Pr, 1998.
[31] "Balsa," The Wood Database. (), [Online]. Available: https://www.wood-database.com/balsa/ (visited on 06/08/2022).
[32] "Mechanical properties of carbon fibre composite materials, fibre / epoxy resin (120°c cure)," Performance Composites Limited. (), [Online]. Available: http://www.performance-composites.com/carbonfibre/mechanicalproperties_2.asp (visited on 06/06/2022).
[33] "7075 aluminum alloy properties, aa 7075-t6, t7351, t651, density, composition, yield strength," The World Material. (), [Online]. Available: https://www.theworldmaterial.com/al-7075-aluminum-alloy/ (visited on 06/08/2022).
[34] Vaisala. "Ozone sounding with radiosonde rs41." (), [Online]. Available: https://www.vaisala.com/en/products/weather-environmental-sensors/ozone-sounding-radiosonde-rs41 (visited on 06/16/2022).
[35] J. V.-L. Halis C. Polat and M. Romano, "Survey, statistical analysis and classification of launched cubesat missions with emphasis on the attitude control method," *Journal of Small Satellites*, vol. 5, no. 3, 2016.
[36] M. O. Kenjiro S. Lay Lingqi Li, "High altitude balloon testing of arduino and environmental sensors for cubesat prototype," *HardwareX*, Jun. 2022. DOI: 10.17605/OSF.IO/7XR38.
[37] R. Lehtinen, P. Survo, and H. Jauhiainen, "Comparison of two radiosonde pressure measurements," Jan. 2016.
[38] O. Teichert, S. Link, J. Schneider, S. Wolff, and M. Lienkamp, "Techno-economic cell selection for battery-electric long-haul trucks," *eTransportation*, vol. 16, p. 100 225, 2023, ISSN: 2590-1168. DOI: https://doi.org/10.1016/j.etran.2022.100225. [Online]. Available: https://www.sciencedirect.com/science/article/pii/S2590116822000704.
[39] J. B. Quinn, T. Waldmann, K. Richter, M. Kasper, and M. Wohlfahrt-Mehrens, "Energy density of cylindrical li-ion cells: A comparison of commercial 18650 to the 21700 cells," *Journal of The Electrochemical Society*, vol. 165, no. 14, A3284, Oct. 2018. DOI: 10.1149/2.0281814jes. [Online]. Available: https://dx.doi.org/10.1149/2.0281814jes.
[40] M. A. Hannan, M. M. Hoque, A. Hussain, Y. Yusof, and P. J. Ker, "State-of-the-art and energy management system of lithium-ion batteries in electric vehicle applications: Issues and recommendations," *IEEE Access*, vol. 6, pp. 19 362–19 378, 2018. DOI: 10.1109/ACCESS.2018.2817655.
[41] R. Hann, A. Enache, M. C. Nielsen, *et al.*, "Experimental heat loads for electrothermal anti-icing and de-icing on uavs," *Aerospace*, vol. 8, no. 3, 2021, ISSN: 2226-4310. DOI: 10.3390/aerospace8030083. [Online]. Available: https://www.mdpi.com/2226-4310/8/3/83.
[42] "Flight planning map - benelux," NOTAM info. (), [Online]. Available: https://notaminfo.com/netherlandsmap (visited on 06/05/2023).
[43] "Aeret preflight drone basic," Aeret. (), [Online]. Available: https://aeret.kaartviewer.nl/index.php?@dpf_basic (visited on 06/05/2023).
[44] "Integrated global radiosonde archive (igra)," National Centers for Environmental Information. (), [Online]. Available: https://www.ncei.noaa.gov/products/weather-balloon/integrated-global-radiosonde-archivel (visited on 06/12/2023).
[45] "Sonde," Network for the Detection of Atmospheric Composition Change. (), [Online]. Available: https://ndacc.larc.nasa.gov/instruments/sonde (visited on 06/12/2023).
[46] "Graph of drag of a sphere," NASA. (), [Online]. Available: https://www1.grc.nasa.gov/beginners-guide-to-aeronautics/drag-of-a-sphere/ (visited on 05/13/2023).
[47] "Understanding high-altitude balloon flight fundamentals," Taylor University. (), [Online]. Available: https://www.iastatedigitalpress.com/ahac/article/8327/galley/7923/view/ (visited on 05/13/2023).
[48] "Cotton morphology and chemistry." (Jun. 2020), [Online]. Available: https://www.cottoninc.com/quality-products/nonwovens/cotton-fiber-tech-guide/cotton-morphology-and-chemistry/.

[49] A. Hodges, A. L. Hoang, G. Tsekouras, *et al.*, "A high-performance capillary-fed electrolysis cell promises more cost-competitive renewable hydrogen," *Nature Communications*, vol. 13, no. 1, Mar. 2022. DOI: 10.1038/s41467-022-28953-x. [Online]. Available: https://doi.org/10.1038/s41467-022-28953-x.

[50] "Drones (uas)," EASA. (), [Online]. Available: https://www.easa.europa.eu/en/the-agency/faqs/drones-uas#category-regulations-on-uas-drone-explained (visited on 06/06/2023).

[51] R. voor Ondernemend Nederland. "Generiek richtsnoer waterstofveiligheid, eerste versie." (2022), [Online]. Available: %5Cbegin%7Bverbatim%7D%20https://www.rvo.nl/sites/default/files/2022-10/Generiek%20richtsnoer%20Waterstofveiligheid%20%28eerste%20vastgestelde%20versie%2C%205%20oktober%202022%29.pdf%20%5Cend%7Bverbatim%7D (visited on 05/10/2022).

[52] D. C. Knowledge. "The environmental impact of lithium-ion batteries – how green are they really?" (), [Online]. Available: https://www.datacenterknowledge.com/hardware/environmental-impact-lithium-ion-batteries-how-green-are-they-really (visited on 06/16/2022).

[53] T. Delft. "Flight altitude determines climate impact of hypersonic aircraft." (), [Online]. Available: https://www.tudelft.nl/en/2022/lr/flight-altitude-determines-climate-impact-of-hypersonic-aircraft (visited on 06/16/2022).

[54] Wikipedia. "Atmospheric escape." (), [Online]. Available: https://en.wikipedia.org/wiki/Atmospheric_escape (visited on 06/16/2022).

[55] HSV. "Epp." (), [Online]. Available: https://www.hsv-pi.nl/en/epp/ (visited on 06/16/2022).

[56] E. Forum. "Epp as a raw material – light and stable." (), [Online]. Available: https://epp-forum.com/en/sustainability/raw-material/ (visited on 06/16/2022).

[57] I. Group. "4 facts about expanded polypropylene." (), [Online]. Available: https://www.isowall.co.za/4-facts-about-expanded-polypropylene-epp/ (visited on 06/16/2022).

[58] Wordpress. "Environmental impact and sustainability." (), [Online]. Available: https://kevlarweb.wordpress.com/environmental-impact-and-sustainability (visited on 06/18/2022).

[59] A. Cleantech. "Environmental impacts of lithium-ion batteries." (), [Online]. Available: https://www.azocleantech.com/article.aspx?ArticleID=1520 (visited on 06/18/2022).

[60] L. cenex. "What is the environmental impact of lithium batteries?" (), [Online]. Available: https://www.cenex-lcv.co.uk/news-media/exhibitor/what-is-the-environmental-impact-of-lithium-batteries (visited on 06/18/2022).

[61] U. Nations. "The 17 goals." (), [Online]. Available: https://sdgs.un.org/goals (visited on 06/16/2022).

[62] C. Kensche, "Service life of sailplanes made of cfrp," *Fibre Science and Technology*, vol. 18, no. 2, pp. 95–108, 1983, ISSN: 0015-0568. DOI: https://doi.org/10.1016/0015-0568(83)90007-6.

[63] Stratodynamics. (), [Online]. Available: http://www.stratodynamics.ca/about/ (visited on 06/13/2023).

[64] E. L. Hernandez, Axios Denver. (Jun. 27, 2023), [Online]. Available: https://www.axios.com/local/denver/2022/06/27/denver-urban-sky-balloon-startup-expands (visited on 06/13/2023).

[65] L. Grush, The Verge. (Jun. 23, 2022), [Online]. Available: https://www.theverge.com/2022/6/23/23177434/urban-sky-stratosphere-microballoons-earth-imaging-remote-sensing (visited on 06/13/2023).

[66] R. Lea. "Making earth observation cost-efficient with nanosatellites," AZO nano. (Oct. 13, 2021), [Online]. Available: https://www.azonano.com/article.aspx?ArticleID=5836 (visited on 06/14/2023).

[67] Aerostar. (), [Online]. Available: https://aerostar.com/products/balloons-airships/super-pressure-balloons (visited on 06/13/2023).

[68] "Remote sensing technology market size, share & trends analysis report by technology (active, passive), by application (agriculture, military, disaster management, weather), by platform, by region, and segment forecasts, 2020 - 2027," 2020. [Online]. Available: https://www.grandviewresearch.com/industry-analysis/remote-sensing-technologies-market (visited on 06/14/2023).

[69] E. Hand, "Aircraft spies gravity waves being sucked into antarctica's polar vortex," *Science*, May 12, 2020. DOI: 10.1126/science.abc7687.

[70] Rijkswaterstaat. "Leidraad rams, sturen op prestaties van systemen." (2013), [Online]. Available: https://www.leidraadse.nl/assets/files/downloads/Publicaties/leidraad_rams_-_sturen_op_prestaties_van_systemen.pdf (visited on 11/01/2013).

[71] M. Ohring, *Engineering Materialis Science*, 1st edition. The Netherlands: Elsevier, 1995.

[72] "Energy-based safety risk assessment: Doesmagnitude and intensity of energy predict injuryseverity?," DOI: https://doi.org/10.1080/01446193.2016.1274418.

[73] WorldoMeters. "Netherlands population." (2023), [Online]. Available: %5Cbegin%7Bverbatim%7D%20https://www.worldometers.info/world-population/netherlands-population/%5Cend%7Bverbatim%7D (visited on 06/20/2023).

[74] Velux. "Nederlanders brengen te weinig tijd door in de buitenlucht." (2019), [Online]. Available: %5Cbegin%7Bverbatim%7Dhttps://pers.velux.nl/nederlanders-brengen-te-weinig-tijd-door-in-de-buitenlucht/%5Cend%7Bverbatim%7D (visited on 06/20/2023).